AD-A128 005 A COMPARISON OF THE MSIS AND JACCHIA-70 MODELS WITH MEASURED ATMOSPHERIC..(U) AEROSPACE CORP EL SEGUNDO CA SPACE SCIENCES LAB A B PRAG 20 APR 83 1/2

UNCLASSIFIED TR-0083(3940-04)-1 SD-TR-83-25 F/G 4/1 NL

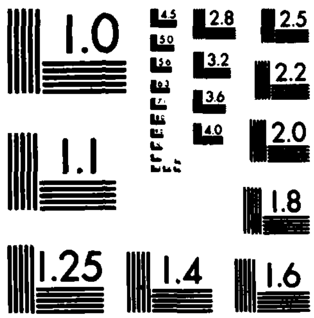

MICROCOPY RESOLUTION TEST CHART
NATIONAL BUREAU OF STANDARDS-1963-A

Prepared for

SPACE DIVISION
AIR FORCE SYSTEMS COMMAND
Los Angeles Air Force Station
P.O. Box 92960, Worldway postal Center
Los Angeles, Calif. 90009

This report was submitted by The Aerospace Corporation, El Segundo, CA 90245, under Contract No. F04701-82-C-0083 with the Space Division, Deputy for Technology, P.O. Box 92960, Worldway Postal Center, Los Angeles, CA 90009. It was reviewed and approved for The Aerospace Corporation by H. R. Rugge, Director, Space Sciences Laboratory.

Lt Ken R. Hasegawa, SD/YLVM, was the project officer for the Mission-Oriented Investigation and Experimentation (MOIE) Program.

This report has been reviewed by the Public Affairs Office (PAS) and is releasable to the National Technical Information Service (NTIS). At NTIS, it will be available to the general public, including foreign nationals.

This technical report has been reviewed and is approved for publication. Publication of this report does not constitute Air Force approval of the report's findings or conclusions. It is published only for the exchange and stimulation of ideas.

Ken R. Hasegawa

Ken R. Hasegawa, 2nd Lt, USAF
Project Officer

Norman W. Lee

Norman W. Lee, Jr., Colonel, USAF
Commander, Det 1, AFSTC

REPORT DOCUMENTATION PAGE

READ INSTRUCTIONS BEFORE COMPLETING FORM

1. REPORT NUMBER: SD-TR-83-25
2. GOVT ACCESSION NO.: AD-A128005
3. RECIPIENT'S CATALOG NUMBER:
4. TITLE (and Subtitle): A COMPARISON OF THE MSIS AND JACCHIA-70 MODELS WITH MEASURED ATMOSPHERIC DENSITY DATA IN THE 120 TO 200 km ALTITUDE RANGE
5. TYPE OF REPORT & PERIOD COVERED:
6. PERFORMING ORG. REPORT NUMBER: TR-0083(3940-04)-1
7. AUTHOR(s): A. B. Prag
8. CONTRACT OR GRANT NUMBER(s): F04701-82-C-0083
9. PERFORMING ORGANIZATION NAME AND ADDRESS: The Aerospace Corporation, El Segundo, CA 90245
10. PROGRAM ELEMENT, PROJECT, TASK AREA & WORK UNIT NUMBERS:
11. CONTROLLING OFFICE NAME AND ADDRESS: Space Division, Air Force Systems Command, Los Angeles, CA 90009
12. REPORT DATE: 20 April 1983
13. NUMBER OF PAGES: 137
14. MONITORING AGENCY NAME & ADDRESS (if different from Controlling Office):
15. SECURITY CLASS. (of this report): Unclassified
15a. DECLASSIFICATION/DOWNGRADING SCHEDULE:
16. DISTRIBUTION STATEMENT (of this Report): Approved for public release; distribution unlimited
17. DISTRIBUTION STATEMENT (of the abstract entered in Block 20, if different from Report):
18. SUPPLEMENTARY NOTES:
19. KEY WORDS (Continue on reverse side if necessary and identify by block number):
Lower thermosphere
atmospheric density
density models
20. ABSTRACT (Continue on reverse side if necessary and identify by block number):

The MSIS and Jacchia-70 (J70) models have been evaluated at each of the nearly 55,000 points for which we have measurements of the atmospheric density between 120 and 200 km. The density measurements were made by nine different instruments of five types (ion gauge, capacitance manometer, mass spectrometer, calorimeter, and accelerometer) flown on five satellites during the 1974-1977 solar minimum. Except for the solar flux, all the

19. KEY WORDS (Continued)

20. ABSTRACT (Continued)

parameters used in the models (geomagnetic activity, altitude, latitude, local time, season, etc.) were well represented.

The density measurements at any one altitude were found to be consistent with a lognormal distribution; that is, the fractional variations in the density were normally distributed, rather than the variations themselves. If a model correctly predicted the average variation in density, the log of the ratio of the measurements to the predictions should be normally distributed with skewness of 0.0 and kurtosis of 3.0. In fact, the skewness when the J70 model was used was -0.10 and the kurtosis was 3.51. For the MSIS model, the corresponding numbers were -0.06 and 4.42.

The J70 model has systematic errors in both the altitude and local time dependence; when these were corrected, the standard deviation of the log ratio dropped to about 14 percent from about 16 percent. When the MSIS model was used, without any corrections, the standard deviation was 13 percent.

The MSIS model is significantly more accurate than the J70 model, but because the log ratios are not normally distributed, the confidence interval about any one prediction must be estimated empirically rather than analytically. From our data, the probability that the magnitude of the log ratio is less than (0.075, 0.155, 0.205) is (0.5, 0.8, 0.9).

CONTENTS

FIGURES

FIGURES (Continued)

FIGURES (Continued)

FIGURES (Continued)

FIGURES (Continued)

FIGURES (Continued)

TABLES

1.0 SUMMARY AND CONCLUSIONS

1.1 INTRODUCTION

This report documents a comparison that has been made between the Aerospace low altitude atmospheric density data base and two widely-used models, MSIS (Hedin, et al., 1977), and J70 (Jacchia, 1970). By "low altitude" we mean the altitude range between 120 km (the lower limit of the measured densities) and 200 km.

There were five different types of measurements made with nine separate instruments on five satellites. The instruments were ion gauges, capacitance manometers, an accelerometer, a mass spectrometer, and calorimeters. Three of these instruments were flown on the same satellite, AE-E, and so a direct intercomparison allows us to estimate instrumental bias.

1.2 DATA ANALYSIS

The five satellites were all flown in the 1974-1977 period of low solar activity, which limits the generality of the results reported here. However many parameters other than solar flux are of interest, and the data base provides reasonable coverage for all of them. The coverage for latitude, longitude, altitude, geomagnetic index, local time, and month are shown for each instrument (except the capacitance manometers, which are included with the ionization gauges) in Section 2.

There are several possible ways of comparing the data to the models; we have chosen to use the logarithm of the ratio of the measurement to the model prediction as the objective function. Figure 1.1 is a histogram of the measured density from AE-C at 175 km, and is typical of all the measurements. It has a pronounced high- density tail, and the two "Pearson parameters" RB1 and B2 are not consistent with a normal distribution. (RB1, (Root Beta 1) is the third moment about the mean divided by the variance raised to the 1.5 power; it is a measure of skewness, and is zero for a normal distribution. B2 (Beta 2) is the fourth moment about the mean divided by the variance squared, and is called the kurtosis. For a normal distribution it has a value of 3.0. If the kurtosis is larger than this, it indicates that the distribution has an excess number of points near the mean and out in the tails.) The histograms of measured densities at fixed altitudes are consistent with a lognormal distribution, so that the log of the density is normally distributed. (That is, the fractional variations in the density are normally distributed, not the variations themselves.) If the models accurately represent the average variability of the density, we would expect our chosen objective function to be normally distributed, and the usual confidence limits would apply.

Section 3 presents histograms of the log ratio for each instrument for both models. The MSIS model was slightly modified from that which has been published. The original model used average solar flux parameters and geomagnetic indices which were centered at the time of interest; we felt that it was more realistic to use averages that ended at the time of the measurement. Tables 1 and 2 summarize the statistical data. In these tables, AE-C, AE-D, etc. are the satellites, "Density" is the combination of the ion gauges and capacitance manometers, "OSS" is the open-source mass spectrometer, "MESA" is the miniature electrostatic accelerometer, and "Cal" is a calorimeter. The square root of the variances of the standard deviation, RB1, and B2 have been calculated assuming that the underlying distribution is a normal one; in only one case, the AE-E density measurements compared with the J70 model, is RB1 and B2 consistent with a normal distribution.

Figures 1.2 to 1.9 show the mean, standard deviation, skewness and kurtosis for the AE-C density gauges and the AE-E MESA (accelerometer) residuals as a function of altitude. The MSIS model yields a uniformly smaller standard deviation than does J70, but its kurtosis, in particular, is much larger, so that an estimate of the confidence interval about any prediction cannot be made other than empirically.

Because the J70 model residuals were more normally distributed, we examined those residuals in more detail, hoping to be able to improve the standard deviation while maintaining the favorable skewness and kurtosis. Section 4 presents plots of the average log ratio versus local solar time for two altitudes, and for both the J70 and the MSIS model. In these figures, the diamonds represent the mean and the error bars through the diamonds are the standard deviation of the mean (not of the individual data points). There are strong, systematic, trends in the J70 residuals, and no obvious trends in the MSIS residuals. Accordingly, we fit the J70 residuals at each altitude with a low-order Fourier time series: a constant term and a diurnal, semi-diurnal, and ter-diurnal cosine. The coefficients were always significant in some altitude range, although no term was significant at all altitudes. The amplitudes and phases so derived are also shown in Section 4, where it can be seen that the semi-diurnal and ter-diurnal terms become increasingly important at lower altitudes and the diurnal term has the opposite behavior. The phase of each of the terms also shows an altitude dependence; perhaps the most surprising is the shift of the diurnal bulge to early morning at the lower altitudes.

If these empirical corrections to the model are applied to the very same data that were used to derive them, we would expect to see a significant change in the standard deviation of the corrected residuals. Histograms of the "before" and "after" distributions are shown in the final part of Section 4. While there is a (statistically) significant reduction in the standard deviation, it is still larger than that obtained using the MSIS model with no corrections at all.

1.3 CONCLUSIONS

We have compared over 50,000 separate measurements of atmospheric density between 120 km and 200 km with the predictions of two models, the MSIS and the J70. The MSIS model produces a considerably smaller standard deviation of the residuals than does the J70, even after the observed systematic errors in local time and altitude have been removed. The kurtosis of the MSIS residuals is large: this may indicate that there are still nonrandom effects that this model has failed to capture, so there is still hope that it may be significantly improved in the future. Until that time, however, we have no choice but to use empirical cumulative probability functions to estimate confidence limits of the accuracy of its predictions. These are shown in Figures 1.10 to 1.17.

The average bias of the log ratio is near zero for both models (cf. Tables 1 and 2), and, in particular, is near zero for the three instruments on AE-E concidered separately. This indicates that a major portion of the average error is due to instrumental bias rather than model bias, so there is justification in subtracting the individual biases and amalgamating the data. The cumulative empirical probability function for all the data using the MSIS model is shown in Figure 1.18, and represents our best estimate of the true distribution function for times near solar minimum.

1.4 REFERENCES

Hedin, A. E., et al., "A Global Thermospheric Model Based on Mass Spectrometer and Incoherent Scatter Data, 1, N2 Density and Temperature", J. Geophys. Res. 82, 2139-2147, 1977.

Hedin, A. E., et al., "A Global Thermospheric Model Based on Mass spectrometer and Incoherent Scatter Data MSIS, 2, Composition", J. Geophys. Res. 82, 2148-2156, 1977.

Jacchia, L. G., "New Static Models of the Thermosphere and Exosphere with Empirical Temperature Profiles", Smithsonian Astrophys. Obs. Special Report No. 313, 87 pp., 1970.

2.0 GEOPHYSICAL PARAMETER COVERAGE

2.1 ALTITUDE DISTRIBUTION

Figures 2.1 through 2.8 show the altitude coverage of the eight instruments (the ion gauges and the capacitance manometers are considered as one instrument). Only the AE-C density gauges and the calorimeters have a significant number of points below 135 km, and only Calorimeter-3 measured data below 125 km. The combined altitude distribution is given in Fig. 2.9. The total number of points, 54,606, is different from the numbers given in Tables One and Two of Section 1 because these data were not editted; measurements were retained in Section One only if the log of the ratio (measurement/model) were between plus and minus one.

2.2 LATITUDE DISTRIBUTION

Figures 2.10 through 2.17 show the latitude distribution of the measurements. The northern hemisphere is well covered, as is the equatorial region (AE-E had an inclination of 19.6 degrees), but only AE-C and AE-D collected a significant amount of data below 20 S.

2.3 LONGITUDE DISTRIBUTION

Figures 2.18 through 2.25 show the longitude distribution of the measurements. Overall, there is excellent longitude coverage.

2.4 LOCAL TIME DISTRIBUTION

Figures 2.26 through 2.33 show the local time distribution of the measurements. AE-C and AE-E have nearly uniform coverage; the measurements on AE-D are concentrated in the morning and evening sectors. S3-1 and Calorimeter-3 made measurements primarily in the late morning and afternoon, while the data from Calorimeter-4 is almost exclusively between 1100 and 1300.

2.5 MONTHLY DISTRIBUTION

Figures 2.34 through 2.41 show the monthly distribution of the measurements. AE-C and AE-E cover all four seasons, AE-D took data between September and January, S3-1 was useful primarily in October, Calorimeter-3 in March and April, and Calorimeter-4 in September and October.

2.6 24-HOUR AP DISTRIBUTION

Figures 2.42 through 2.49 show the distribution of the 24-hour average Ap index. These averages ended at the time of each measurement, and are used in the MSIS model only. This index has a maximum possible value of 400; the Figures show that its values in this data base are stongly concentrated in the lower twenty percent of its range. This is consistent with the fact that this is a sunspot-minimum data base. (Even during sunspot-maximum periods, geomagnetic indices are more frequently in the lower portion of their range. See the discussion in the following sub-section.)

2.7 KP DISTRIBUTION

Figures 2.50 through 2.57 show the distribution of the three-hour geomagnetic index Kp. This index was evaluated six hours prior to each density measurement, and is used only in the J70 model. As with the 24-hour average Ap, most of the data were taken when Kp(6) was in the lower portion of its 0-9 range. The effect is not as dramatic here, however, because Ap and Kp are logarithmically related. Figure 2.58 shows the Kp distribution from 1 January 1932 to 30 June 1981, and so includes periods of both high and low solar activity. Its distribution is not unlike the Kp distribution when the density measurements were made. The average value over this 50 year period was 2.12, with a standard deviation of 1.46. This corresponds to an average Ap of 7.7 (plus 13.3, minus 4.7). Although there were no great geomagnetic storms during the time for which we have data, this is not considered to be operationally significant. (Kp reached its maximum value of 9 only 20 times in 50 years, and exceeded 6+ (Ap equals 94) only one percent of the time.)

3.0 MEASUREMENT/MODEL DISTRIBUTIONS

3.1 THE MSIS MODEL

Figures 3.1 through 3.8 are histograms of the natural log of the ratio of the individual measurements to the predictions of the MSIS model. The data were editted so that the magnitude of this ratio was always between zero and one; this eliminated 28 points (out of 54,606). Most of the editted points were obviously in error: a reported measurement of 1E-3 grams/centimeter-cubed, for instance, instead of 1E-13.

The MSIS model was evaluated using 24-hour average values of Ap and 81-day average values of the solar flux parameter F10.7 ending at the time of the measurement. The original model specified that these averages were to be centered at the time of interest, but it was difficult for us to see the physical justification for that procedure. In fact, histograms comparable to the ones presented in this subsection were generated using the original model; in every case, the standard deviations were slightly larger.

3.2 THE J70 MODEL

Figures 3.9 through 3.16 are histograms of the natural log of the individual density measurements divided by the predictions of the J70 model. As in the previous subsection, these data were editted to exclude points with magnitude greater than one. A single additional measurement was eliminated when the J70 model was used.

4.0 CORRECTIONS TO THE J70 MODEL

4.1 LOCAL TIME DEPENDENCE

Figures 4.1 and 4.2 show the local time dependence of the natural log of the AE-C density gauge measurements between 195 and 200 km divided by the predictions of the J70 and the MSIS models, respectively. Figures 4.3 and 4.4 show the same thing for the AE-E MESA measurements. Figures 4.5 to 4.8 are comparable to the first four, but for the altitude range 150-155 km. It can be seen that the J70 plots exhibit a persistent, reasonably strong, local time dependence for both instruments in both altitude ranges. The MSIS plot at the higher altitude for AE-C also seems to show a local time dependence, but it does not persist across instruments nor at the lower altitude.

We made an empirical model of the error in the time dependence of the J70 model using the AE-C density gauge data. In each five kilometer interval, the log ratio was fit to a third-order Fourier expansion, using a constant term and diurnal, semi-diurnal, and ter-diurnal terms. The coefficients were determined using a weighted least- squares technique, the weights being the reciprocal of the variances of the means at each local time. The altitude dependence of the coefficients is shown in Figures 4.9 through 4.15. The phases are determined such that a negative phase indicates that the model's prediction should be increased at later times. For instance, the -44 degree phase angle for the diurnal term at 165 km, coupled with the 0.092 value for the amplitude, indicates that the model's prediction should be increased by nine percent at about 0300 and decreased by the same amount at 1500.

These corrections were applied to the J70 model, and the histogram of the log ratios was recalculated. The original histogram is shown in Figure 4.16 and the "corrected" one in Figure 4.17. The standard deviation has been reduced from 0.156 to 0.142, a statistically significant amount. It is not operationally significant, however, since the standard deviation using the uncorrected MSIS model is substantially smaller, 0.126, as is shown in Figure 4.18.

Since the correction procedure did not produce very dramatic improvements for the AE-C data, we did not feel it to be worthwhile to pursue the matter with the other data sets.

TABLE 1
MSIS STATISTICS

	N	Mu	Sigma	$\sqrt{var(sig)}$	RB1	$\sqrt{var(RB1)}$	B2	$\sqrt{var(B2)}$
AE-C Density	17415	0.055	0.126	0.001	-0.304	0.030	5.246	0.135
AE-D Density	10935	-0.090	0.132	0.001	0.120	0.037	3.243	0.128
AE-E Density	4977	0.089	0.130	0.001	-0.098	0.055	3.123	0.187
AE-E OSS	7574	-0.058	0.132	0.001	-0.054	0.045	4.589	0.187
AE-E MESA	8280	-0.006	0.127	0.001	0.035	0.043	5.140	0.193
S3-1 Density	1454	0.100	0.144	0.003	0.289	0.103	3.088	0.344
Cal-3	1492	-0.018	0.174	0.003	0.256	0.101	4.849	0.436
Cal-4	2451	0.145	0.136	0.002	0.201	0.079	3.919	0.299
All Data	54578	0.008	0.130	0.007	-0.058	0.189	4.180	0.920

TABLE 2
J70 STATISTICS

	N	Mu	Sigma	$\sqrt{var(sig)}$	RB1	$\sqrt{var(RB1)}$	B2	$\sqrt{var(B2)}$
AE-C Density	17415	0.050	0.156	0.001	-0.298	0.030	3.935	0.112
AE-D Density	10935	-0.113	0.147	0.001	-0.064	0.037	3.006	0.124
AE-E density	4977	0.084	0.160	0.002	-0.008	0.055	2.924	0.182
AE-E OSS	7573	-0.063	0.170	0.001	-0.128	0.045	3.253	0.154
AE-E MESA	8280	-0.017	0.156	0.001	-0.011	0.043	3.763	0.159
S3-1 Density	1454	0.012	0.138	0.003	0.412	0.104	3.528	0.367
Cal-3	1492	-0.004	0.192	0.004	0.324	0.102	4.171	0.397
Cal-4	2451	0.010	0.129	0.002	0.212	0.079	3.545	0.283
All Data	54577	-0.011	0.156	0.011	-0.097	0.175	3.462	0.415

Tables 1 and 2

SECTION 1

PRECEDING PAGE BLANK-NOT FILMED

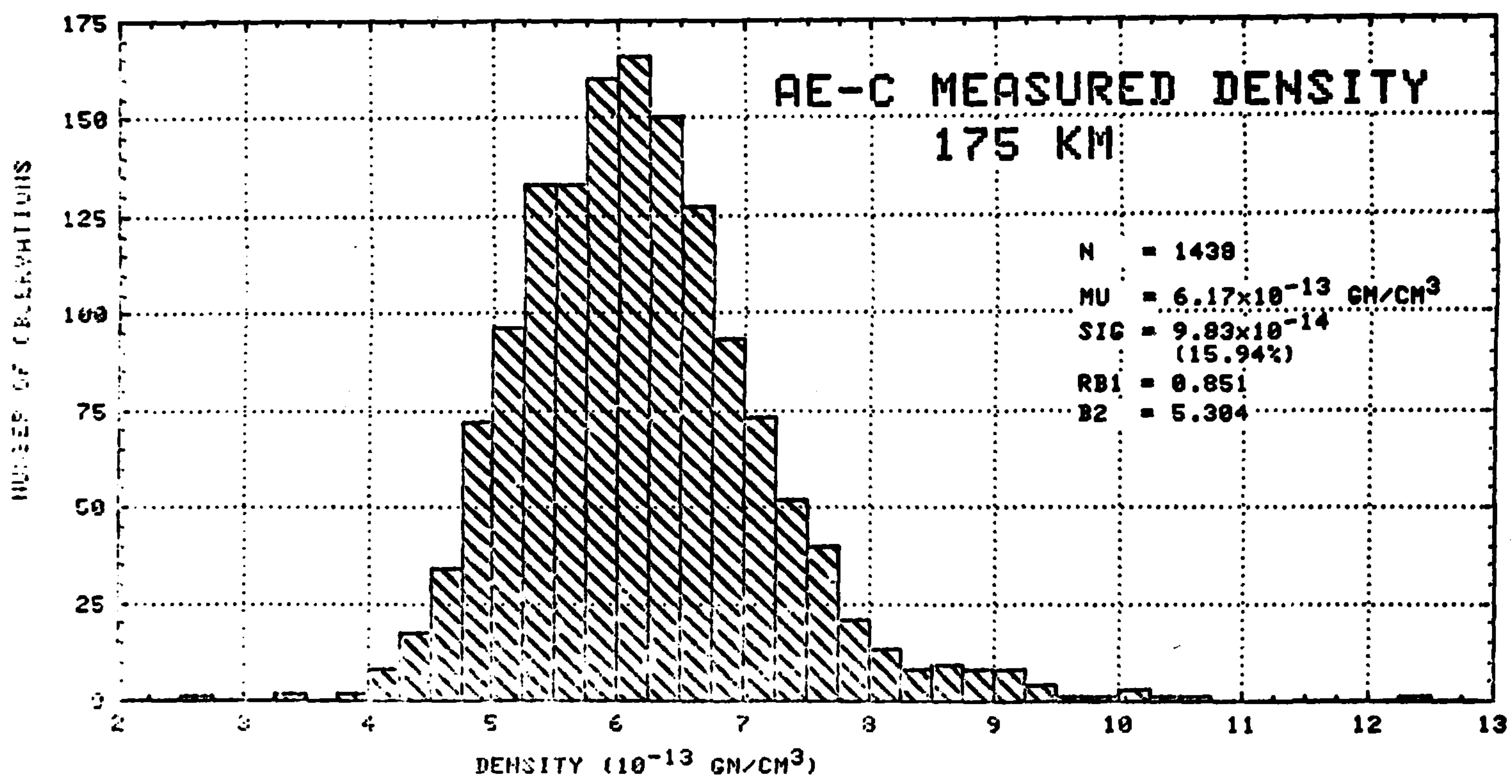
AE-C MEASURED DENSITY
175 KM
N = 1430
MU = 6.17x10^-13 GM/CM^3
SIG = 9.83x10^-14
(15.94%)
RB1 = 0.851
B2 = 5.304
175
150
125
100
75
50
25
0
2
3
4
5
6
7
8
9
10
11
12
13
DENSITY (10^-13 GM/CM^3)
NUMBER OF OBSERVATIONS

Figure 1-1.

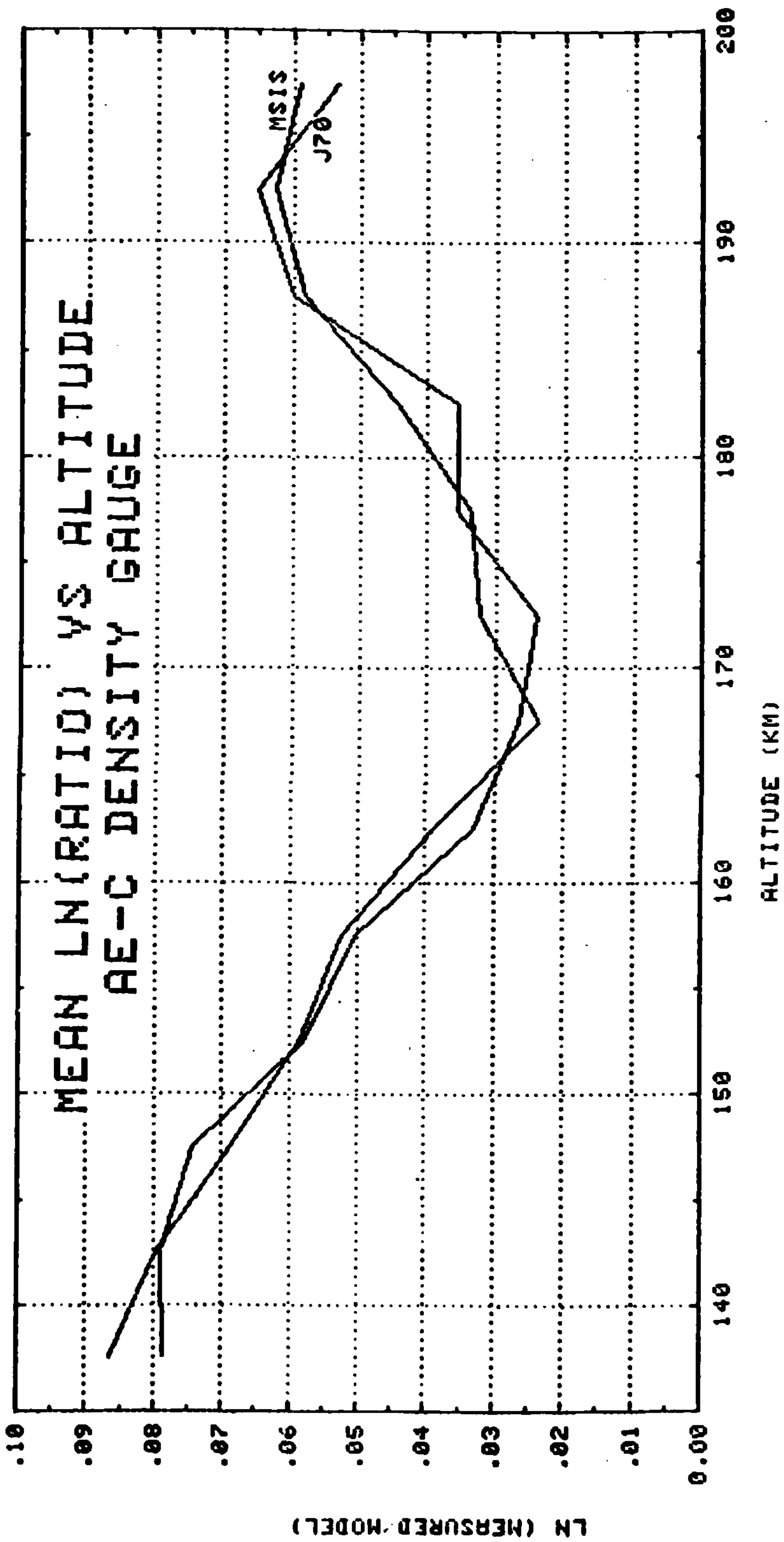

MEAN LN(RATIO) VS ALTITUDE
AE-C DENSITY GAUGE
MSIS
J70
.10
.09
.08
.07
.06
.05
.04
.03
.02
.01
0.00
LN (MEASURED-MODEL)
140
150
160
170
180
190
200
ALTITUDE (KM)

Figure 1-2.

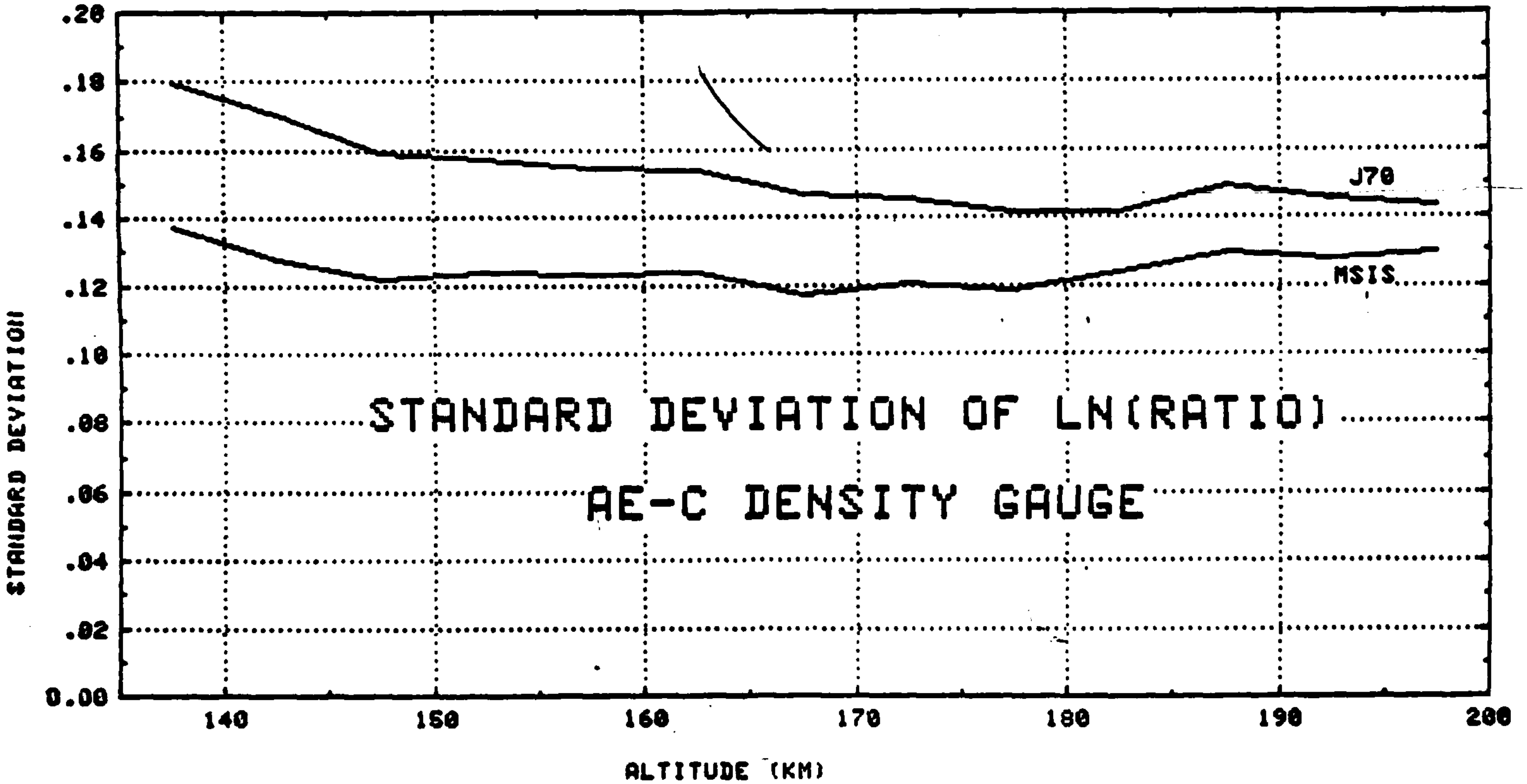
STANDARD DEVIATION OF LN(RATIO)
AE-C DENSITY GAUGE
J70
MSIS
STANDARD DEVIATION
.20
.18
.16
.14
.12
.10
.08
.06
.04
.02
0.00
ALTITUDE (KM)
140
150
160
170
180
190
200

Figure 1-3.

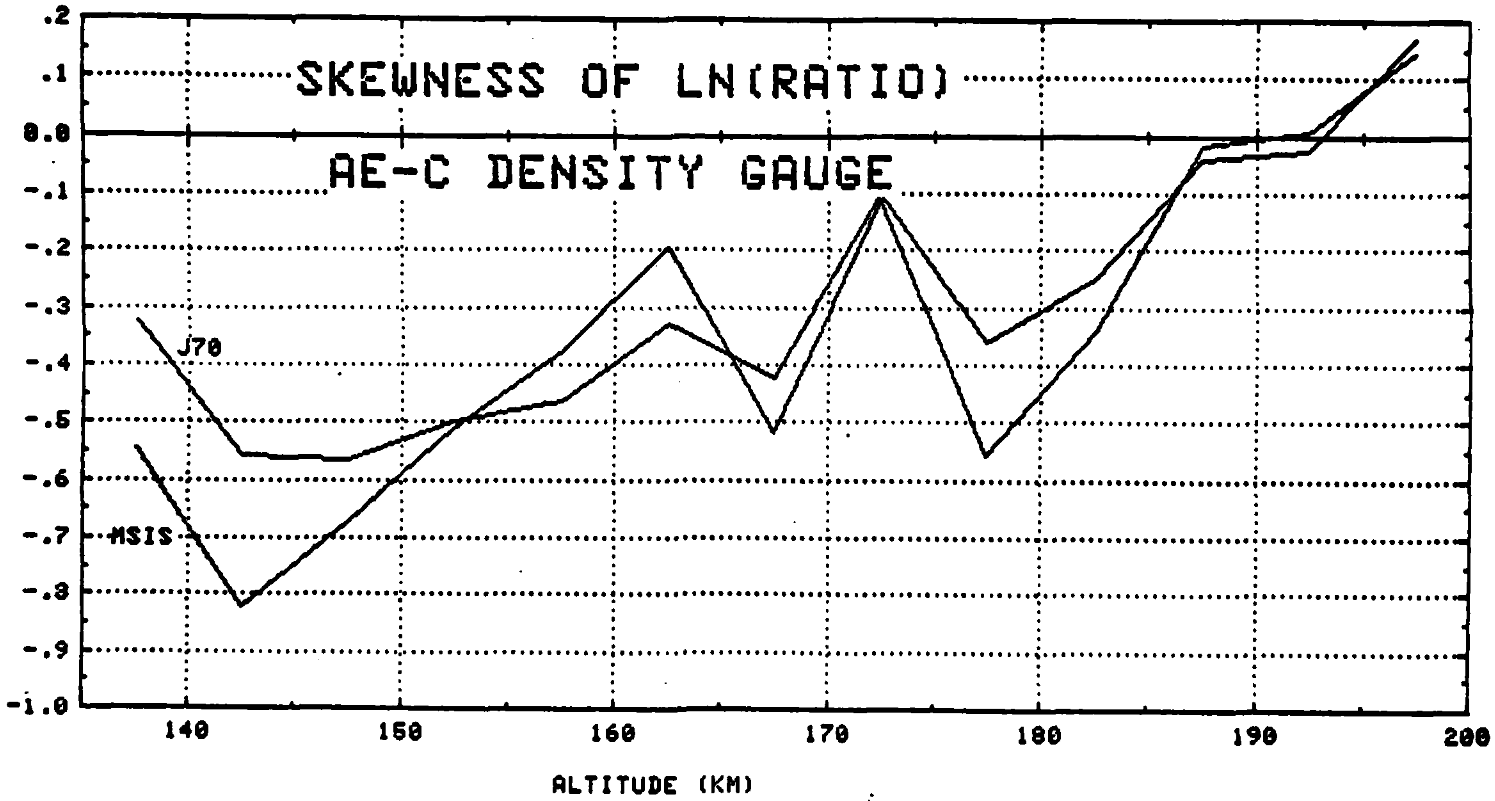
SKEWNESS OF LN(RATIO)
AE-C DENSITY GAUGE
J70
MSIS
.2
.1
0.0
-.1
-.2
-.3
-.4
-.5
-.6
-.7
-.8
-.9
-1.0
140
150
160
170
180
190
200
ALTITUDE (KM)

Figure 1-4.

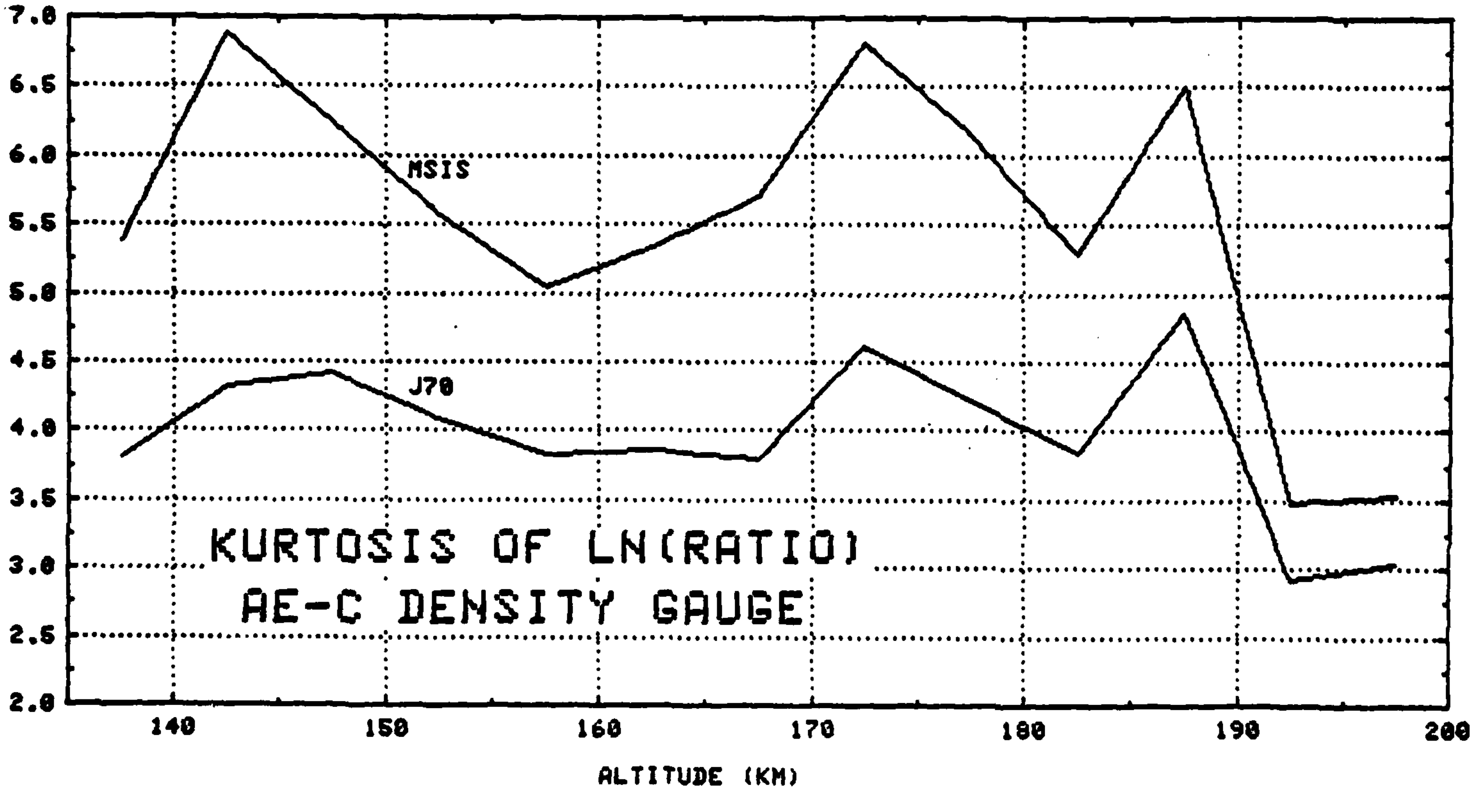
KURTOSIS OF LN(RATIO)
AE-C DENSITY GAUGE
MSIS
J70
7.0
6.5
6.0
5.5
5.0
4.5
4.0
3.5
3.0
2.5
2.0
140
150
160
170
180
190
200
ALTITUDE (KM)

Figure 1-5.

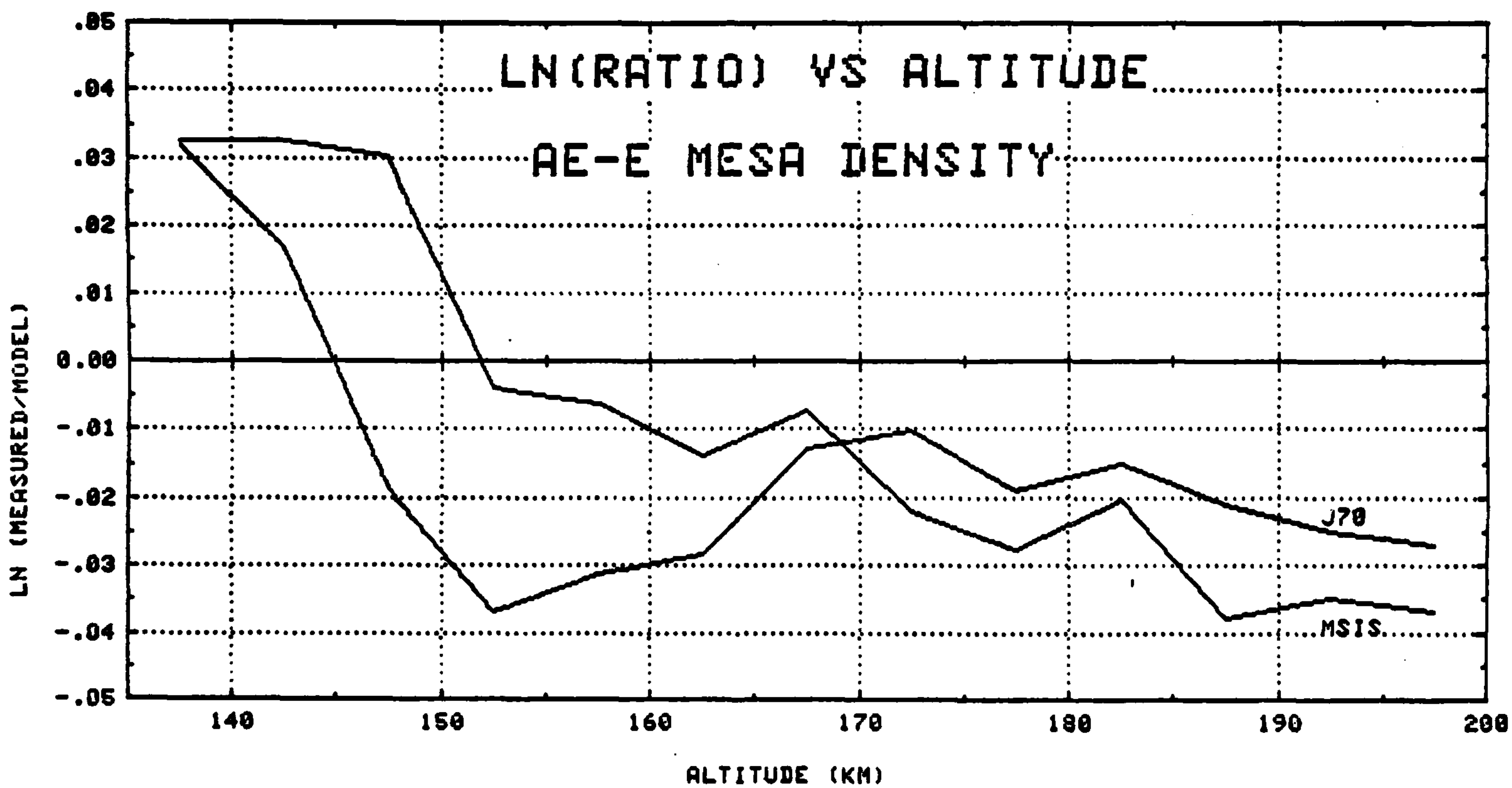

LN(RATIO) VS ALTITUDE
AE-E MESA DENSITY
.05
.04
.03
.02
.01
0.00
-.01
-.02
-.03
-.04
-.05
LN (MEASURED/MODEL)
140
150
160
170
180
190
200
ALTITUDE (KM)
J70
MSIS

Figure 1-6.

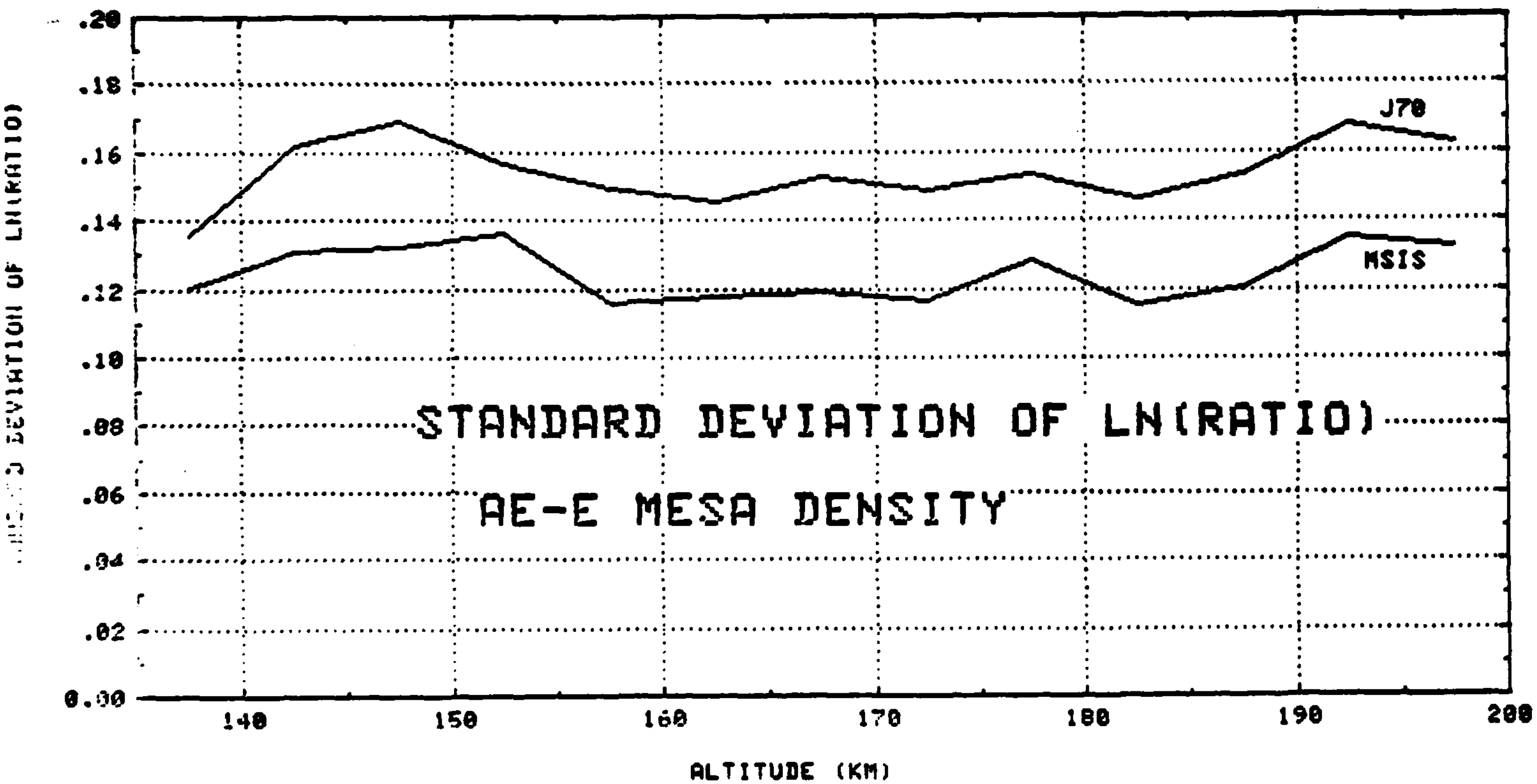
STANDARD DEVIATION OF LN(RATIO)
AE-E MESA DENSITY
J70
MSIS
.20
.18
.16
.14
.12
.10
.08
.06
.04
.02
0.00
140
150
160
170
180
190
200
ALTITUDE (KM)
DEVIATION OF LN(RATIO)

Figure 1-7.

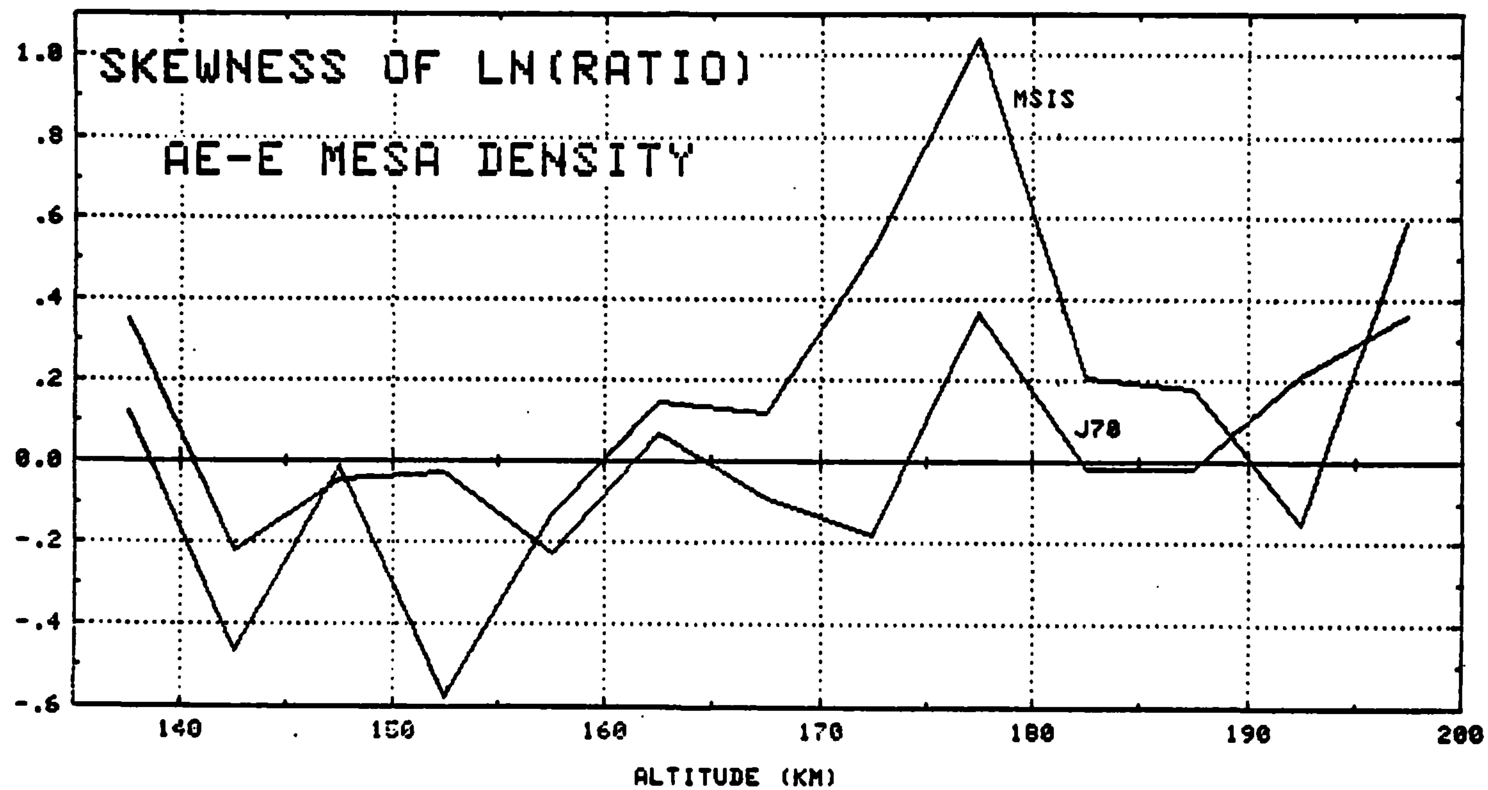

SKEWNESS OF LN(RATIO)
AE-E MESA DENSITY
MSIS
J70
1.0
.8
.6
.4
.2
0.0
-.2
-.4
-.6
140
150
160
170
180
190
200
ALTITUDE (KM)

Figure 1-8.

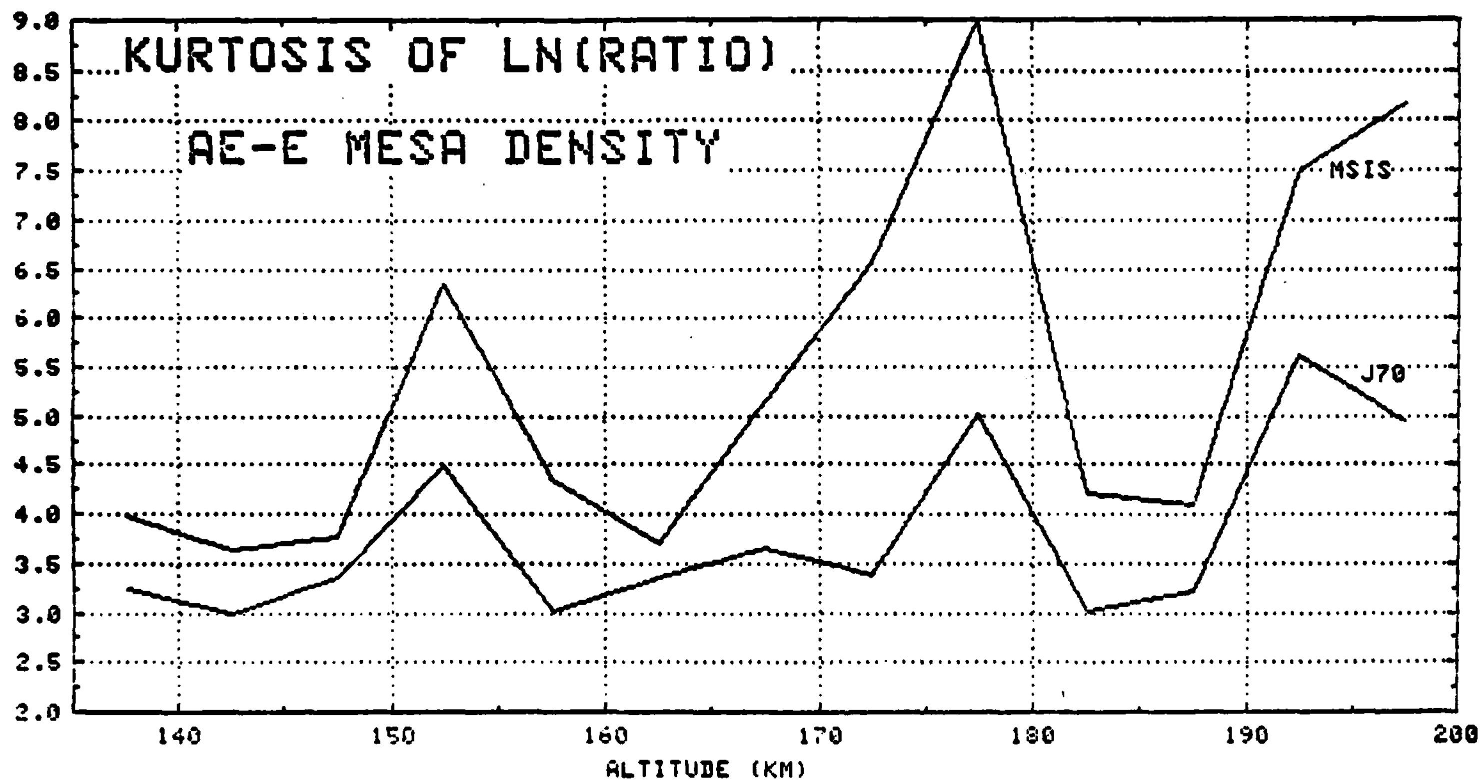
KURTOSIS OF LN(RATIO)
AE-E MESA DENSITY
9.0
8.5
8.0
7.5
7.0
6.5
6.0
5.5
5.0
4.5
4.0
3.5
3.0
2.5
2.0
140
150
160
170
180
190
200
ALTITUDE (KM)
MSIS
J70

Figure 1-9.

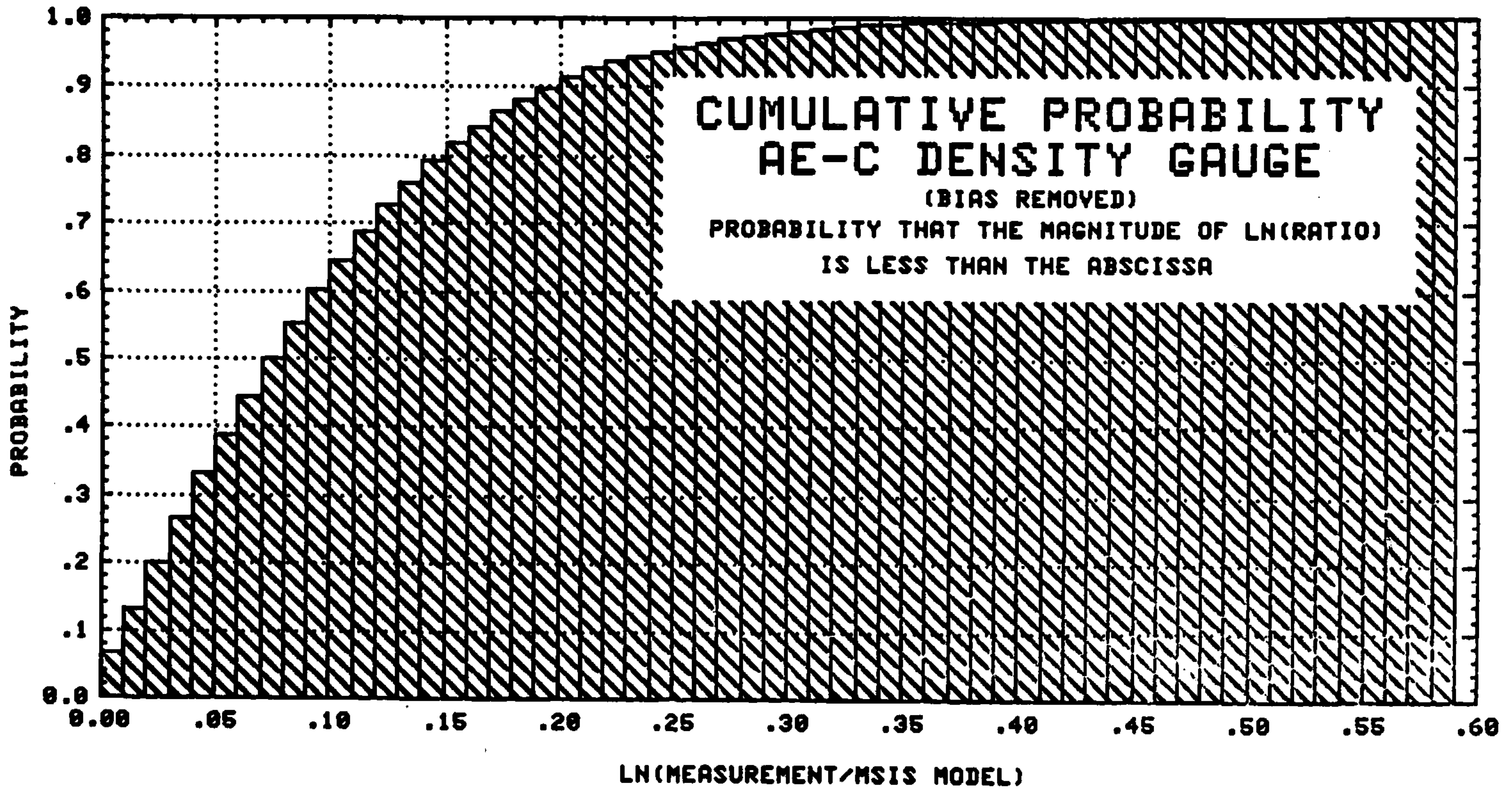
CUMULATIVE PROBABILITY
AE-C DENSITY GAUGE
(BIAS REMOVED)
PROBABILITY THAT THE MAGNITUDE OF LN(RATIO)
IS LESS THAN THE ABSCISSA
PROBABILITY
1.0
.9
.8
.7
.6
.5
.4
.3
.2
.1
0.0
0.00
.05
.10
.15
.20
.25
.30
.35
.40
.45
.50
.55
.60
LN(MEASUREMENT/MSIS MODEL)

Figure 1-10.

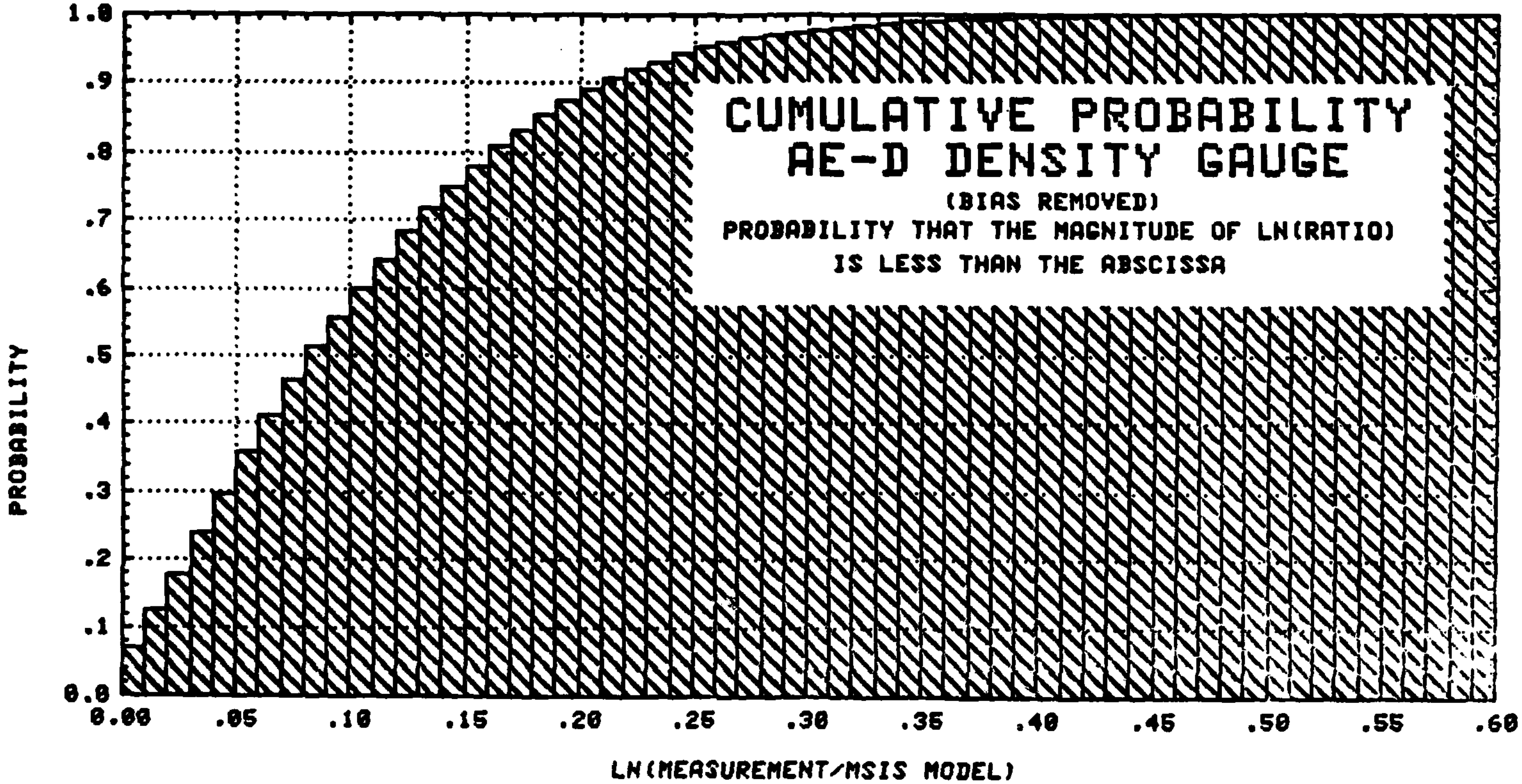
CUMULATIVE PROBABILITY
AE-D DENSITY GAUGE
(BIAS REMOVED)
PROBABILITY THAT THE MAGNITUDE OF LN(RATIO)
IS LESS THAN THE ABSCISSA
PROBABILITY
1.0
.9
.8
.7
.6
.5
.4
.3
.2
.1
0.0
0.00
.05
.10
.15
.20
.25
.30
.35
.40
.45
.50
.55
.60
LN(MEASUREMENT/MSIS MODEL)

Figure 1-11.

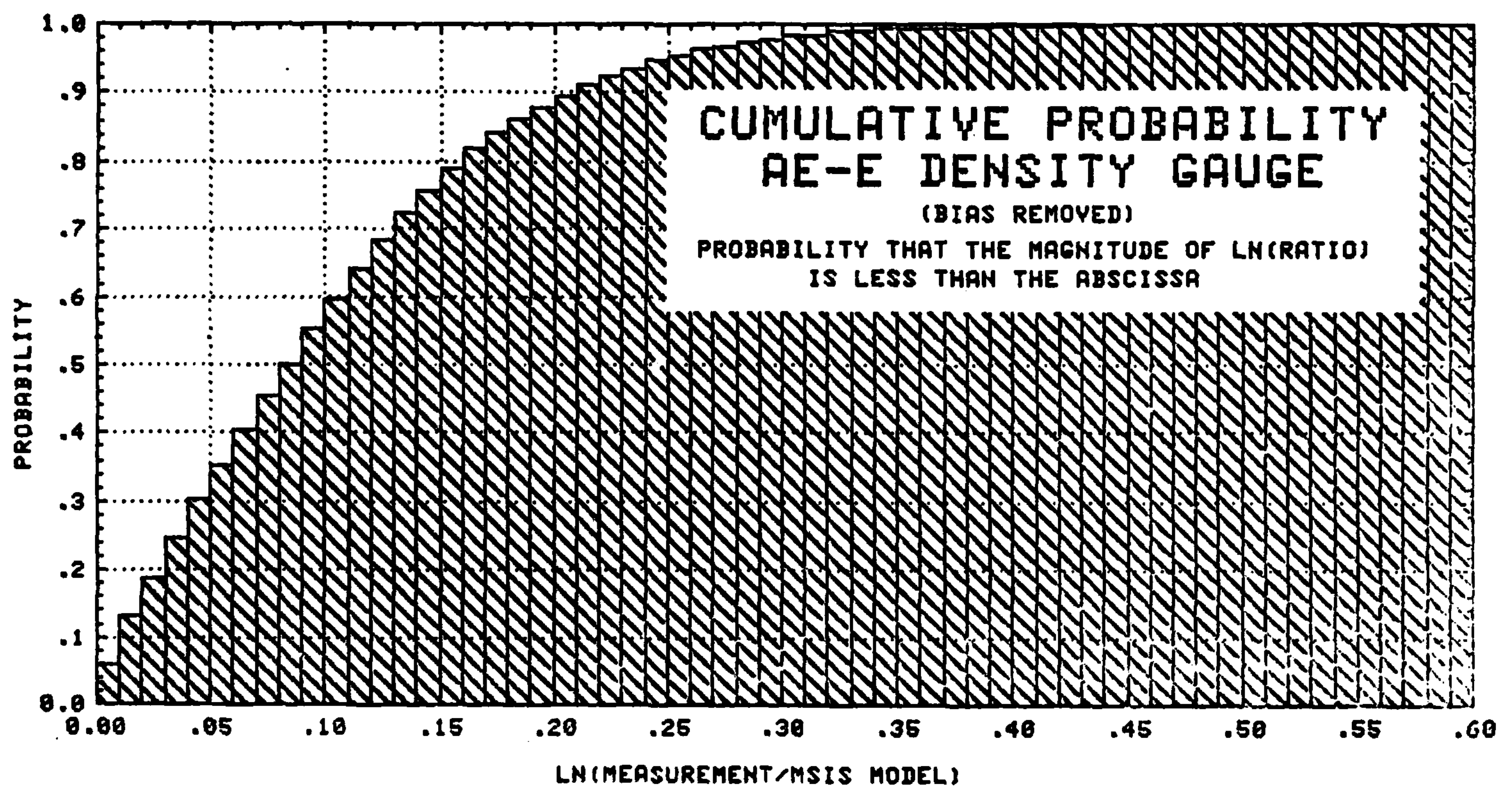
CUMULATIVE PROBABILITY
AE-E DENSITY GAUGE
(BIAS REMOVED)
PROBABILITY THAT THE MAGNITUDE OF LN(RATIO)
IS LESS THAN THE ABSCISSA
PROBABILITY
1.0
.9
.8
.7
.6
.5
.4
.3
.2
.1
0.0
0.00
.05
.10
.15
.20
.25
.30
.35
.40
.45
.50
.55
.60
LN(MEASUREMENT/MSIS MODEL)

Figure 1-12.

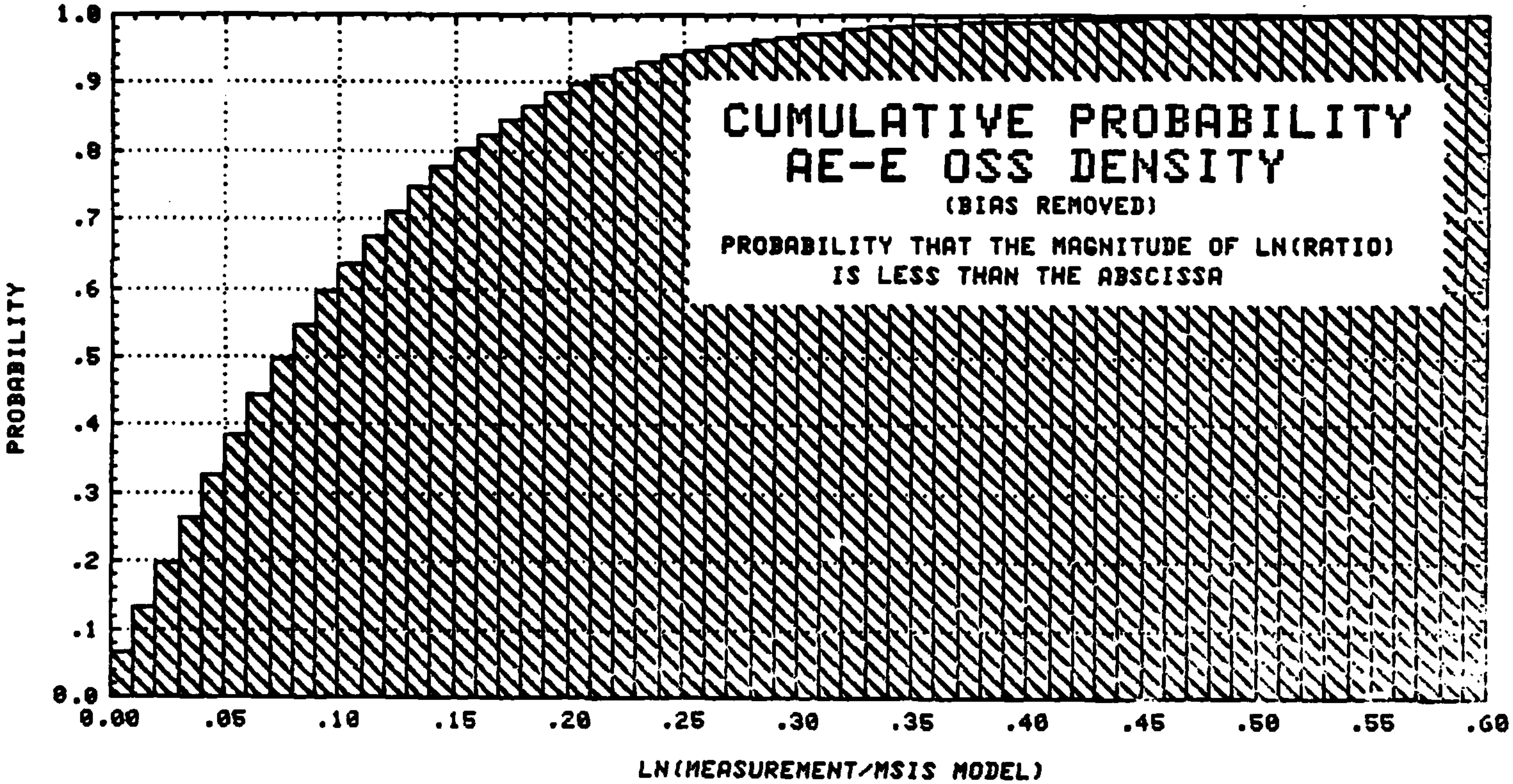
CUMULATIVE PROBABILITY
AE-E OSS DENSITY
(BIAS REMOVED)
PROBABILITY THAT THE MAGNITUDE OF LN(RATIO)
IS LESS THAN THE ABSCISSA
PROBABILITY
1.0
.9
.8
.7
.6
.5
.4
.3
.2
.1
0.0
0.00
.05
.10
.15
.20
.25
.30
.35
.40
.45
.50
.55
.60
LN(MEASUREMENT/MSIS MODEL)

Figure 1-13.

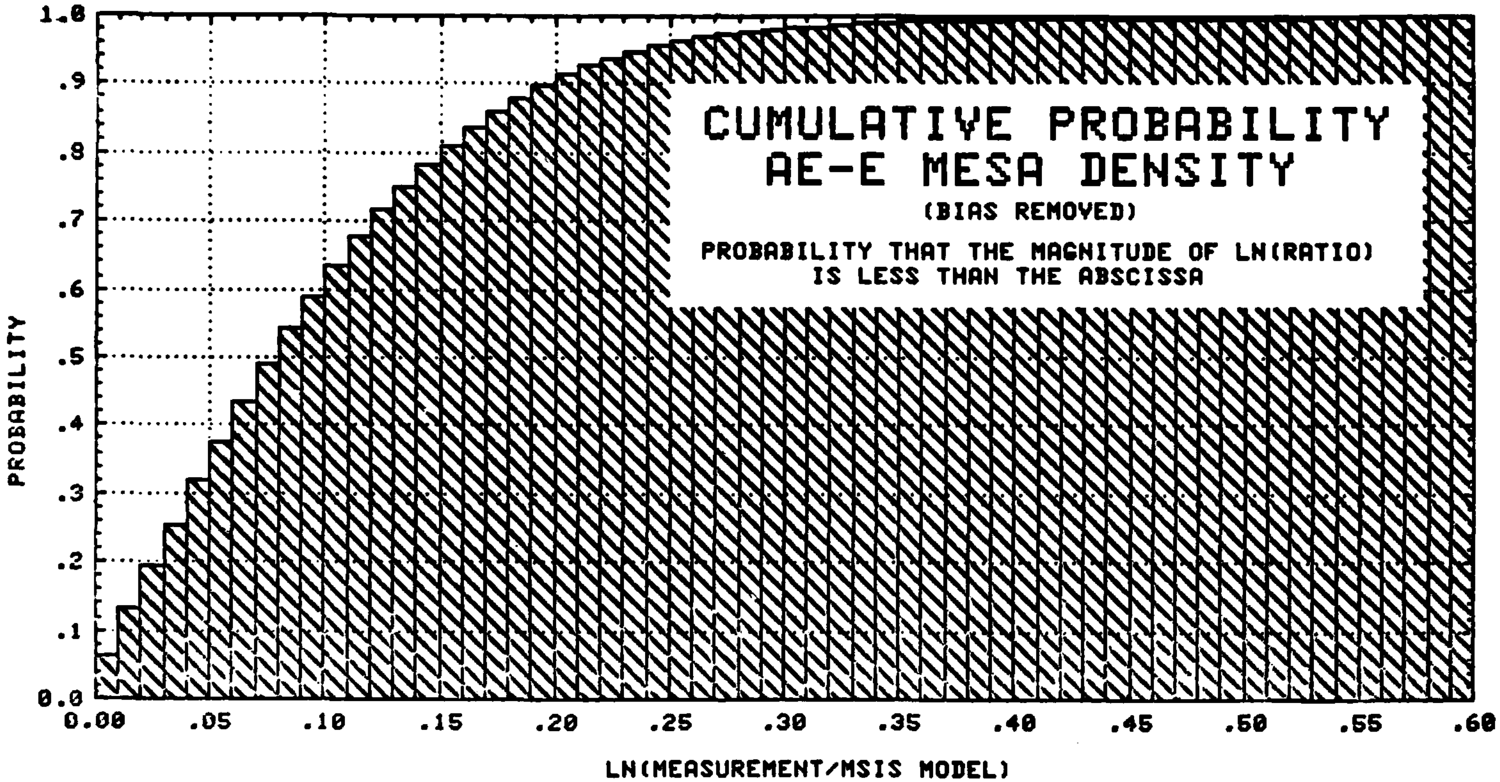
CUMULATIVE PROBABILITY
AE-E MESA DENSITY
(BIAS REMOVED)
PROBABILITY THAT THE MAGNITUDE OF LN(RATIO)
IS LESS THAN THE ABSCISSA
PROBABILITY
1.0
.9
.8
.7
.6
.5
.4
.3
.2
.1
0.0
0.00
.05
.10
.15
.20
.25
.30
.35
.40
.45
.50
.55
.60
LN(MEASUREMENT/MSIS MODEL)

Figure 1-14.

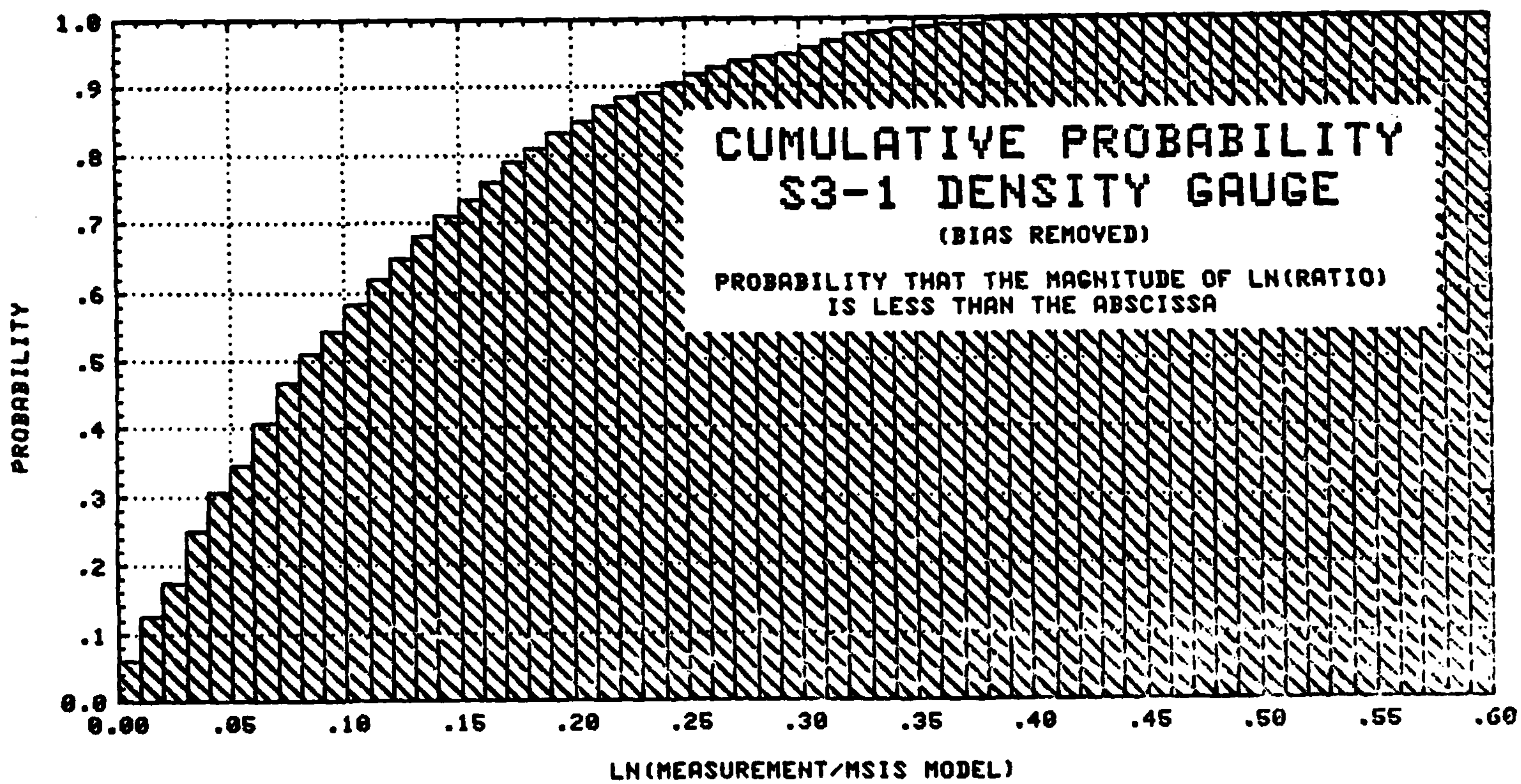
CUMULATIVE PROBABILITY
S3-1 DENSITY GAUGE
(BIAS REMOVED)
PROBABILITY THAT THE MAGNITUDE OF LN(RATIO)
IS LESS THAN THE ABSCISSA
PROBABILITY
1.0
.9
.8
.7
.6
.5
.4
.3
.2
.1
0.0
0.00
.05
.10
.15
.20
.25
.30
.35
.40
.45
.50
.55
.60
LN(MEASUREMENT/MSIS MODEL)

Figure 1-15.

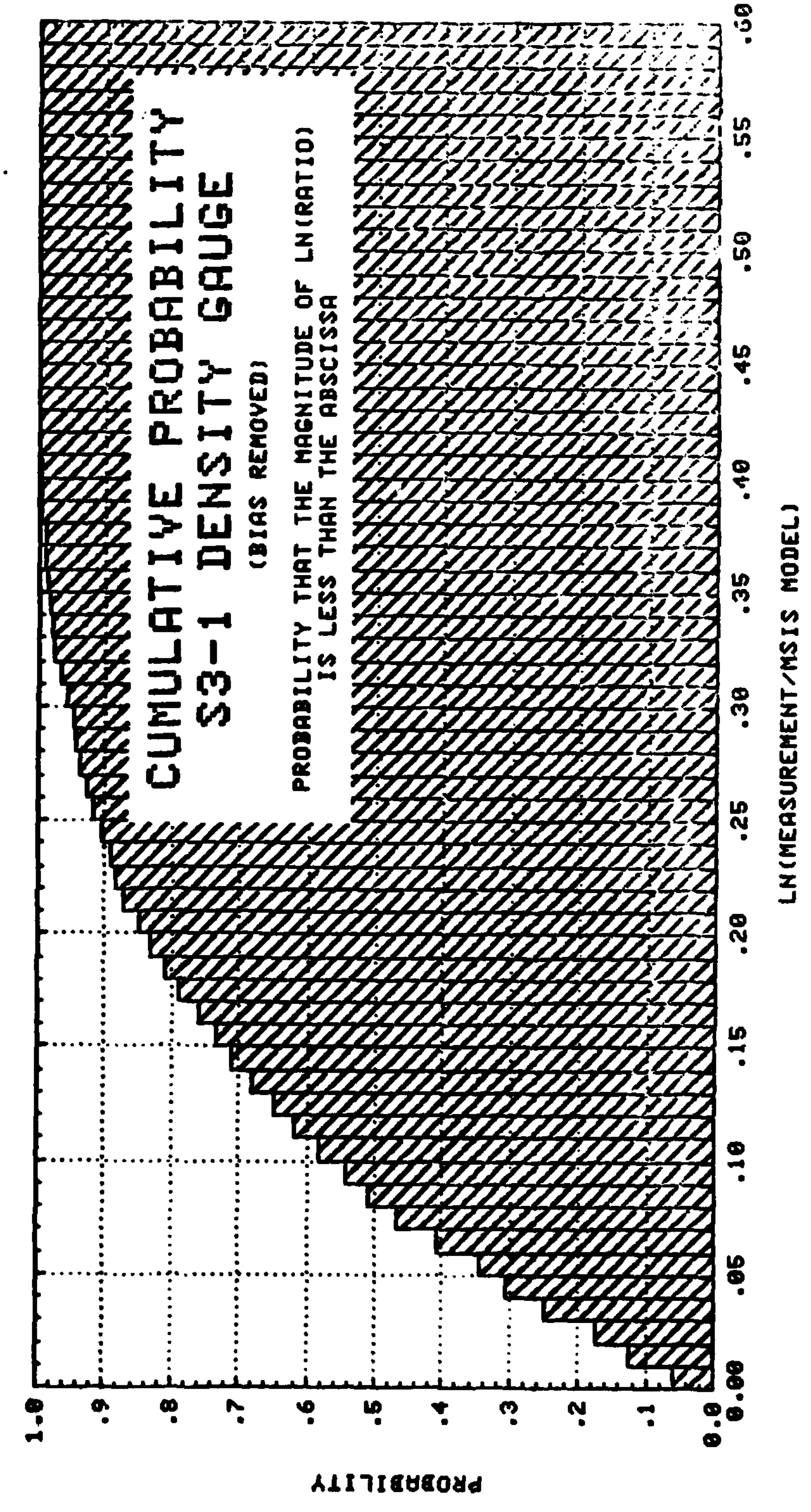

CUMULATIVE PROBABILITY
S3-1 DENSITY GAUGE
(BIAS REMOVED)
PROBABILITY THAT THE MAGNITUDE OF LN(RATIO)
IS LESS THAN THE ABSCISSA
PROBABILITY
1.0
.9
.8
.7
.6
.5
.4
.3
.2
.1
0.0
0.00
.05
.10
.15
.20
.25
.30
.35
.40
.45
.50
.55
.60
LN(MEASUREMENT/MSIS MODEL)

Figure 1-15.

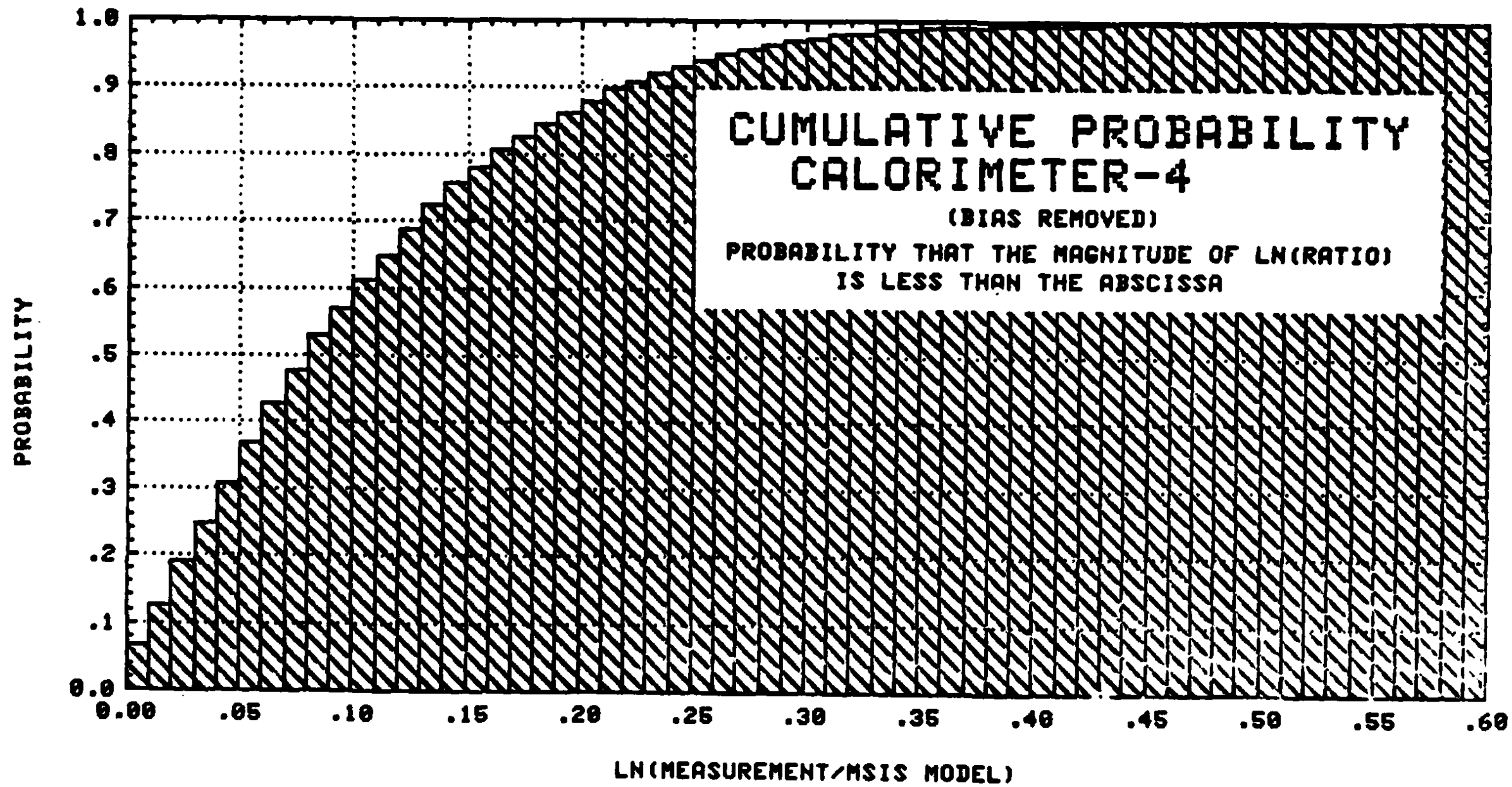
CUMULATIVE PROBABILITY
CALORIMETER-4
(BIAS REMOVED)
PROBABILITY THAT THE MAGNITUDE OF LN(RATIO)
IS LESS THAN THE ABSCISSA
PROBABILITY
1.0
.9
.8
.7
.6
.5
.4
.3
.2
.1
0.0
0.00
.05
.10
.15
.20
.25
.30
.35
.40
.45
.50
.55
.60
LN(MEASUREMENT/MSIS MODEL)

Figure 1-17.

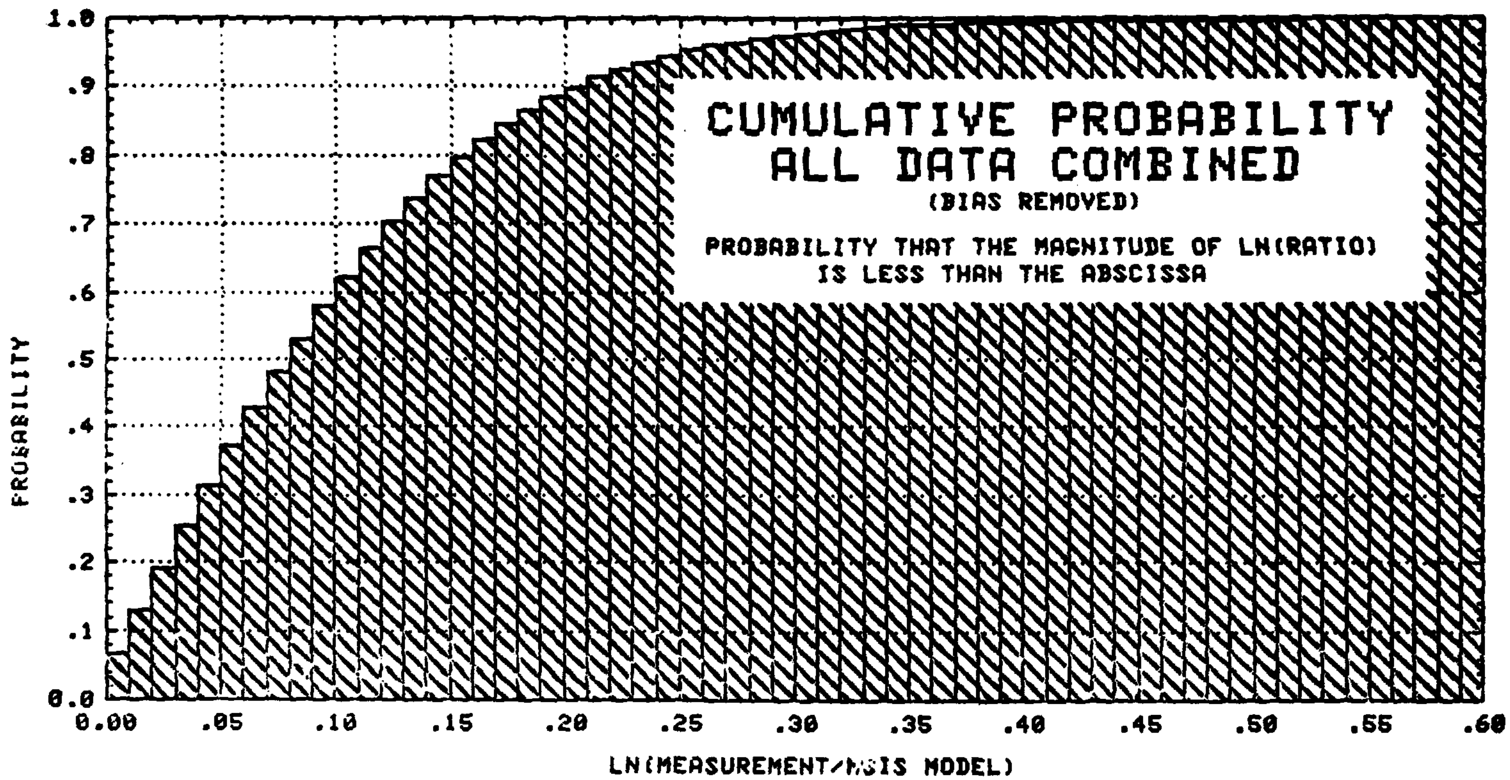
CUMULATIVE PROBABILITY
ALL DATA COMBINED
(BIAS REMOVED)
PROBABILITY THAT THE MAGNITUDE OF LN(RATIO)
IS LESS THAN THE ABSCISSA
PROBABILITY
1.0
.9
.8
.7
.6
.5
.4
.3
.2
.1
0.0
0.00
.05
.10
.15
.20
.25
.30
.35
.40
.45
.50
.55
.60
LN(MEASUREMENT/MSIS MODEL)

Figure 1-18.

SECTION 2

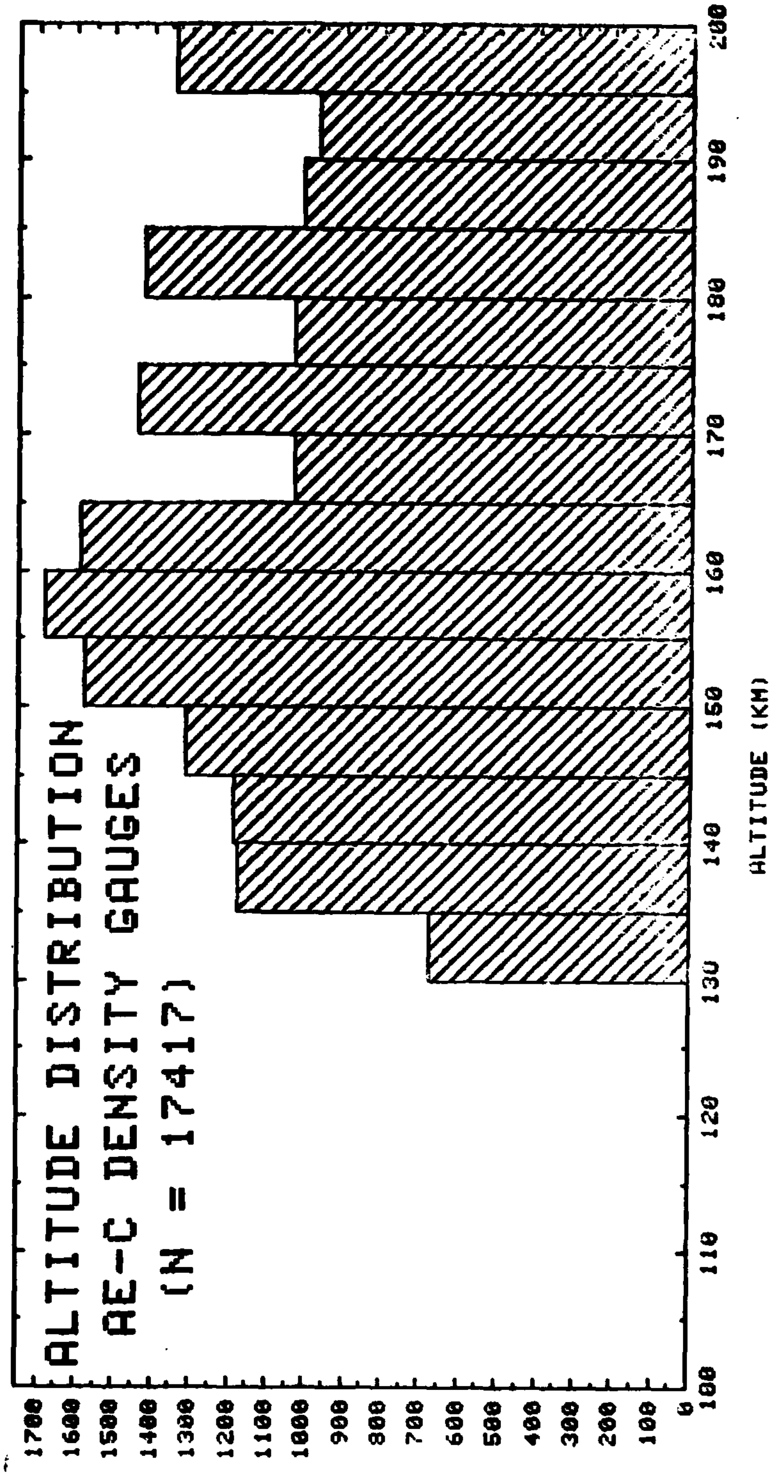

ALTITUDE DISTRIBUTION
AE-C DENSITY GAUGES
(N = 17417)
1700
1600
1500
1400
1300
1200
1100
1000
900
800
700
600
500
400
300
200
100
0
100
110
120
130
140
150
160
170
180
190
200
ALTITUDE (KM)

Figure 2-1.

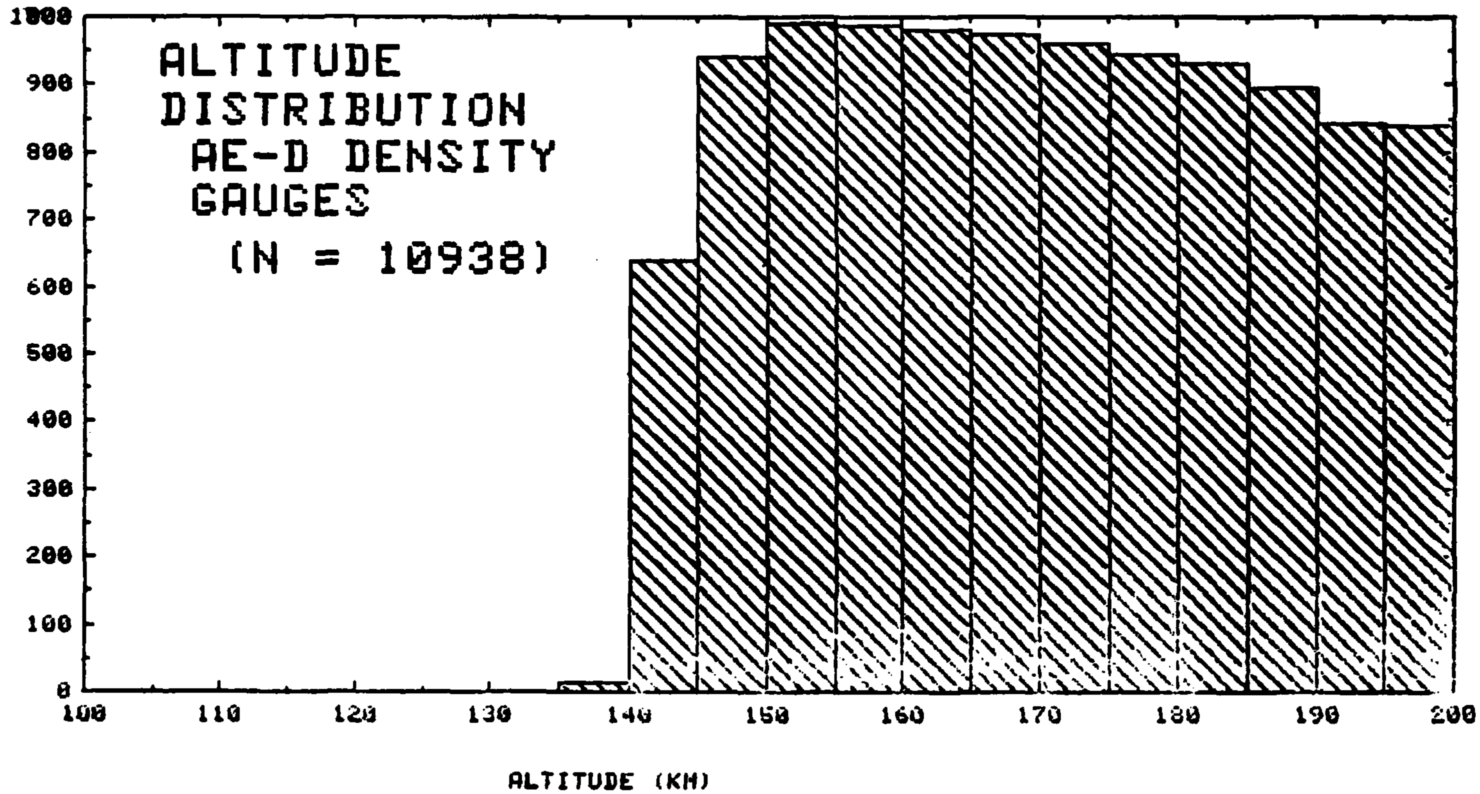
ALTITUDE
DISTRIBUTION
AE-D DENSITY
GAUGES
(N = 10938)
1000
900
800
700
600
500
400
300
200
100
0
100
110
120
130
140
150
160
170
180
190
200
ALTITUDE (KM)

Figure 2-2.

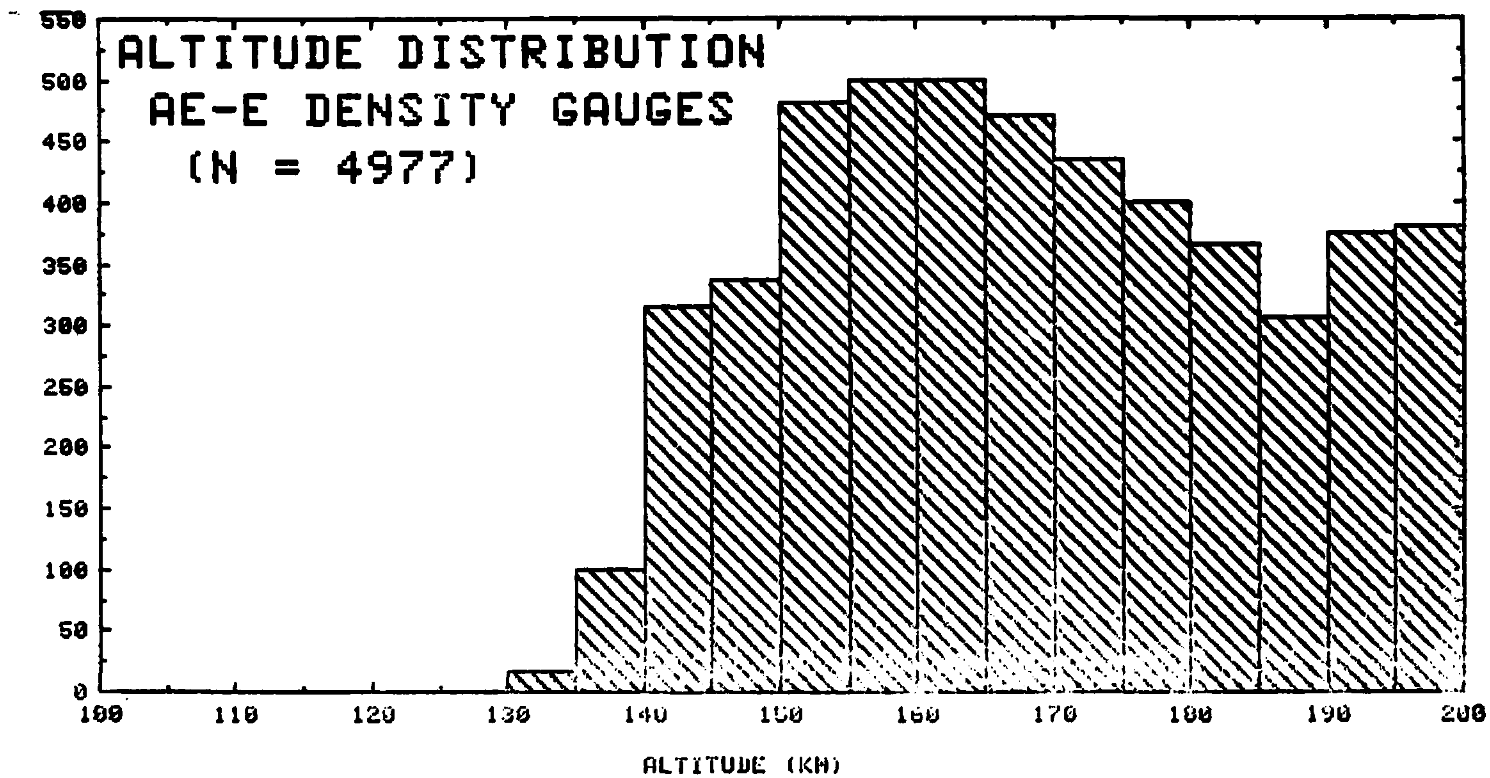
ALTITUDE DISTRIBUTION
AE-E DENSITY GAUGES
(N = 4977)
550
500
450
400
350
300
250
200
150
100
50
0
100
110
120
130
140
150
160
170
180
190
200
ALTITUDE (KM)

Figure 2-3.

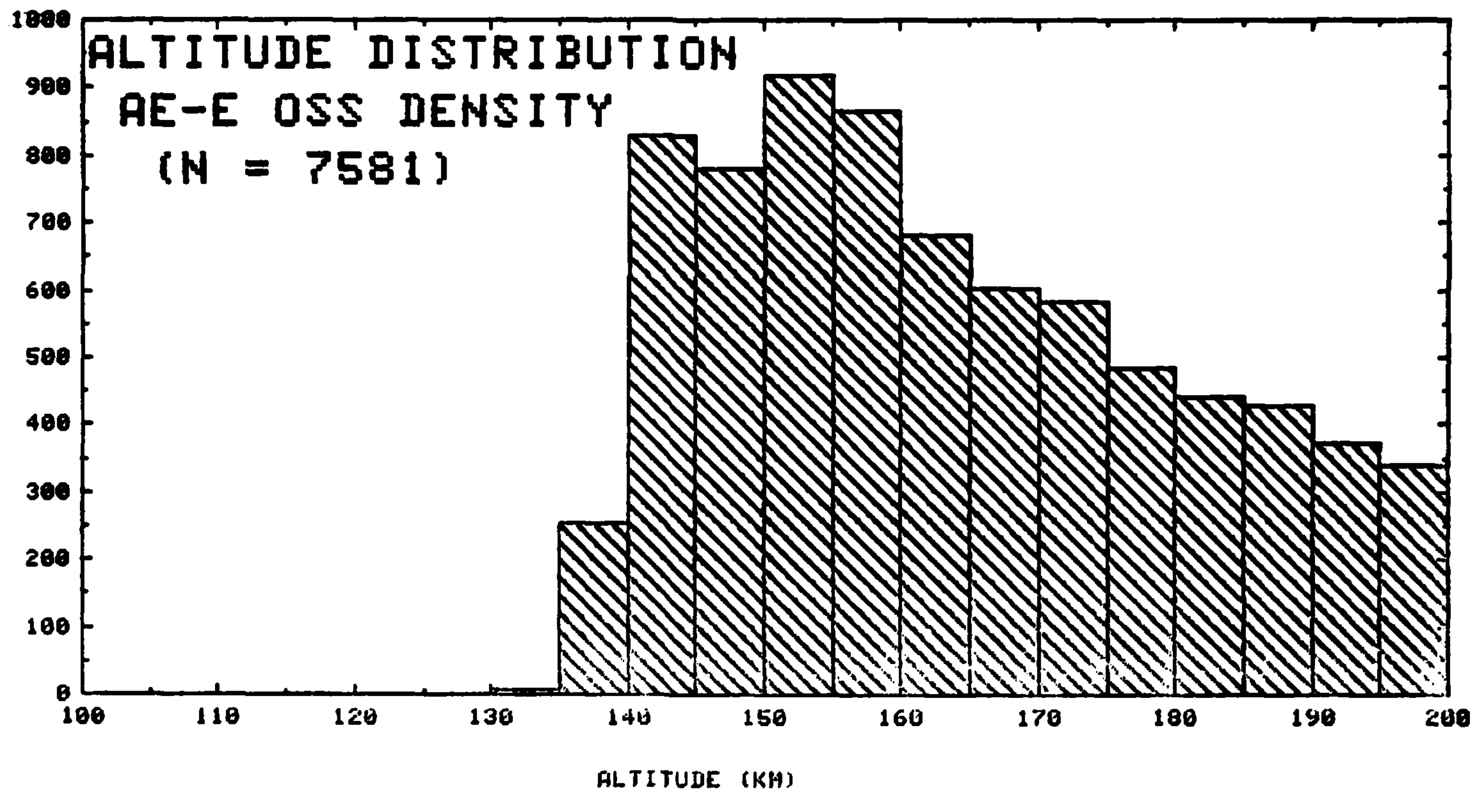

ALTITUDE DISTRIBUTION
AE-E OSS DENSITY
(N = 7581)
1000
900
800
700
600
500
400
300
200
100
0
100
110
120
130
140
150
160
170
180
190
200
ALTITUDE (KM)

Figure 2-4.

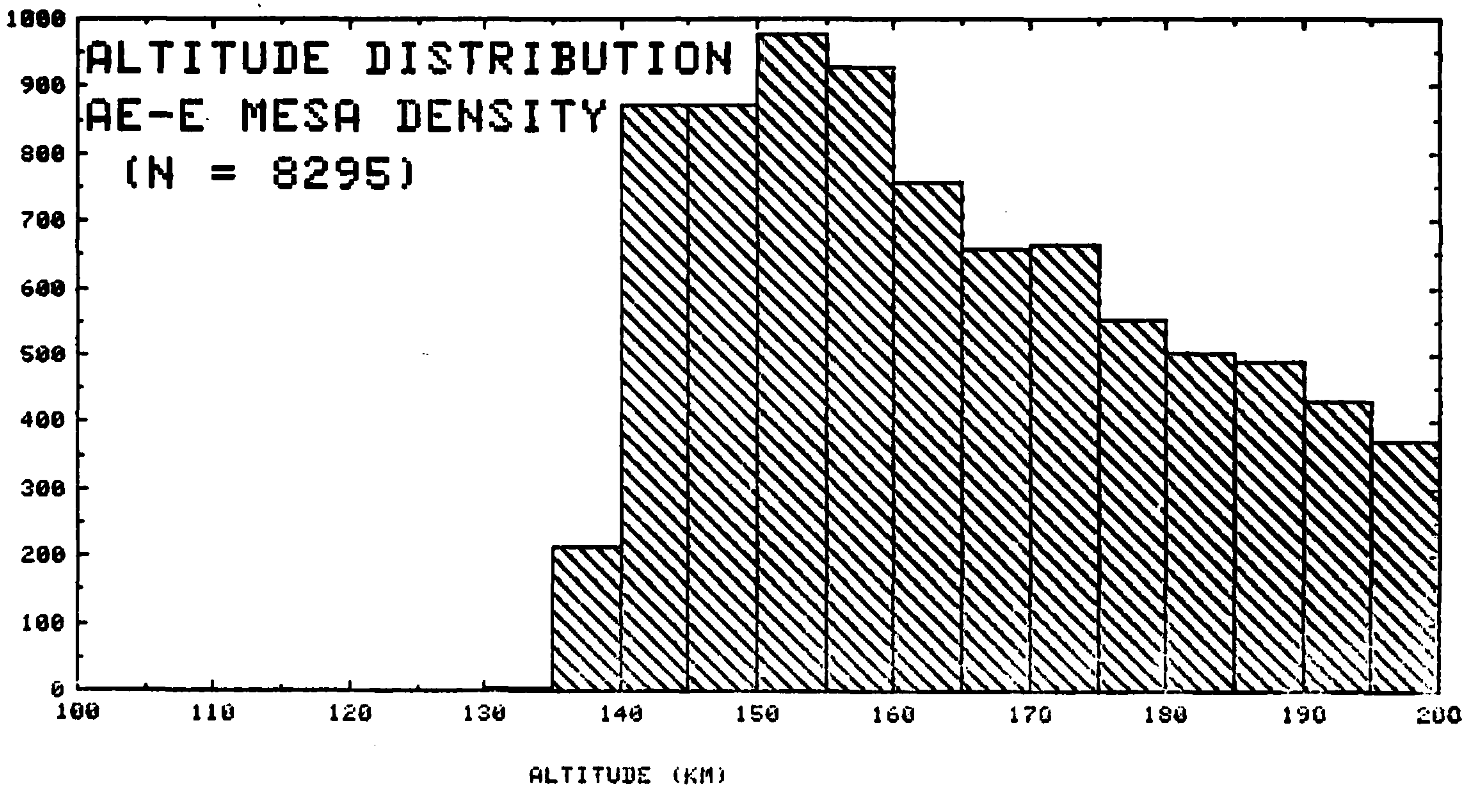

ALTITUDE DISTRIBUTION
AE-E MESA DENSITY
(N = 8295)
1000
900
800
700
600
500
400
300
200
100
0
100
110
120
130
140
150
160
170
180
190
200
ALTITUDE (KM)

Figure 2-5.

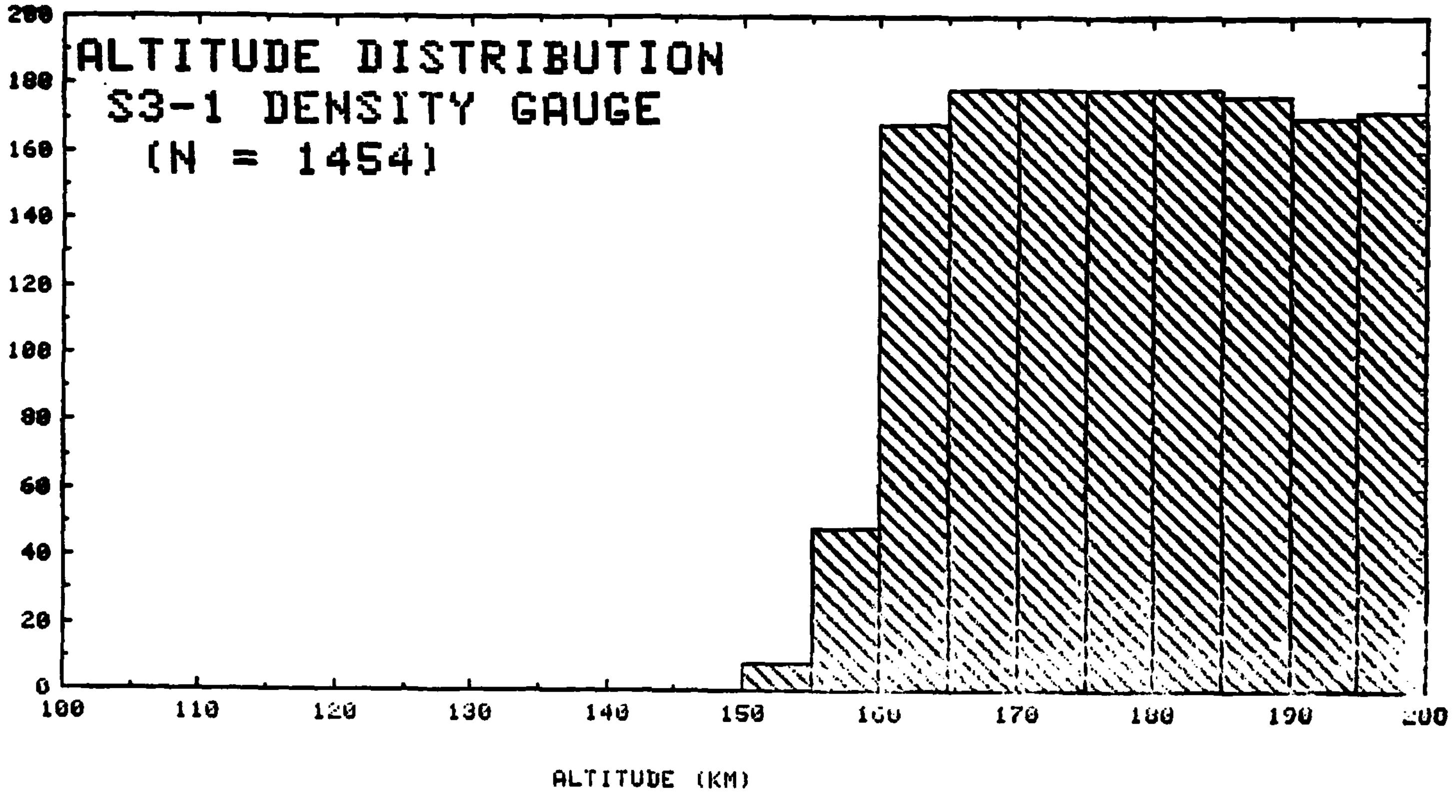
ALTITUDE DISTRIBUTION
S3-1 DENSITY GAUGE
(N = 1454)
200
180
160
140
120
100
80
60
40
20
0
100
110
120
130
140
150
160
170
180
190
200
ALTITUDE (KM)

Figure 2-6.

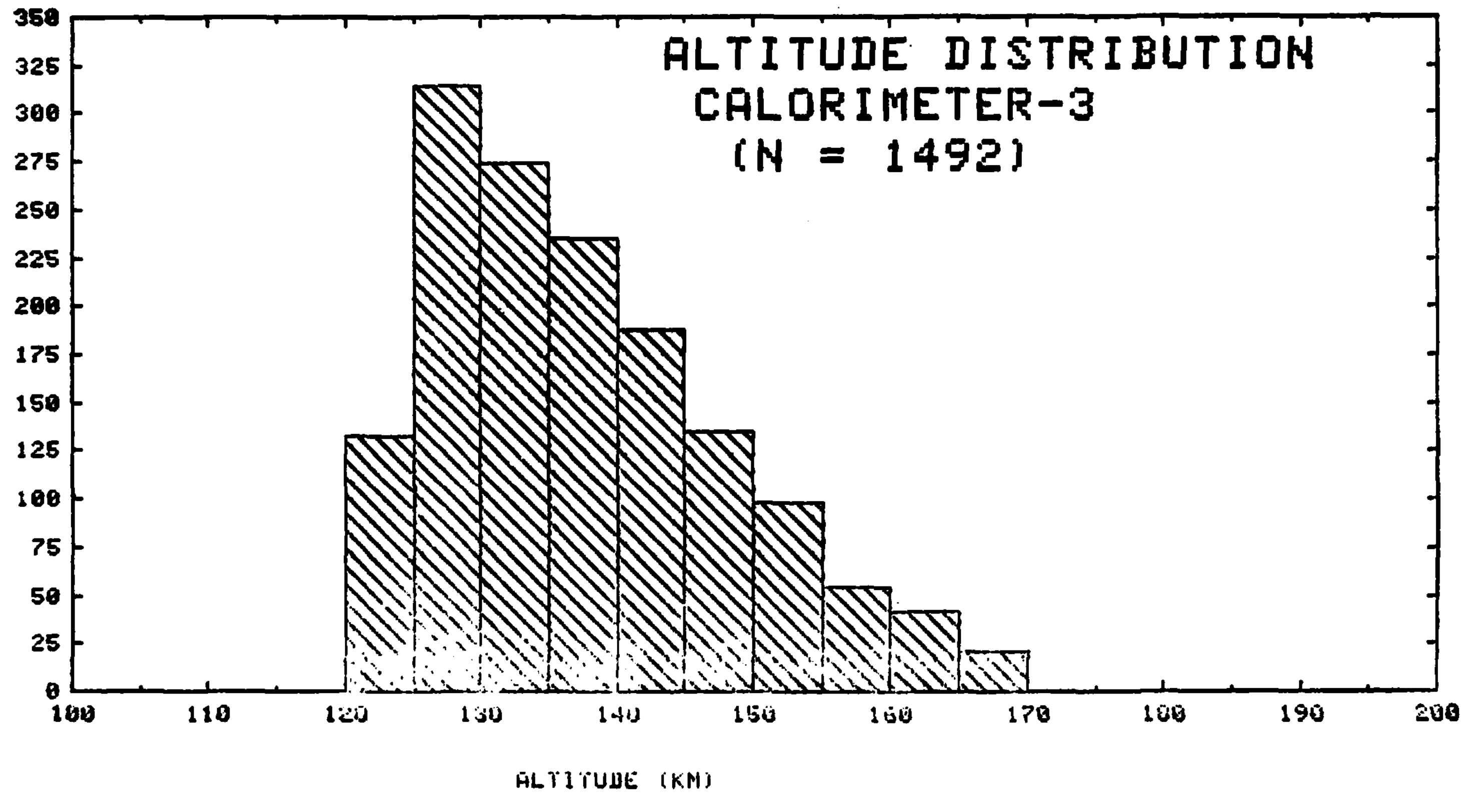
ALTITUDE DISTRIBUTION
CALORIMETER-3
(N = 1492)
350
325
300
275
250
225
200
175
150
125
100
75
50
25
0
100
110
120
130
140
150
160
170
180
190
200
ALTITUDE (KM)

Figure 2-7.

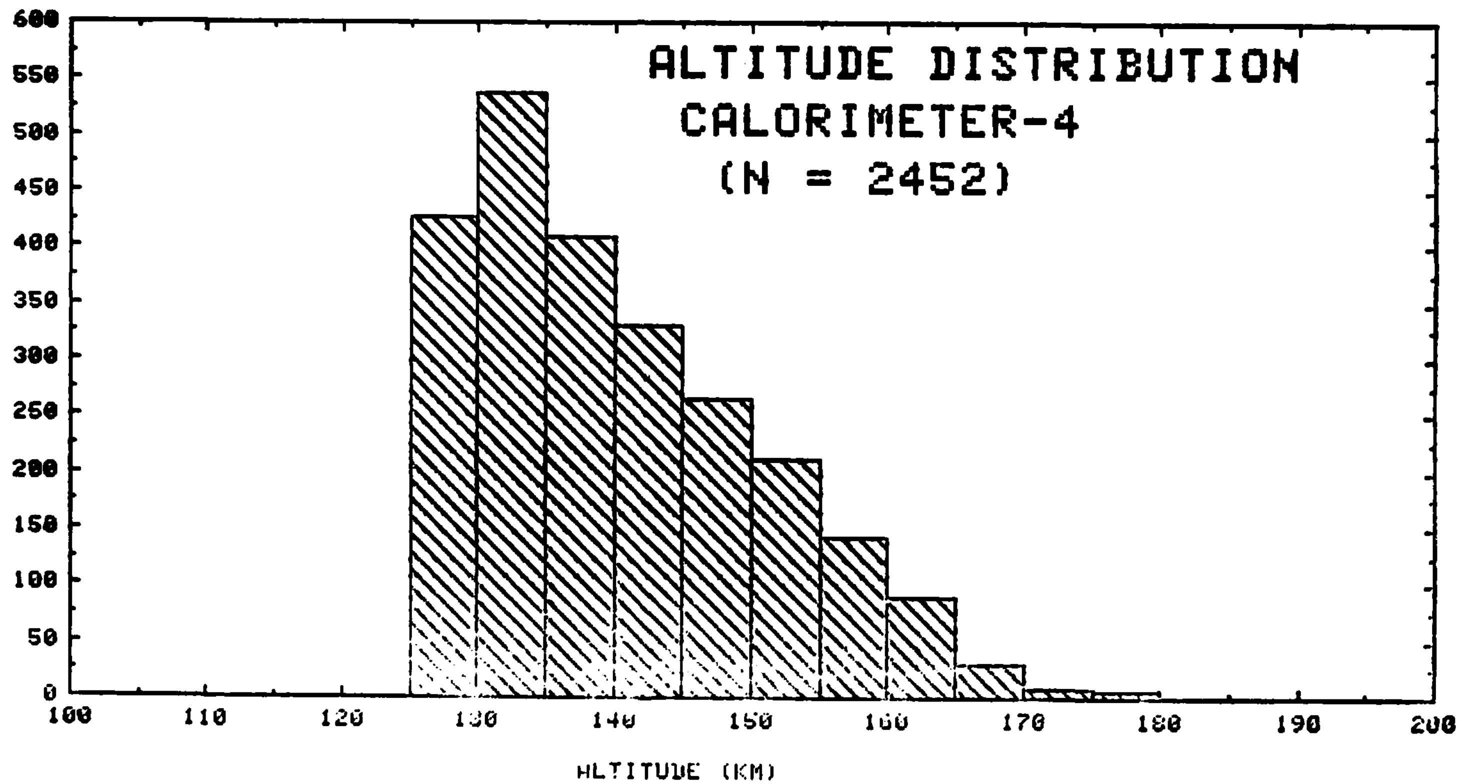
ALTITUDE DISTRIBUTION
CALORIMETER-4
(N = 2452)
0
50
100
150
200
250
300
350
400
450
500
550
600
100
110
120
130
140
150
160
170
180
190
200
ALTITUDE (KM)

Figure 2-8.

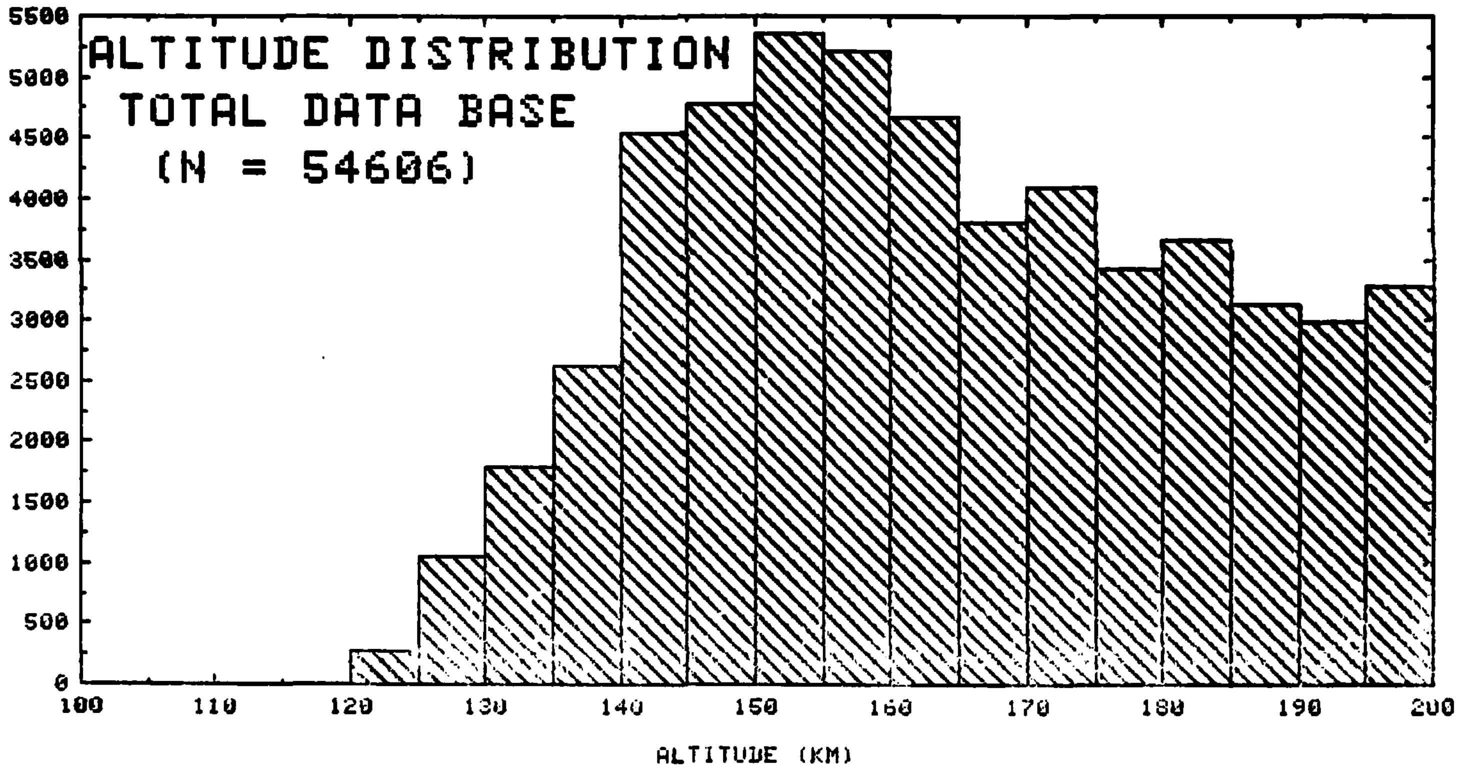
ALTITUDE DISTRIBUTION
TOTAL DATA BASE
(N = 54606)
5500
5000
4500
4000
3500
3000
2500
2000
1500
1000
500
0
100
110
120
130
140
150
160
170
180
190
200
ALTITUDE (KM)

Figure 2-9.

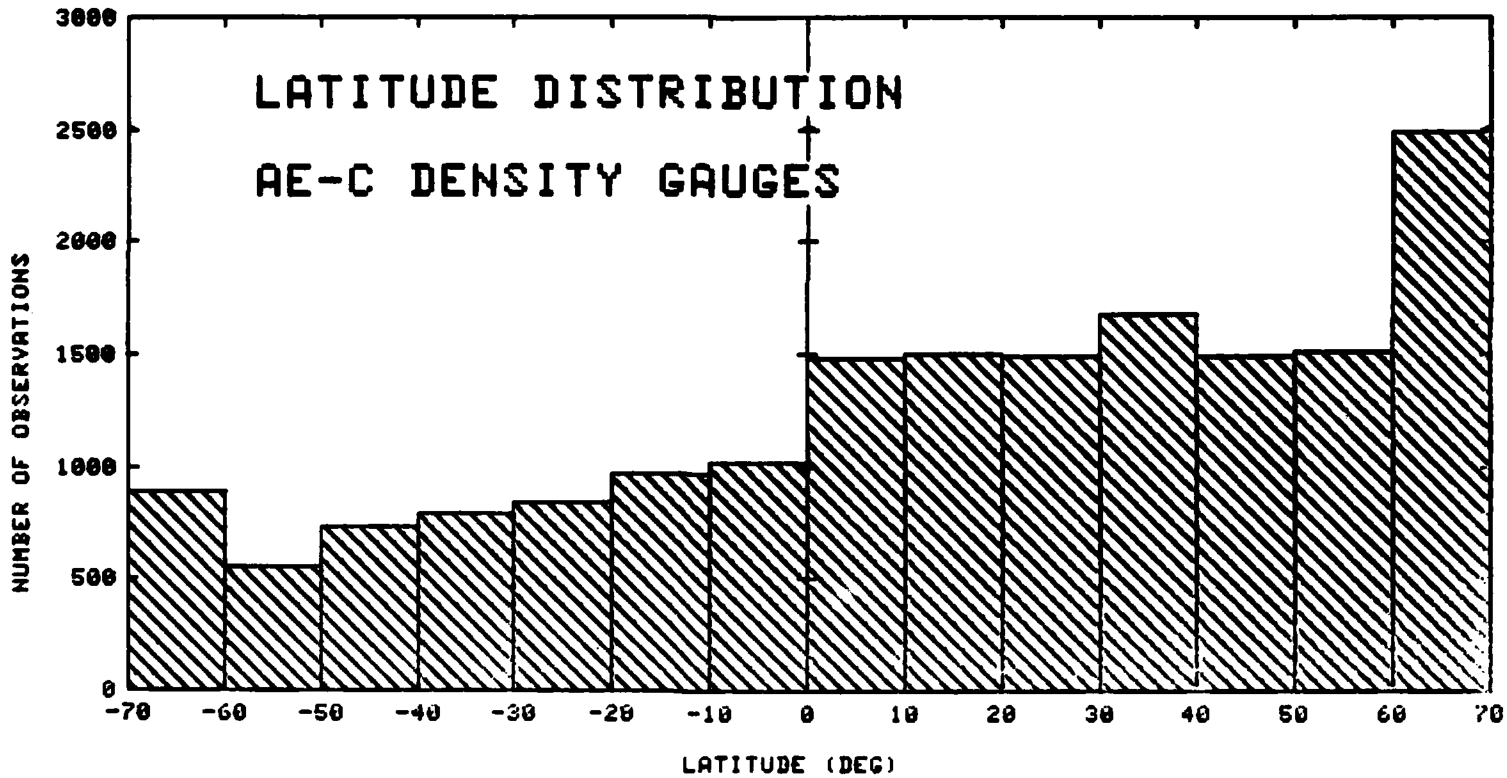
LATITUDE DISTRIBUTION
AE-C DENSITY GAUGES
NUMBER OF OBSERVATIONS
0
500
1000
1500
2000
2500
3000
-70
-60
-50
-40
-30
-20
-10
0
10
20
30
40
50
60
70
LATITUDE (DEG)

Figure 2-10.

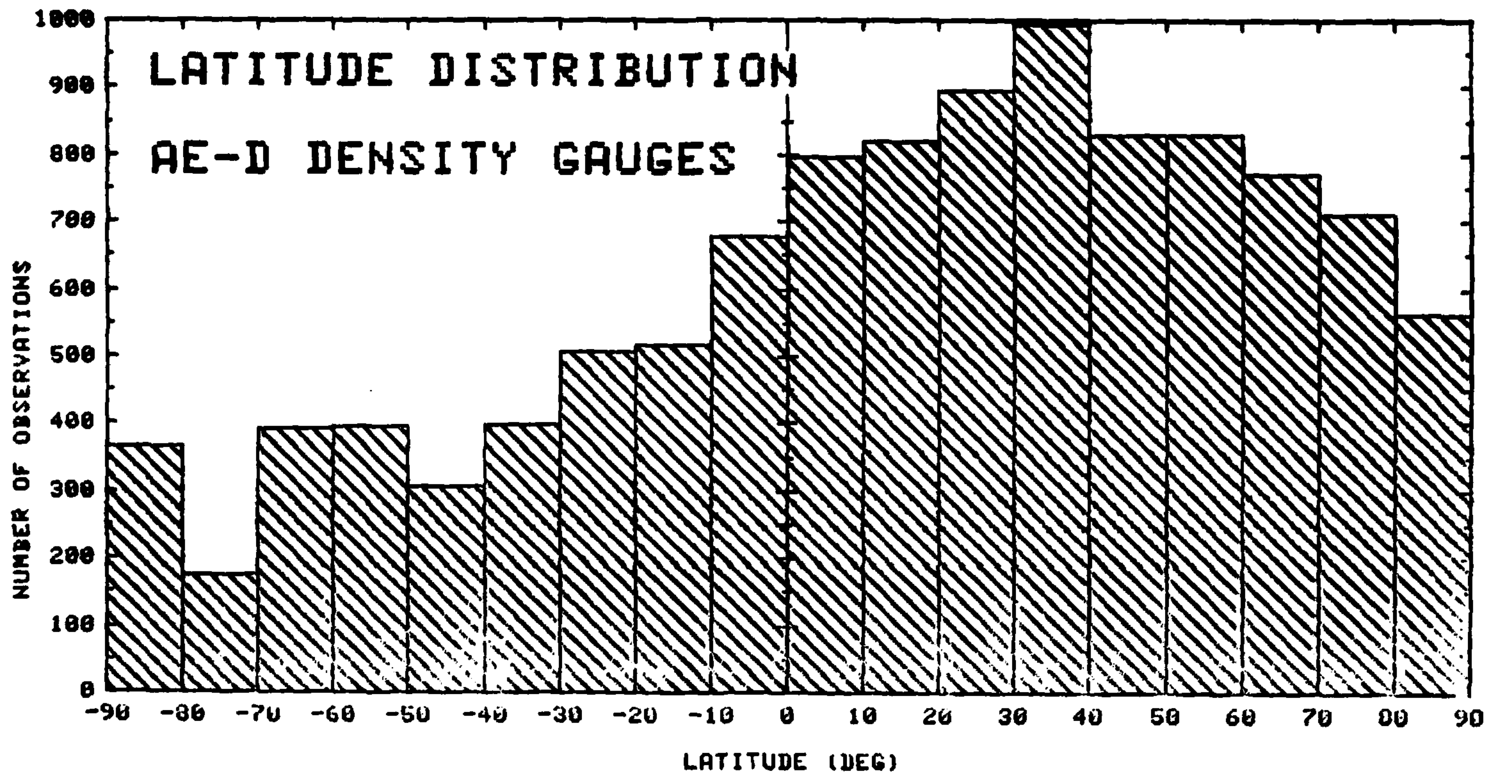
LATITUDE DISTRIBUTION
AE-D DENSITY GAUGES
NUMBER OF OBSERVATIONS
1000
900
800
700
600
500
400
300
200
100
0
-90 -80 -70 -60 -50 -40 -30 -20 -10 0 10 20 30 40 50 60 70 80 90
LATITUDE (DEG)

Figure 2-11.

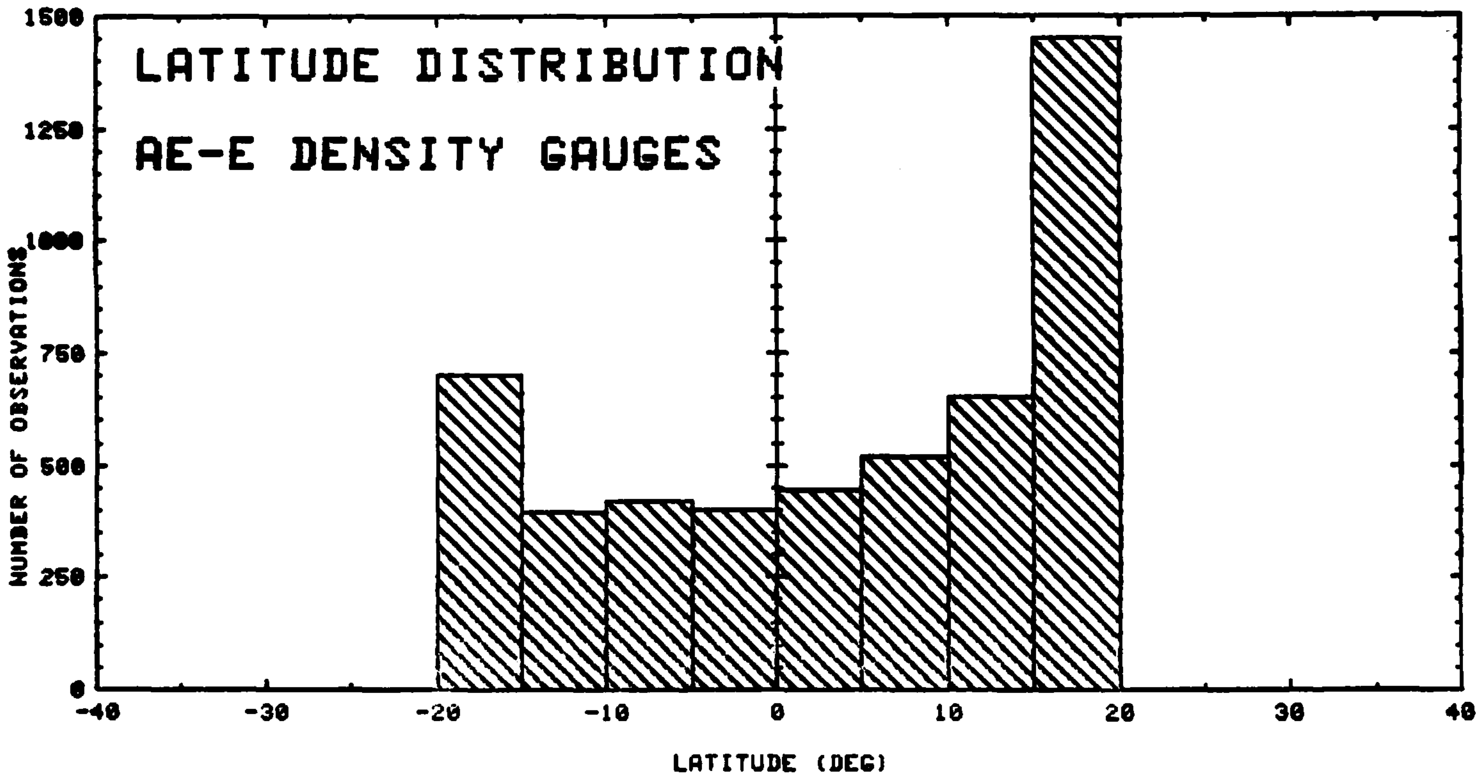
LATITUDE DISTRIBUTION
AE-E DENSITY GAUGES
NUMBER OF OBSERVATIONS
1500
1250
1000
750
500
250
0
-40
-30
-20
-10
0
10
20
30
40
LATITUDE (DEG)

Figure 2-12.

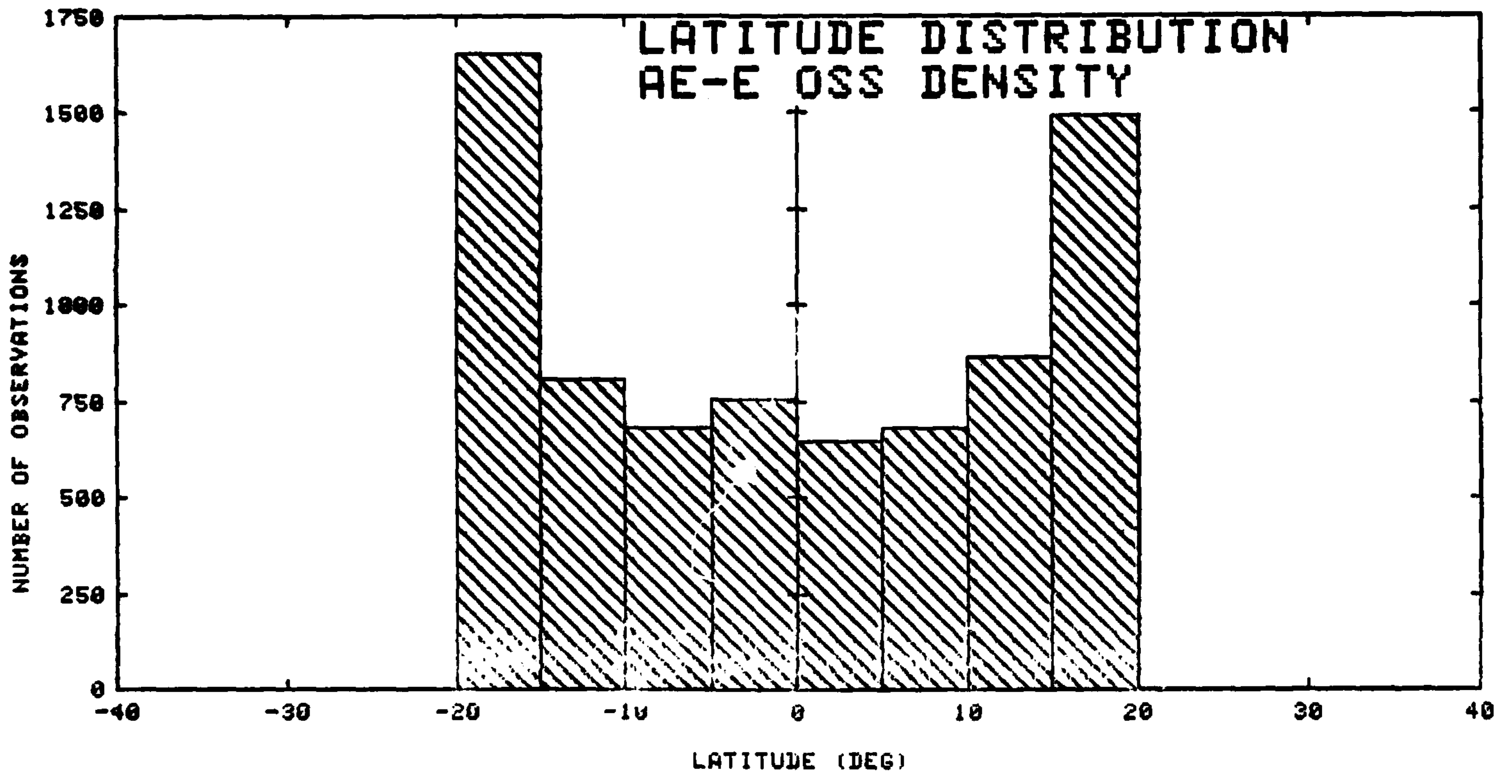
LATITUDE DISTRIBUTION
AE-E OSS DENSITY
NUMBER OF OBSERVATIONS
0
250
500
750
1000
1250
1500
1750
-40
-30
-20
-10
0
10
20
30
40
LATITUDE (DEG)

Figure 2-13.

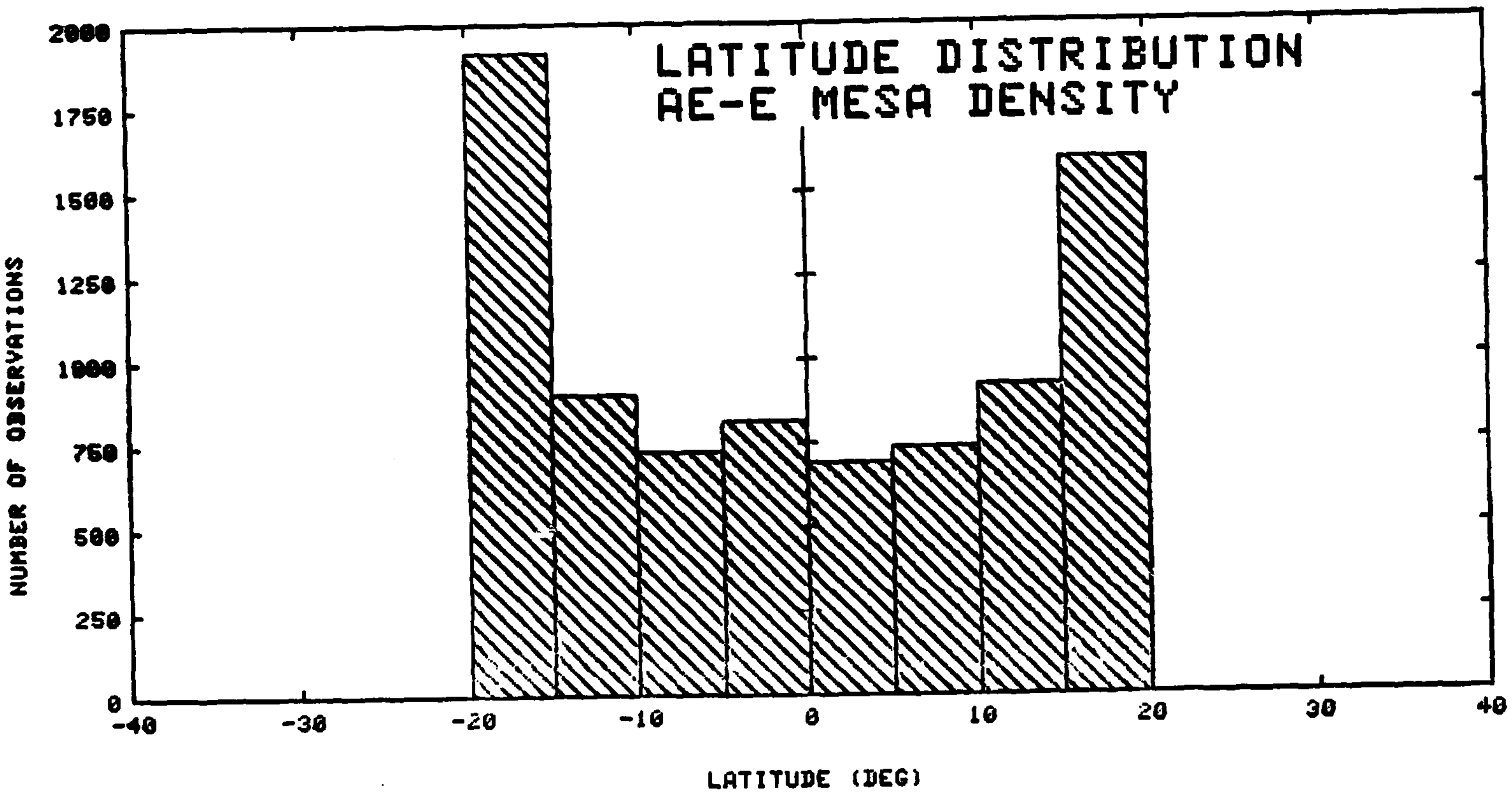

LATITUDE DISTRIBUTION
AE-E MESA DENSITY
2000
1750
1500
1250
1000
750
500
250
0
NUMBER OF OBSERVATIONS
-40
-30
-20
-10
0
10
20
30
40
LATITUDE (DEG)

Figure 2-14.

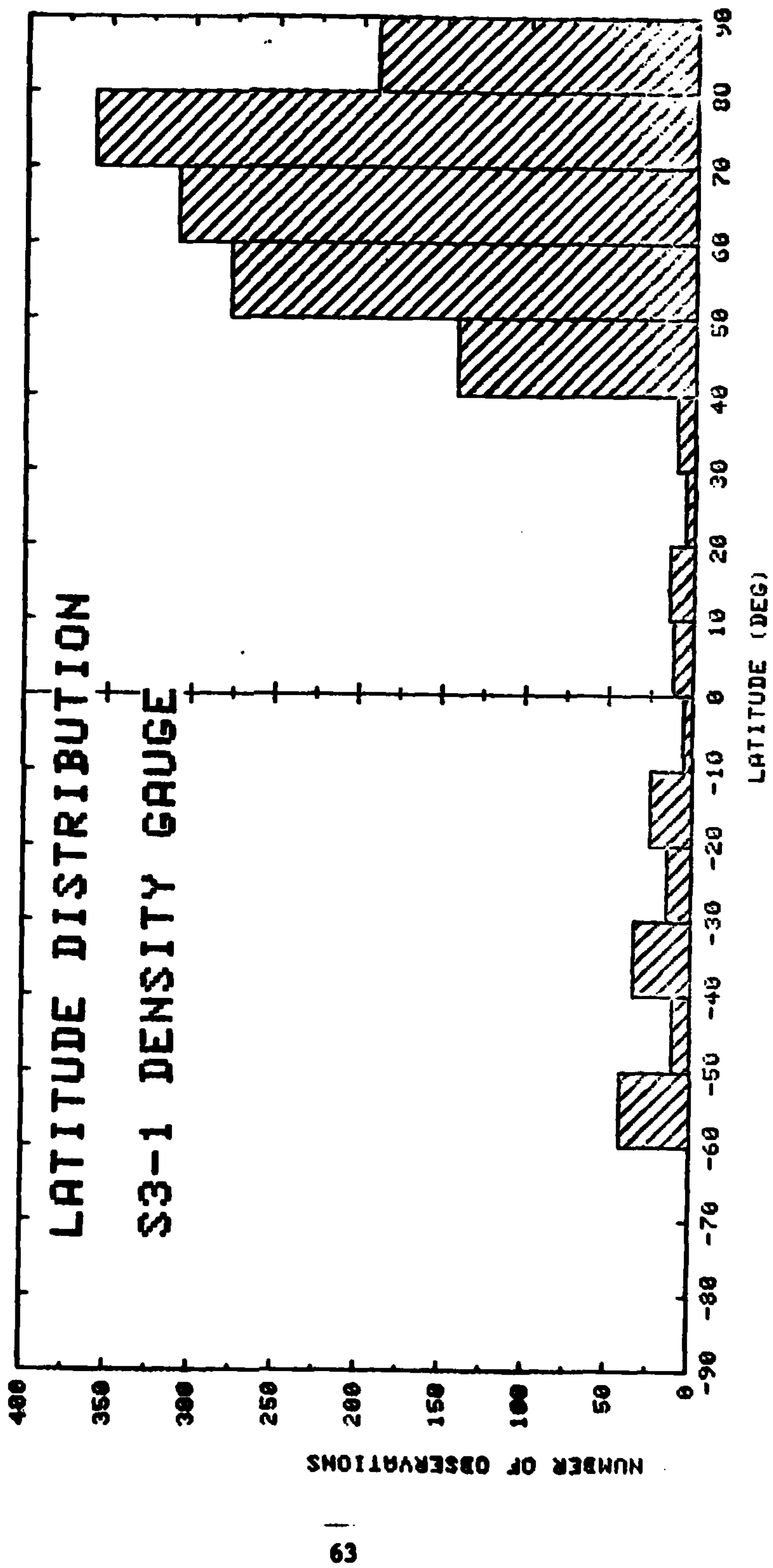
LATITUDE DISTRIBUTION
S3-1 DENSITY GAUGE
LATITUDE (DEG)
NUMBER OF OBSERVATIONS
-90
-80
-70
-60
-50
-40
-30
-20
-10
0
10
20
30
40
50
60
70
80
90
0
50
100
150
200
250
300
350
400

Figure 2-15.

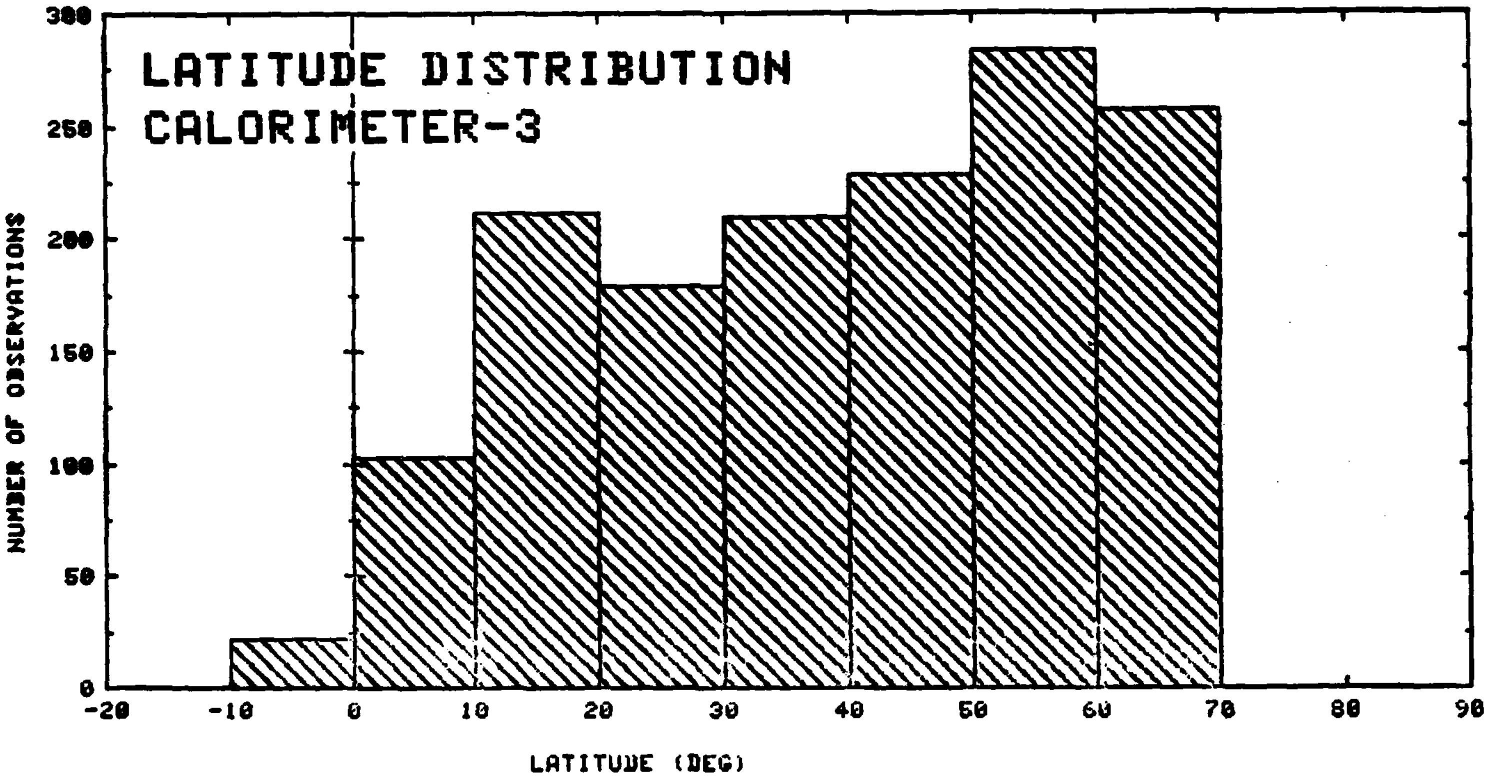
LATITUDE DISTRIBUTION
CALORIMETER-3
NUMBER OF OBSERVATIONS
LATITUDE (DEG)
300
250
200
150
100
50
0
-20
-10
0
10
20
30
40
50
60
70
80
90

Figure 2-16.

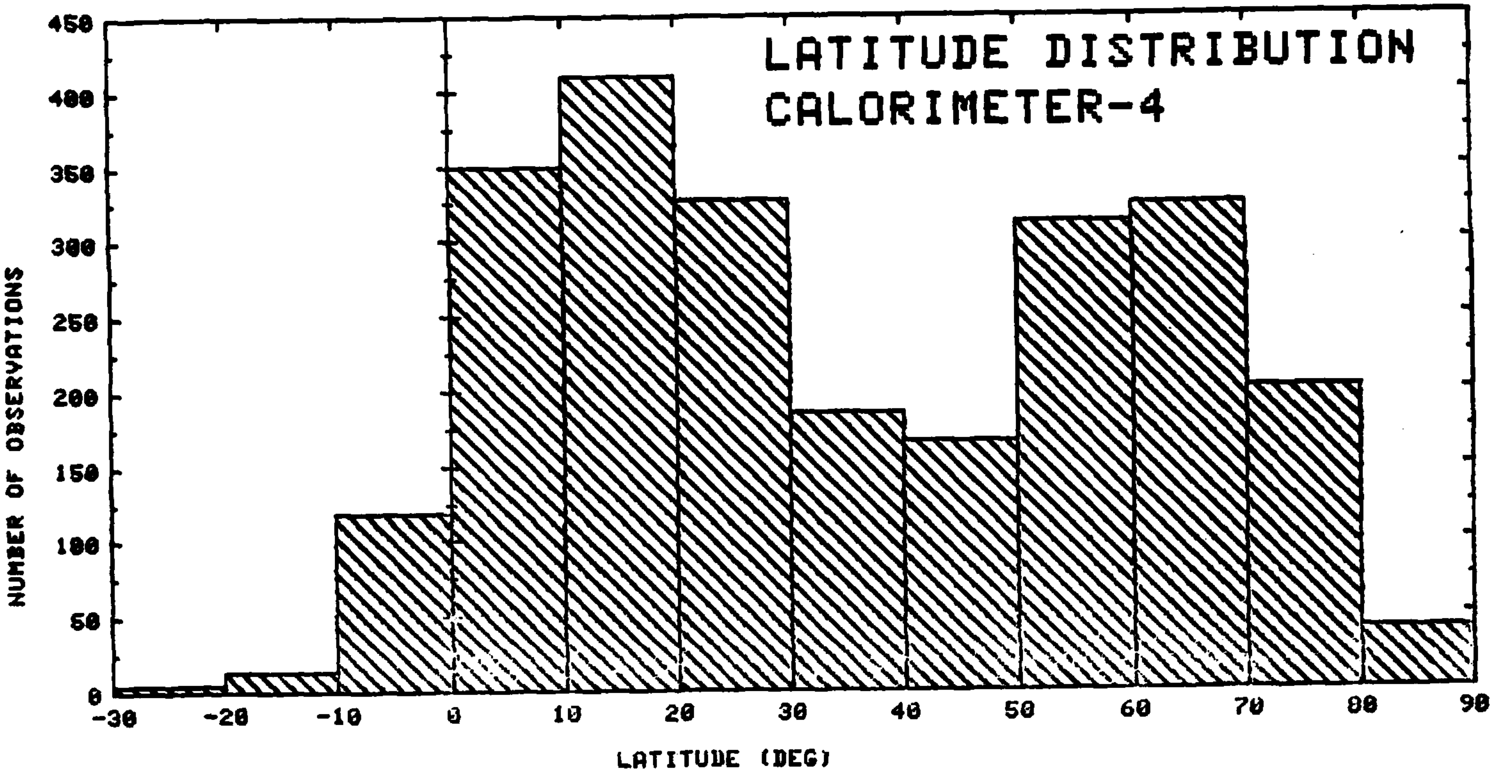
LATITUDE DISTRIBUTION
CALORIMETER-4
NUMBER OF OBSERVATIONS
LATITUDE (DEG)
450
400
350
300
250
200
150
100
50
0
-30
-20
-10
0
10
20
30
40
50
60
70
80
90

Figure 2-17.

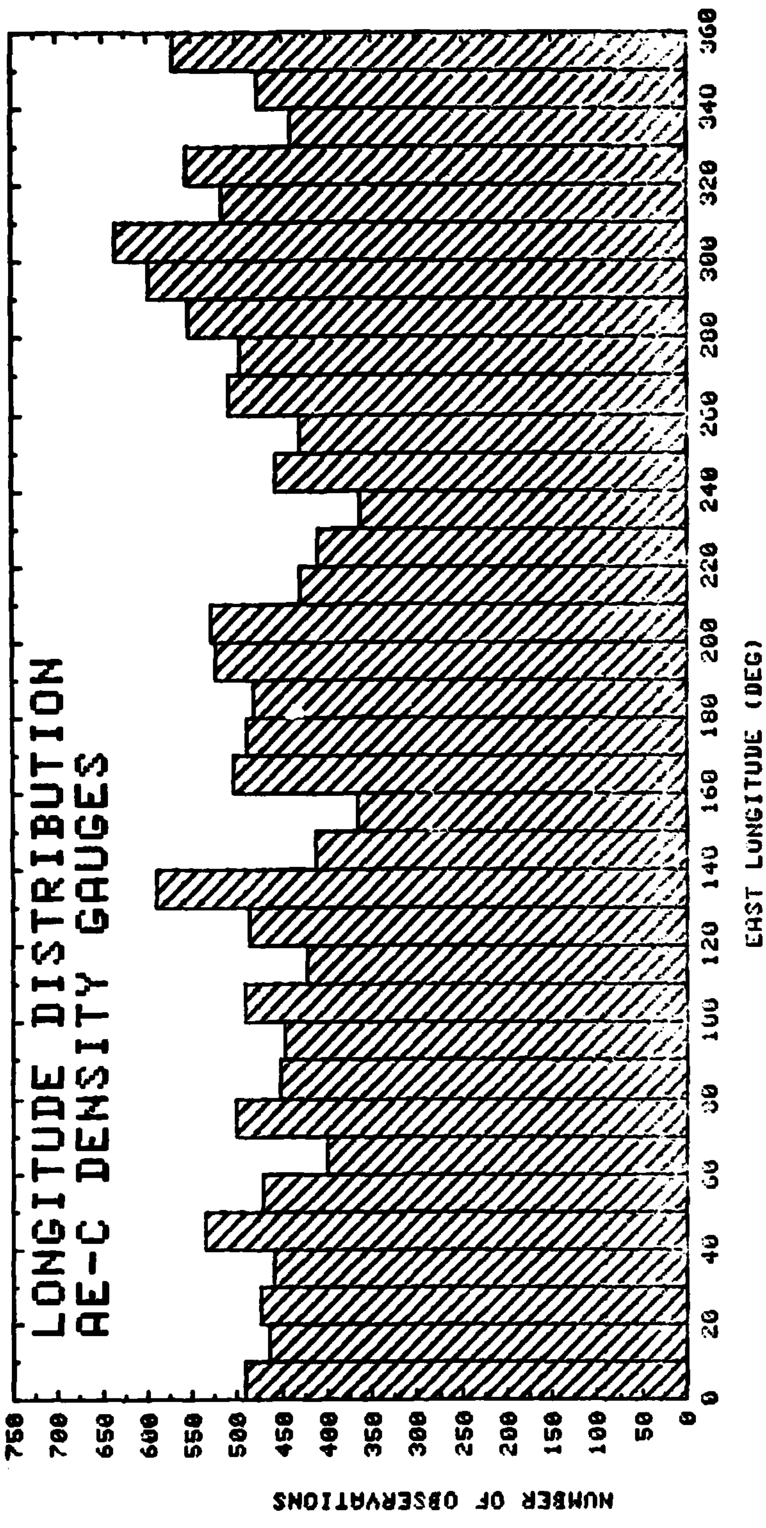
LONGITUDE DISTRIBUTION
AE-C DENSITY GAUGES
NUMBER OF OBSERVATIONS
EAST LONGITUDE (DEG)

Figure 2-18.

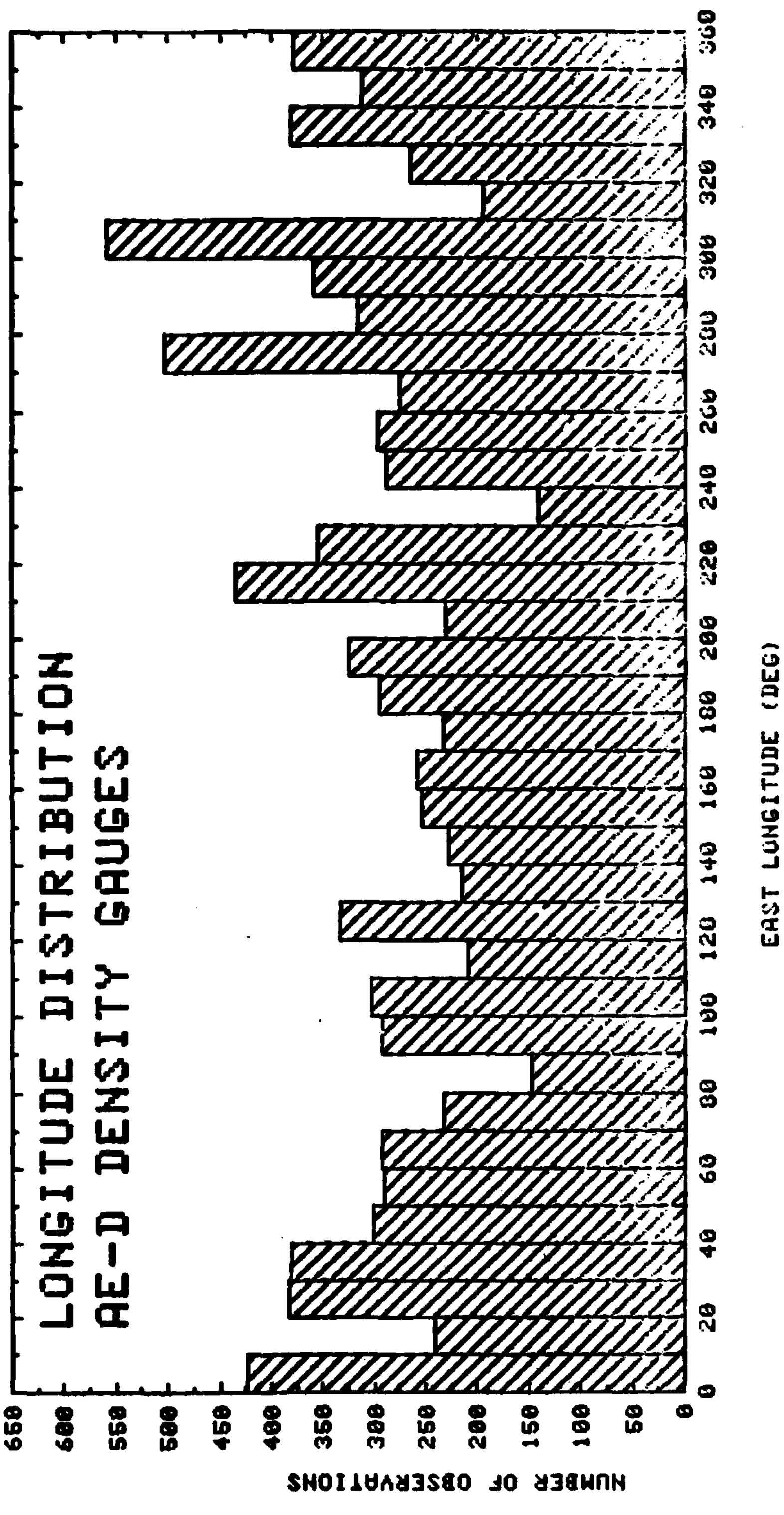
LONGITUDE DISTRIBUTION
AE-D DENSITY GAUGES
NUMBER OF OBSERVATIONS
EAST LONGITUDE (DEG)
0
50
100
150
200
250
300
350
400
450
500
550
600
650
0
20
40
60
80
100
120
140
160
180
200
220
240
260
280
300
320
340
360

Figure 2-19.

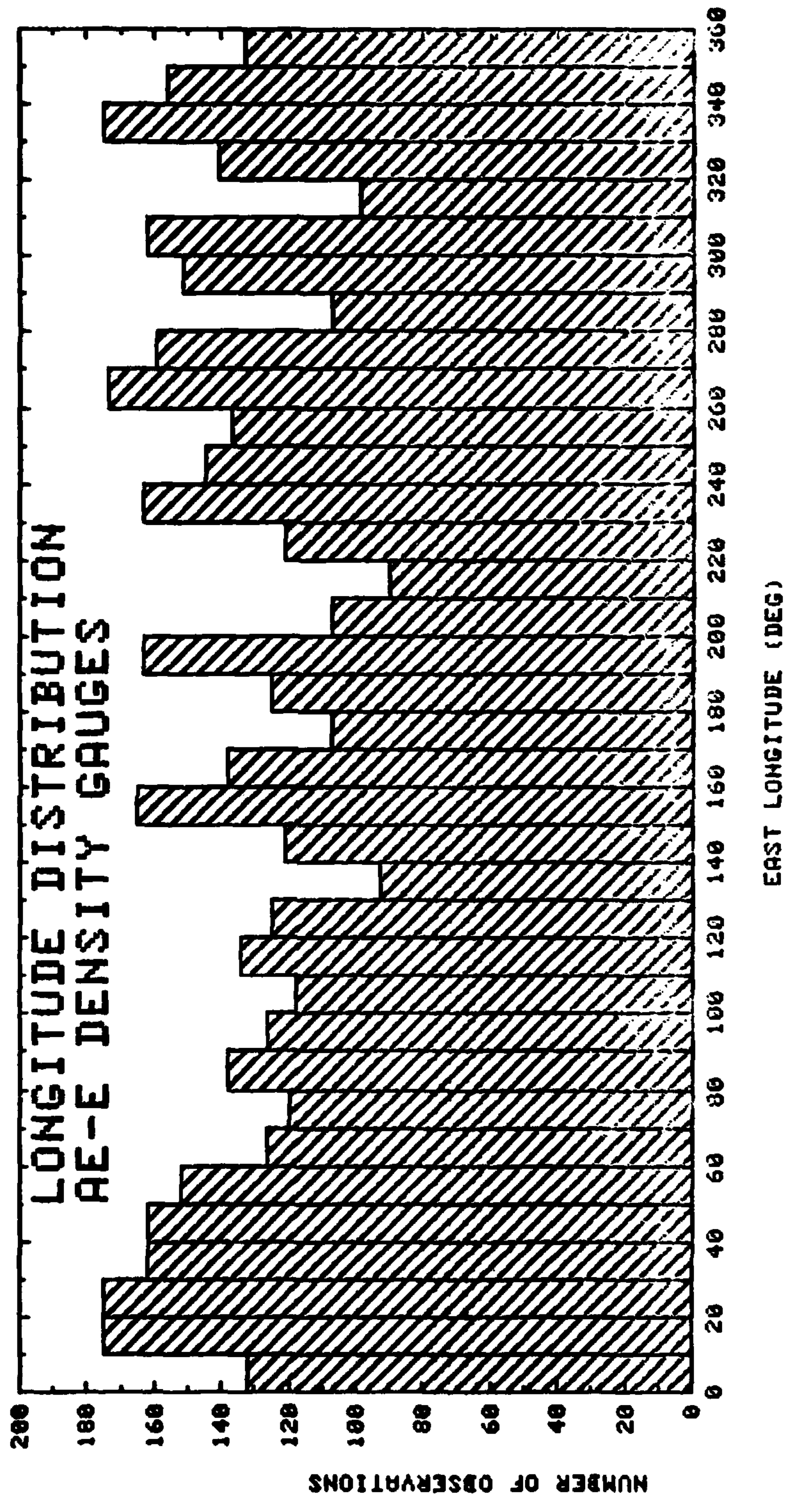
LONGITUDE DISTRIBUTION
AE-E DENSITY GAUGES
NUMBER OF OBSERVATIONS
EAST LONGITUDE (DEG)
0
20
40
60
80
100
120
140
160
180
200
220
240
260
280
300
320
340
360

Figure 2-20.

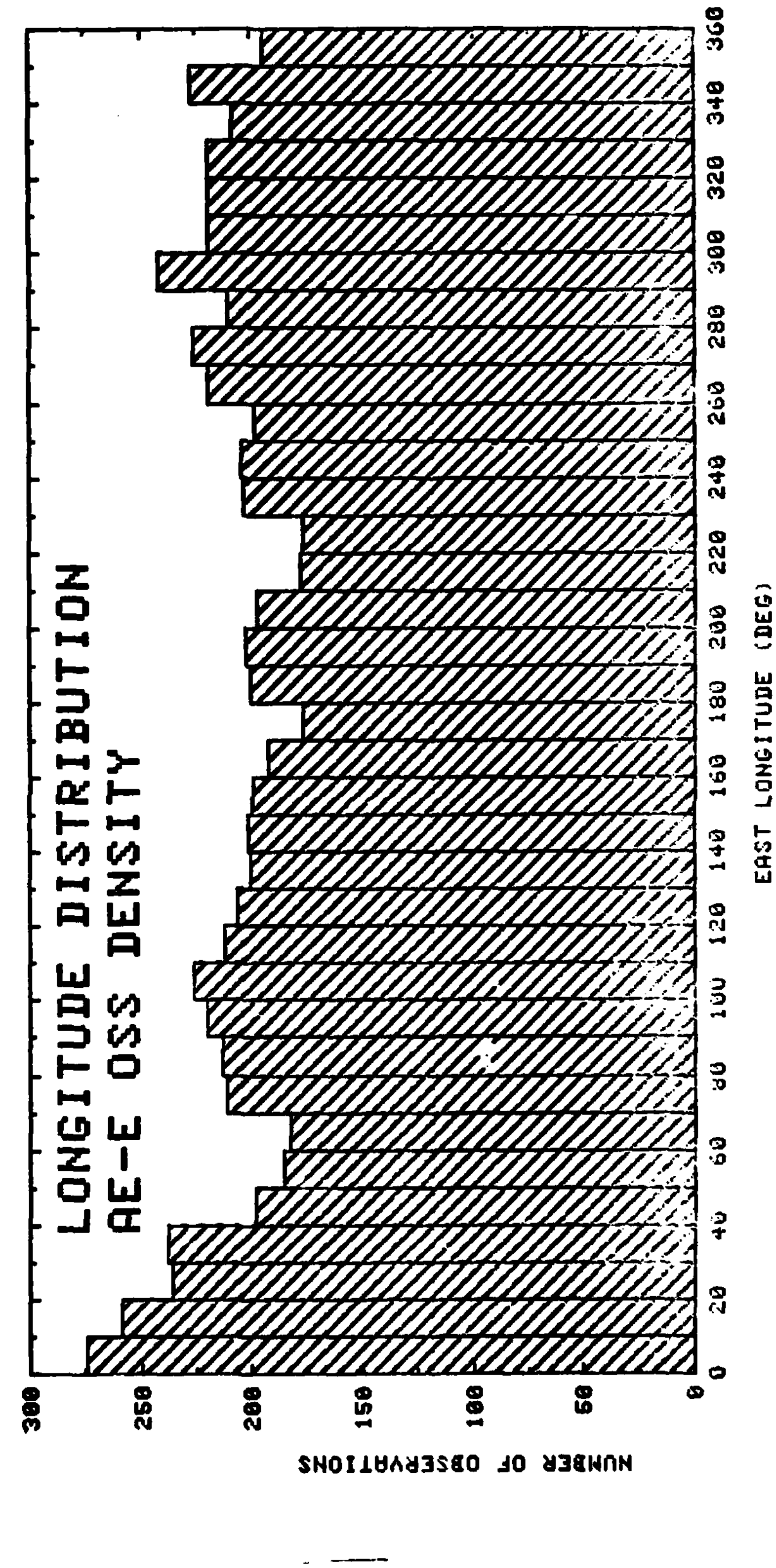
LONGITUDE DISTRIBUTION
AE-E OSS DENSITY
NUMBER OF OBSERVATIONS
EAST LONGITUDE (DEG)
0
50
100
150
200
250
300
0
20
40
60
80
100
120
140
160
180
200
220
240
260
280
300
320
340
360

Figure 2-21.

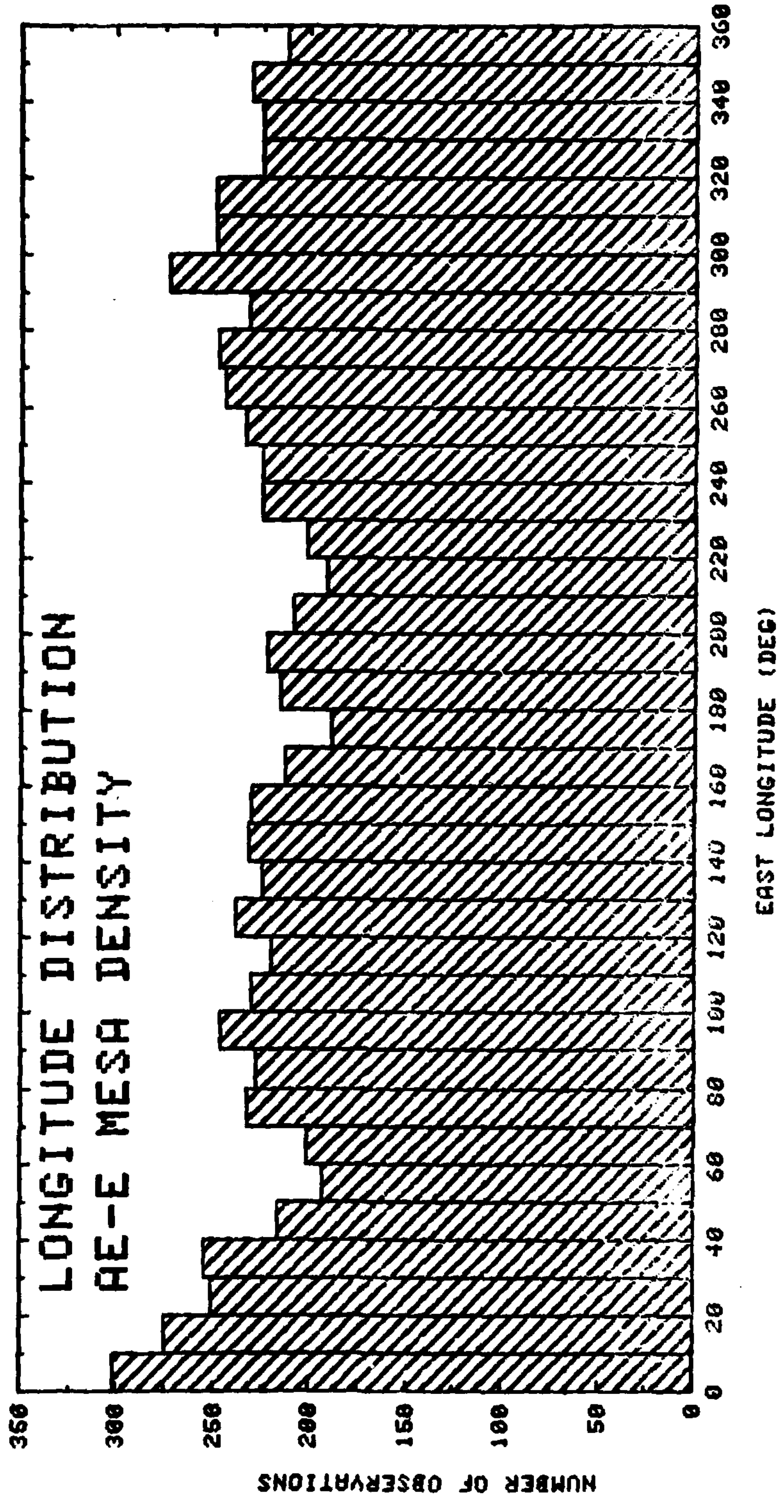
LONGITUDE DISTRIBUTION
AE-E MESA DENSITY
NUMBER OF OBSERVATIONS
EAST LONGITUDE (DEG)
0
50
100
150
200
250
300
350
0
20
40
60
80
100
120
140
160
180
200
220
240
260
280
300
320
340
360

Figure 2-22.

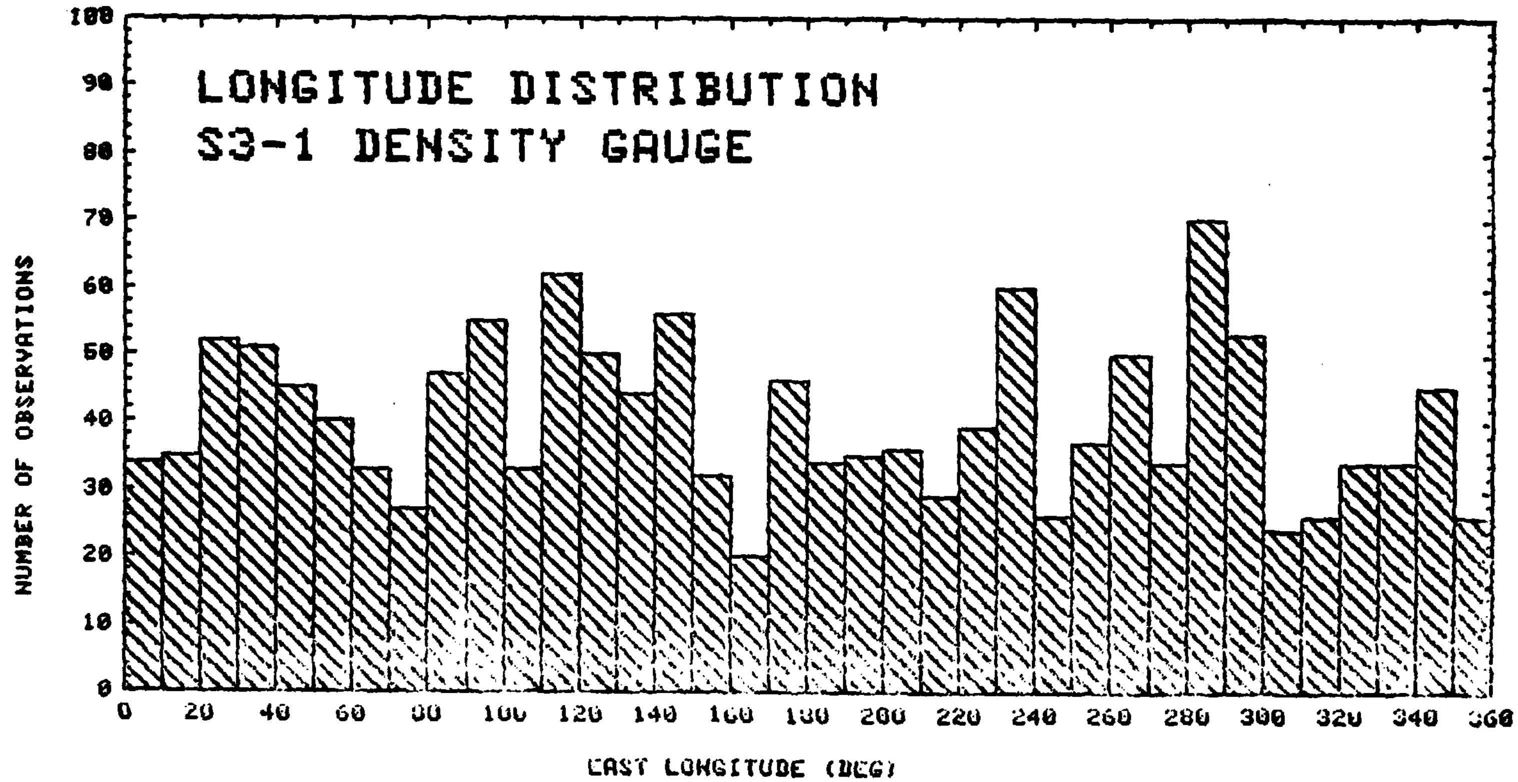
LONGITUDE DISTRIBUTION
S3-1 DENSITY GAUGE
NUMBER OF OBSERVATIONS
0
10
20
30
40
50
60
70
80
90
100
0 20 40 60 80 100 120 140 160 180 200 220 240 260 280 300 320 340 360
EAST LONGITUDE (DEG)

Figure 2-23.

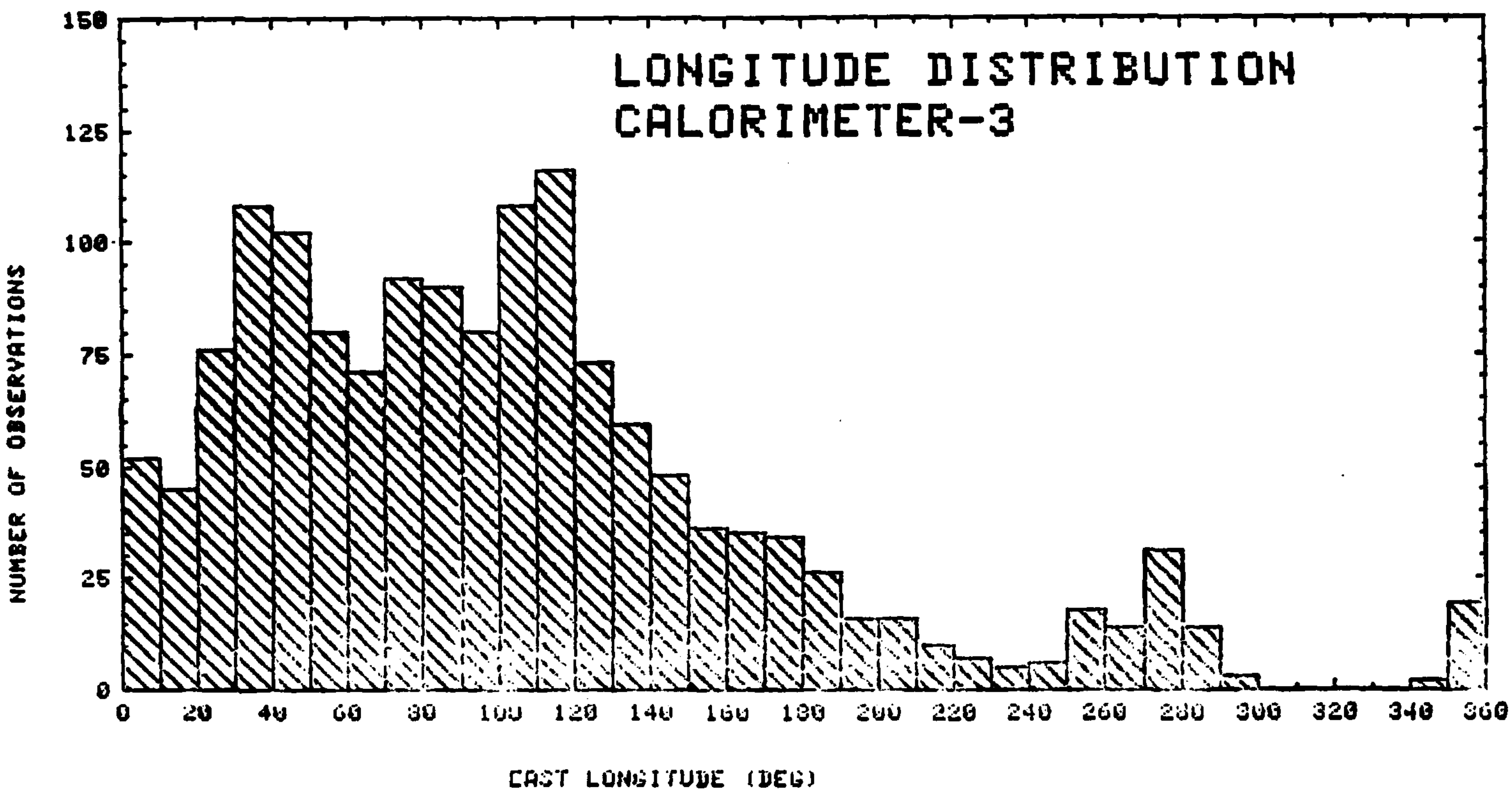
LONGITUDE DISTRIBUTION
CALORIMETER-3
150
125
100
75
50
25
0
NUMBER OF OBSERVATIONS
0 20 40 60 80 100 120 140 160 180 200 220 240 260 280 300 320 340 360
EAST LONGITUDE (DEG)

Figure 2-24.

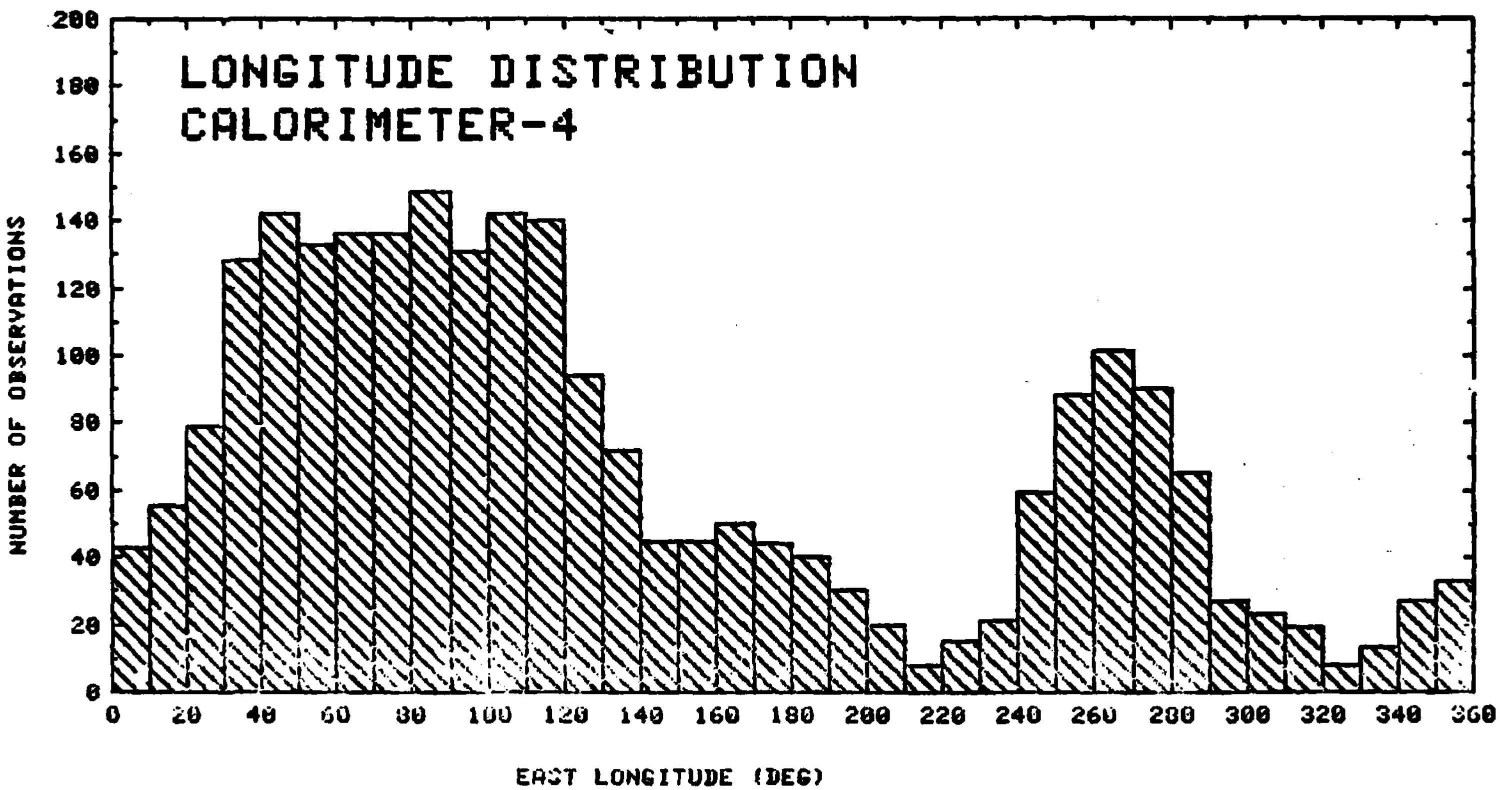
LONGITUDE DISTRIBUTION
CALORIMETER-4
NUMBER OF OBSERVATIONS
0
20
40
60
80
100
120
140
160
180
200
220
240
260
280
300
320
340
360
EAST LONGITUDE (DEG)

Figure 2-25.

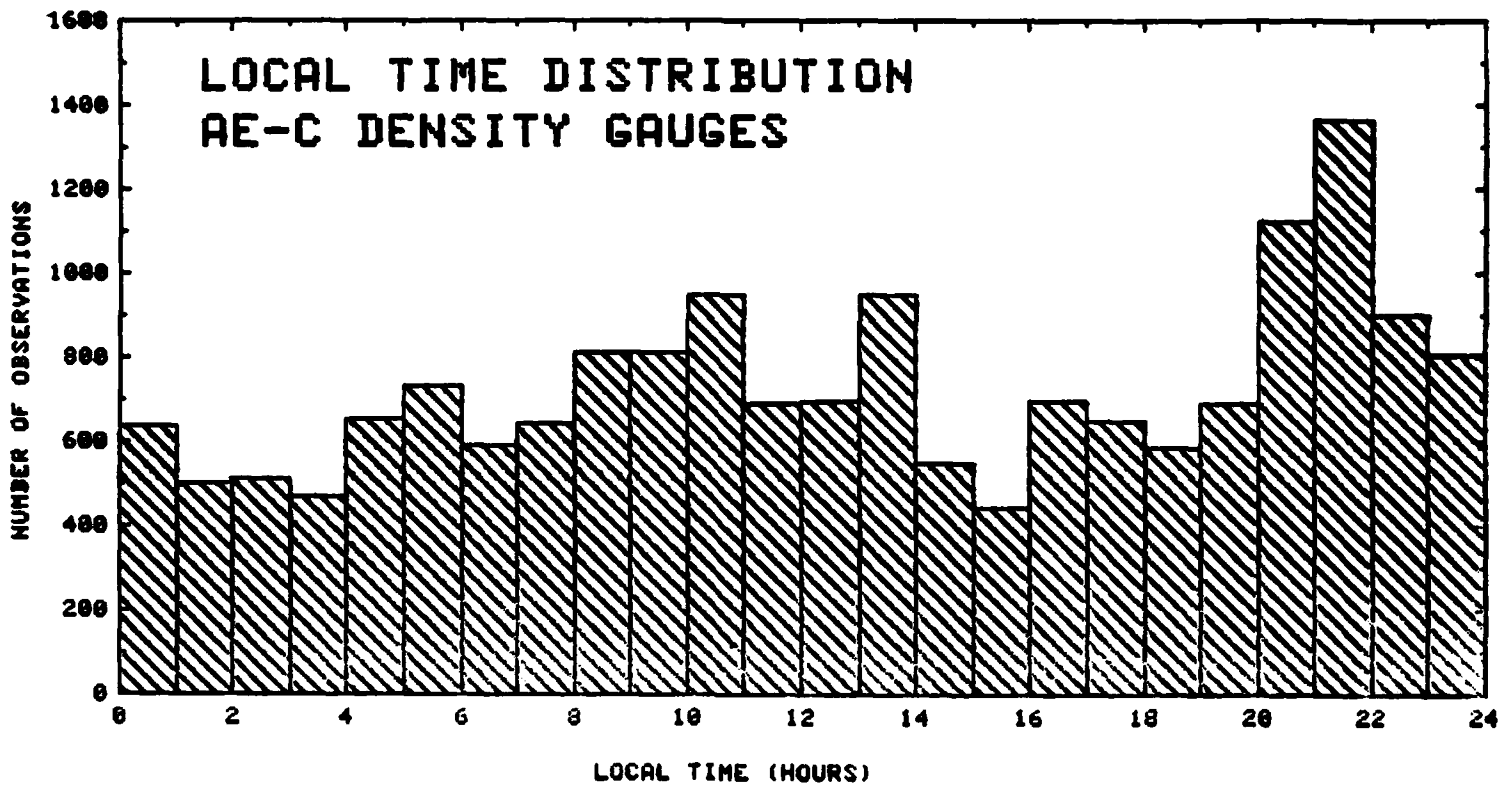
LOCAL TIME DISTRIBUTION
AE-C DENSITY GAUGES
NUMBER OF OBSERVATIONS
1600
1400
1200
1000
800
600
400
200
0
0
2
4
6
8
10
12
14
16
18
20
22
24
LOCAL TIME (HOURS)

Figure 2-26.

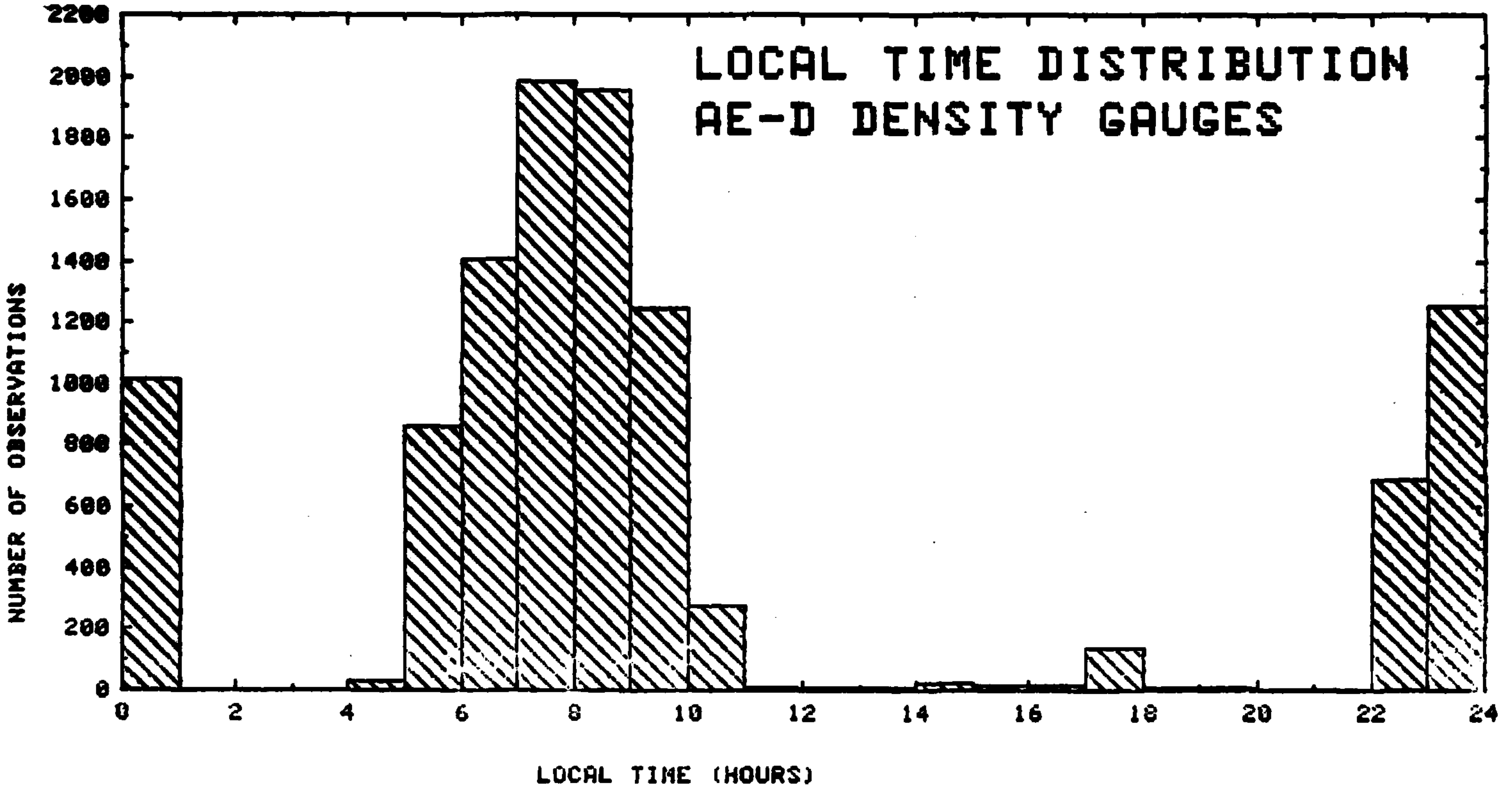
LOCAL TIME DISTRIBUTION
AE-D DENSITY GAUGES
NUMBER OF OBSERVATIONS
0
200
400
600
800
1000
1200
1400
1600
1800
2000
2200
0
2
4
6
8
10
12
14
16
18
20
22
24
LOCAL TIME (HOURS)

Figure 2-27.

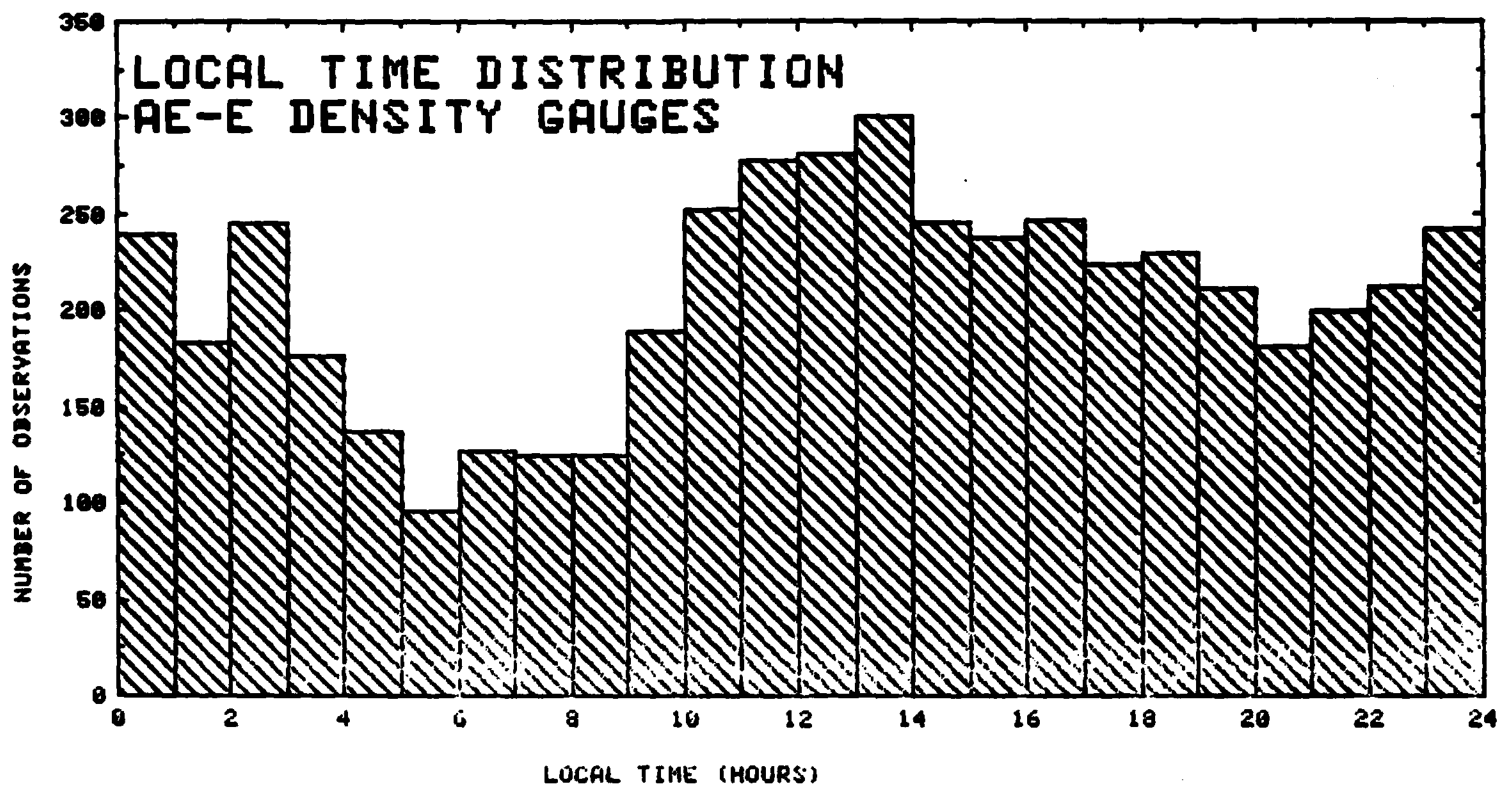
LOCAL TIME DISTRIBUTION
AE-E DENSITY GAUGES
NUMBER OF OBSERVATIONS
0
50
100
150
200
250
300
350
0
2
4
6
8
10
12
14
16
18
20
22
24
LOCAL TIME (HOURS)

Figure 2-28.

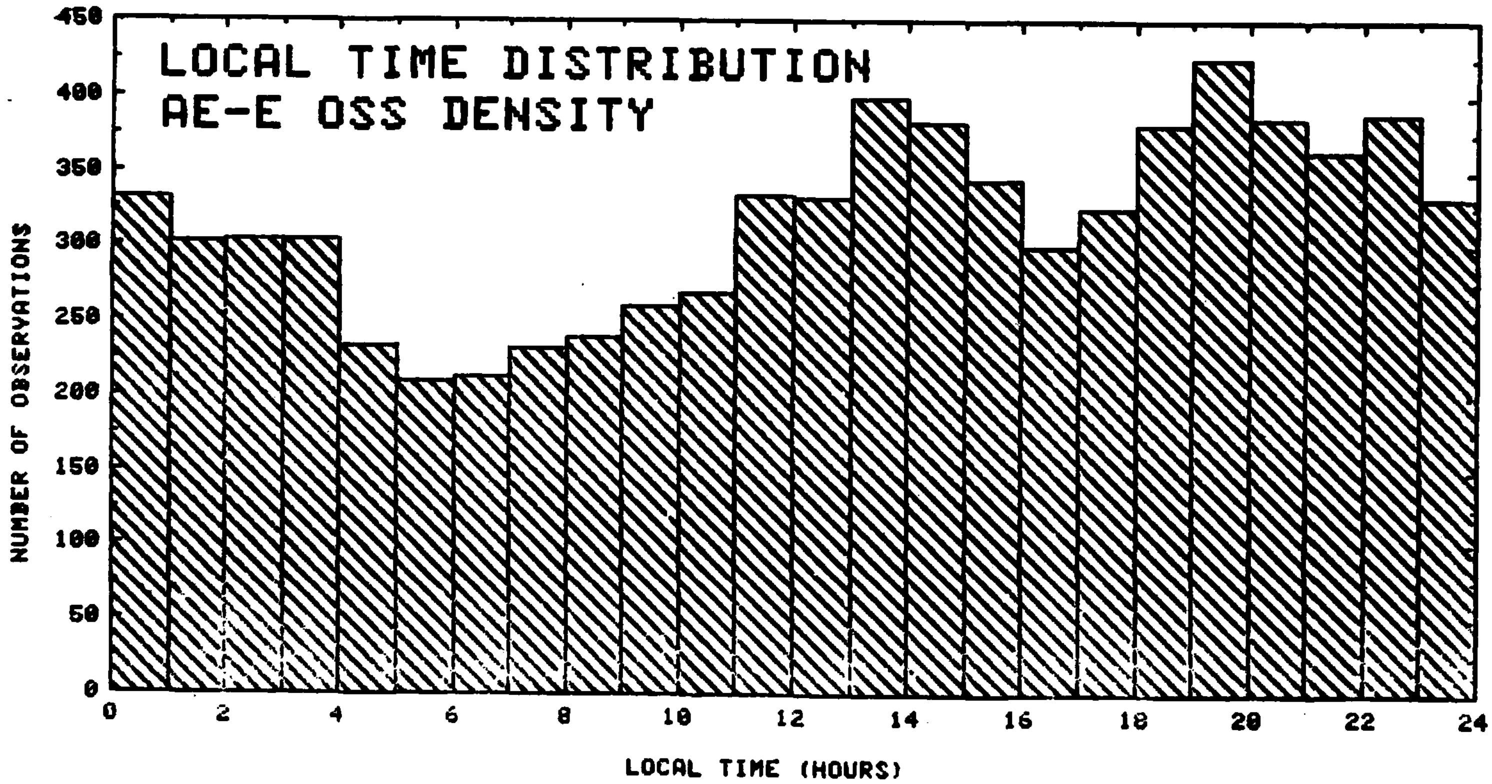

LOCAL TIME DISTRIBUTION
AE-E OSS DENSITY
NUMBER OF OBSERVATIONS
0
50
100
150
200
250
300
350
400
450
0
2
4
6
8
10
12
14
16
18
20
22
24
LOCAL TIME (HOURS)

Figure 2-29.

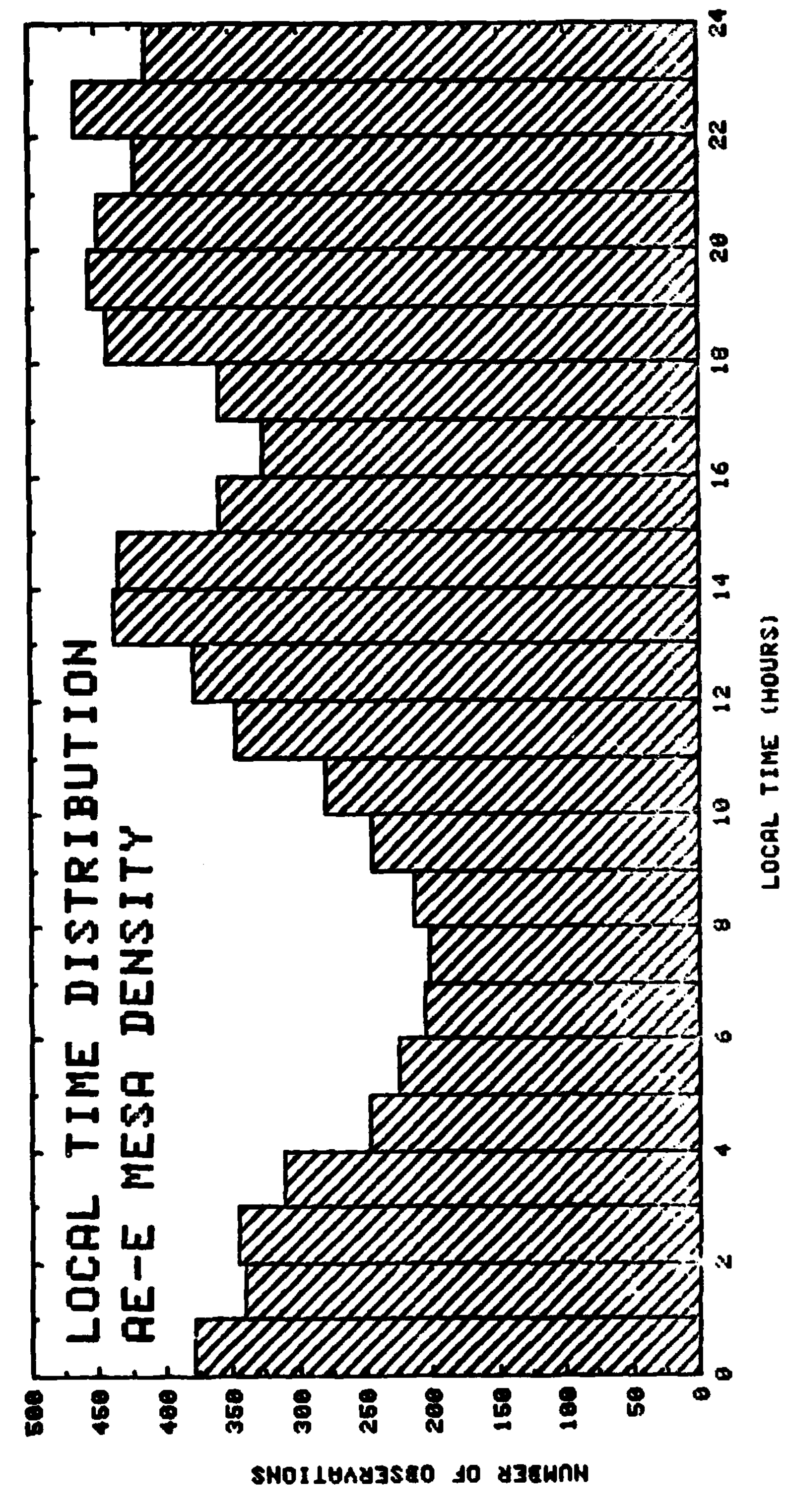
LOCAL TIME DISTRIBUTION
AE-E MESA DENSITY
NUMBER OF OBSERVATIONS
0
50
100
150
200
250
300
350
400
450
500
LOCAL TIME (HOURS)
0
2
4
6
8
10
12
14
16
18
20
22
24

Figure 2-30.

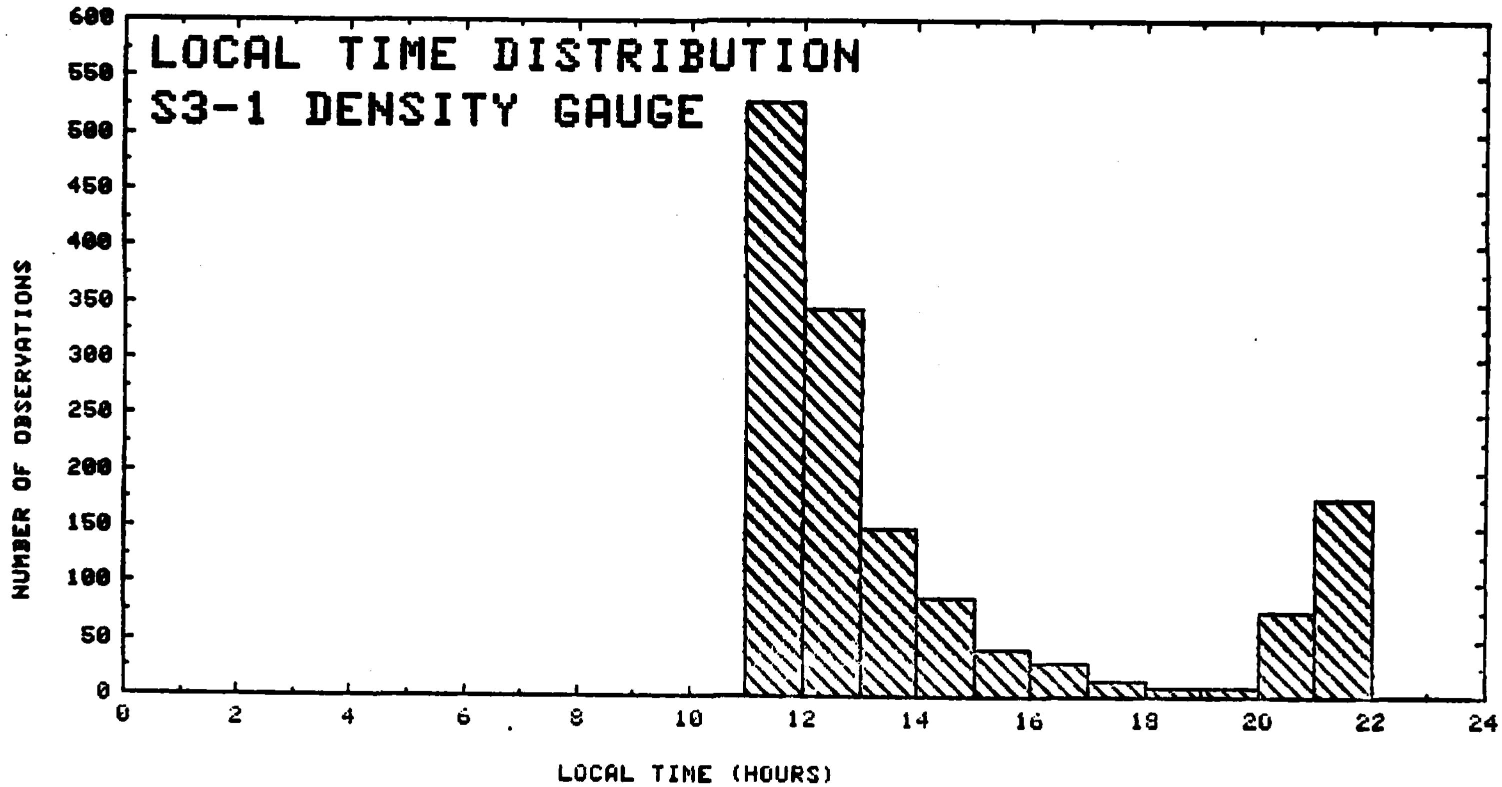
LOCAL TIME DISTRIBUTION
S3-1 DENSITY GAUGE
NUMBER OF OBSERVATIONS
LOCAL TIME (HOURS)
0
50
100
150
200
250
300
350
400
450
500
550
600
0
2
4
6
8
10
12
14
16
18
20
22
24

Figure 2-31.

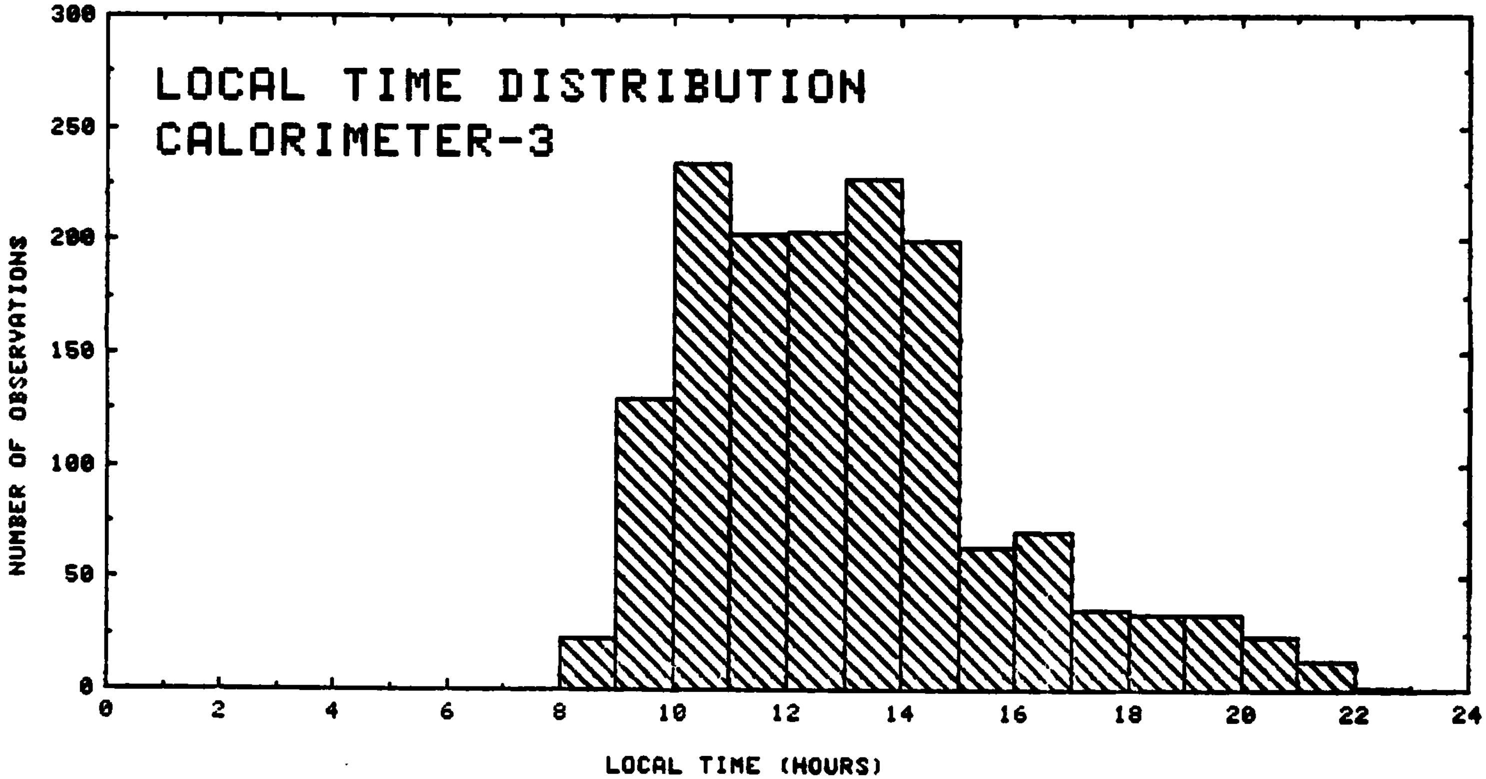
LOCAL TIME DISTRIBUTION
CALORIMETER-3
NUMBER OF OBSERVATIONS
0
50
100
150
200
250
300
0
2
4
6
8
10
12
14
16
18
20
22
24
LOCAL TIME (HOURS)

Figure 2-32.

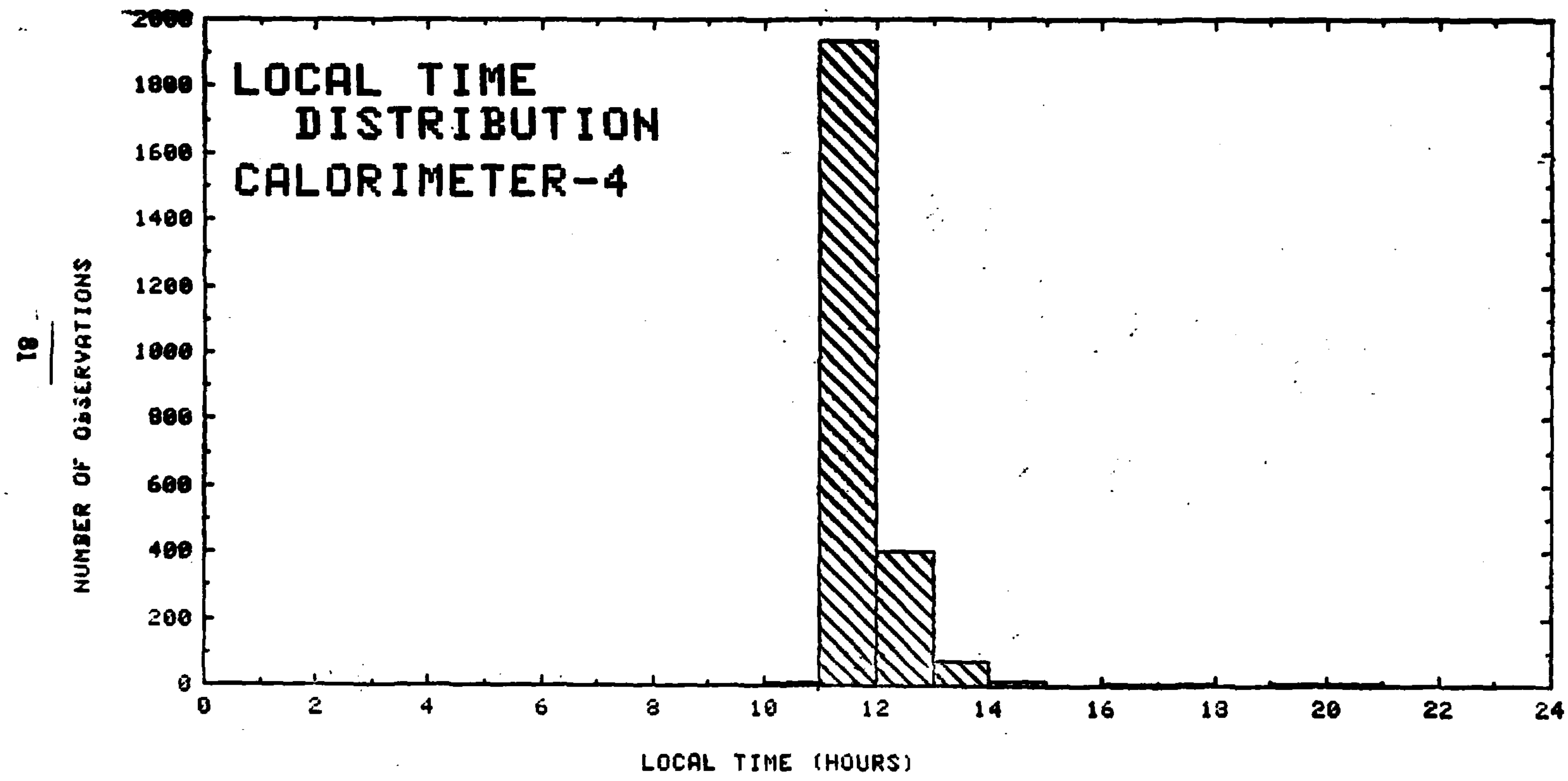
LOCAL TIME
DISTRIBUTION
CALORIMETER-4
NUMBER OF OBSERVATIONS
2000
1800
1600
1400
1200
1000
800
600
400
200
0
0
2
4
6
8
10
12
14
16
18
20
22
24
LOCAL TIME (HOURS)

Figure 2-33.

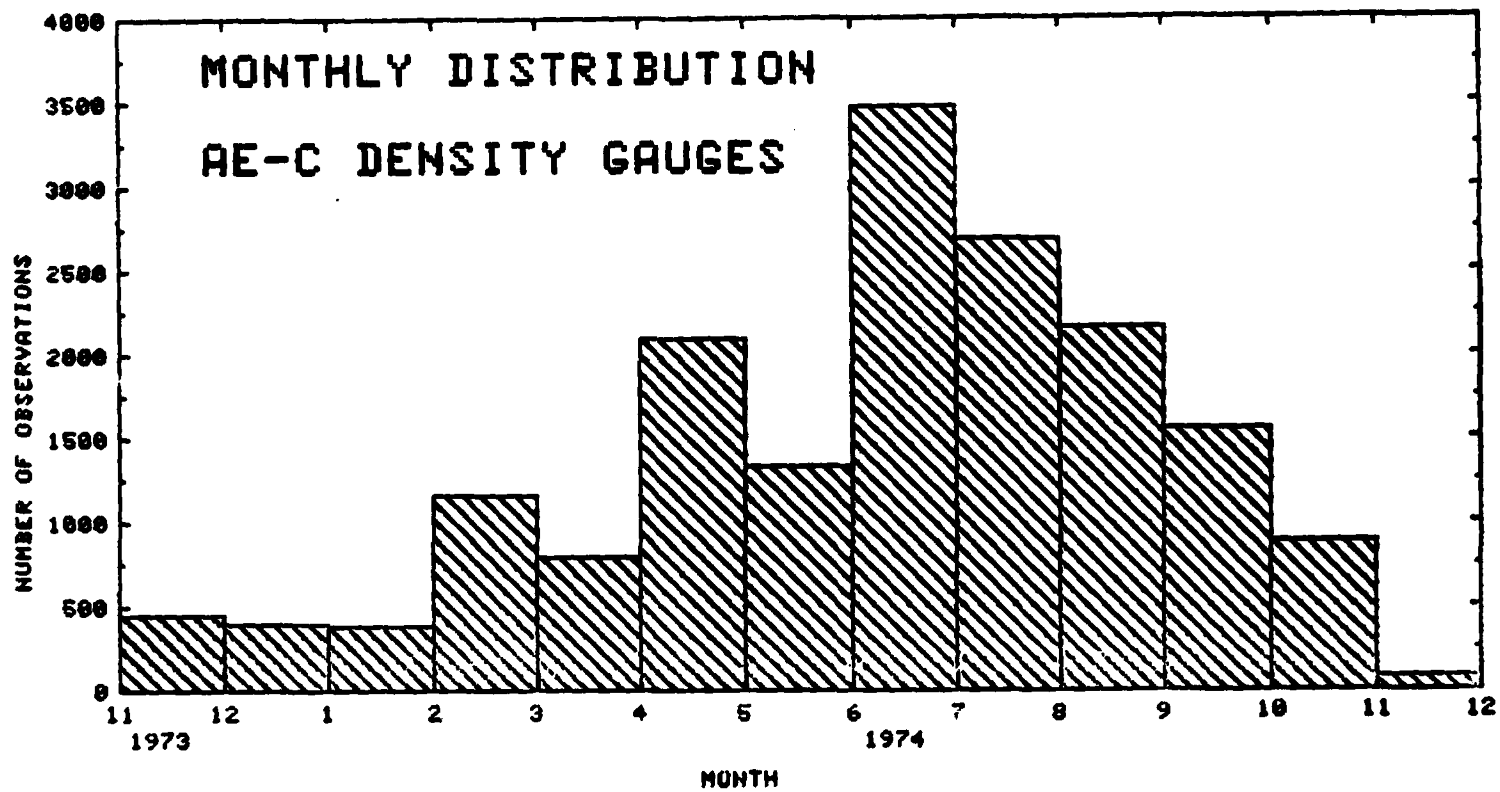
MONTHLY DISTRIBUTION
AE-C DENSITY GAUGES
NUMBER OF OBSERVATIONS
0
500
1000
1500
2000
2500
3000
3500
4000
11
12
1
2
3
4
5
6
7
8
9
10
11
12
1973
1974
MONTH

Figure 2-34.

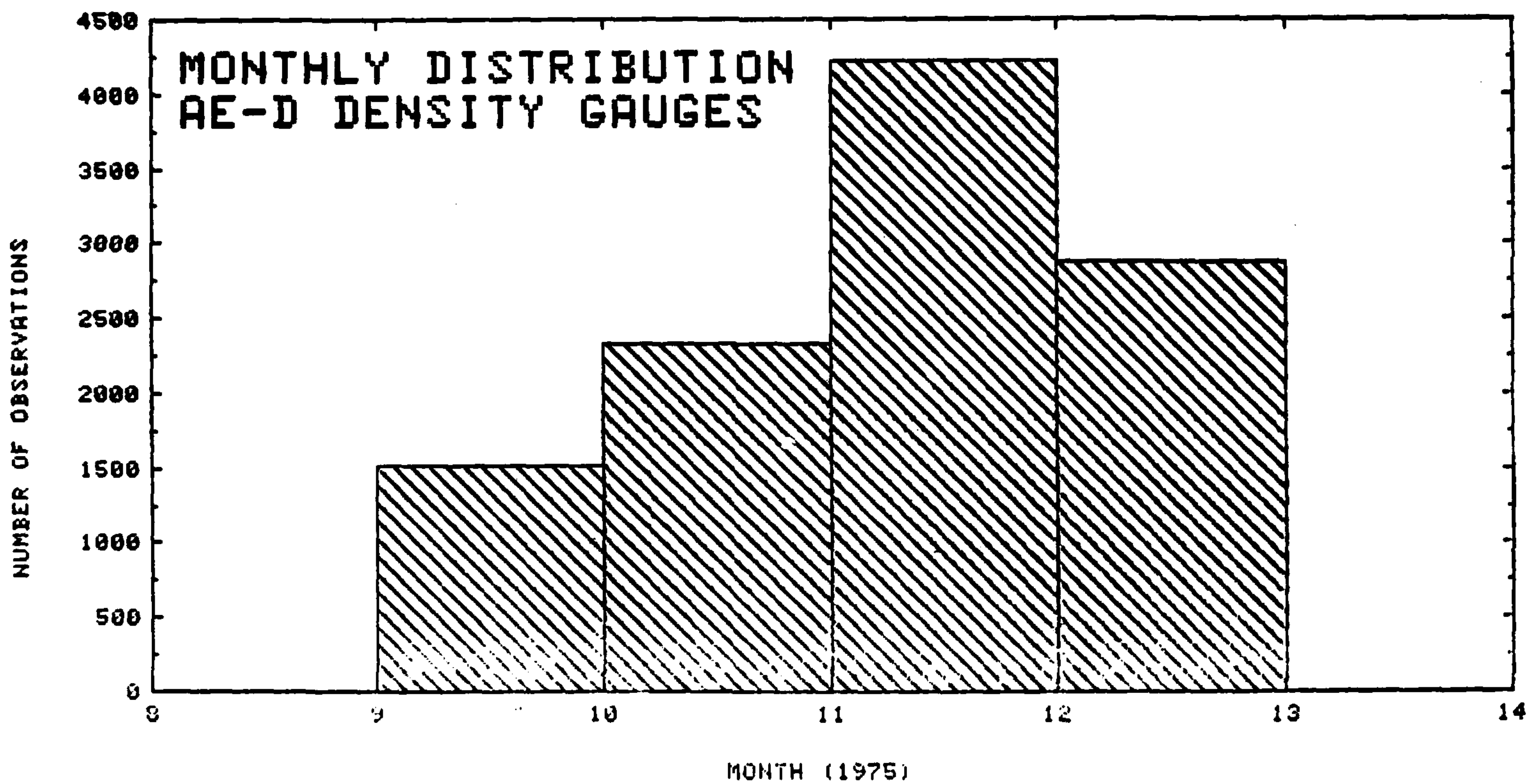
MONTHLY DISTRIBUTION
AE-D DENSITY GAUGES
NUMBER OF OBSERVATIONS
4500
4000
3500
3000
2500
2000
1500
1000
500
0
8
9
10
11
12
13
14
MONTH (1975)

Figure 2-35.

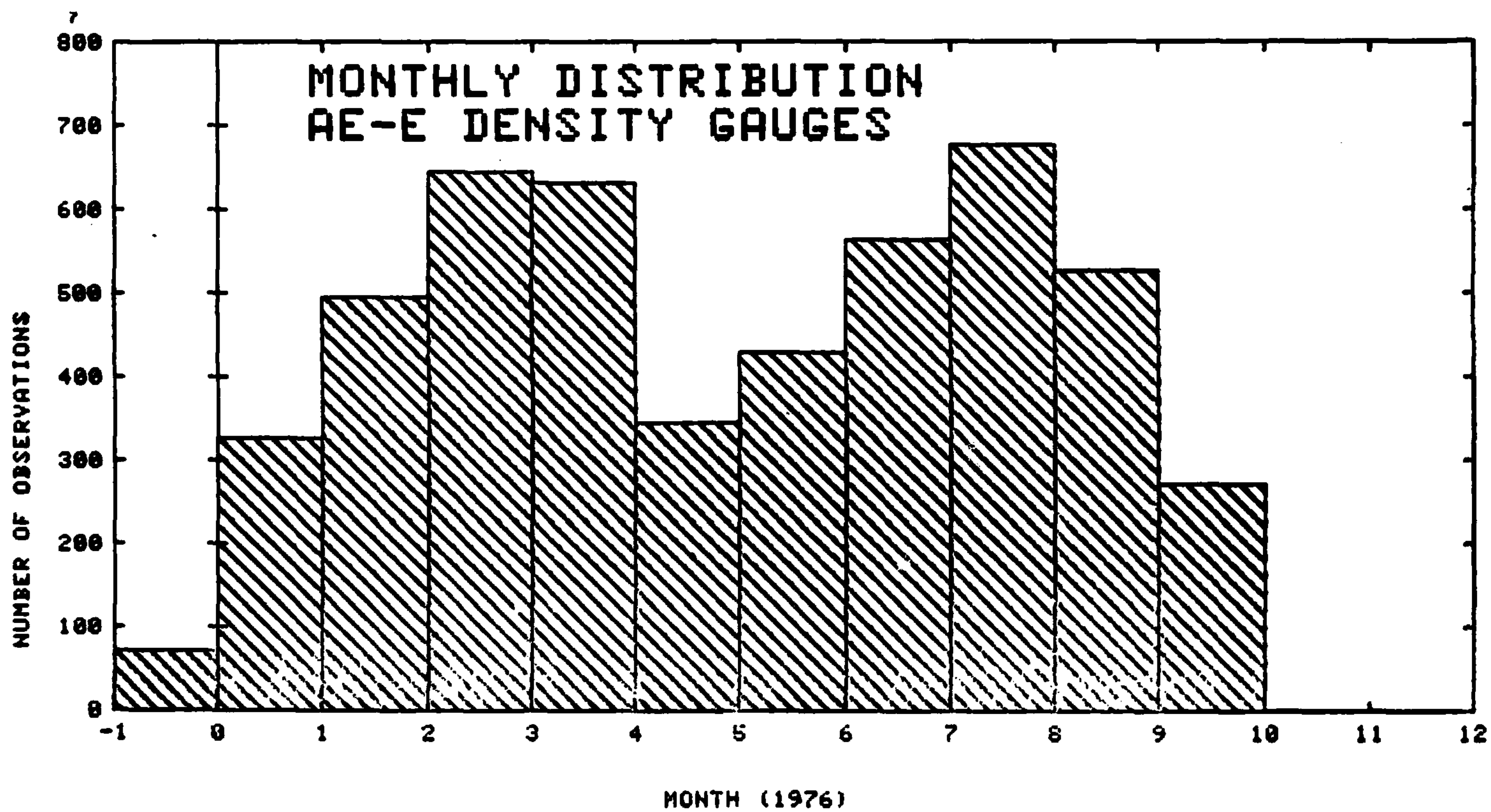
MONTHLY DISTRIBUTION
AE-E DENSITY GAUGES
NUMBER OF OBSERVATIONS
800
700
600
500
400
300
200
100
0
-1
0
1
2
3
4
5
6
7
8
9
10
11
12
MONTH (1976)

Figure 2-36.

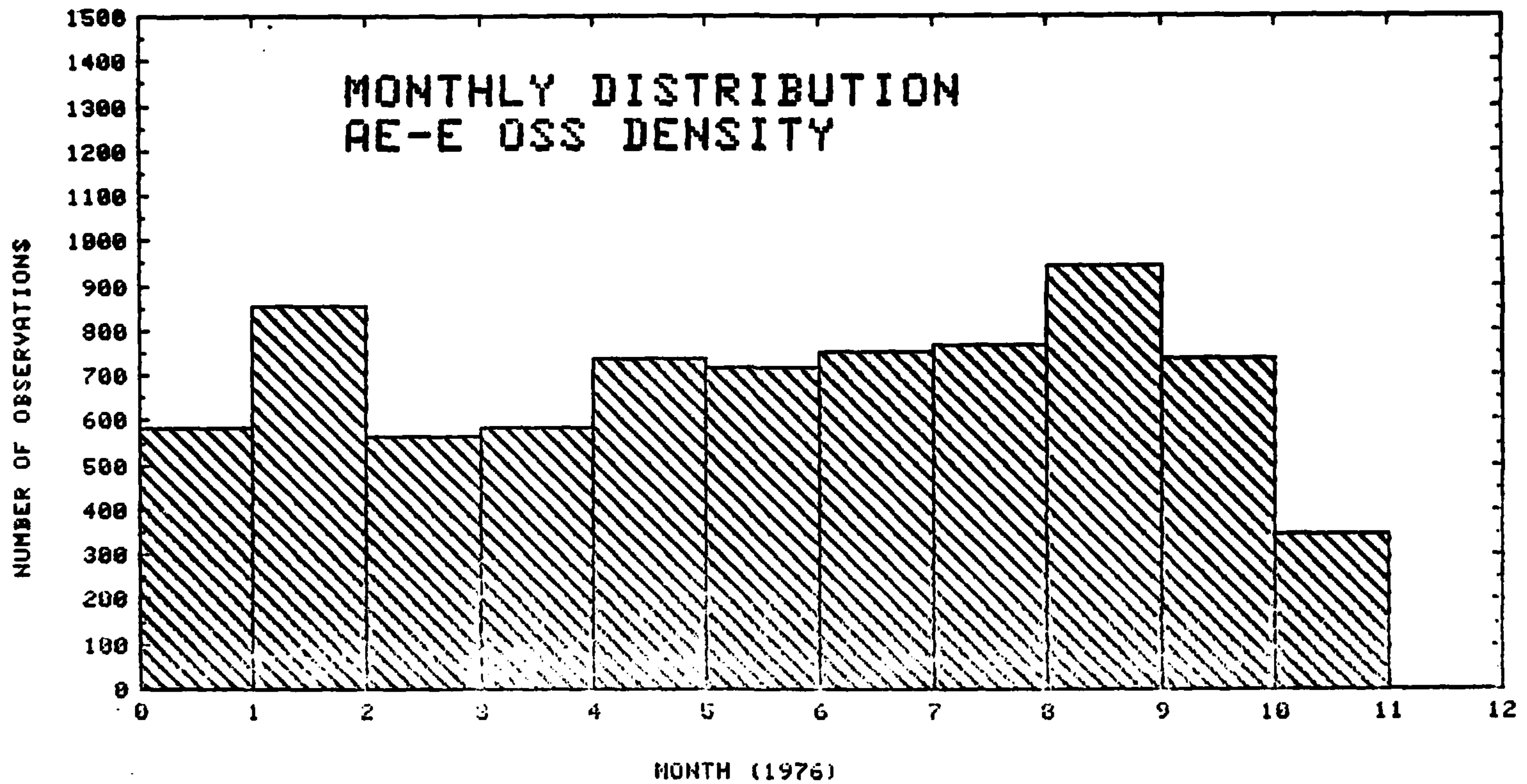
MONTHLY DISTRIBUTION
AE-E OSS DENSITY
NUMBER OF OBSERVATIONS
1500
1400
1300
1200
1100
1000
900
800
700
600
500
400
300
200
100
0
0 1 2 3 4 5 6 7 8 9 10 11 12
MONTH (1976)

Figure 2-37.

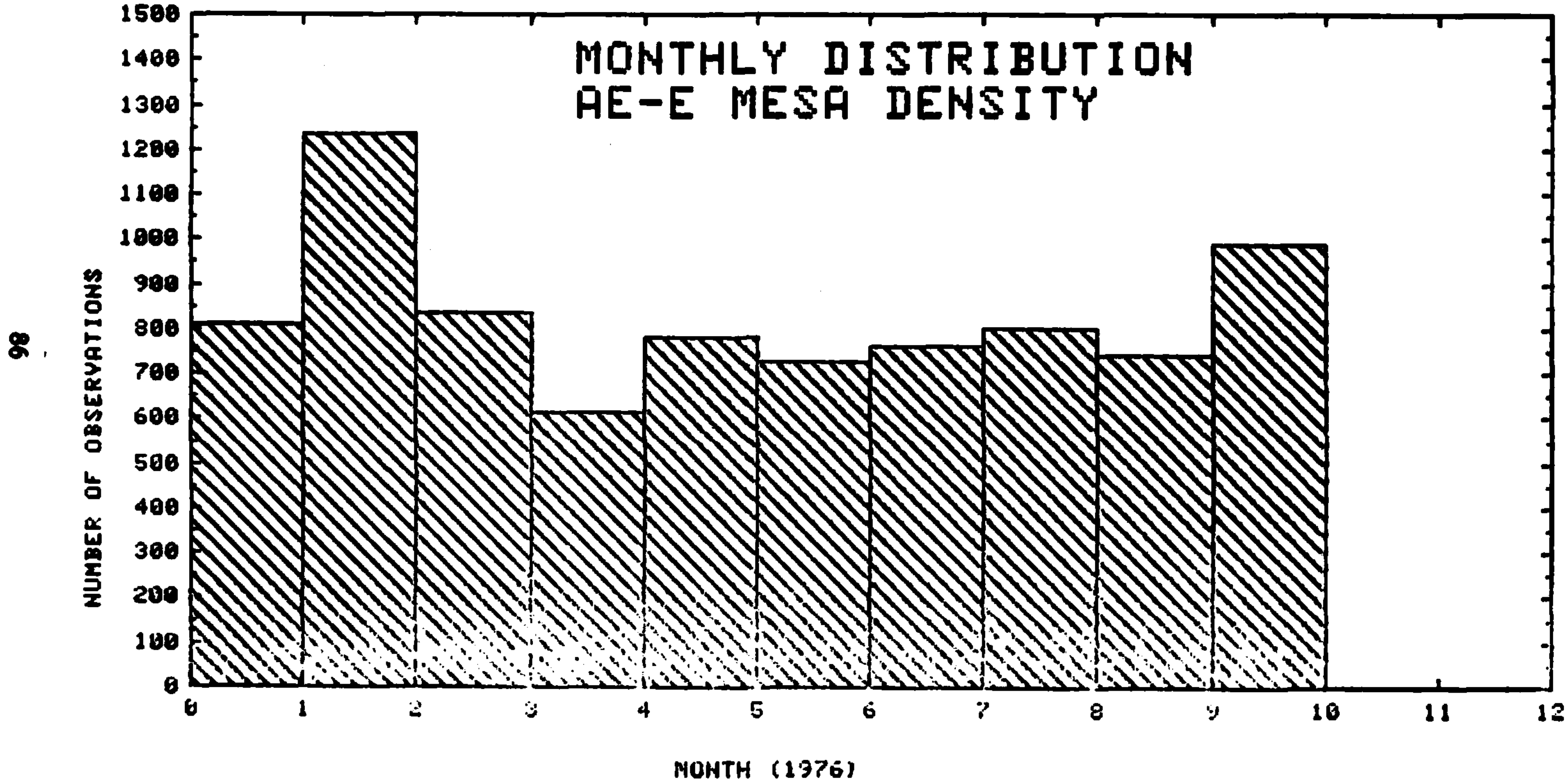
MONTHLY DISTRIBUTION
AE-E MESA DENSITY
NUMBER OF OBSERVATIONS
0
100
200
300
400
500
600
700
800
900
1000
1100
1200
1300
1400
1500
0
1
2
3
4
5
6
7
8
9
10
11
12
MONTH (1976)

Figure 2-38.

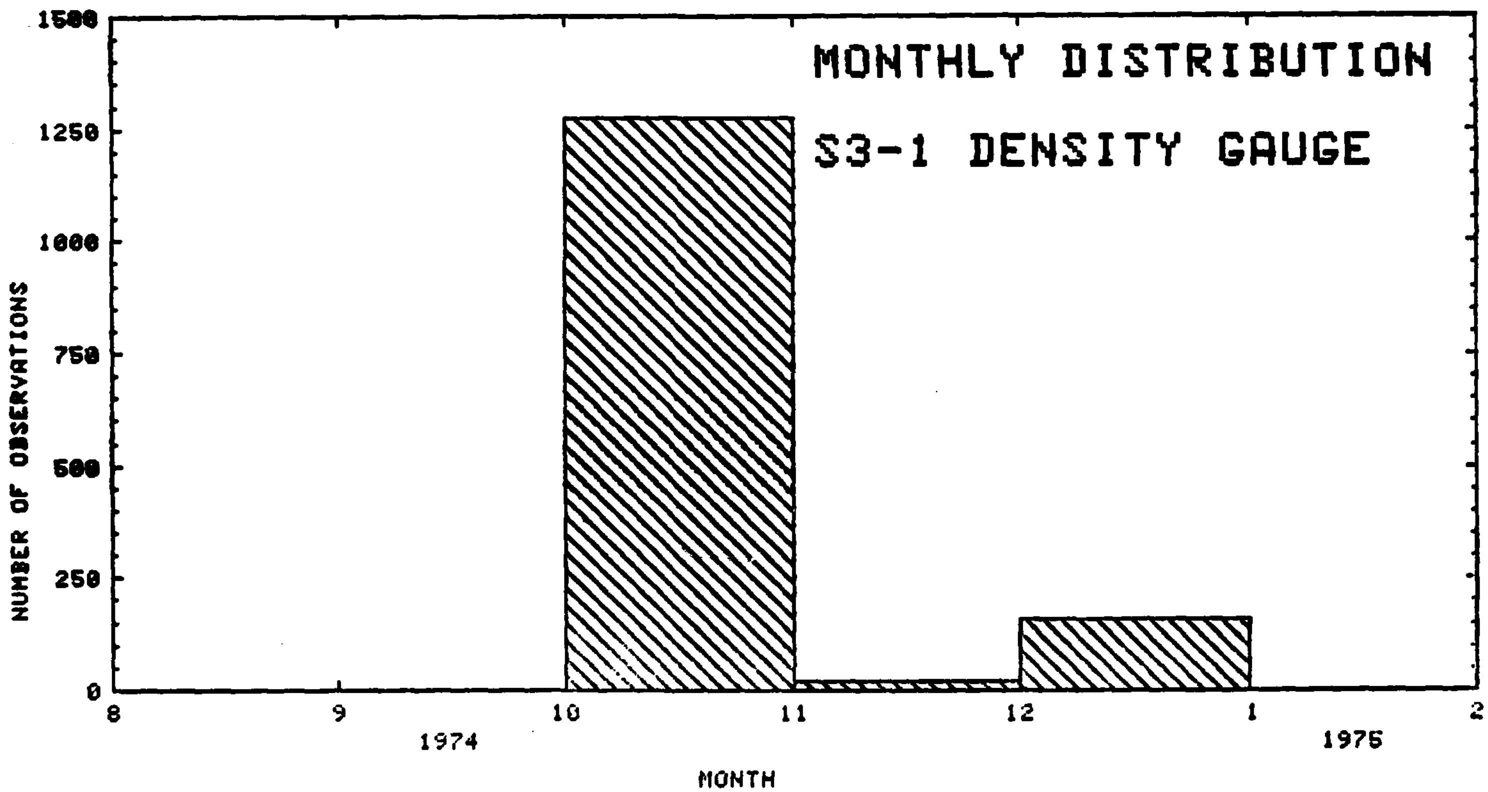
MONTHLY DISTRIBUTION
S3-1 DENSITY GAUGE
NUMBER OF OBSERVATIONS
1500
1250
1000
750
500
250
0
8
9
10
11
12
1
2
1974
1975
MONTH

Figure 2-39.

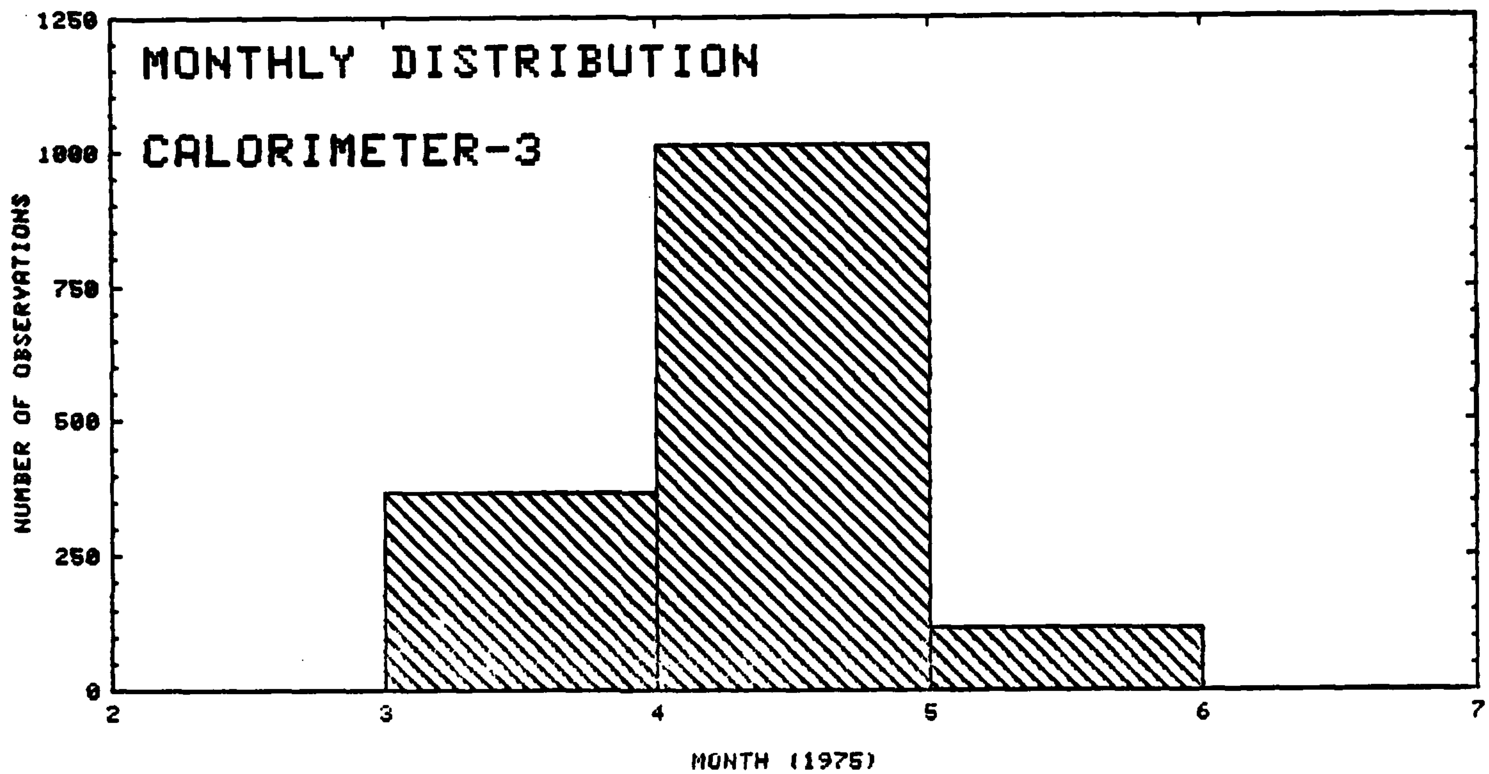

MONTHLY DISTRIBUTION
CALORIMETER-3
1250
1000
750
500
250
0
NUMBER OF OBSERVATIONS
2
3
4
5
6
7
MONTH (1975)

Figure 2-40.

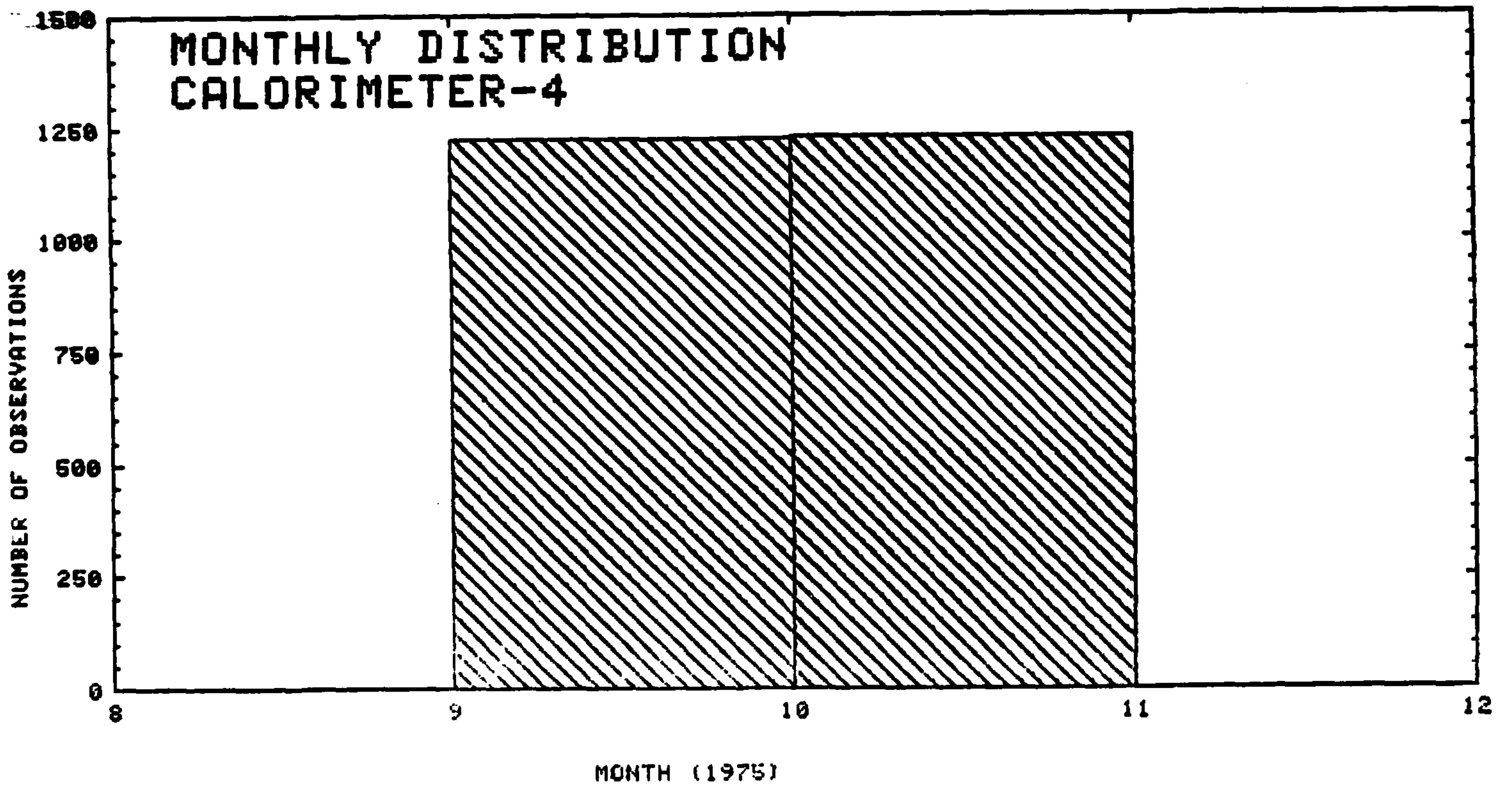
MONTHLY DISTRIBUTION
CALORIMETER-4
NUMBER OF OBSERVATIONS
1500
1250
1000
750
500
250
0
8
9
10
11
12
MONTH (1975)

Figure 2-41.

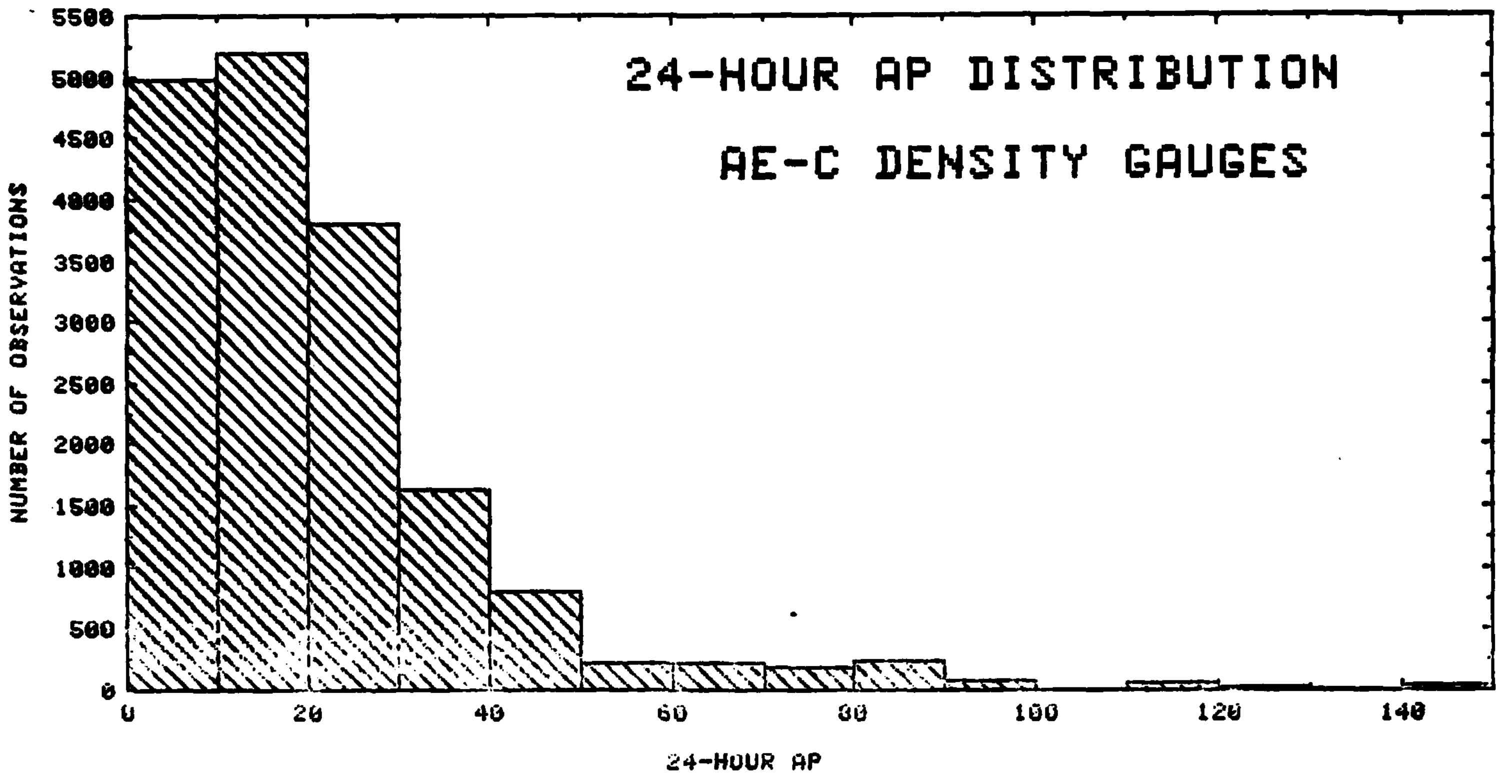
24-HOUR AP DISTRIBUTION
AE-C DENSITY GAUGES
NUMBER OF OBSERVATIONS
5500
5000
4500
4000
3500
3000
2500
2000
1500
1000
500
0
0
20
40
60
80
100
120
140
24-HOUR AP

Figure 2-42.

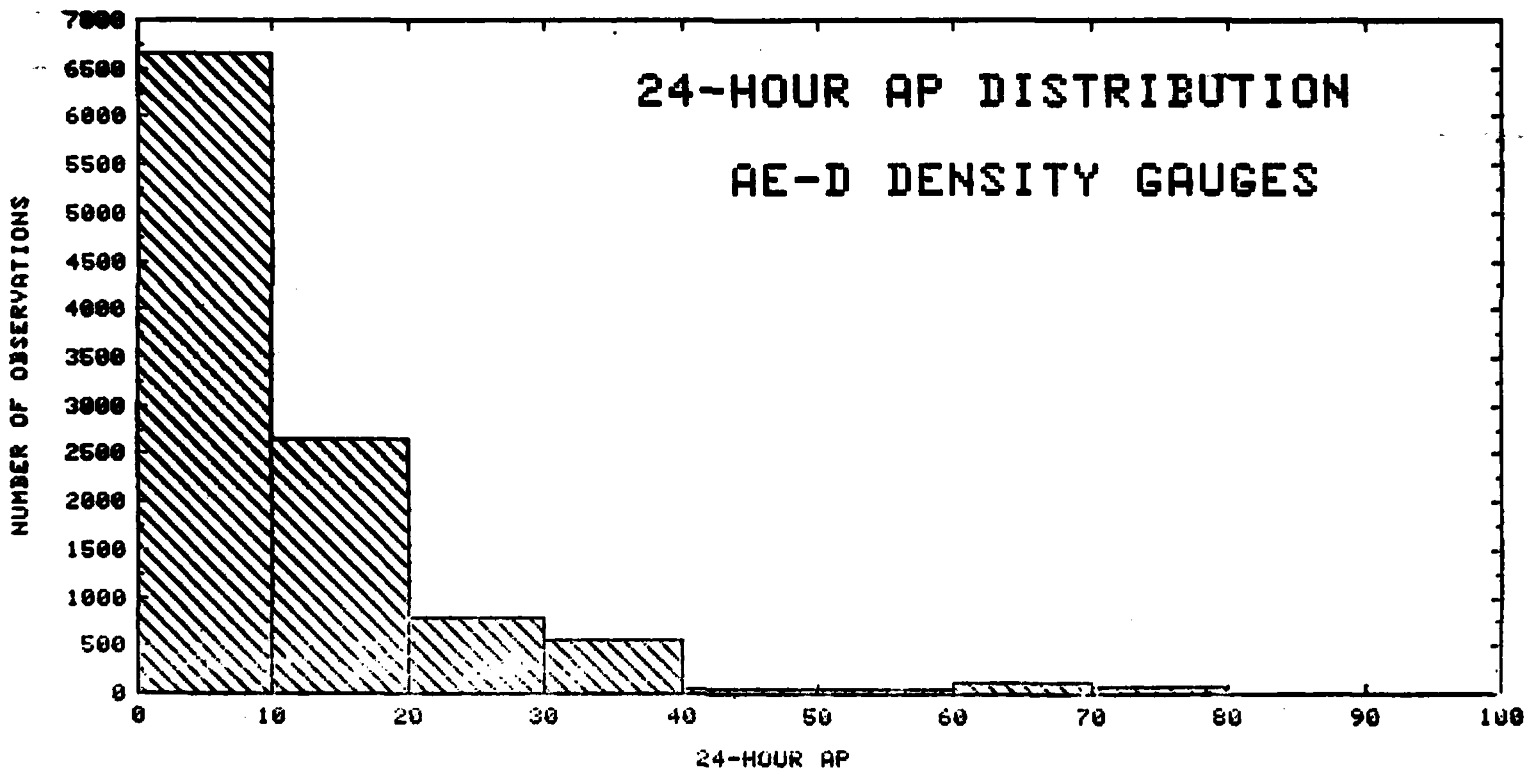
24-HOUR AP DISTRIBUTION
AE-D DENSITY GAUGES
NUMBER OF OBSERVATIONS
7000
6500
6000
5500
5000
4500
4000
3500
3000
2500
2000
1500
1000
500
0
0
10
20
30
40
50
60
70
80
90
100
24-HOUR AP

Figure 2-43.

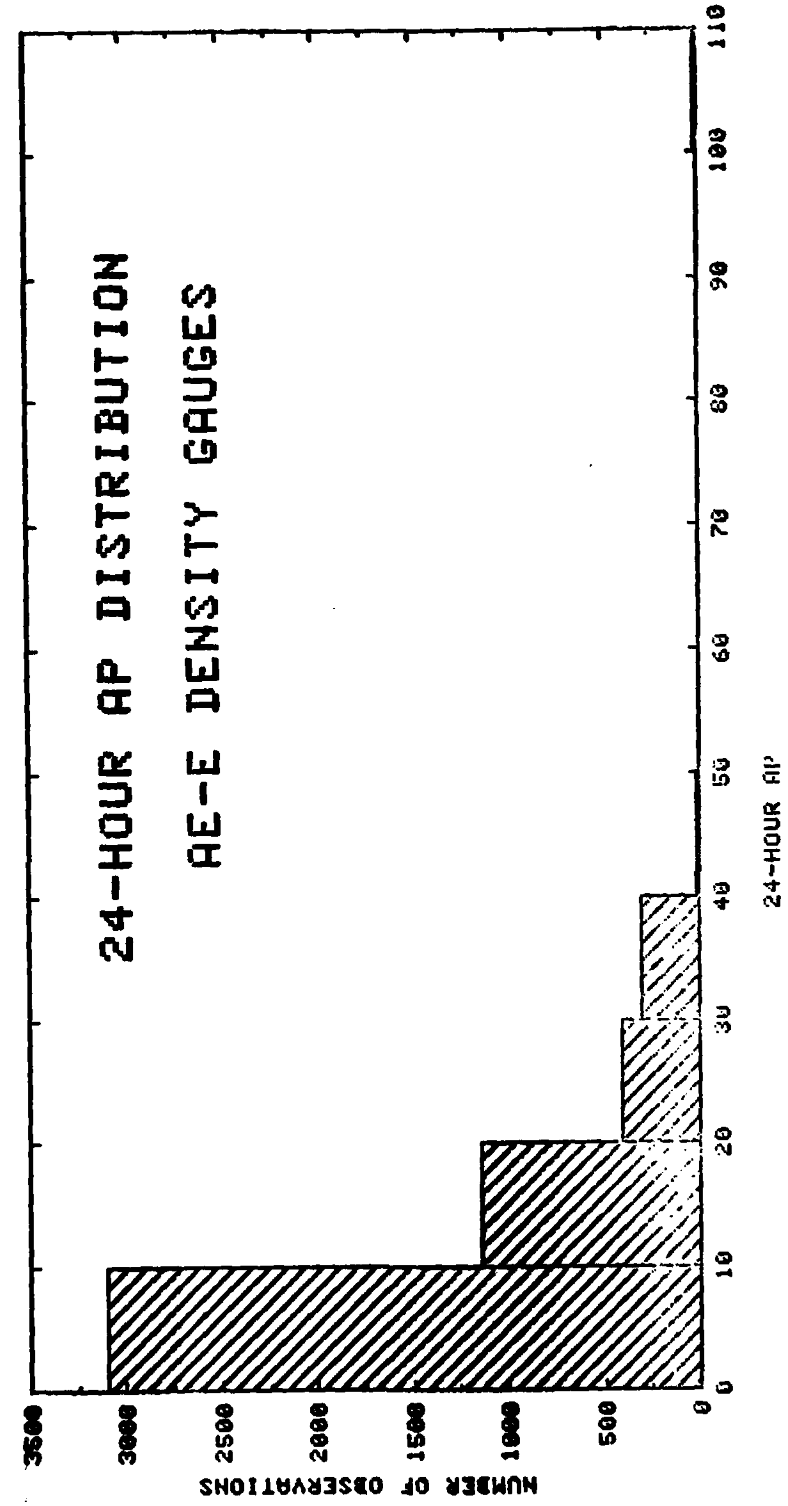
24-HOUR AP DISTRIBUTION
AE-E DENSITY GAUGES
NUMBER OF OBSERVATIONS
0
500
1000
1500
2000
2500
3000
3500
0
10
20
30
40
50
60
70
80
90
100
110
24-HOUR AP

Figure 2-44.

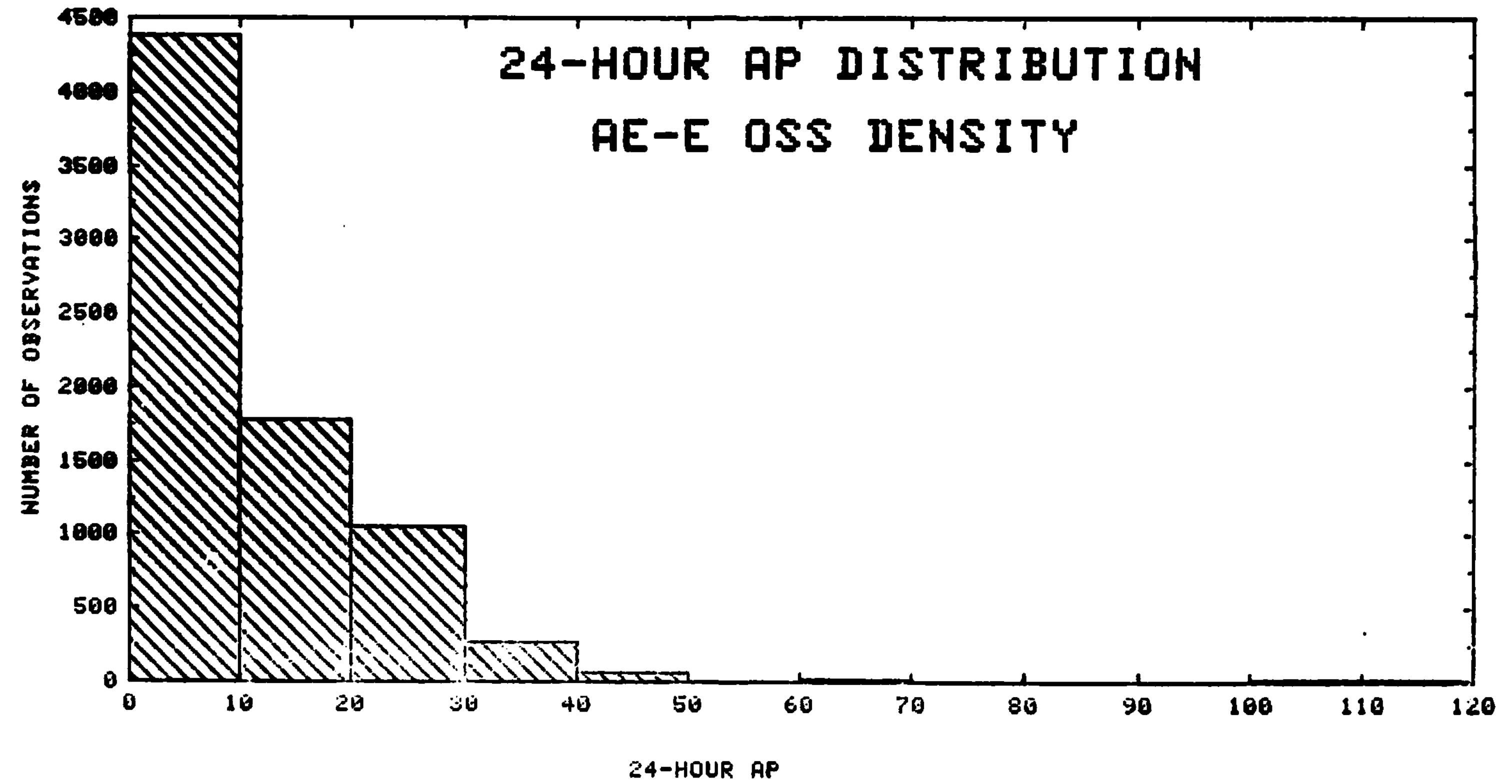
24-HOUR AP DISTRIBUTION
AE-E OSS DENSITY
NUMBER OF OBSERVATIONS
0
500
1000
1500
2000
2500
3000
3500
4000
4500
0
10
20
30
40
50
60
70
80
90
100
110
120
24-HOUR AP

Figure 2-45.

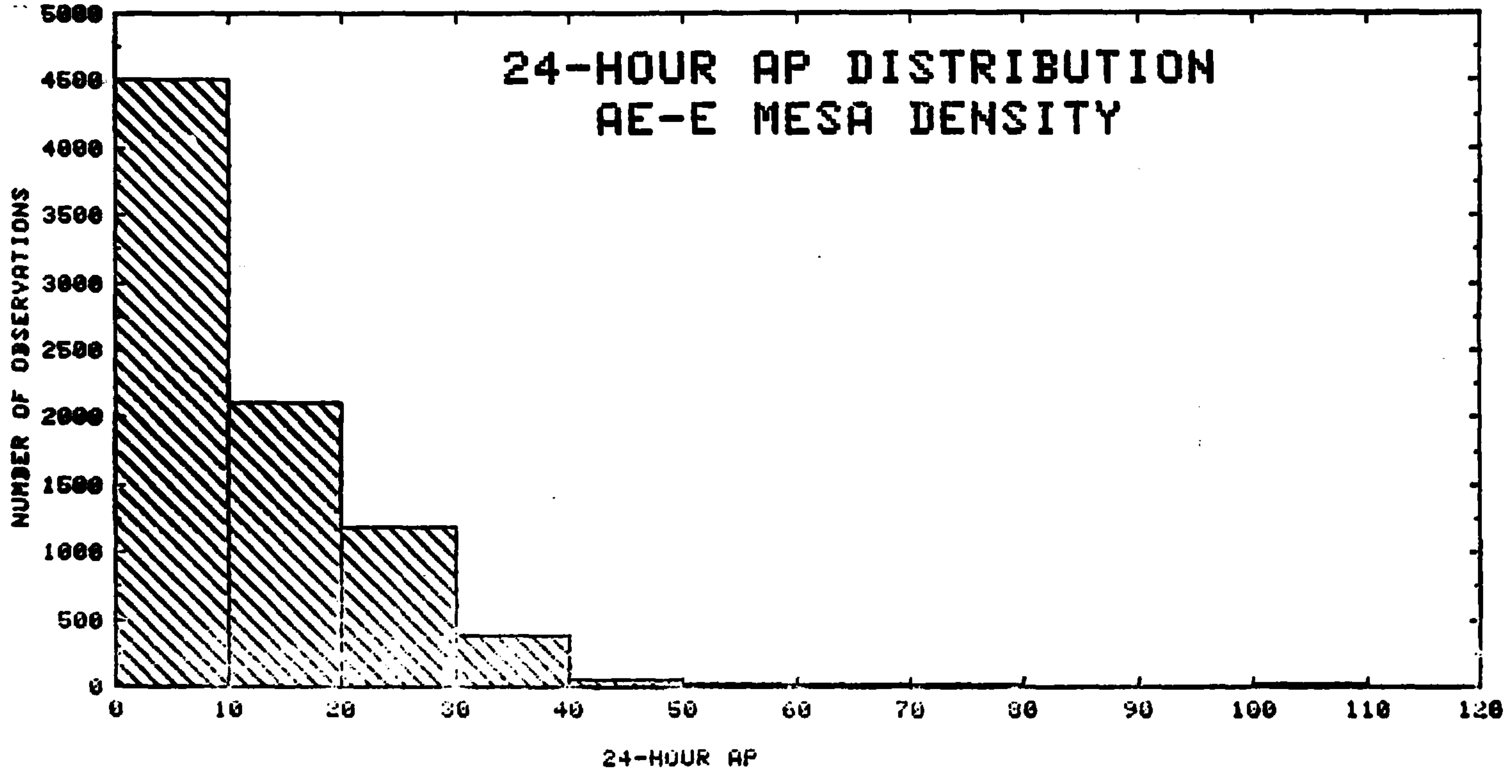

24-HOUR AP DISTRIBUTION
AE-E MESA DENSITY
NUMBER OF OBSERVATIONS
0
500
1000
1500
2000
2500
3000
3500
4000
4500
5000
0
10
20
30
40
50
60
70
80
90
100
110
120
24-HOUR AP

Figure 2-46.

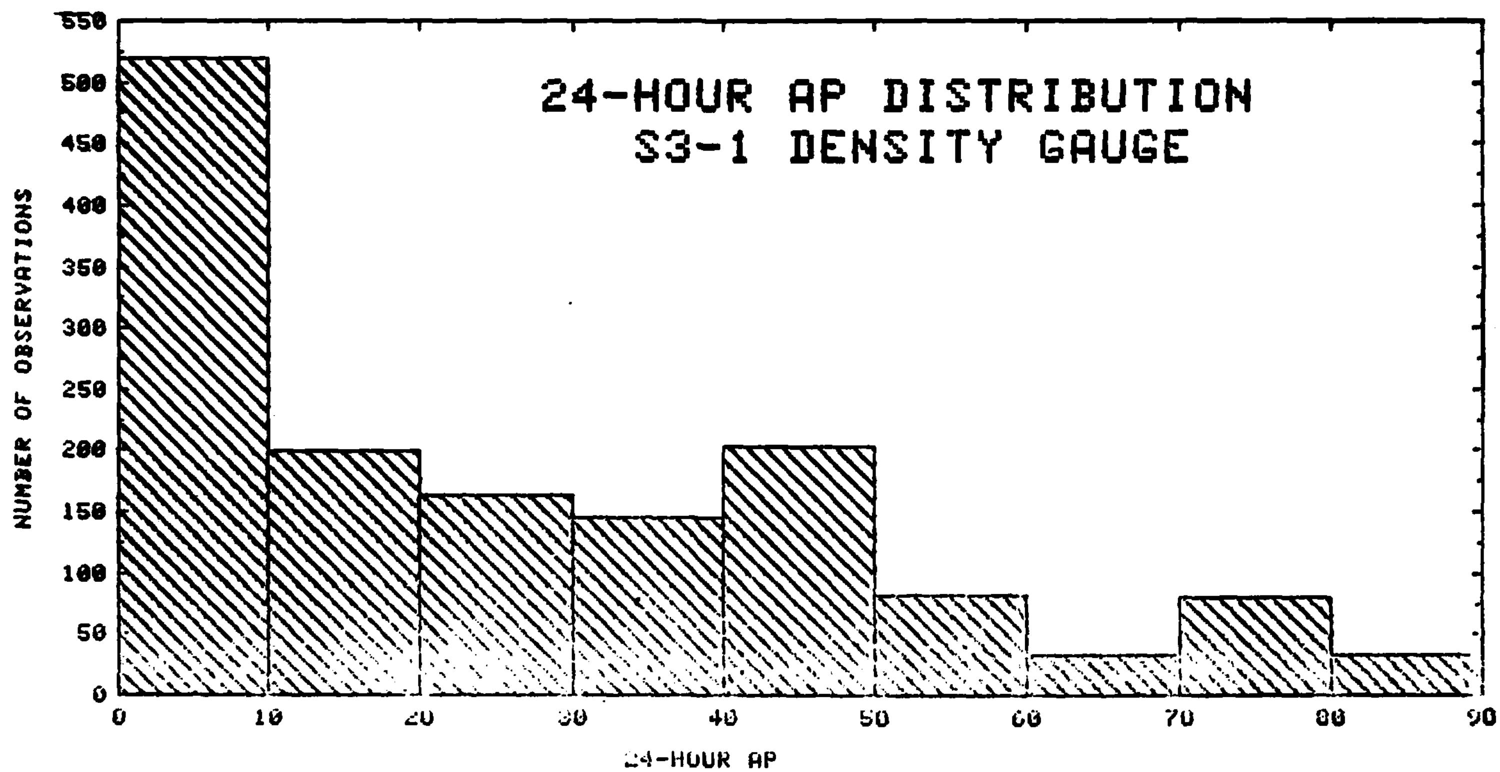
24-HOUR AP DISTRIBUTION
S3-1 DENSITY GAUGE
NUMBER OF OBSERVATIONS
550
500
450
400
350
300
250
200
150
100
50
0
0
10
20
30
40
50
60
70
80
90
24-HOUR AP

Figure 2-47.

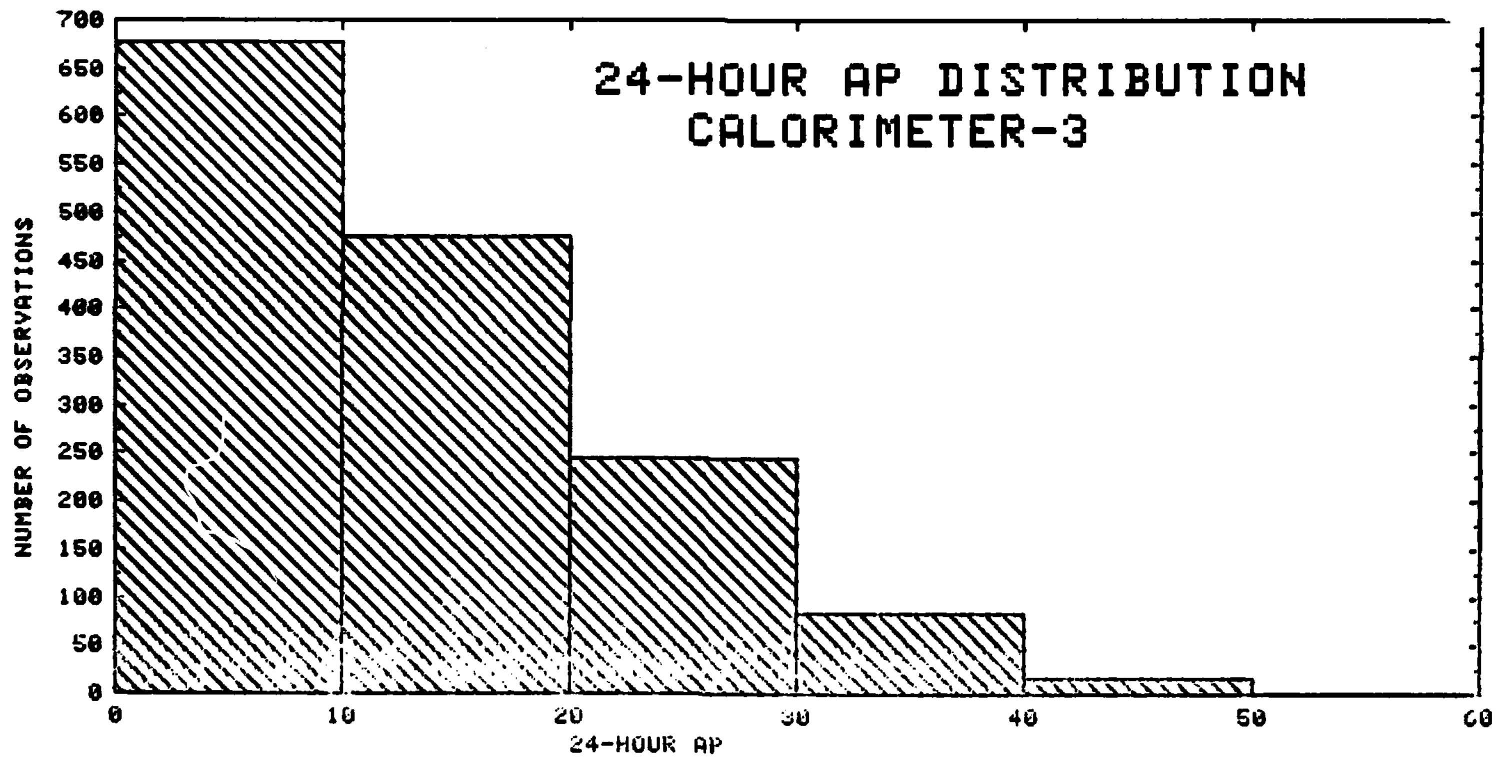
24-HOUR AP DISTRIBUTION
CALORIMETER-3
NUMBER OF OBSERVATIONS
700
650
600
550
500
450
400
350
300
250
200
150
100
50
0
0
10
20
30
40
50
60
24-HOUR AP

Figure 2-48.

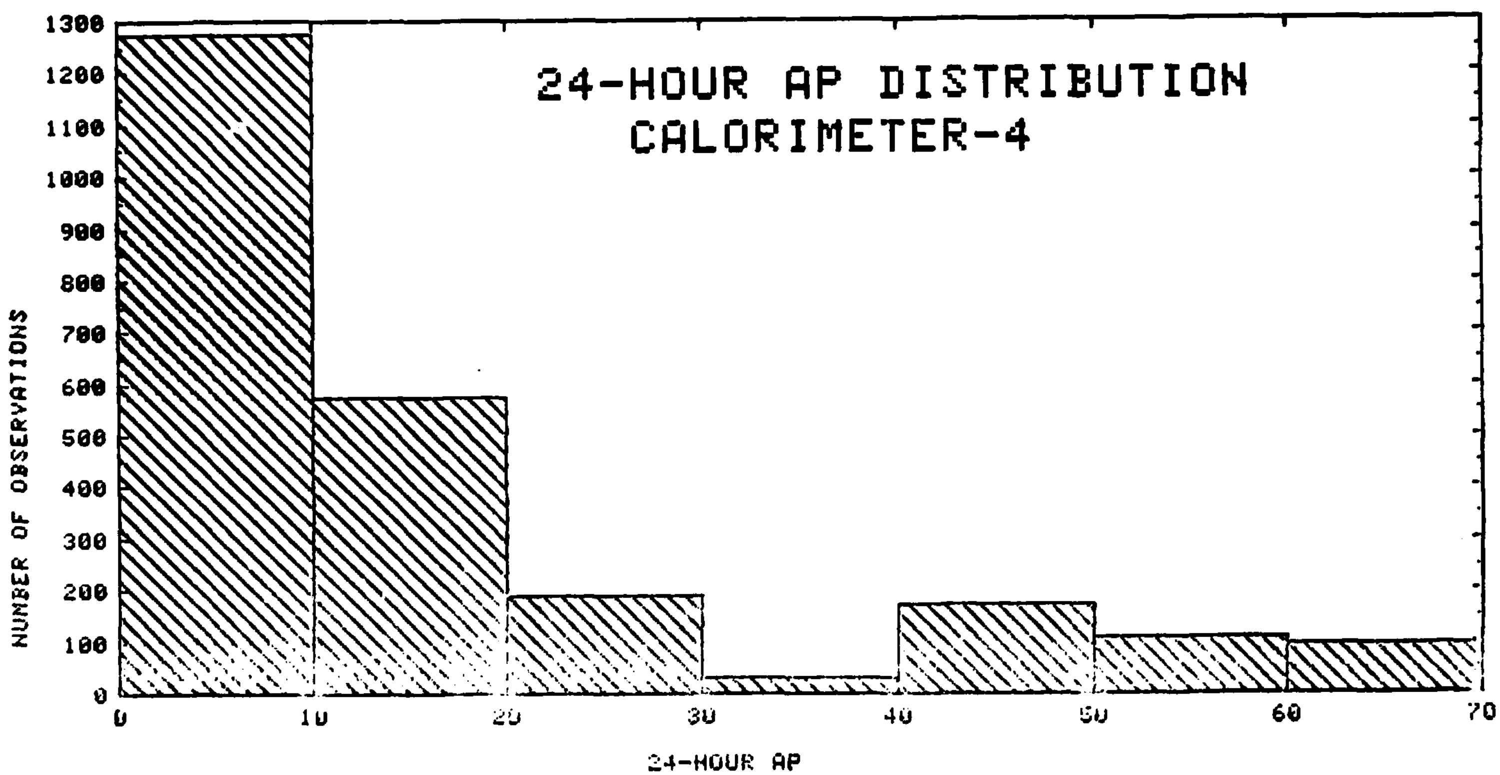
24-HOUR AP DISTRIBUTION
CALORIMETER-4
NUMBER OF OBSERVATIONS
0
100
200
300
400
500
600
700
800
900
1000
1100
1200
1300
24-HOUR AP
0
10
20
30
40
50
60
70

Figure 2-49.

AD-A128 005 A COMPARISON OF THE MSIS AND JACCHIA-70 MODELS WITH MEASURED ATMOSPHERIC..(U) AEROSPACE CORP EL SEGUNDO CA SPACE SCIENCES LAB A B PRAG 20 APR 83 2/2

UNCLASSIFIED TR-0083(3940-04)-1 SD-TR-83-25 F/G 4/1 NL

END
DATE
FILMED
DTIC

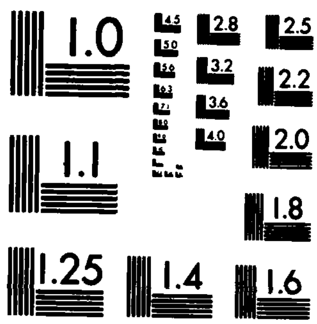

MICROCOPY RESOLUTION TEST CHART
NATIONAL BUREAU OF STANDARDS-1963-A

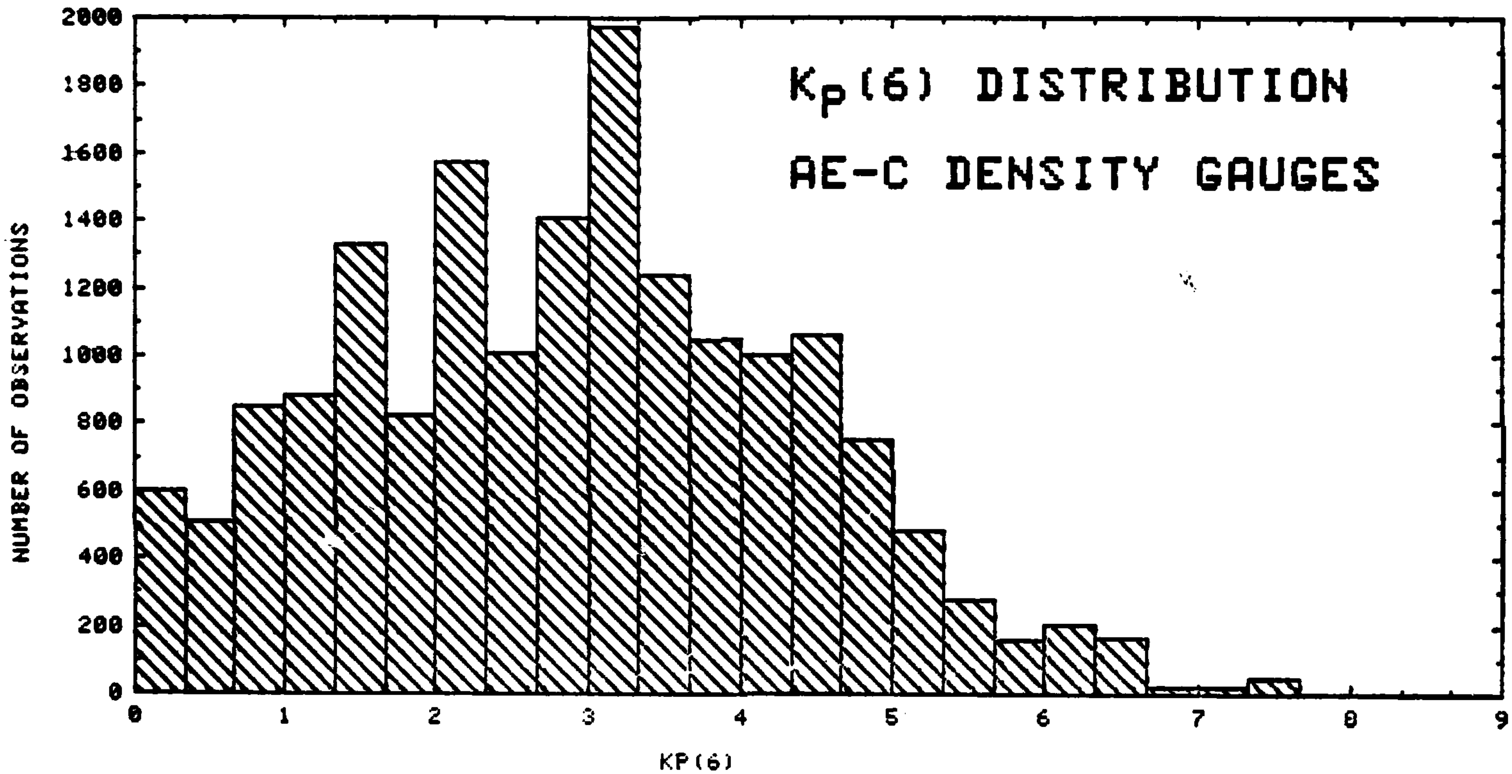

K_p(6) DISTRIBUTION
AE-C DENSITY GAUGES
NUMBER OF OBSERVATIONS
0
200
400
600
800
1000
1200
1400
1600
1800
2000
0
1
2
3
4
5
6
7
8
9
KP(6)

Figure 2-50.

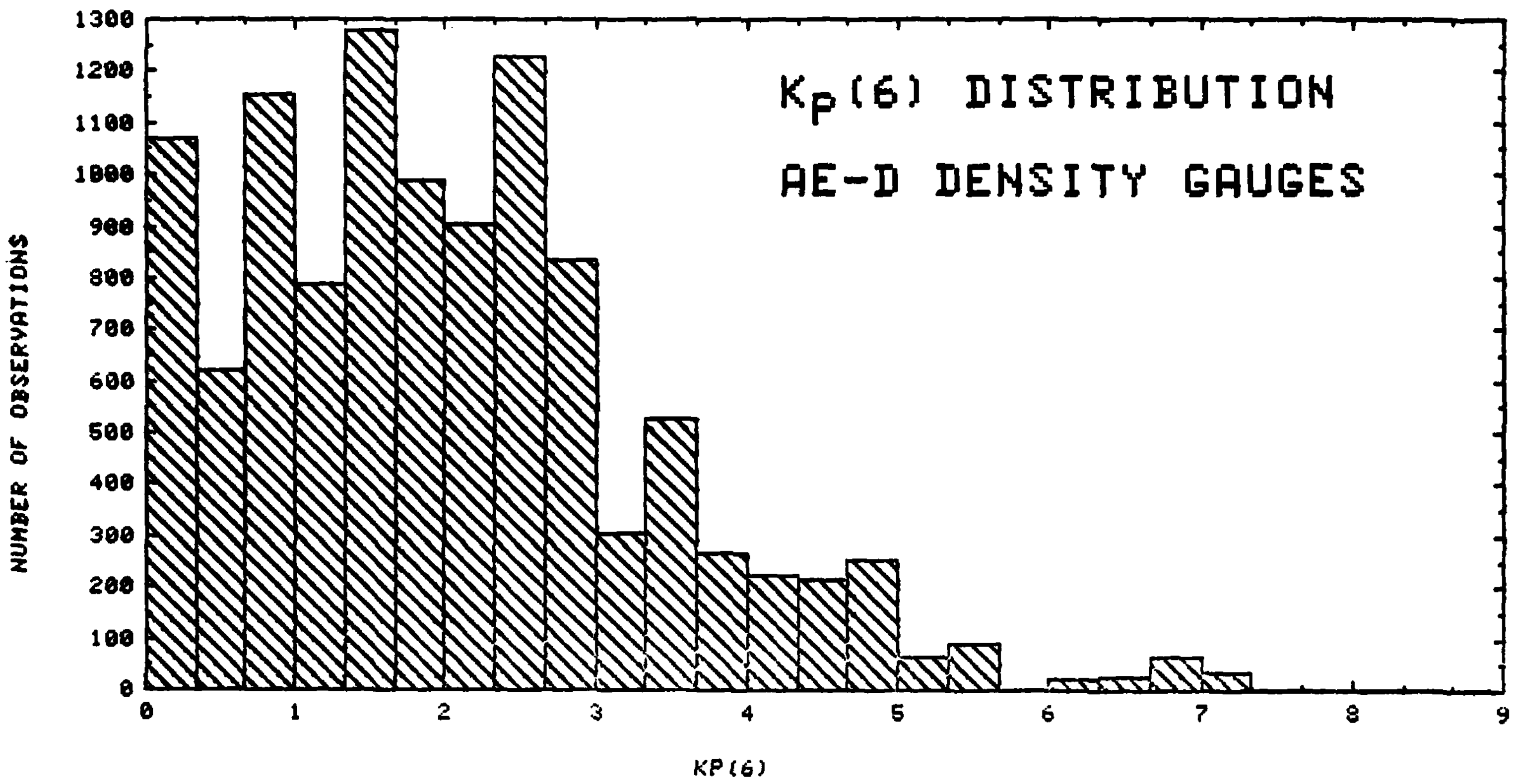

K_p(6) DISTRIBUTION
AE-D DENSITY GAUGES
NUMBER OF OBSERVATIONS
0
100
200
300
400
500
600
700
800
900
1000
1100
1200
1300
0
1
2
3
4
5
6
7
8
9
KP(6)

Figure 2-51.

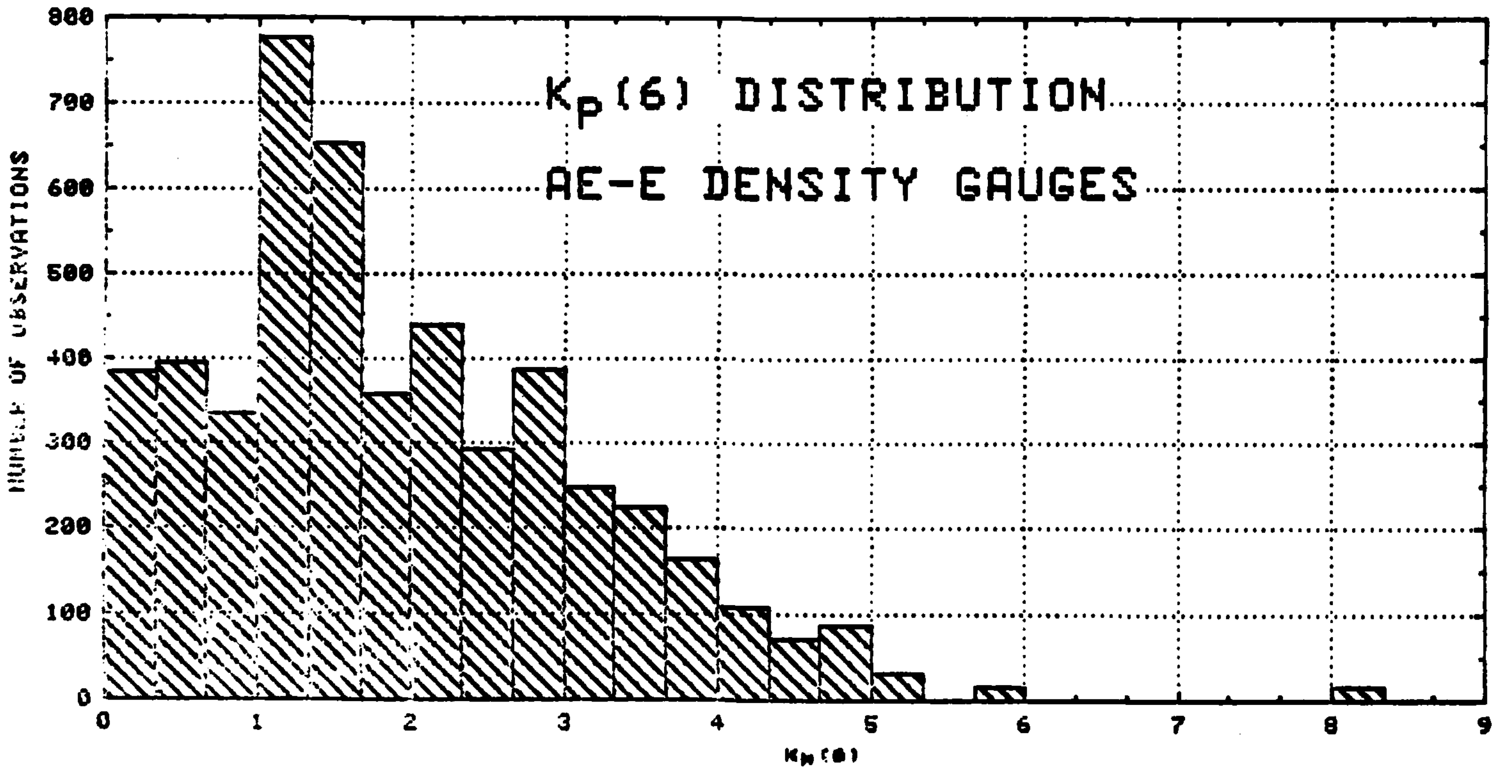

K_p(6) DISTRIBUTION
AE-E DENSITY GAUGES
NUMBER OF OBSERVATIONS
0
100
200
300
400
500
600
700
800
1
2
3
4
5
6
7
8
9

Figure 2-52.

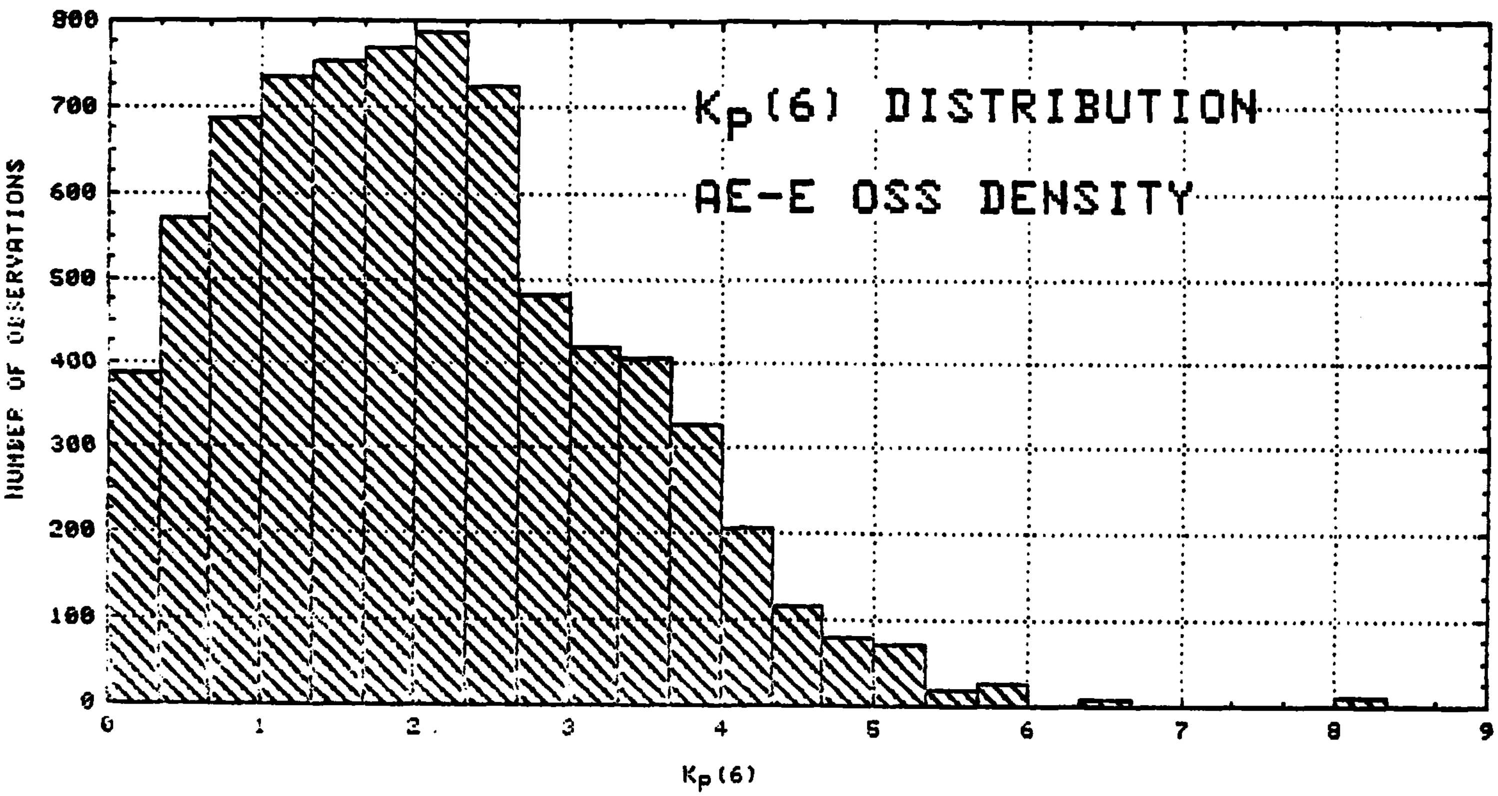
Kp(6) DISTRIBUTION
AE-E OSS DENSITY
NUMBER OF OBSERVATIONS
0
100
200
300
400
500
600
700
800
0
1
2
3
4
5
6
7
8
9
Kp(6)

Figure 2-53.

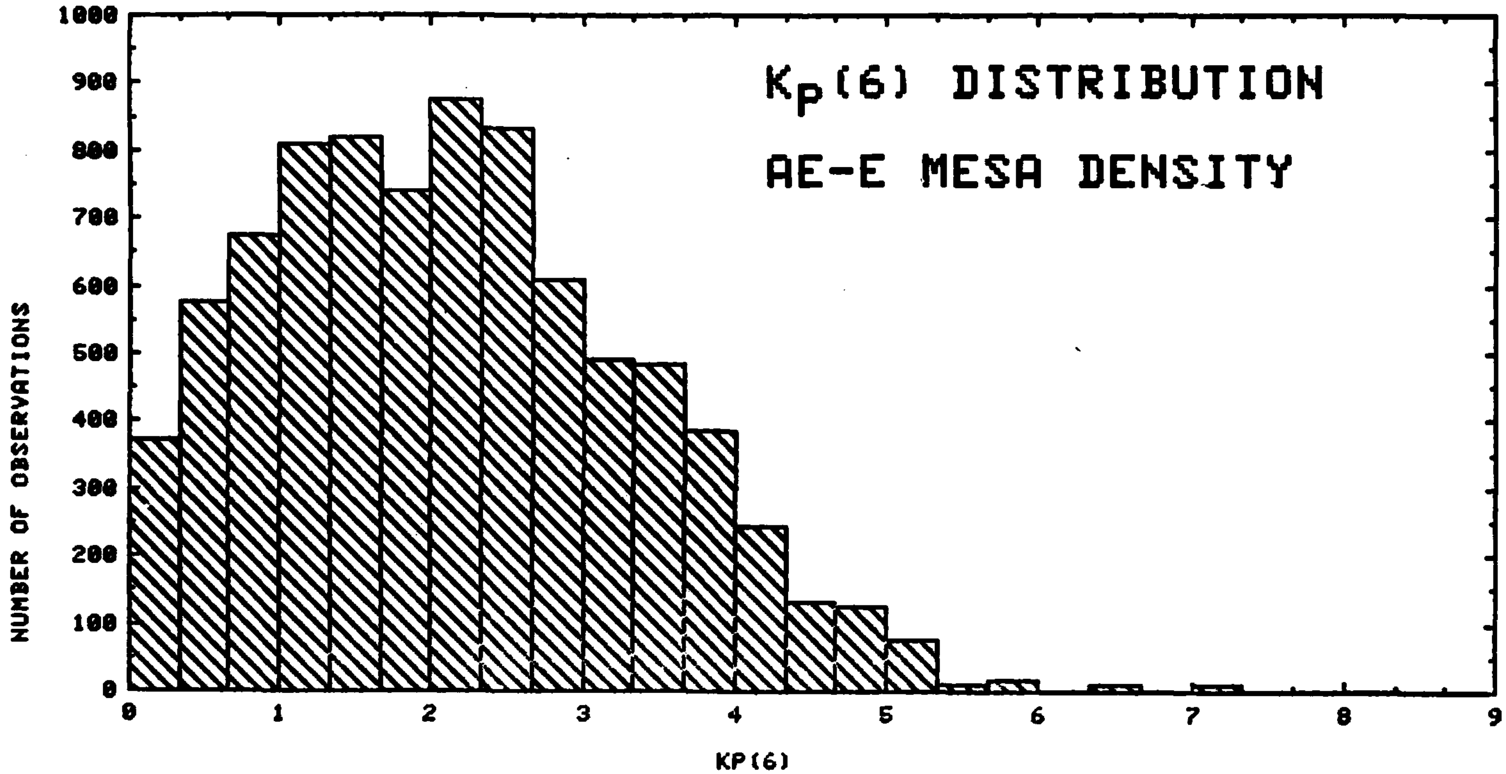

K_p(6) DISTRIBUTION
AE-E MESA DENSITY
NUMBER OF OBSERVATIONS
1000
900
800
700
600
500
400
300
200
100
0
0
1
2
3
4
5
6
7
8
9
KP(6)

Figure 2-54.

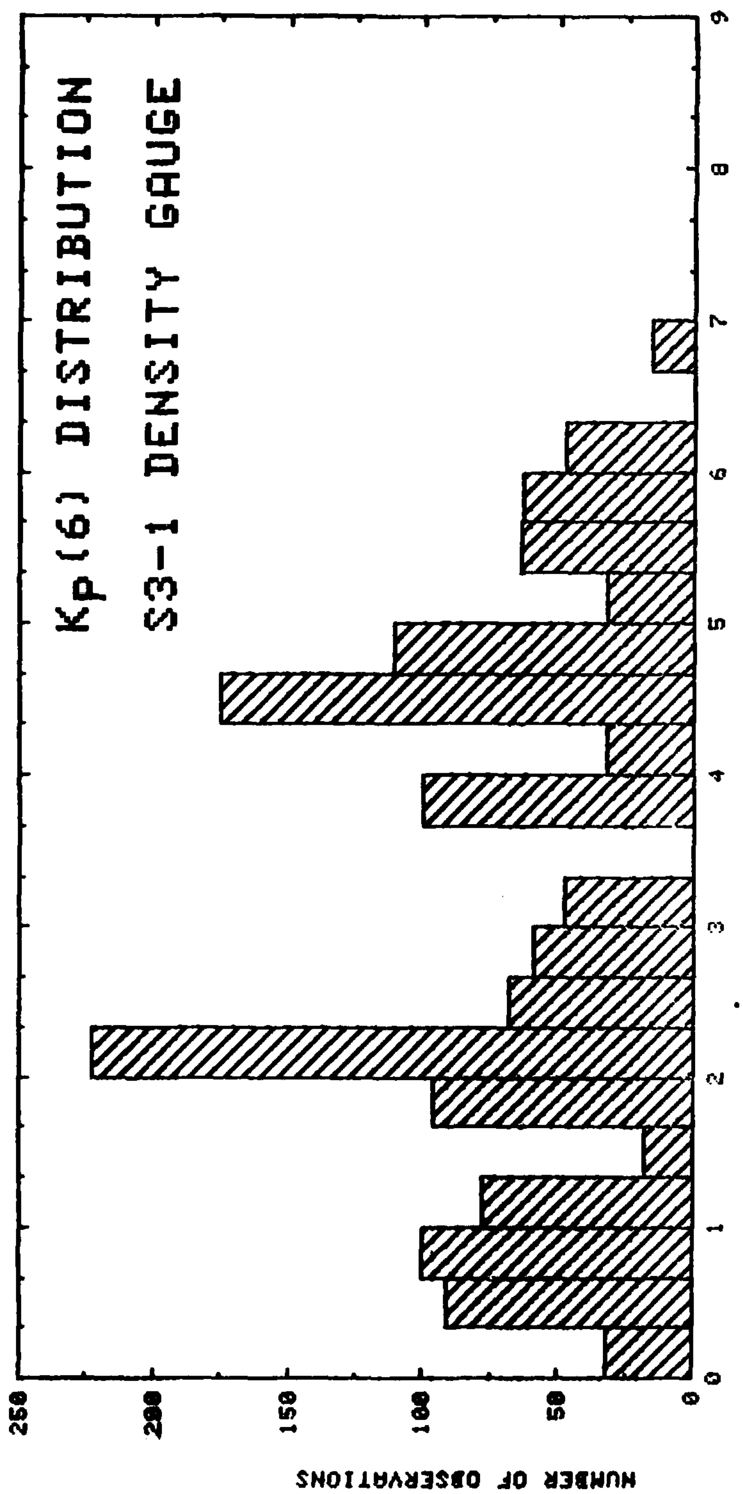
Kp(6) DISTRIBUTION
S3-1 DENSITY GAUGE
NUMBER OF OBSERVATIONS
KP(6)
0
50
100
150
200
250
0
1
2
3
4
5
6
7
8
9

Figure 2-55.

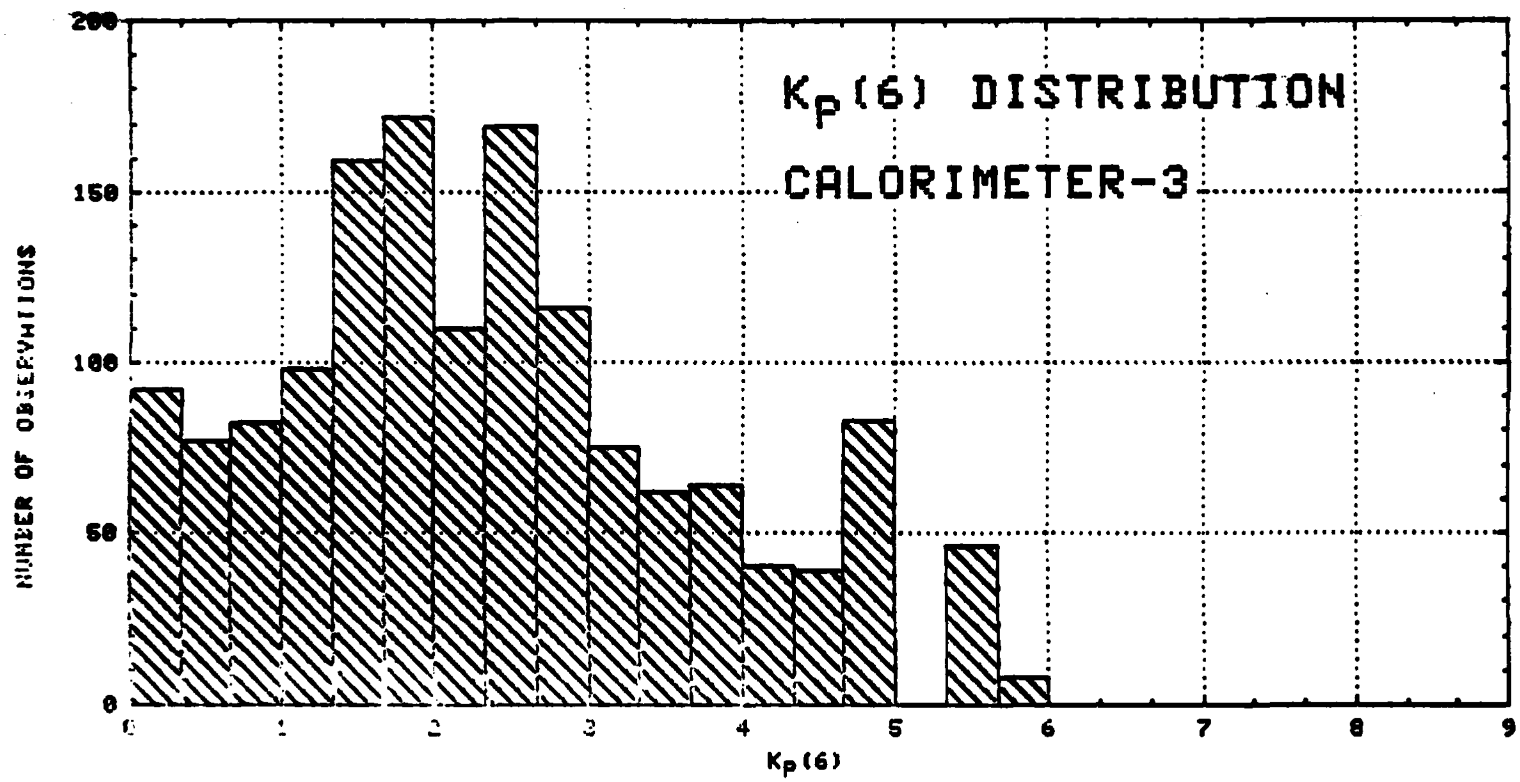
Kp(6) DISTRIBUTION
CALORIMETER-3
NUMBER OF OBSERVATIONS
Kp(6)
0
50
100
150
200
0
1
2
3
4
5
6
7
8
9

Figure 2-56.

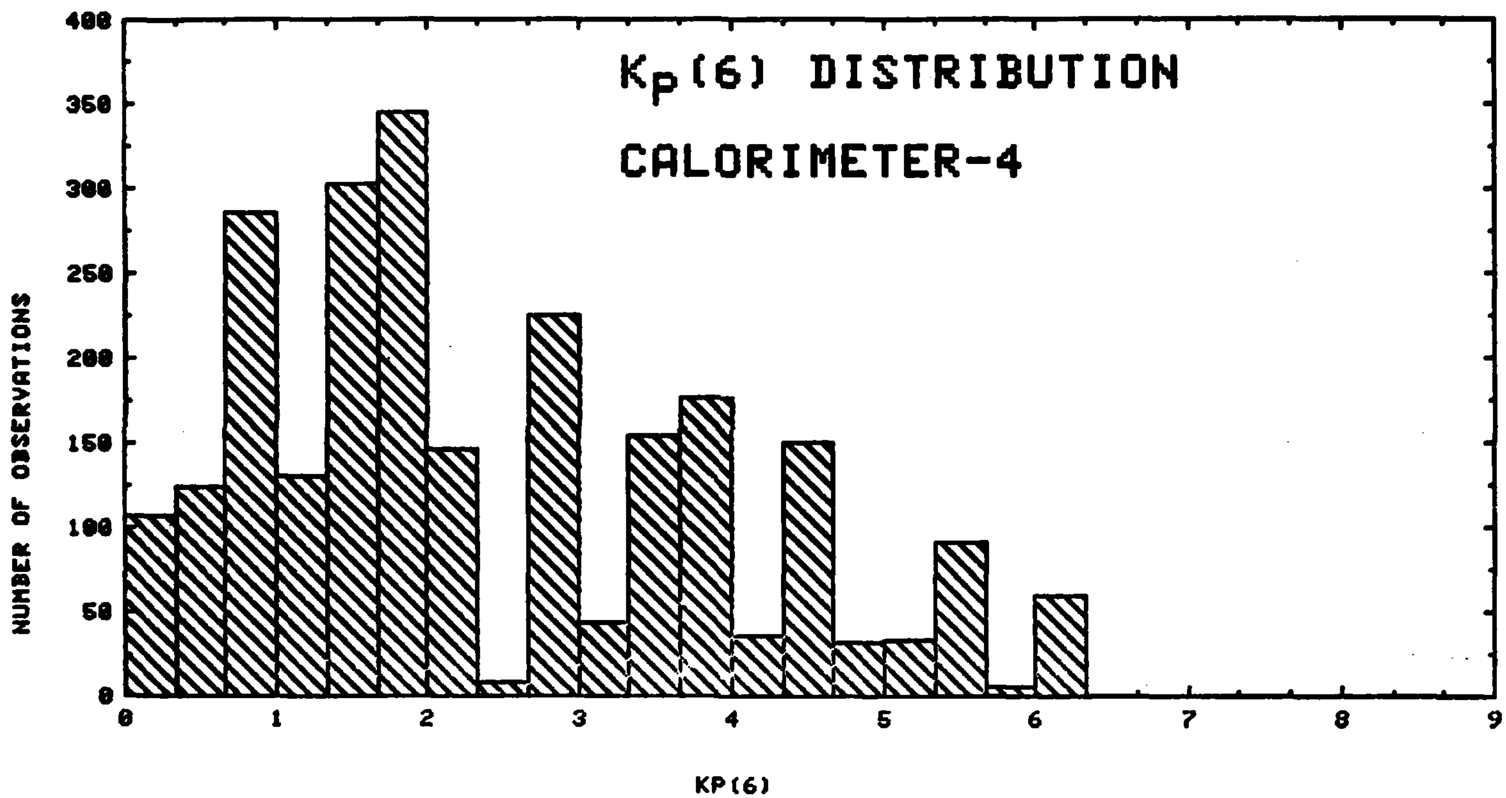
Kp(6) DISTRIBUTION
CALORIMETER-4
NUMBER OF OBSERVATIONS
400
350
300
250
200
150
100
50
0
0
1
2
3
4
5
6
7
8
9
KP(6)

Figure 2-57.

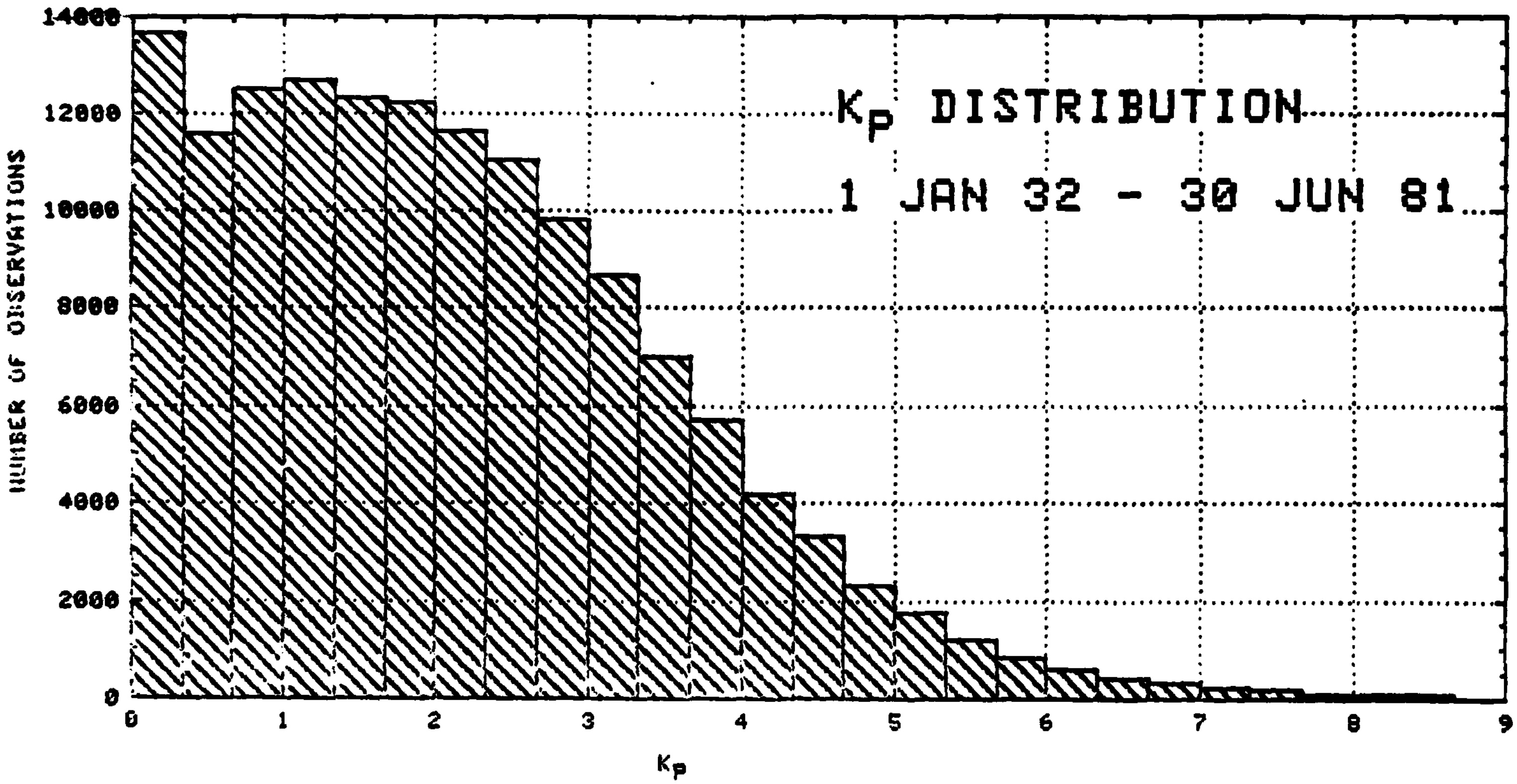

K_P DISTRIBUTION
1 JAN 32 - 30 JUN 81
NUMBER OF OBSERVATIONS
14000
12000
10000
8000
6000
4000
2000
0
0
1
2
3
4
5
6
7
8
9
K_p

Figure 2-58.

SECTION 3

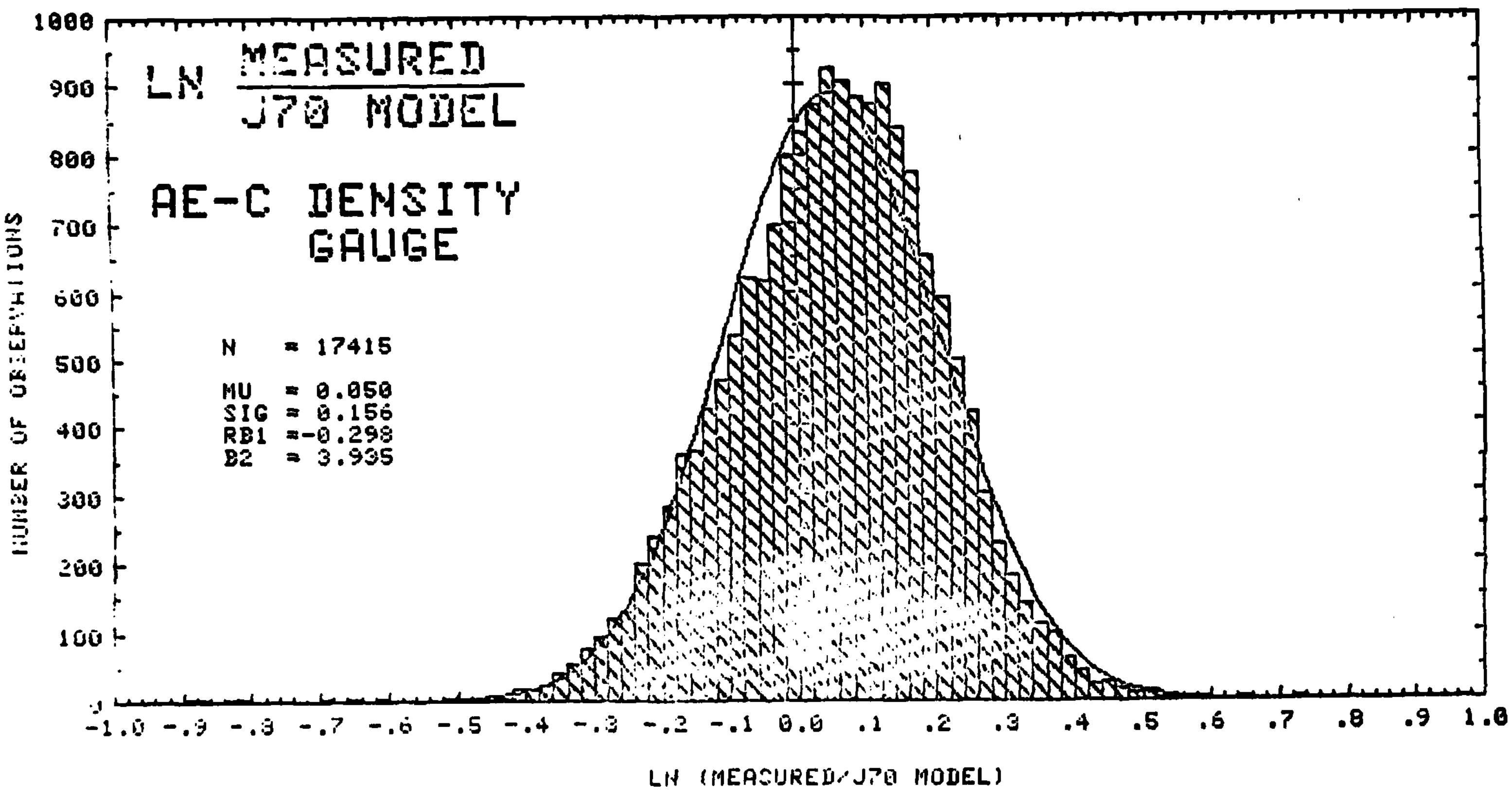

LN MEASURED / J70 MODEL
AE-C DENSITY GAUGE
N = 17415
MU = 0.050
SIG = 0.156
RB1 =-0.298
B2 = 3.935
NUMBER OF OBSERVATIONS
LN (MEASURED/J70 MODEL)

Figure 3-1.

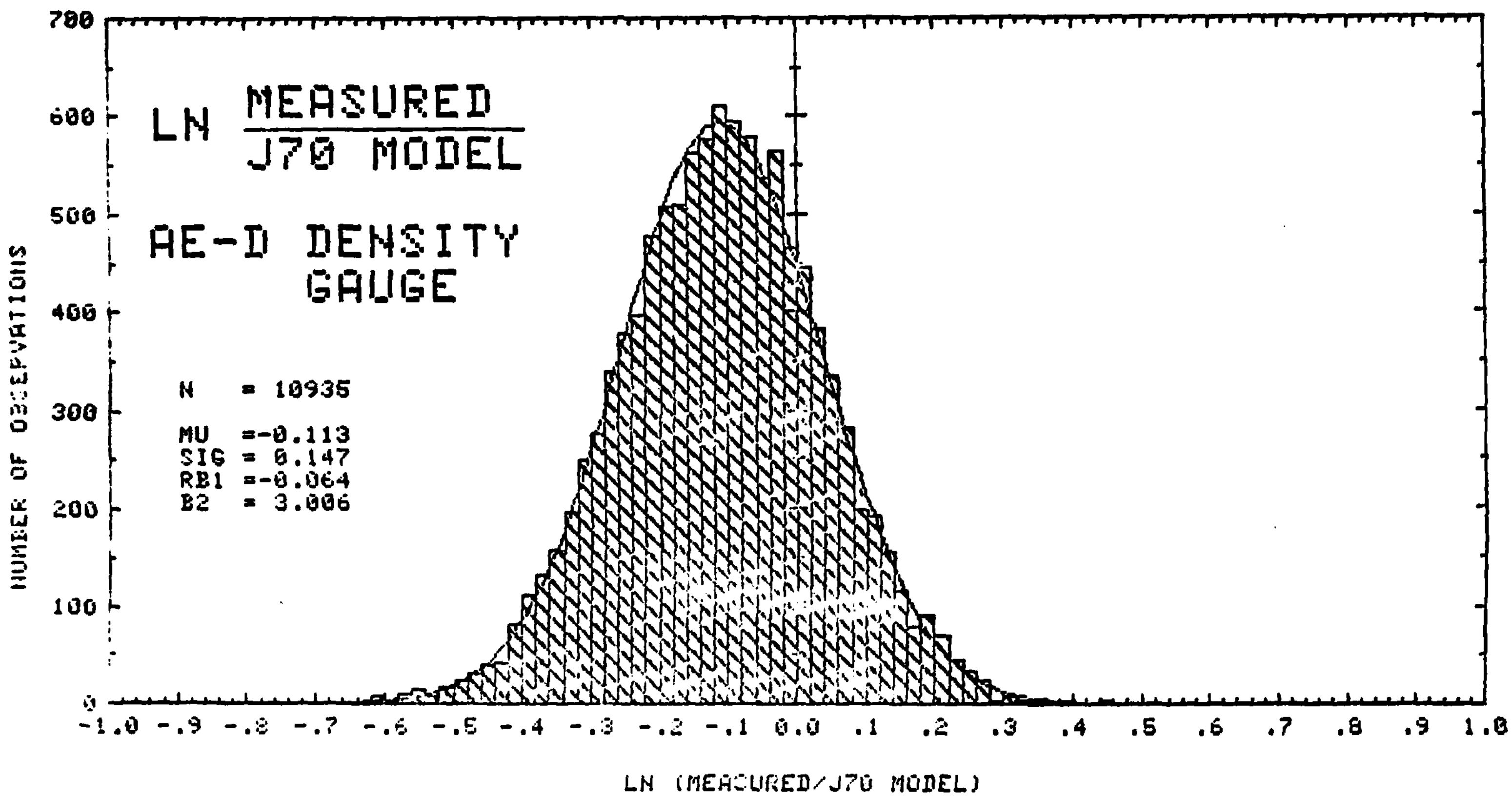
LN MEASURED / J70 MODEL
AE-D DENSITY GAUGE
N = 10935
MU =-0.113
SIG = 0.147
RB1 =-0.064
B2 = 3.006
NUMBER OF OBSERVATIONS
700
600
500
400
300
200
100
0
-1.0 -.9 -.8 -.7 -.6 -.5 -.4 -.3 -.2 -.1 0.0 .1 .2 .3 .4 .5 .6 .7 .8 .9 1.0
LN (MEASURED/J70 MODEL)

Figure 3-2.

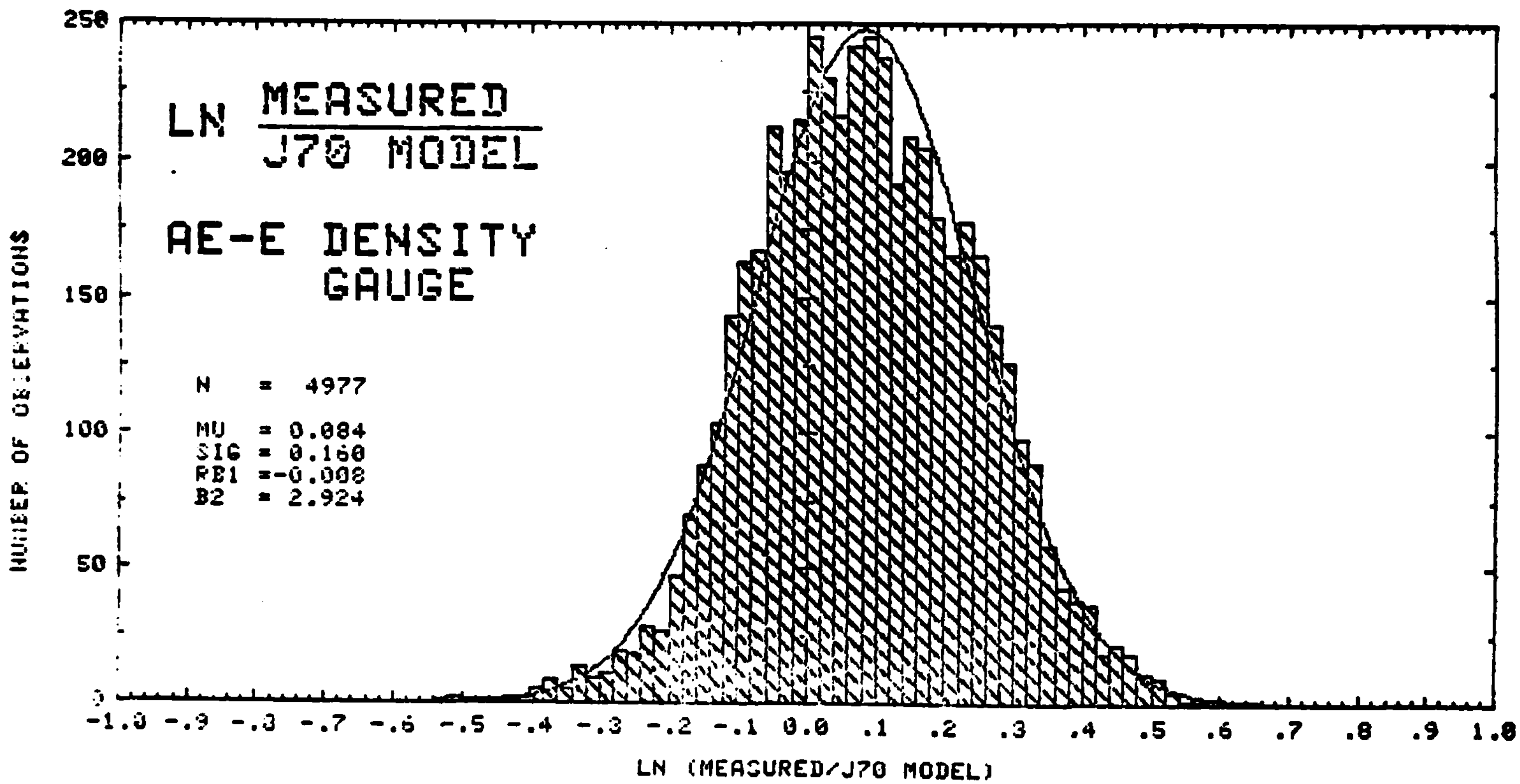
LN MEASURED / J70 MODEL
AE-E DENSITY GAUGE
N = 4977
MU = 0.084
SIG = 0.160
RB1 =-0.008
B2 = 2.924
250
200
150
100
50
0
-1.0 -.9 -.8 -.7 -.6 -.5 -.4 -.3 -.2 -.1 0.0 .1 .2 .3 .4 .5 .6 .7 .8 .9 1.0
NUMBER OF OBSERVATIONS
LN (MEASURED/J70 MODEL)

Figure 3-3.

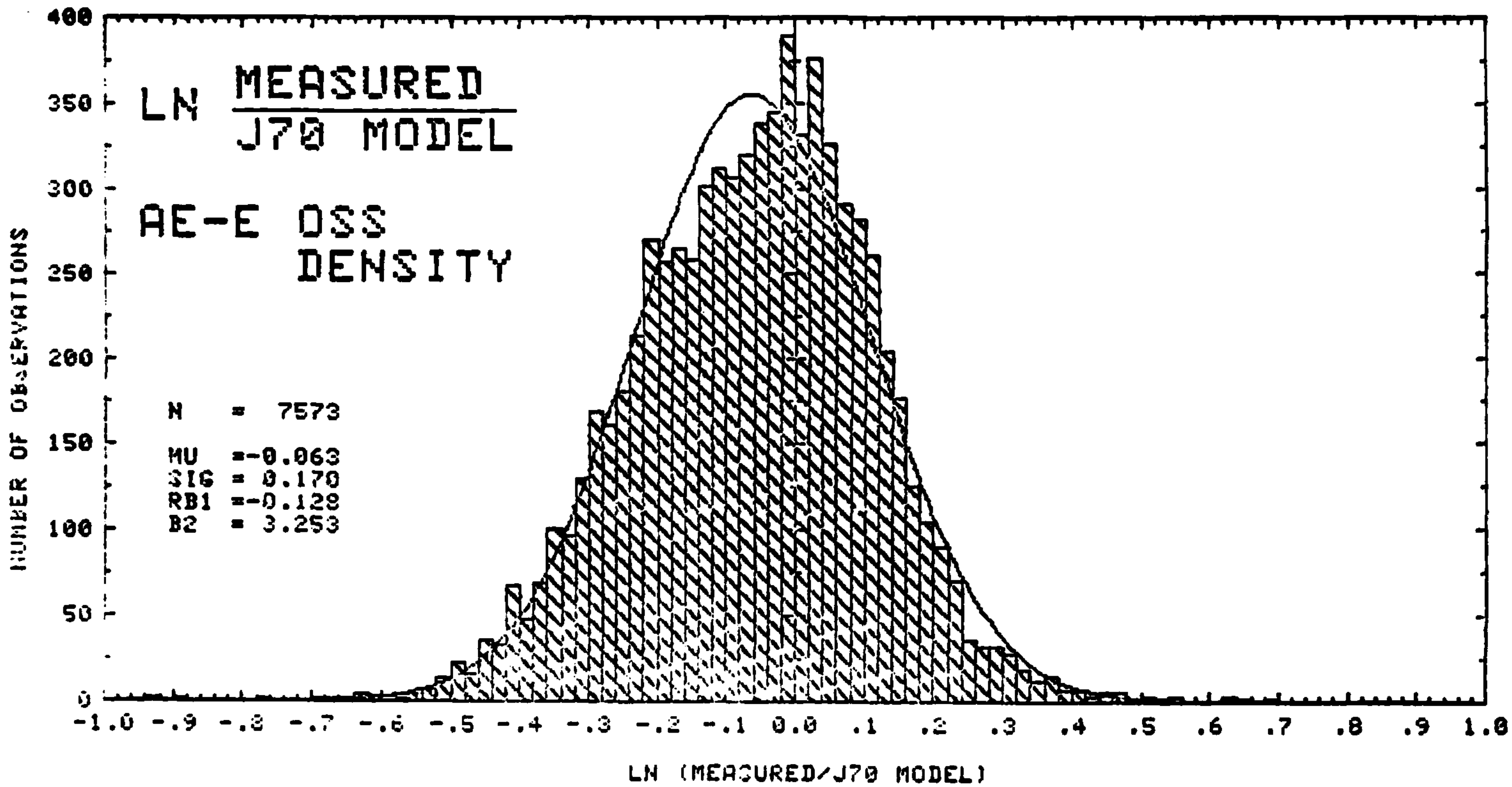
LN MEASURED / J70 MODEL
AE-E OSS DENSITY
N = 7573
MU =-0.063
SIG = 0.170
RB1 =-0.128
B2 = 3.253
NUMBER OF OBSERVATIONS
0
50
100
150
200
250
300
350
400
-1.0 -.9 -.8 -.7 -.6 -.5 -.4 -.3 -.2 -.1 0.0 .1 .2 .3 .4 .5 .6 .7 .8 .9 1.0
LN (MEASURED/J70 MODEL)

Figure 3-4.

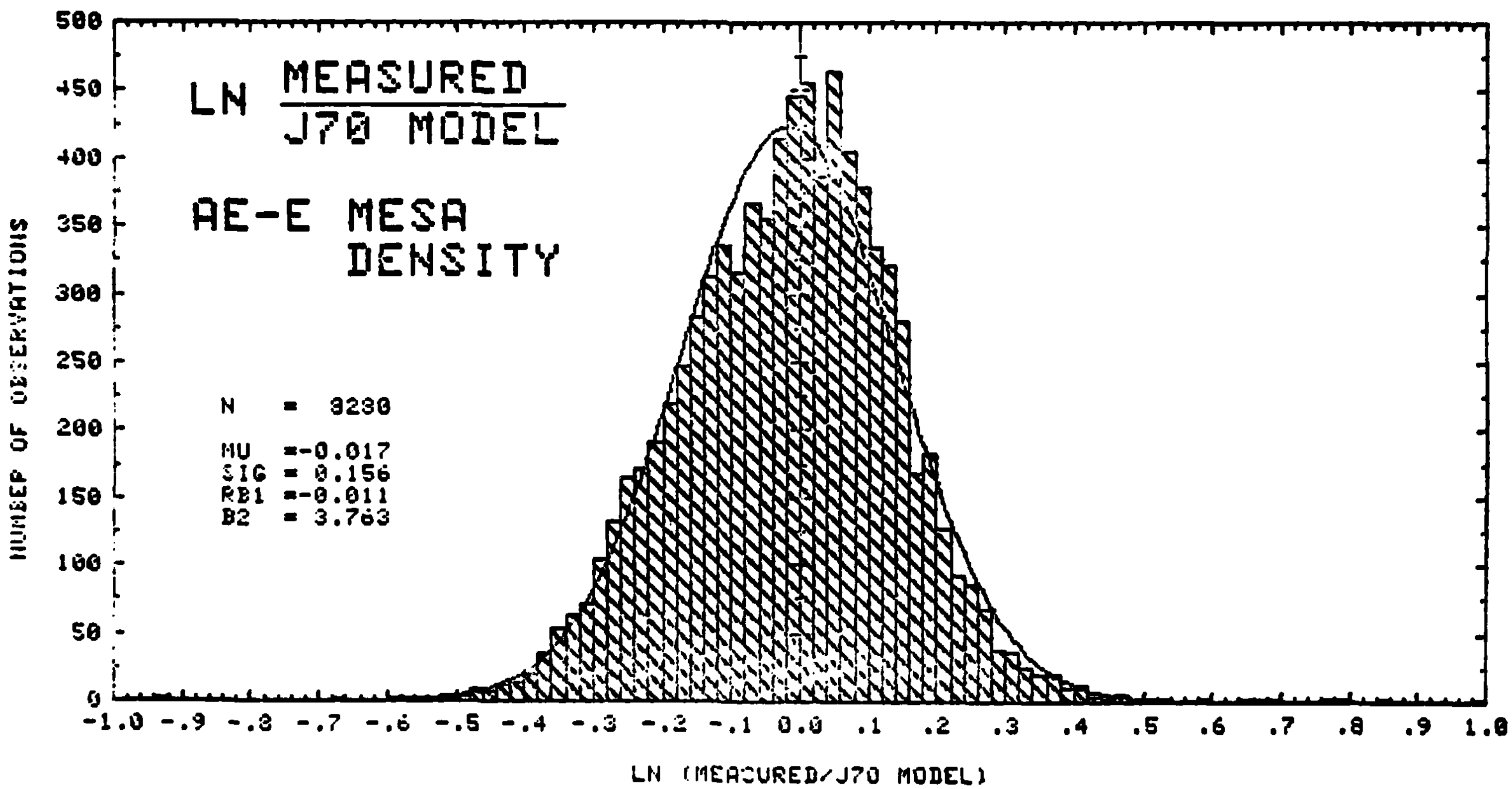
LN MEASURED / J70 MODEL
AE-E MESA
DENSITY
N = 3230
MU =-0.017
SIG = 0.156
RB1 =-0.011
B2 = 3.763
NUMBER OF OBSERVATIONS
LN (MEASURED/J70 MODEL)

Figure 3-5.

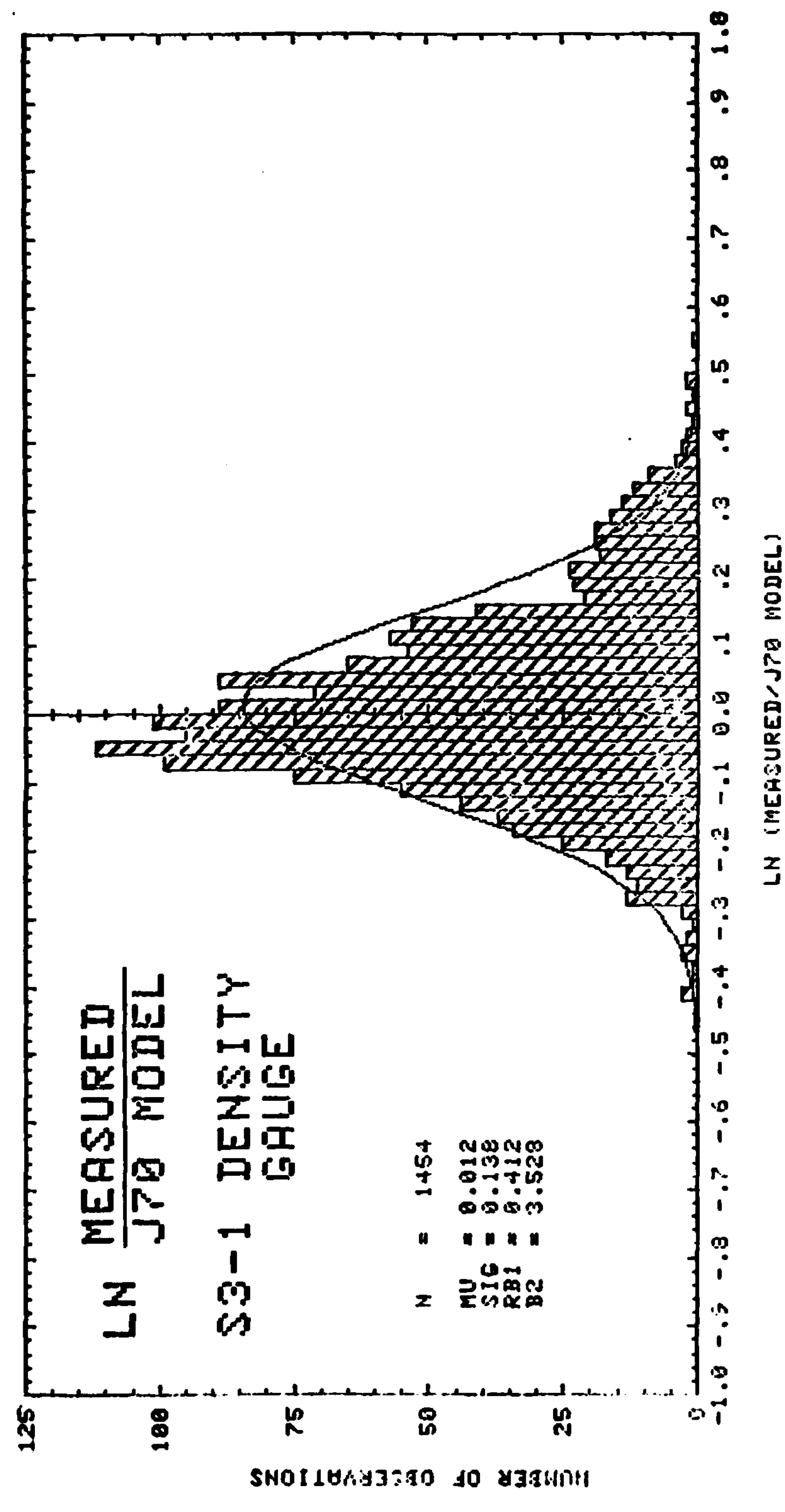
LN MEASURED / J70 MODEL
S3-1 DENSITY GAUGE
N = 1454
MU = 0.012
SIG = 0.138
RB1 = 0.412
B2 = 3.528
NUMBER OF OBSERVATIONS
0
25
50
75
100
125
-1.0 -.9 -.8 -.7 -.6 -.5 -.4 -.3 -.2 -.1 0.0 .1 .2 .3 .4 .5 .6 .7 .8 .9 1.0
LN (MEASURED/J70 MODEL)

Figure 3-6.

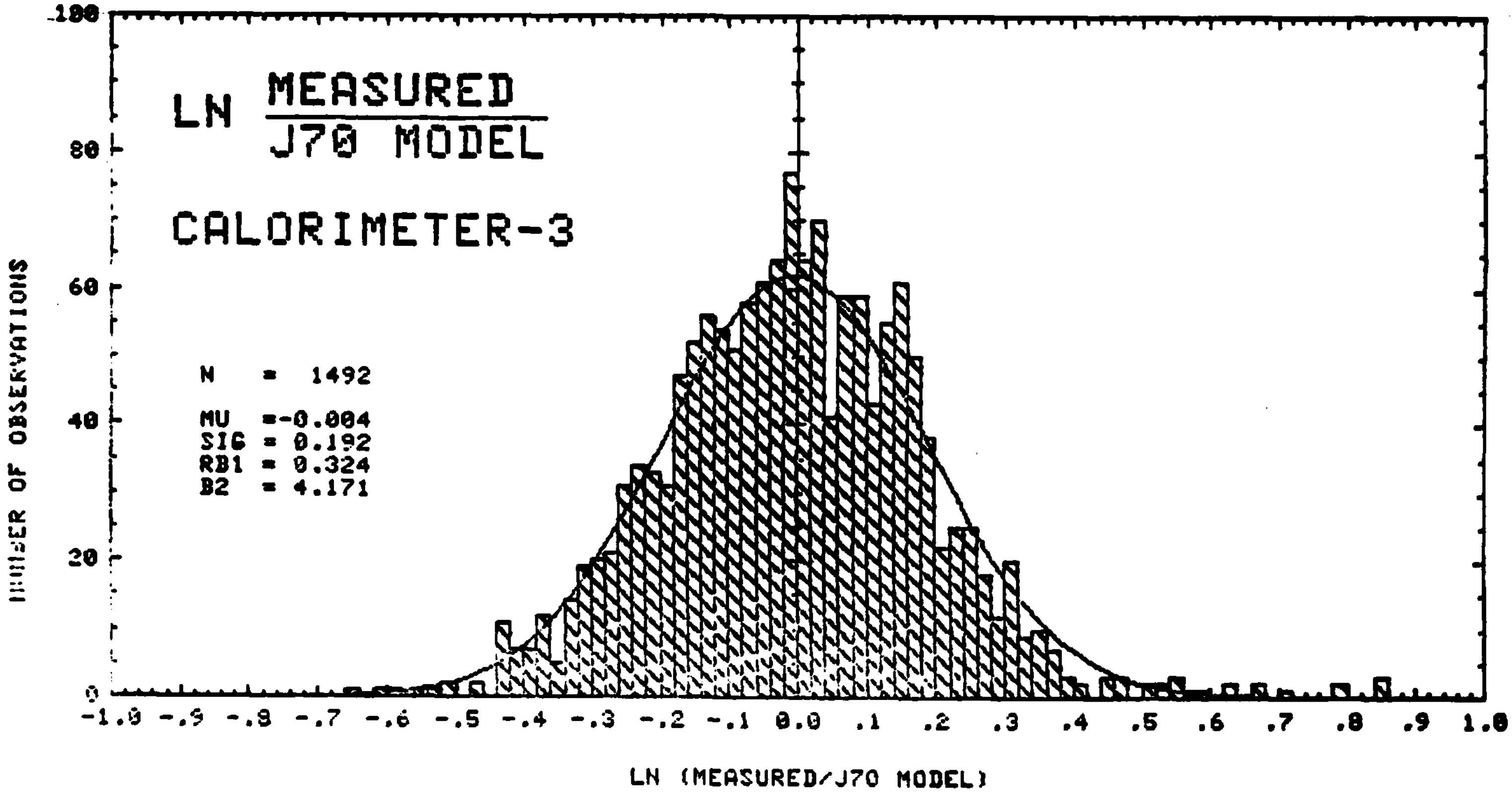
LN MEASURED / J70 MODEL
CALORIMETER-3
N = 1492
MU =-0.004
SIG = 0.192
RB1 = 0.324
B2 = 4.171
100
80
60
40
20
0
NUMBER OF OBSERVATIONS
-1.0 -.9 -.8 -.7 -.6 -.5 -.4 -.3 -.2 -.1 0.0 .1 .2 .3 .4 .5 .6 .7 .8 .9 1.0
LN (MEASURED/J70 MODEL)

Figure 3-7.

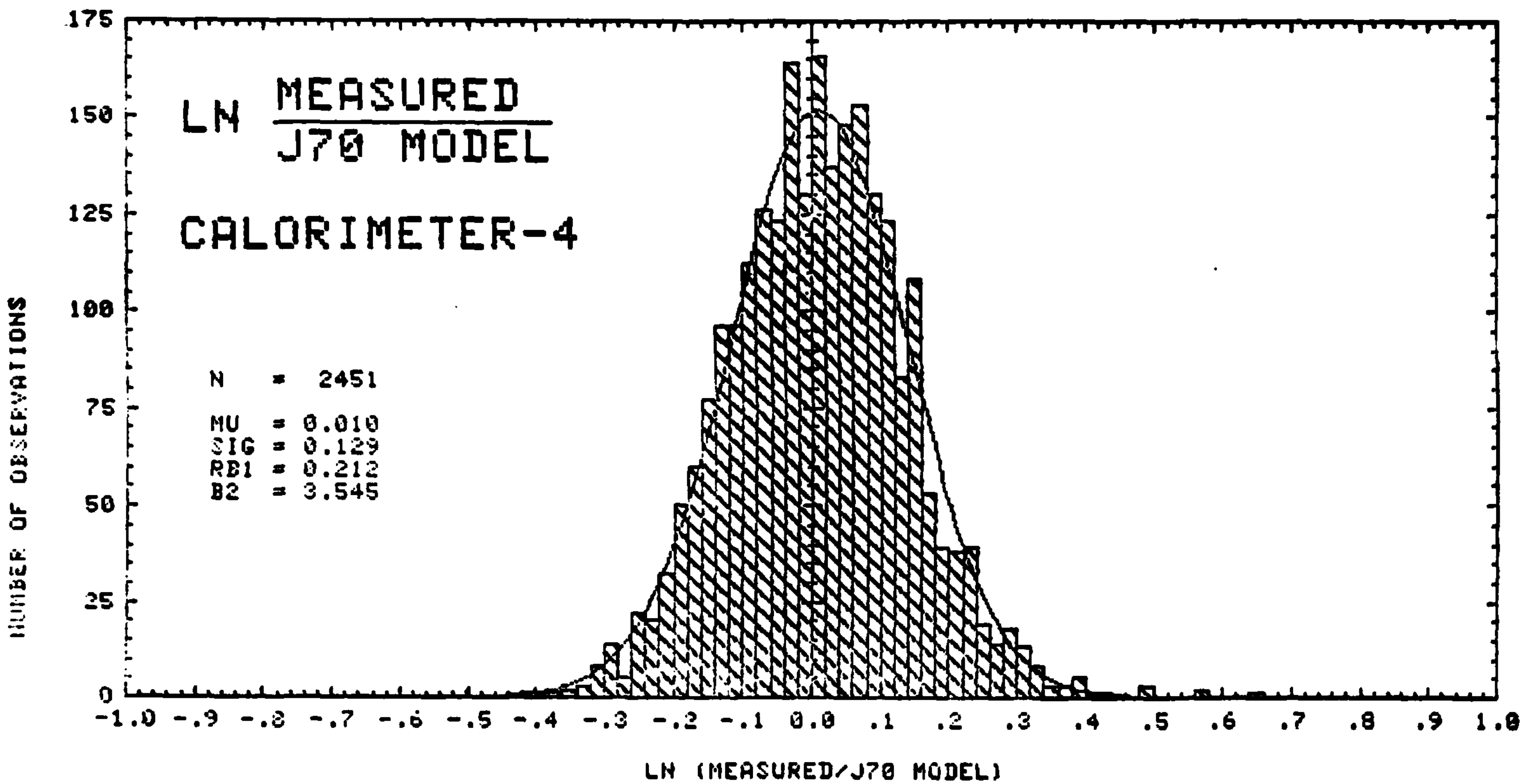

LN MEASURED / J70 MODEL
CALORIMETER-4
N = 2451
MU = 0.010
SIG = 0.129
RB1 = 0.212
B2 = 3.545
NUMBER OF OBSERVATIONS
0
25
50
75
100
125
150
175
-1.0 -.9 -.8 -.7 -.6 -.5 -.4 -.3 -.2 -.1 0.0 .1 .2 .3 .4 .5 .6 .7 .8 .9 1.0
LN (MEASURED/J70 MODEL)

Figure 3-8.

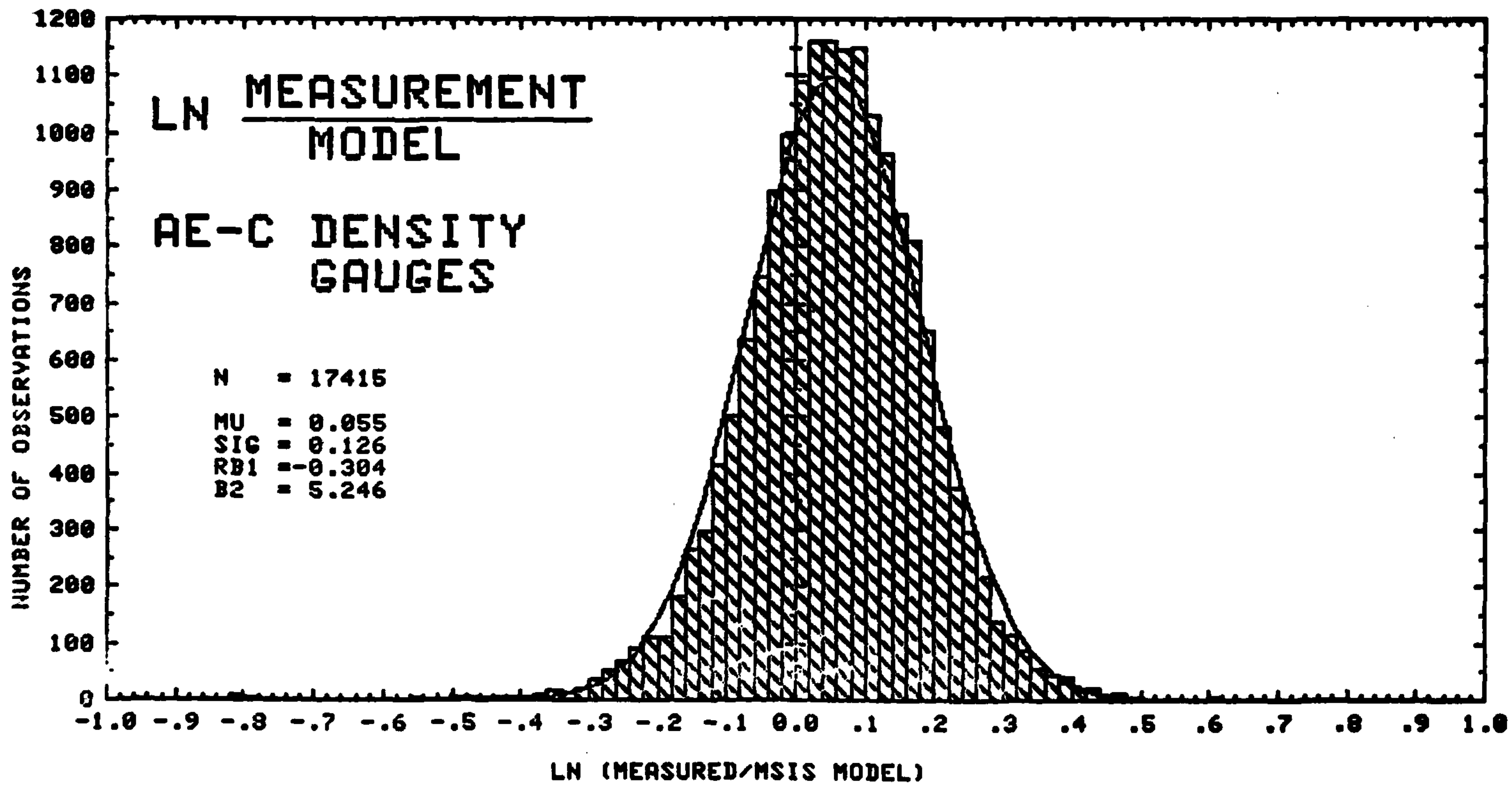
LN MEASUREMENT / MODEL
AE-C DENSITY GAUGES
N = 17415
MU = 0.055
SIG = 0.126
RB1 =-0.304
B2 = 5.246
NUMBER OF OBSERVATIONS
LN (MEASURED/MSIS MODEL)
0
100
200
300
400
500
600
700
800
900
1000
1100
1200
-1.0 -.9 -.8 -.7 -.6 -.5 -.4 -.3 -.2 -.1 0.0 .1 .2 .3 .4 .5 .6 .7 .8 .9 1.0

Figure 3-9.

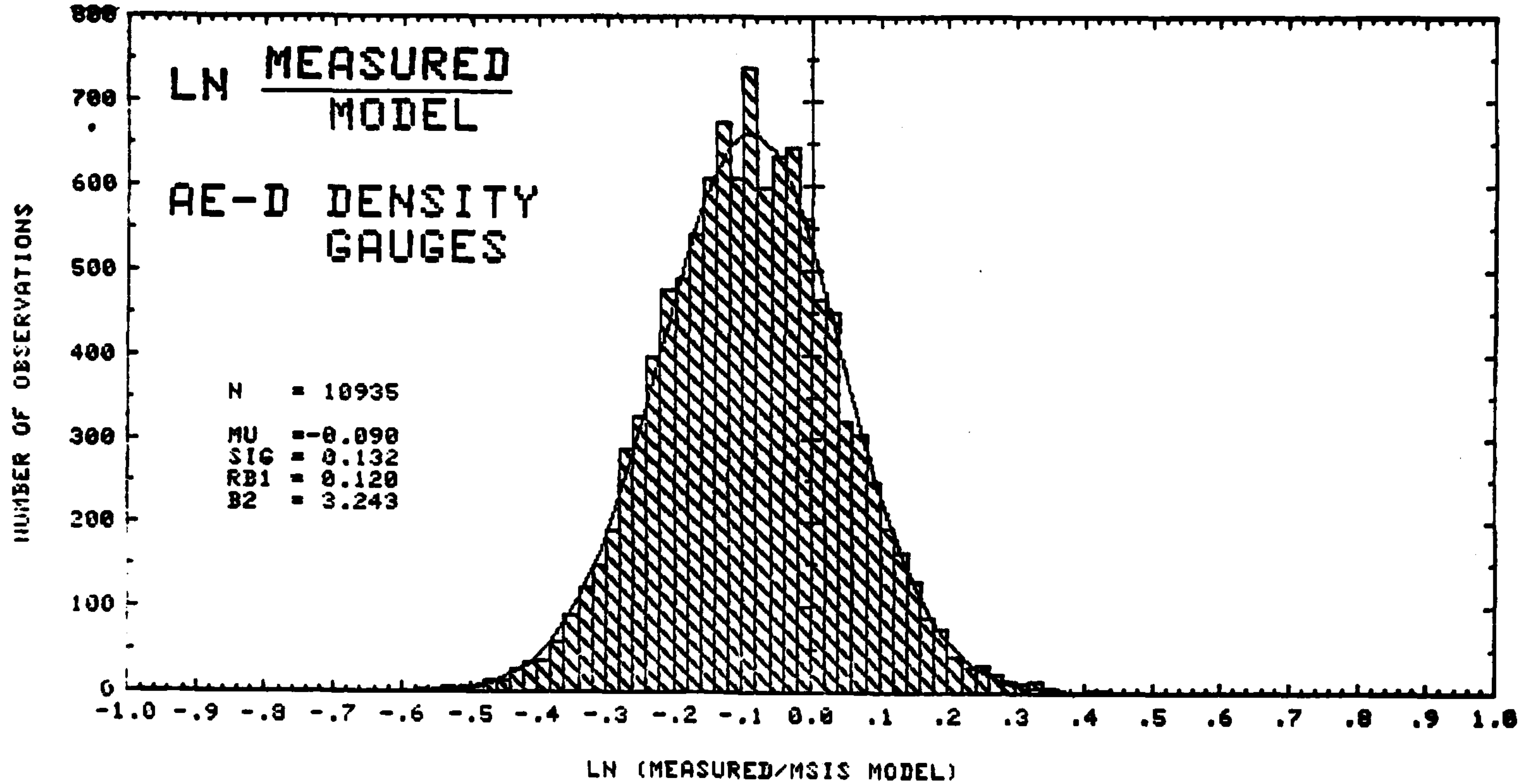

LN MEASURED / MODEL
AE-D DENSITY GAUGES
N = 10935
MU =-0.090
SIG = 0.132
RB1 = 0.120
B2 = 3.243
NUMBER OF OBSERVATIONS
0
100
200
300
400
500
600
700
800
-1.0 -.9 -.8 -.7 -.6 -.5 -.4 -.3 -.2 -.1 0.0 .1 .2 .3 .4 .5 .6 .7 .8 .9 1.0
LN (MEASURED/MSIS MODEL)

Figure 3-10.

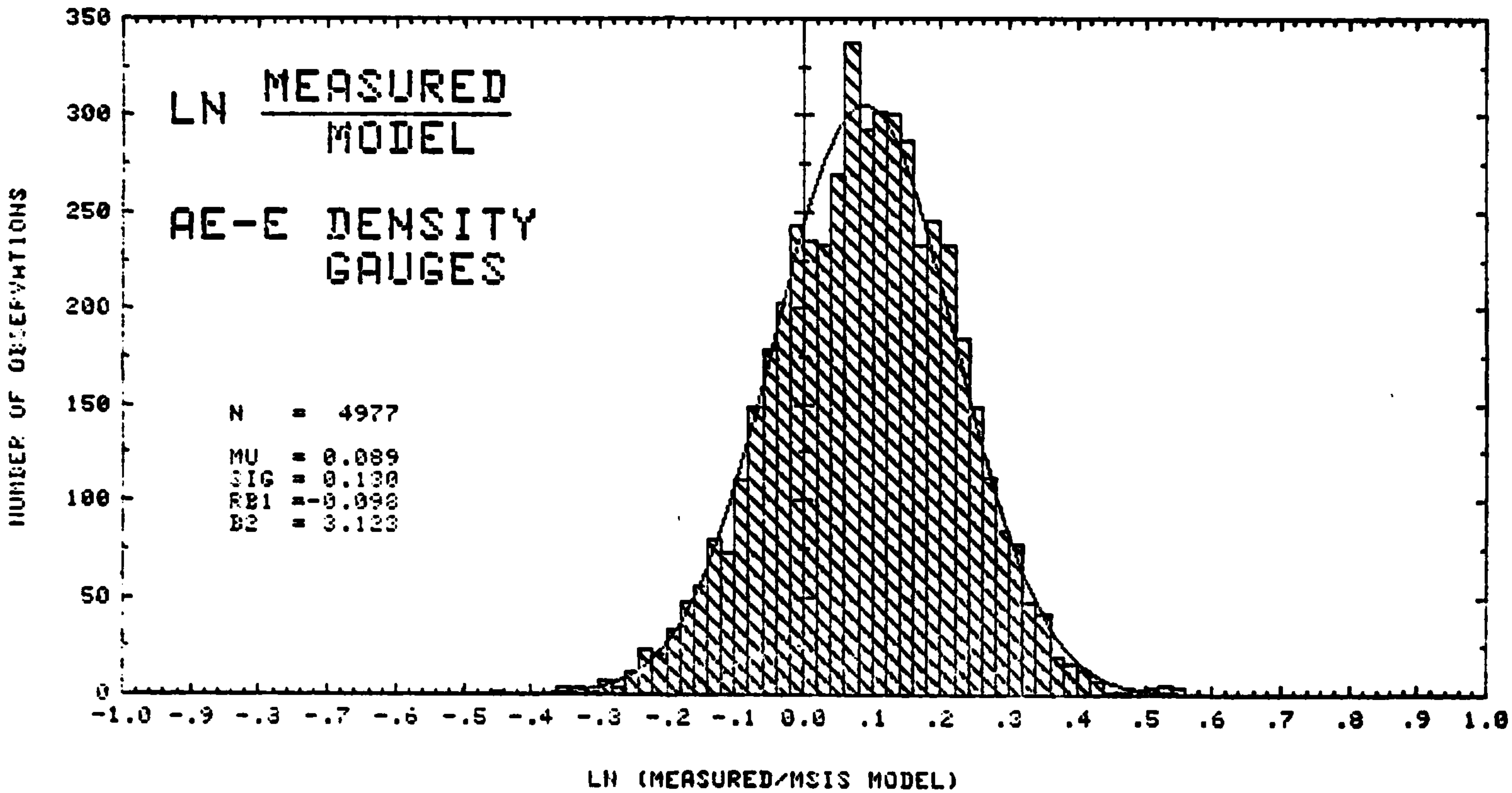
LN MEASURED / MODEL
AE-E DENSITY GAUGES
N = 4977
MU = 0.089
SIG = 0.130
RB1 =-0.098
B2 = 3.123
NUMBER OF OBSERVATIONS
350
300
250
200
150
100
50
0
-1.0 -.9 -.8 -.7 -.6 -.5 -.4 -.3 -.2 -.1 0.0 .1 .2 .3 .4 .5 .6 .7 .8 .9 1.0
LN (MEASURED/MSIS MODEL)

Figure 3-11.

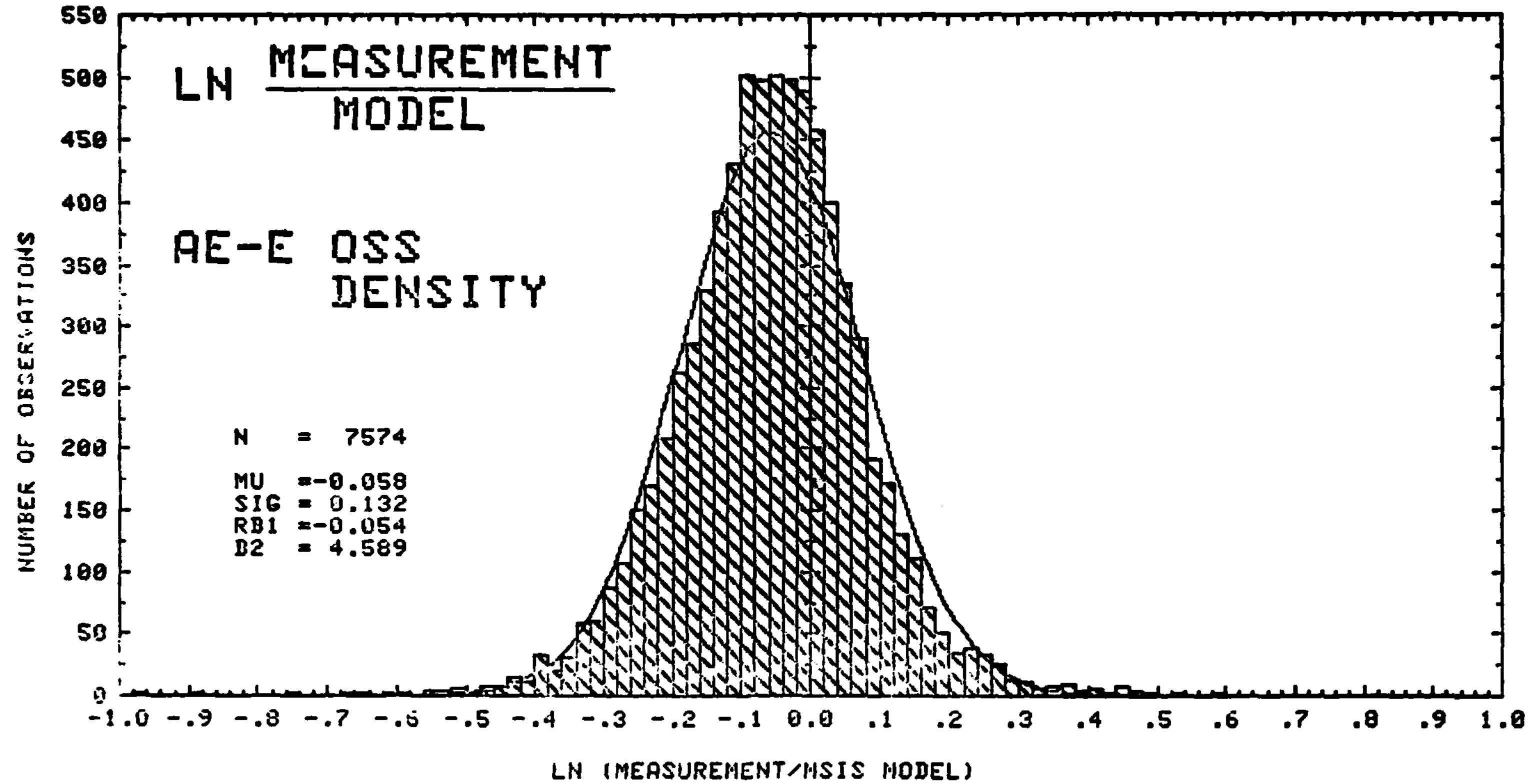
LN MEASUREMENT / MODEL
AE-E OSS DENSITY
N = 7574
MU =-0.058
SIG = 0.132
RB1 =-0.054
B2 = 4.589
NUMBER OF OBSERVATIONS
550
500
450
400
350
300
250
200
150
100
50
0
-1.0 -.9 -.8 -.7 -.6 -.5 -.4 -.3 -.2 -.1 0.0 .1 .2 .3 .4 .5 .6 .7 .8 .9 1.0
LN (MEASUREMENT/MSIS MODEL)

Figure 3-12.

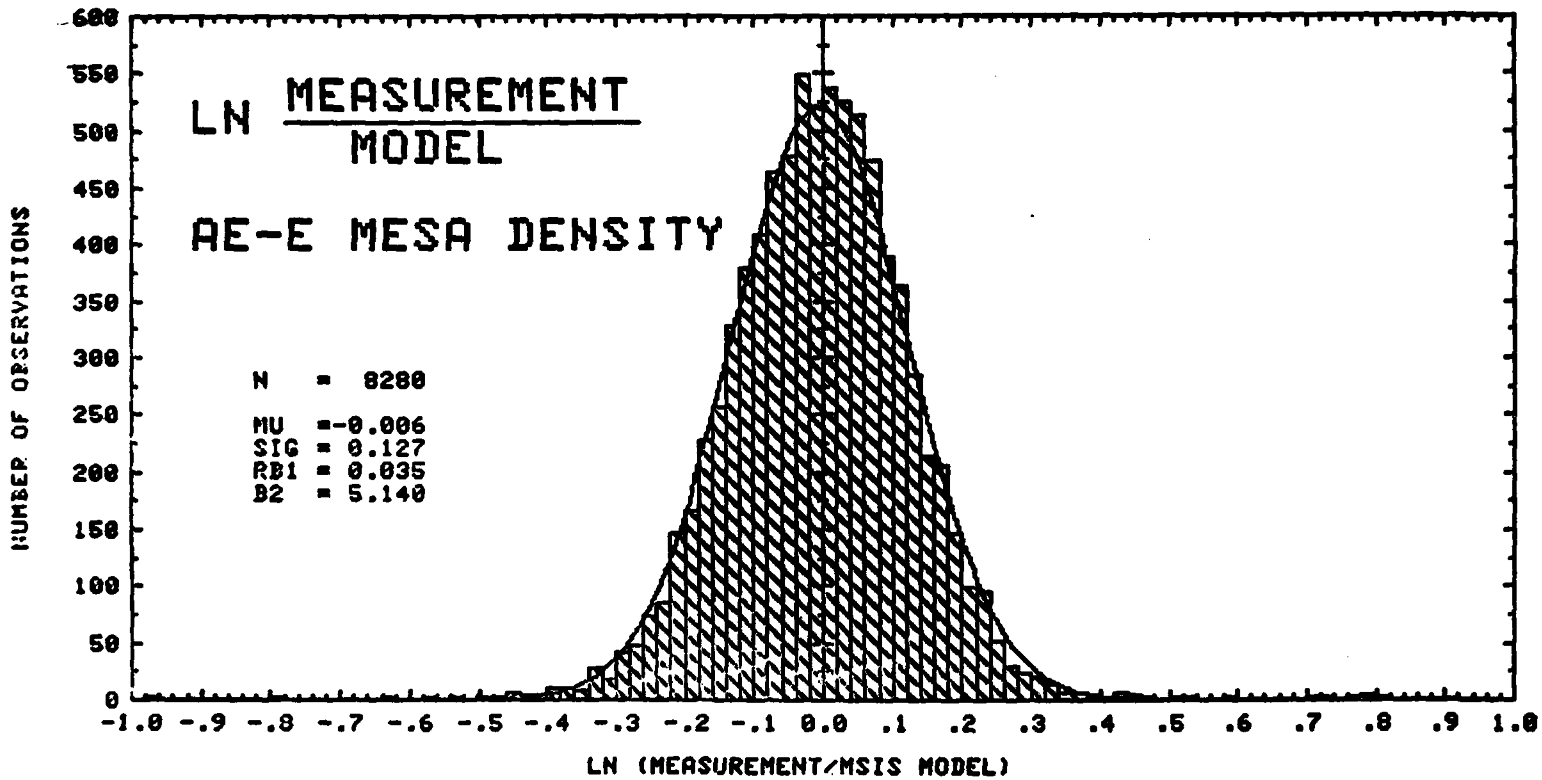
LN MEASUREMENT / MODEL
AE-E MESA DENSITY
N = 8280
MU =-0.006
SIG = 0.127
RB1 = 0.035
B2 = 5.140
NUMBER OF OBSERVATIONS
0
50
100
150
200
250
300
350
400
450
500
550
600
-1.0 -.9 -.8 -.7 -.6 -.5 -.4 -.3 -.2 -.1 0.0 .1 .2 .3 .4 .5 .6 .7 .8 .9 1.0
LN (MEASUREMENT/MSIS MODEL)

Figure 3-13.

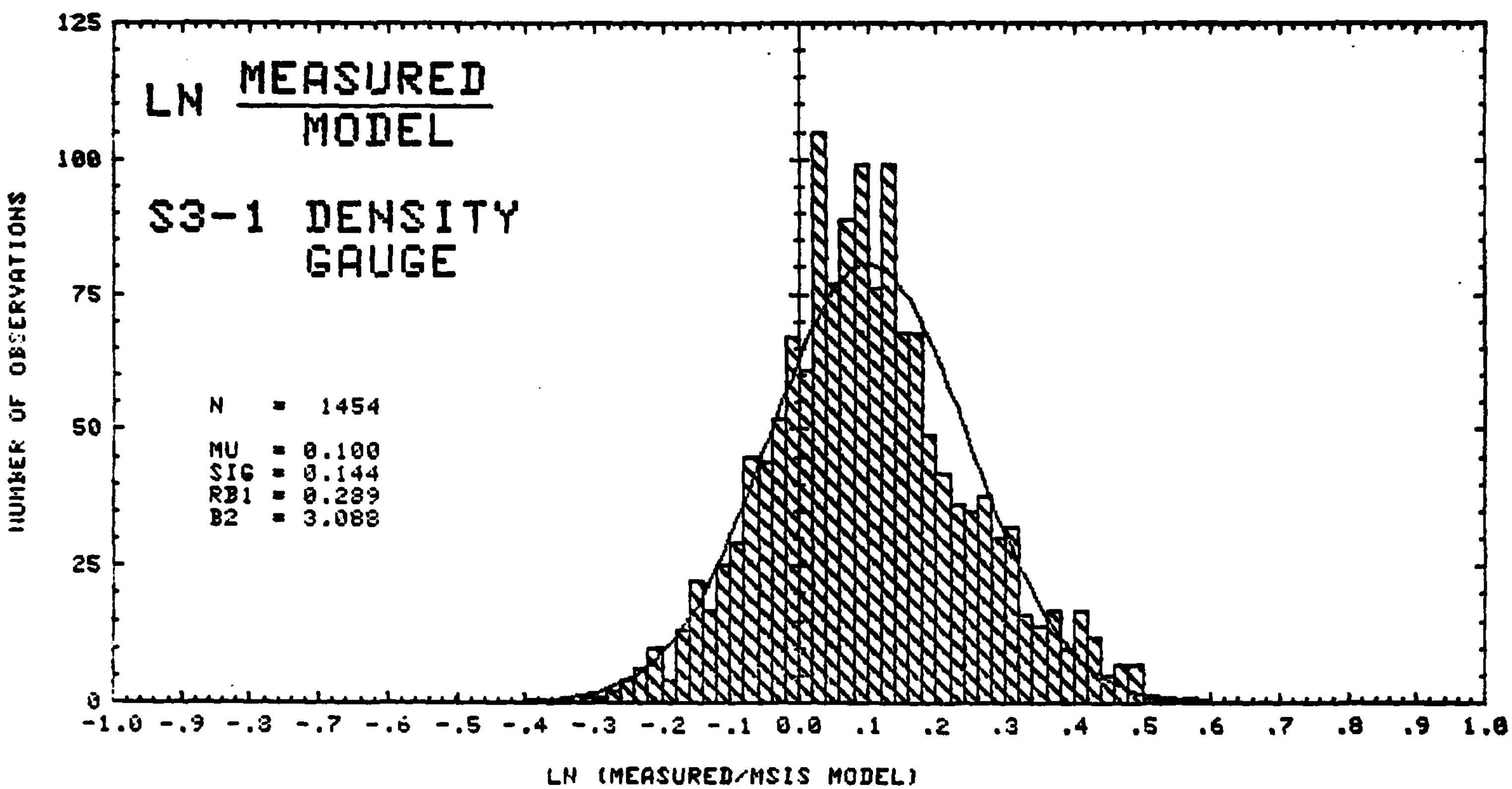
LN MEASURED / MODEL
S3-1 DENSITY GAUGE
N = 1454
MU = 0.100
SIG = 0.144
RB1 = 0.289
B2 = 3.088
NUMBER OF OBSERVATIONS
125
100
75
50
25
0
-1.0 -.9 -.8 -.7 -.6 -.5 -.4 -.3 -.2 -.1 0.0 .1 .2 .3 .4 .5 .6 .7 .8 .9 1.0
LN (MEASURED/MSIS MODEL)

Figure 3-14.

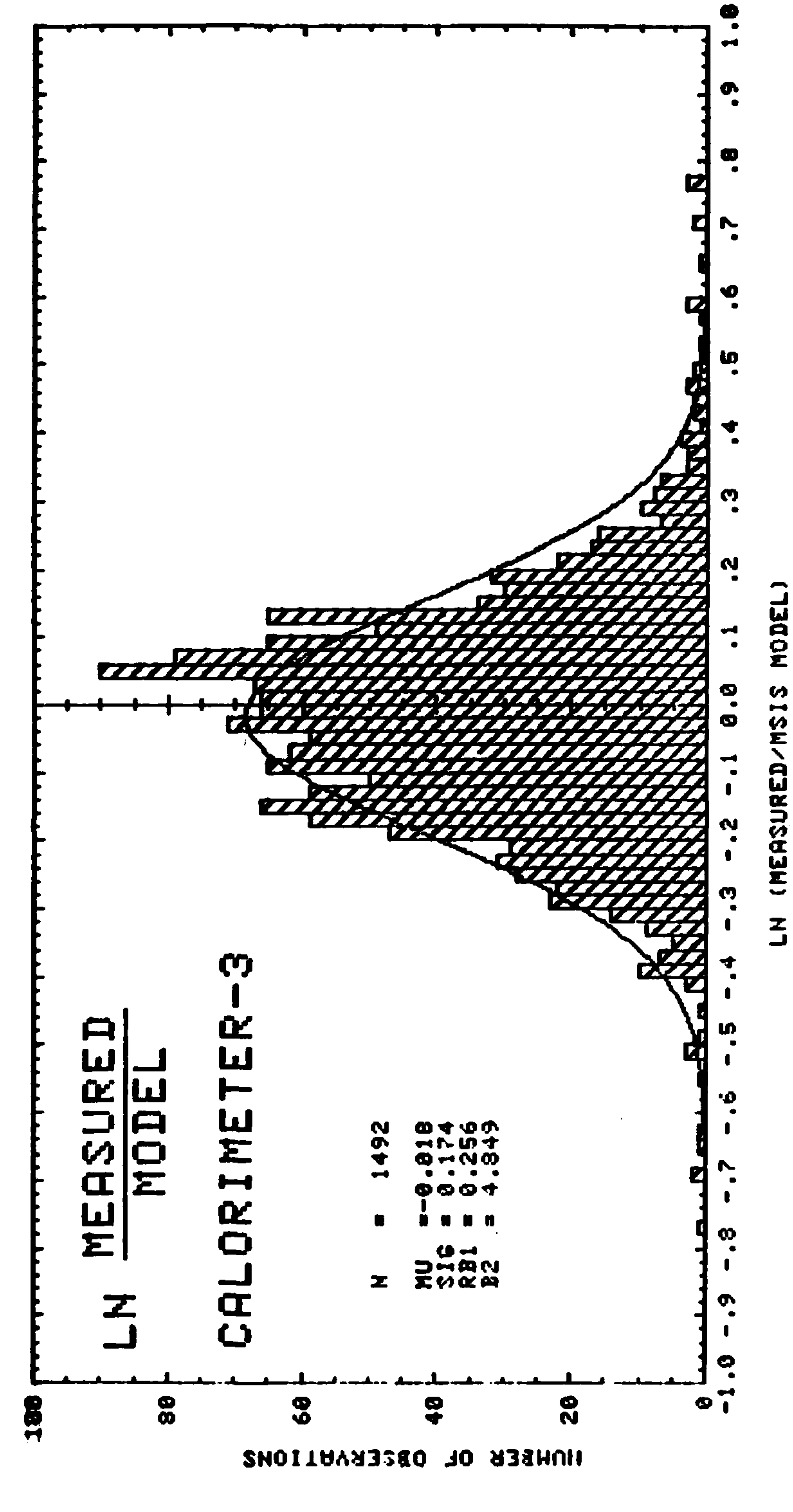

LN MEASURED / MODEL
CALORIMETER-3
N = 1492
MU =-0.018
SIG = 0.174
RB1 = 0.256
B2 = 4.849
NUMBER OF OBSERVATIONS
0
20
40
60
80
100
-1.0 -.9 -.8 -.7 -.6 -.5 -.4 -.3 -.2 -.1 0.0 .1 .2 .3 .4 .5 .6 .7 .8 .9 1.0
LN (MEASURED/MSIS MODEL)

Figure 3-15.

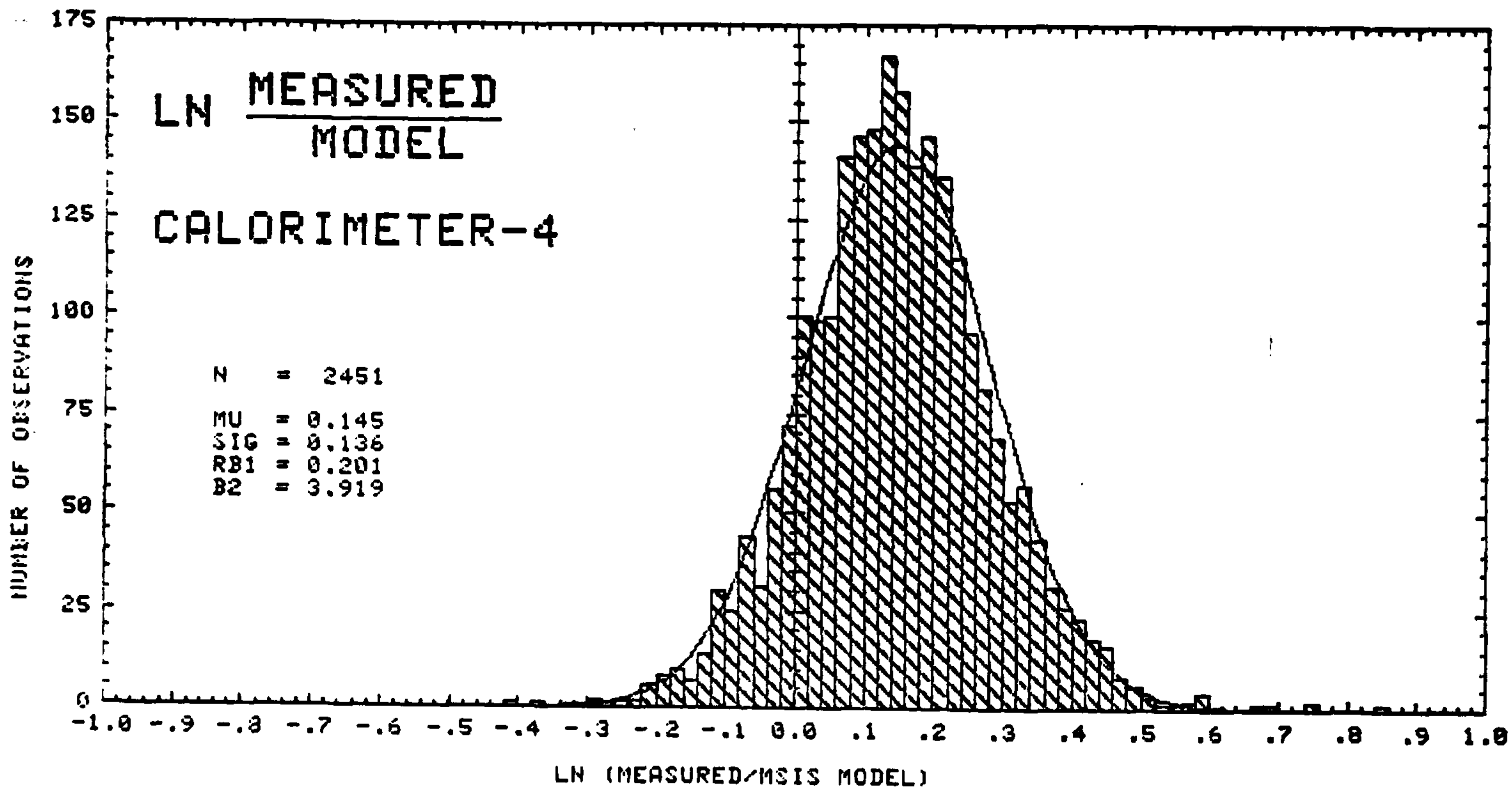
LN MEASURED / MODEL
CALORIMETER-4
N = 2451
MU = 0.145
SIG = 0.136
RB1 = 0.201
B2 = 3.919
NUMBER OF OBSERVATIONS
0
25
50
75
100
125
150
175
-1.0 -.9 -.8 -.7 -.6 -.5 -.4 -.3 -.2 -.1 0.0 .1 .2 .3 .4 .5 .6 .7 .8 .9 1.0
LN (MEASURED/MSIS MODEL)

Figure 3-16.

SECTION 4

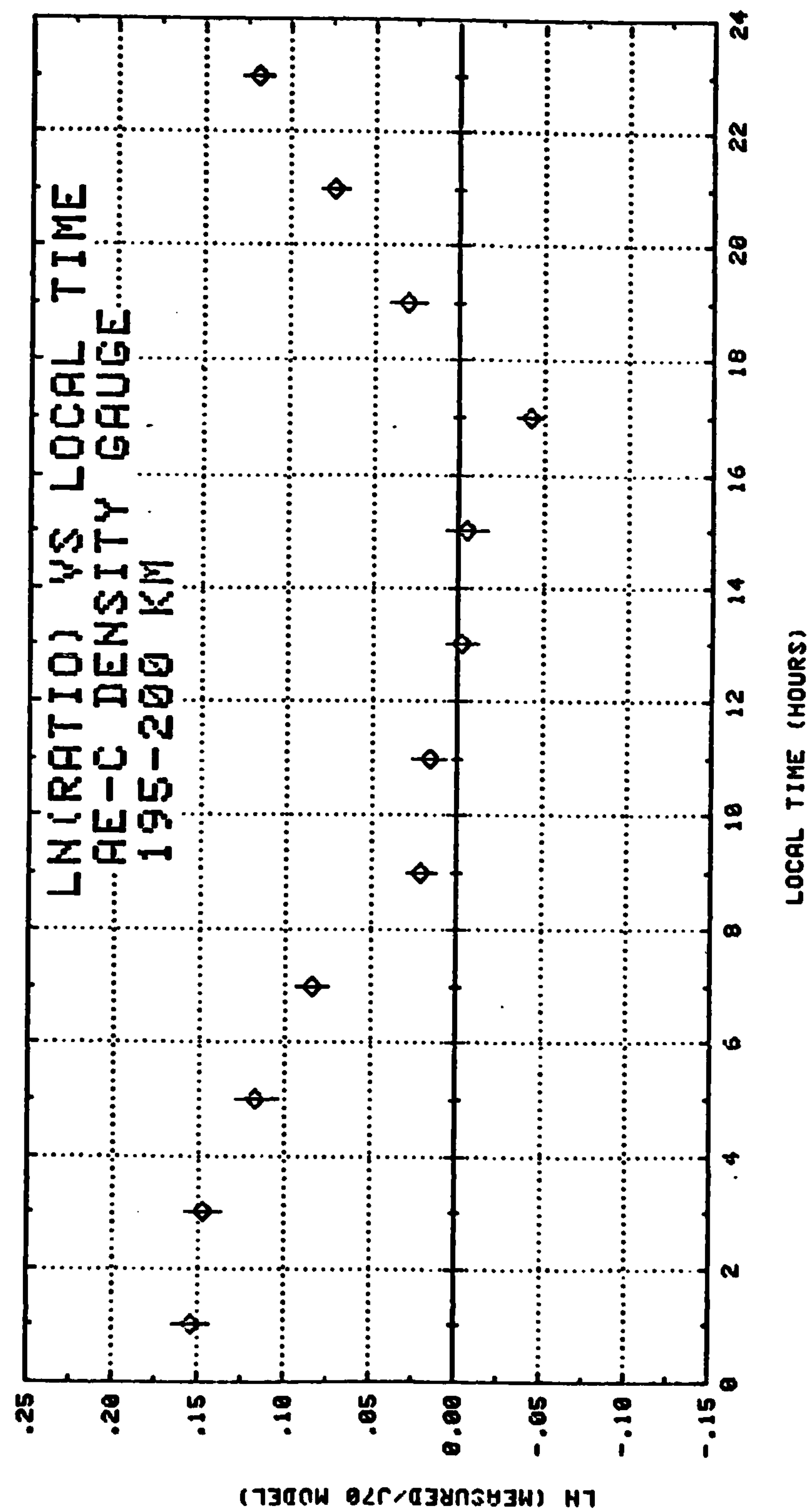

LN(RATIO) VS LOCAL TIME
AE-C DENSITY GAUGE
195-200 KM
LN (MEASURED/J70 MODEL)
LOCAL TIME (HOURS)
.25
.20
.15
.10
.05
0.00
-.05
-.10
-.15
0
2
4
6
8
10
12
14
16
18
20
22
24

Figure 4-1.

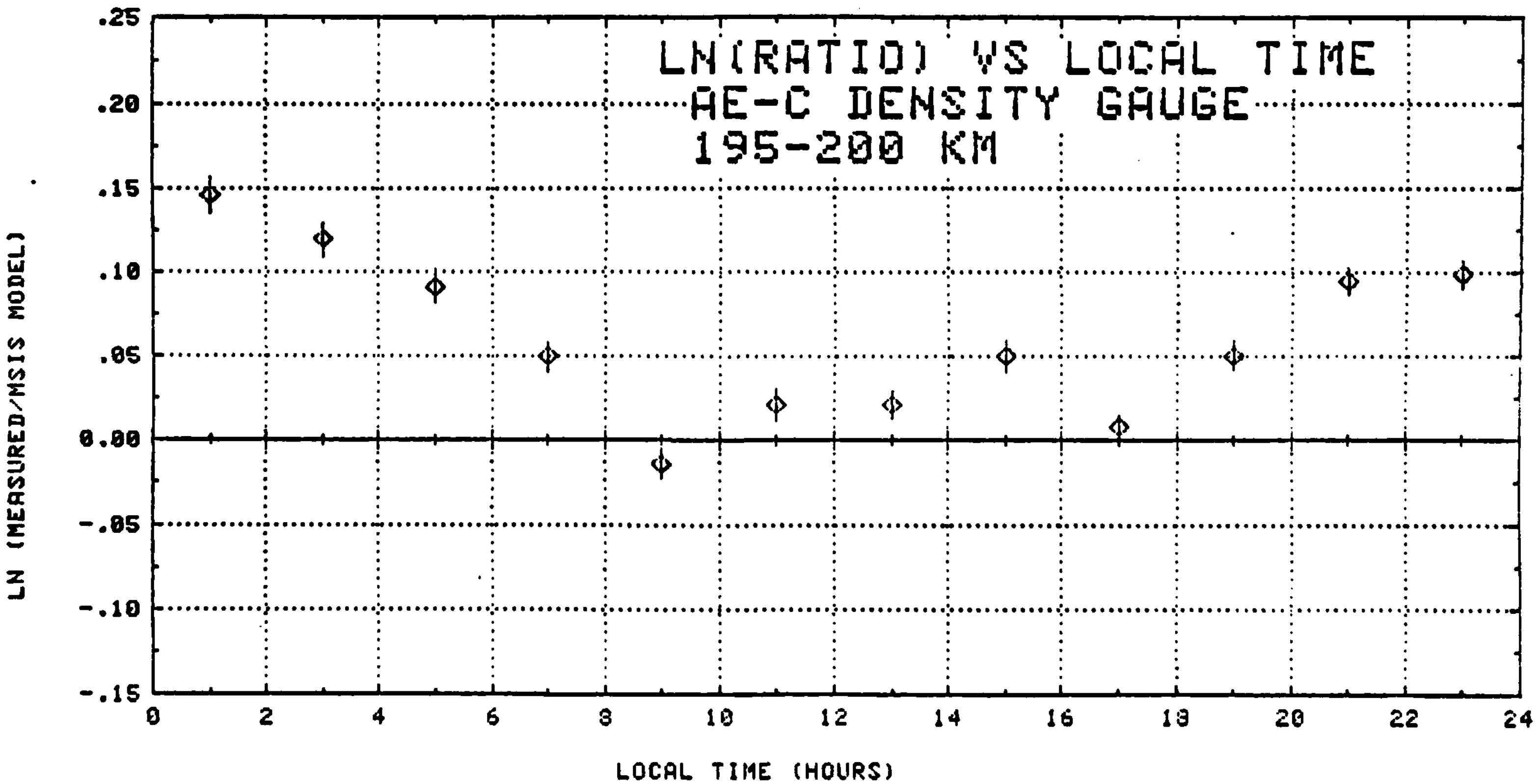
LN(RATIO) VS LOCAL TIME
AE-C DENSITY GAUGE
195-200 KM
.25
.20
.15
.10
.05
0.00
-.05
-.10
-.15
0
2
4
6
8
10
12
14
16
18
20
22
24
LOCAL TIME (HOURS)
LN (MEASURED/MSIS MODEL)

Figure 4-2.

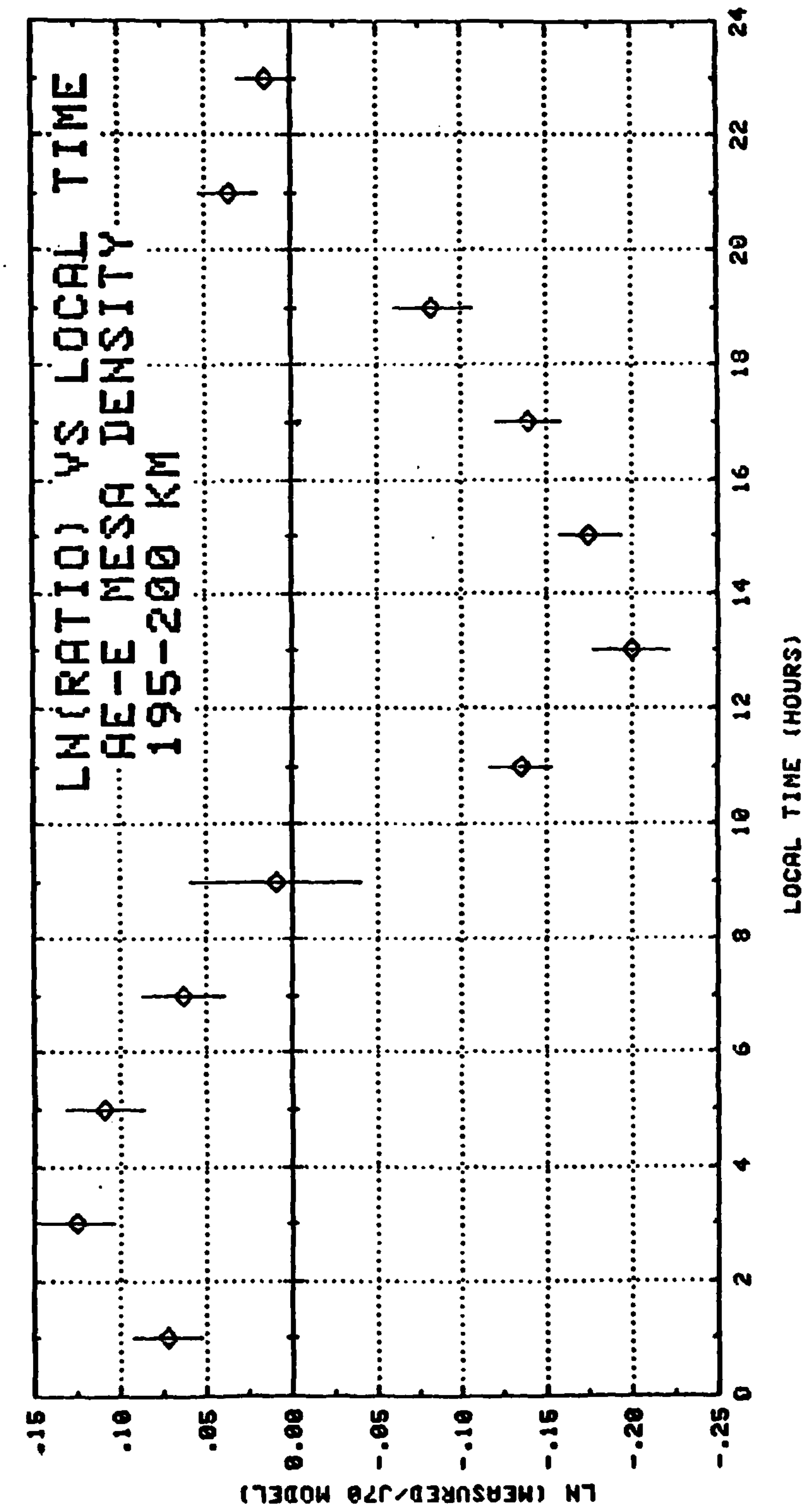
LN(RATIO) VS LOCAL TIME
AE-E MESA DENSITY
195-200 KM
LOCAL TIME (HOURS)
LN (MEASURED/J70 MODEL)
.15
.10
.05
0.00
-.05
-.10
-.15
-.20
-.25
0
2
4
6
8
10
12
14
16
18
20
22
24

Figure 4-3.

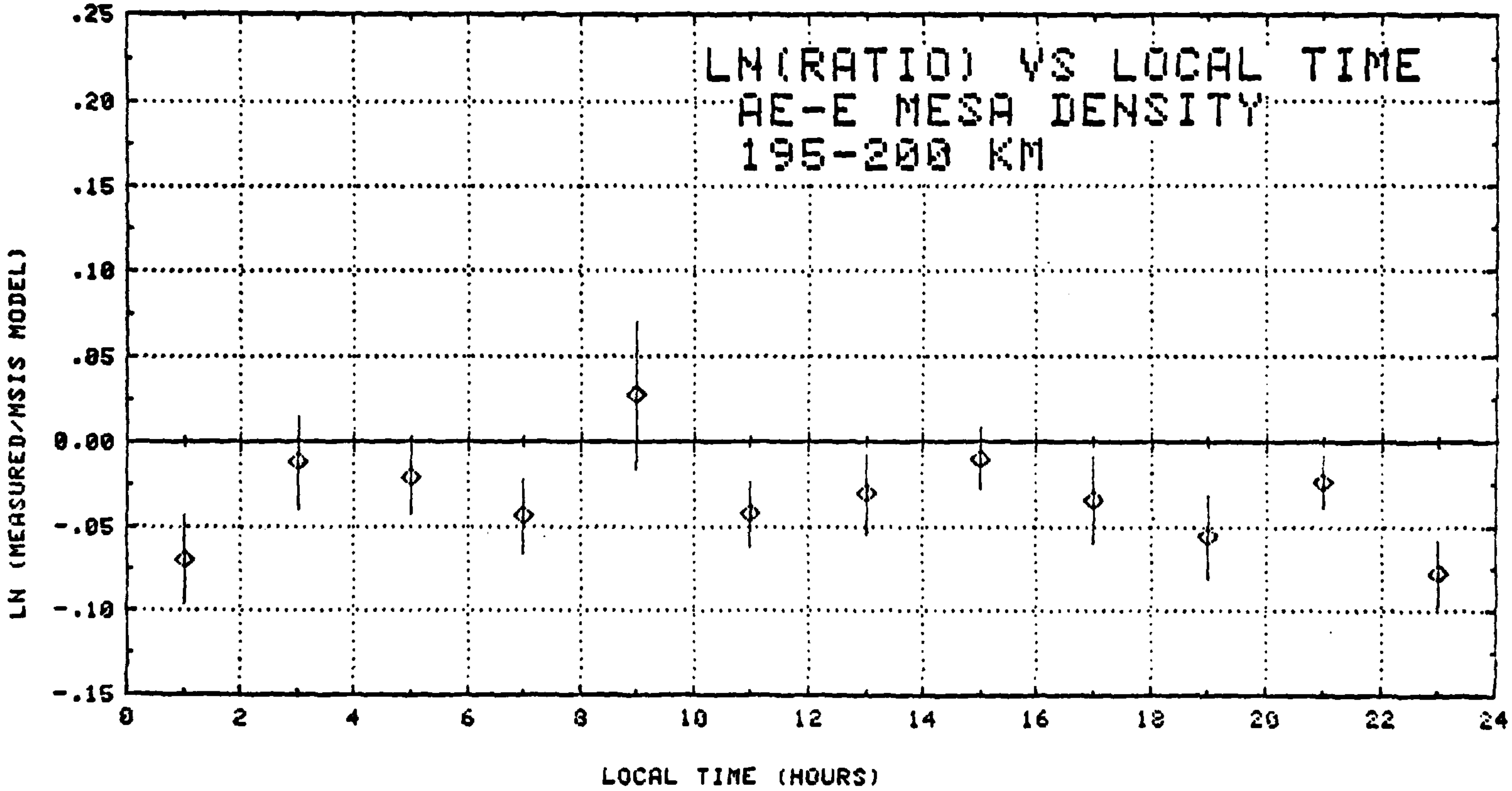
LN(RATIO) VS LOCAL TIME
AE-E MESA DENSITY
195-200 KM
LN (MEASURED/MSIS MODEL)
.25
.20
.15
.10
.05
0.00
-.05
-.10
-.15
0
2
4
6
8
10
12
14
16
18
20
22
24
LOCAL TIME (HOURS)

Figure 4-4.

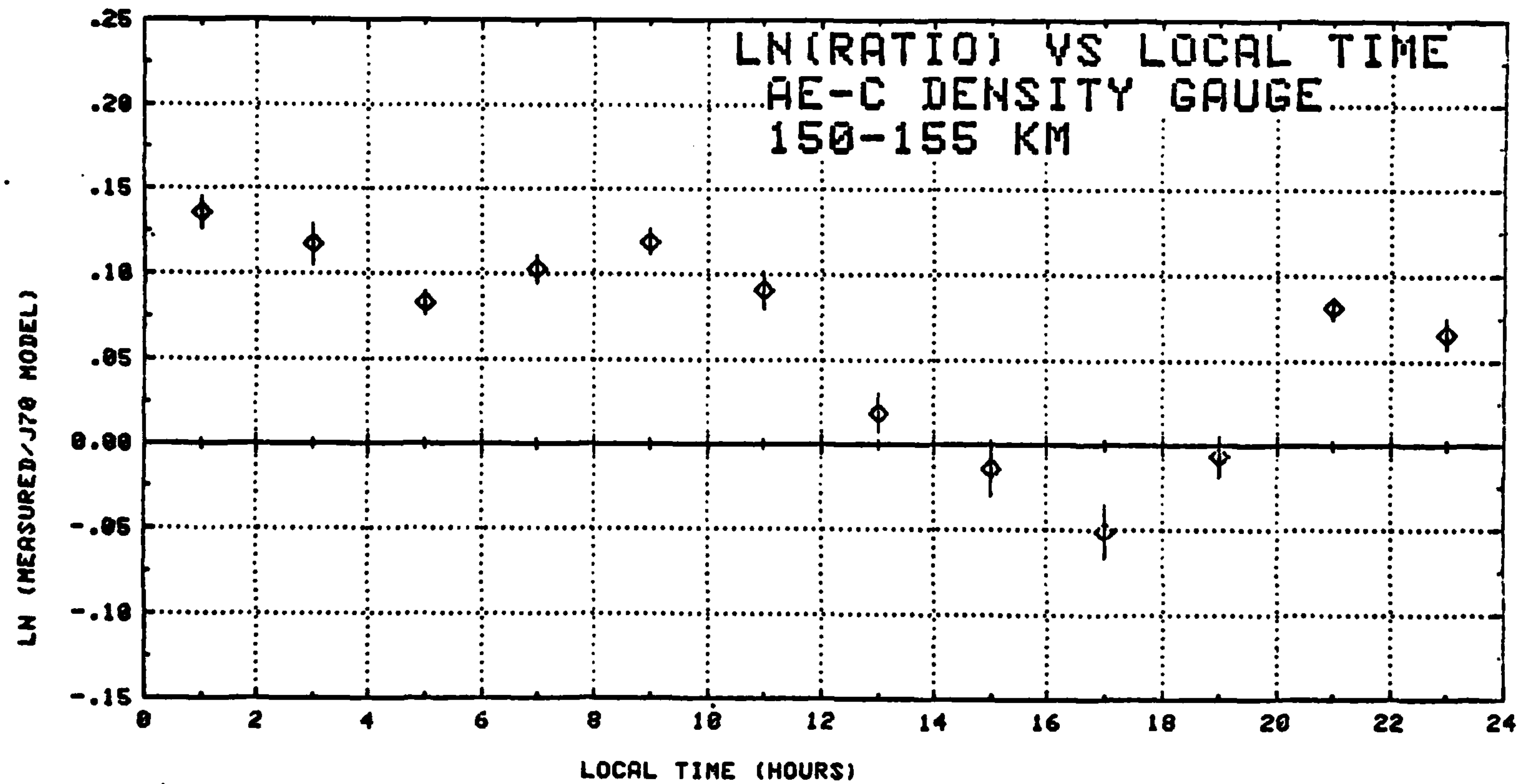
LN(RATIO) VS LOCAL TIME
AE-C DENSITY GAUGE
150-155 KM
.25
.20
.15
.10
.05
0.00
-.05
-.10
-.15
LN (MEASURED/J70 MODEL)
0
2
4
6
8
10
12
14
16
18
20
22
24
LOCAL TIME (HOURS)

Figure 4-5.

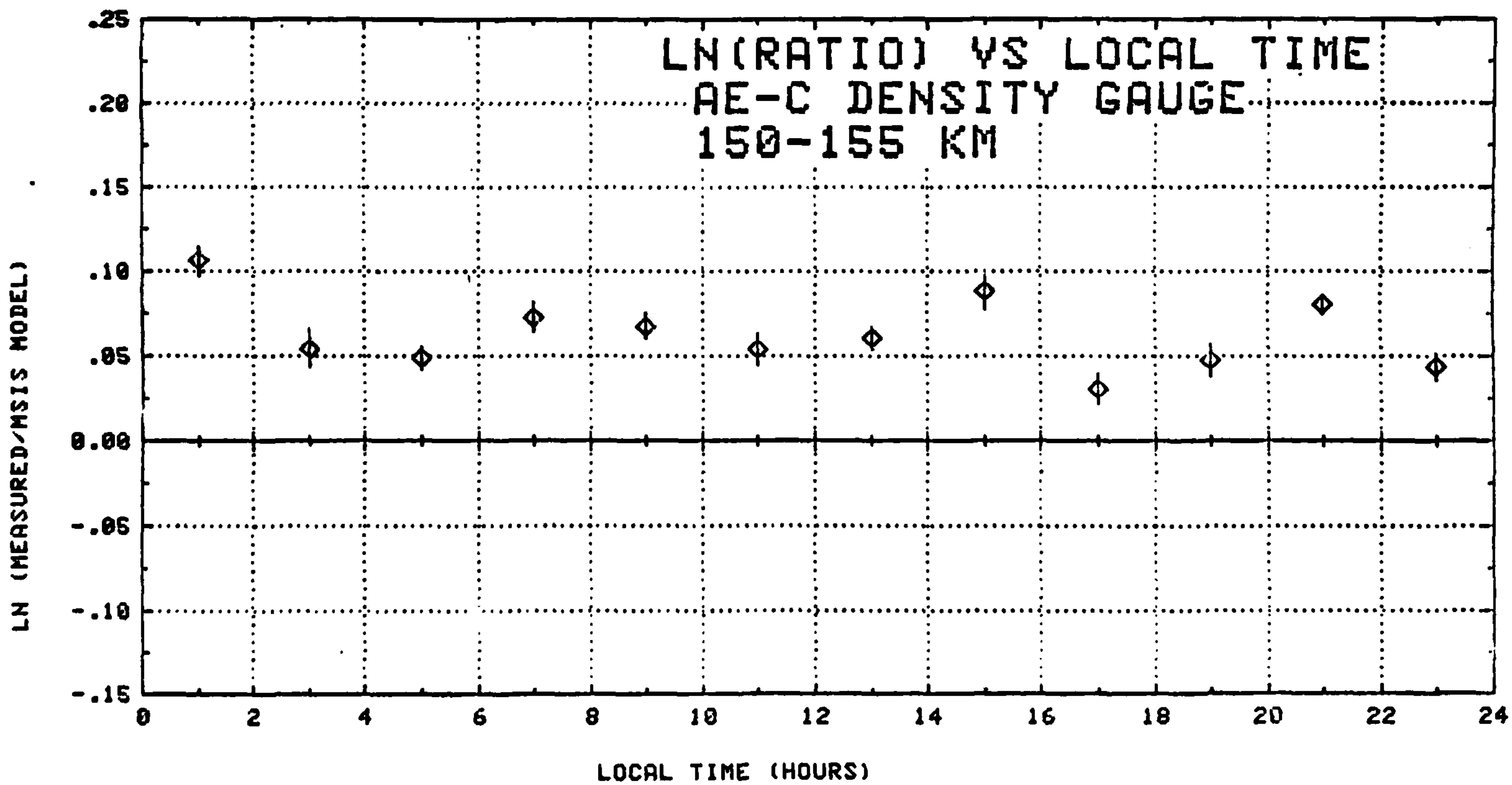
LN(RATIO) VS LOCAL TIME
AE-C DENSITY GAUGE
150-155 KM
.25
.20
.15
.10
.05
0.00
-.05
-.10
-.15
LN (MEASURED/MSIS MODEL)
0
2
4
6
8
10
12
14
16
18
20
22
24
LOCAL TIME (HOURS)

Figure 4-6.

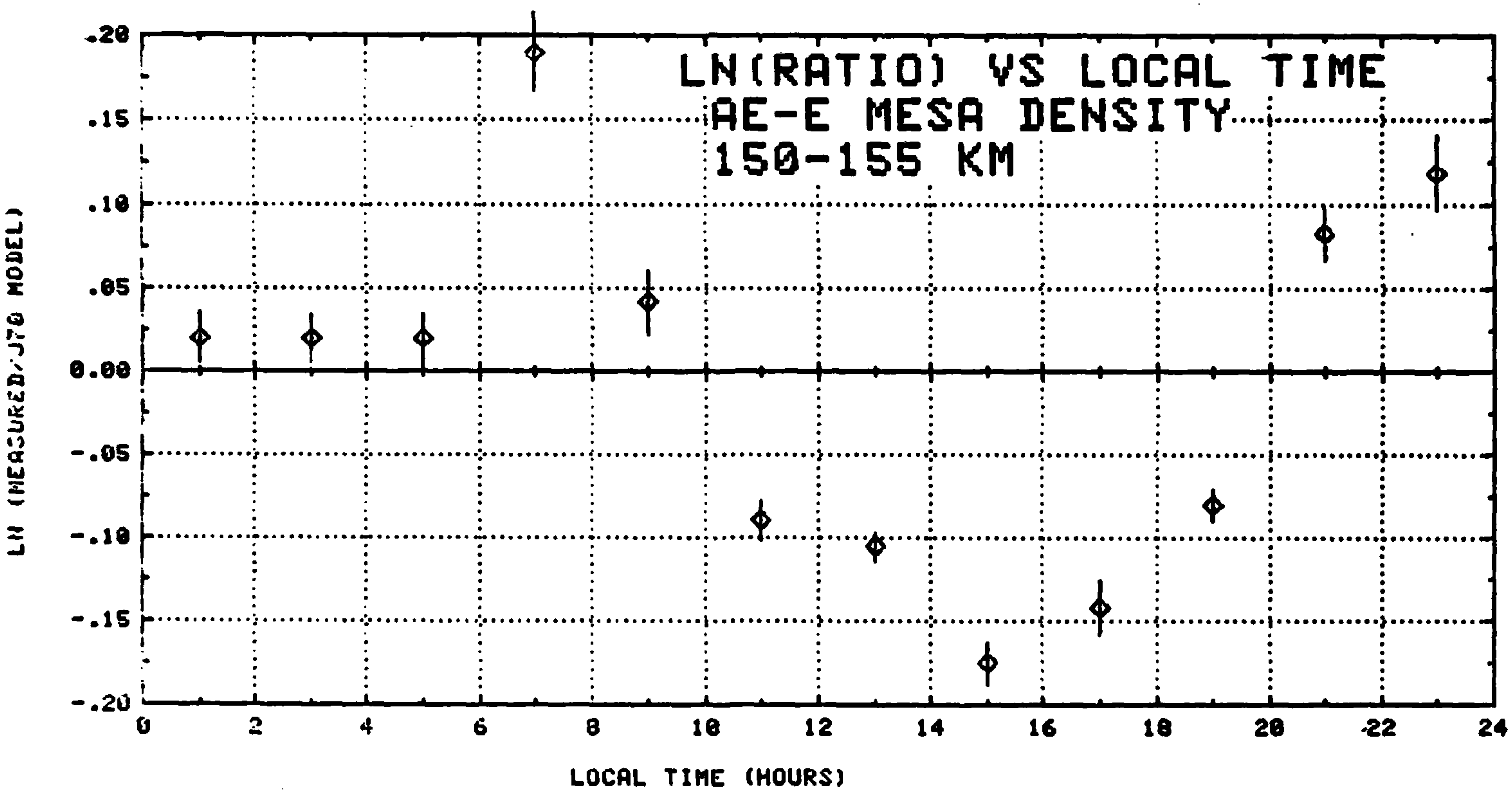
LN(RATIO) VS LOCAL TIME
AE-E MESA DENSITY
150-155 KM
.20
.15
.10
.05
0.00
-.05
-.10
-.15
-.20
LN (MEASURED/J70 MODEL)
0
2
4
6
8
10
12
14
16
18
20
22
24
LOCAL TIME (HOURS)

Figure 4-7.

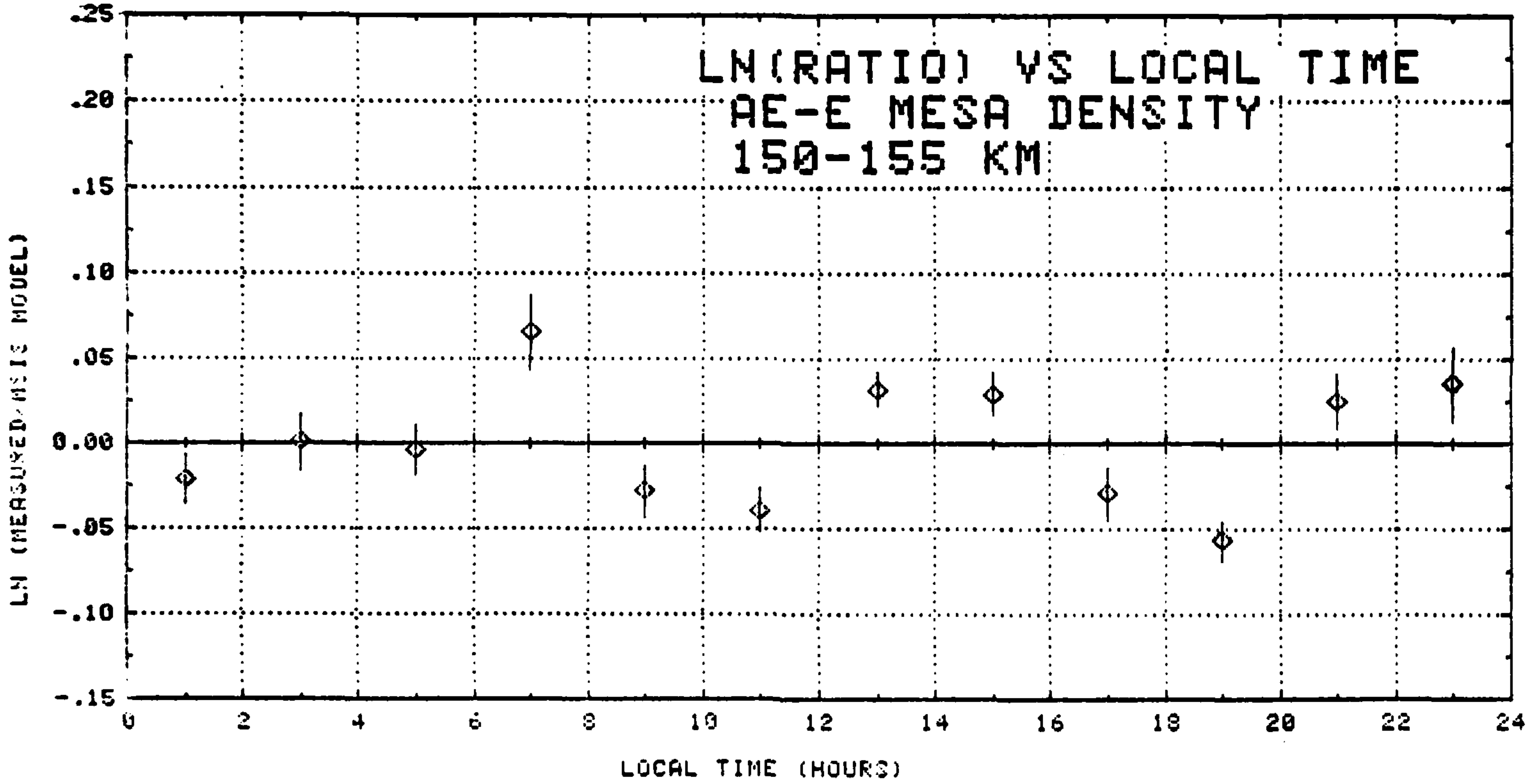
LN(RATIO) VS LOCAL TIME
AE-E MESA DENSITY
150-155 KM
.25
.20
.15
.10
.05
0.00
-.05
-.10
-.15
LN (MEASURED/MSIS MODEL)
0
2
4
6
8
10
12
14
16
18
20
22
24
LOCAL TIME (HOURS)

Figure 4-8.

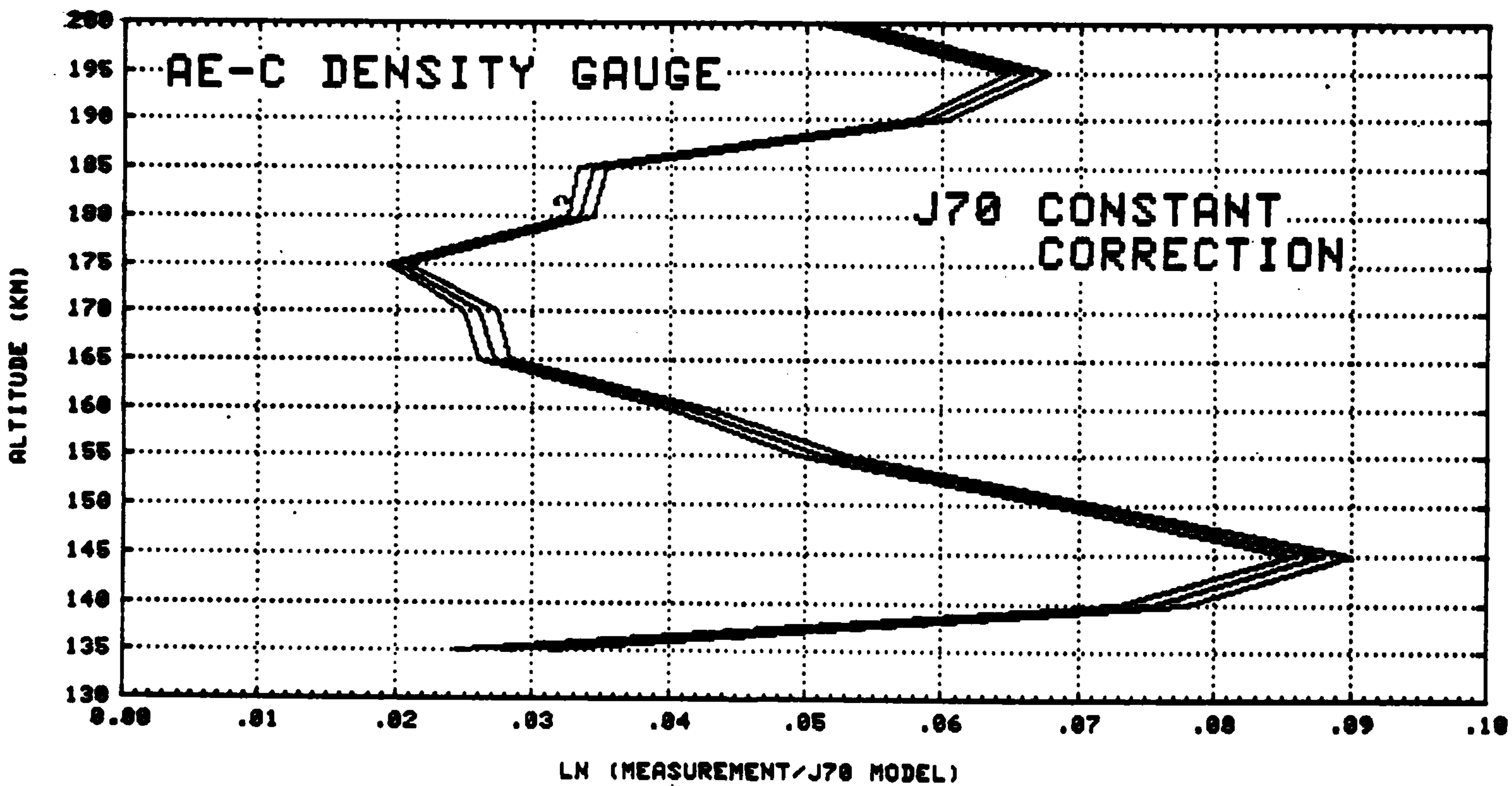

AE-C DENSITY GAUGE
J70 CONSTANT
CORRECTION
200
195
190
185
180
175
170
165
160
155
150
145
140
135
130
ALTITUDE (KM)
0.00
.01
.02
.03
.04
.05
.06
.07
.08
.09
.10
LN (MEASUREMENT/J70 MODEL)

Figure 4-9.

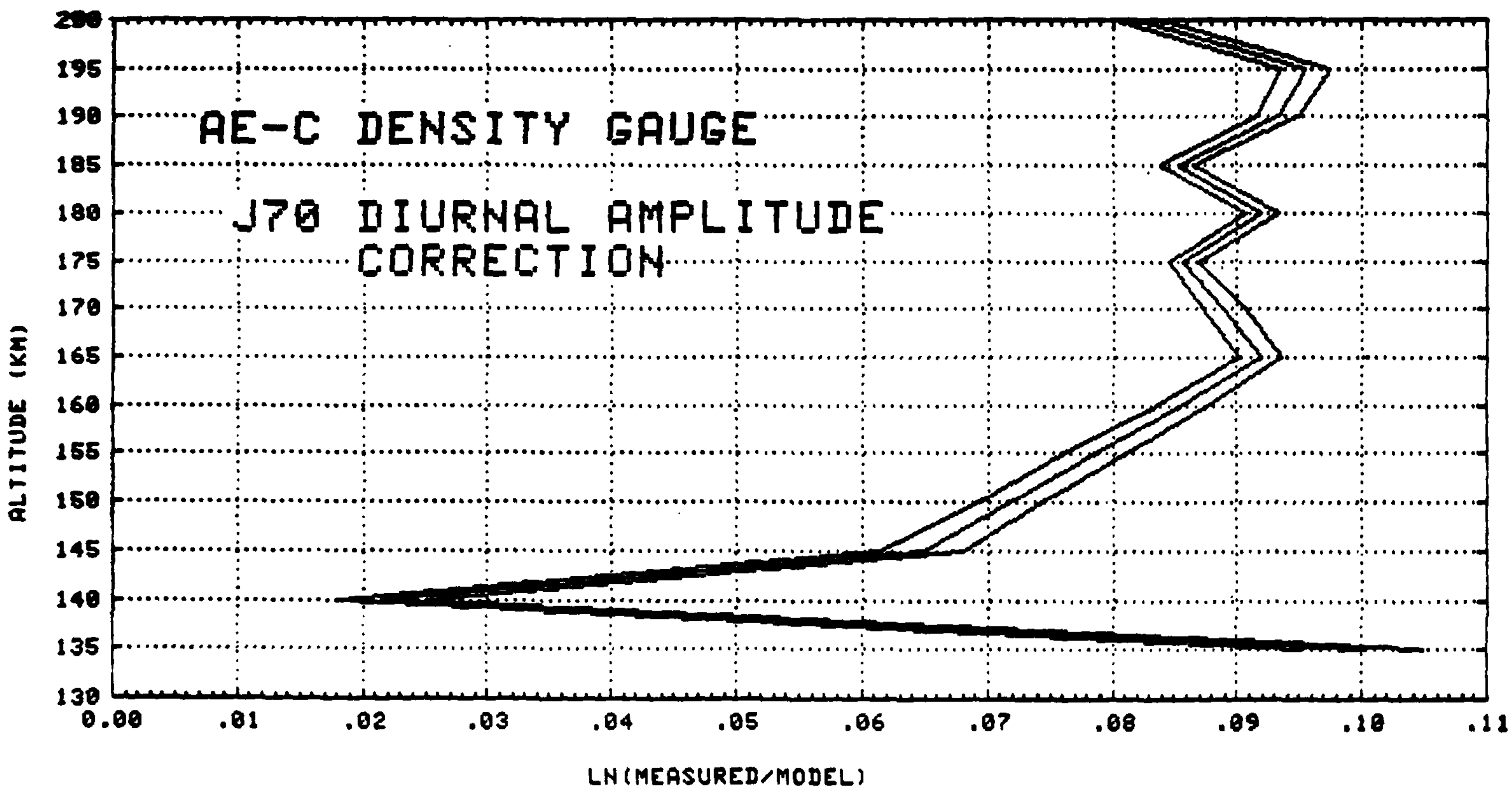
AE-C DENSITY GAUGE
J70 DIURNAL AMPLITUDE
CORRECTION
200
195
190
185
180
175
170
165
160
155
150
145
140
135
130
ALTITUDE (KM)
0.00
.01
.02
.03
.04
.05
.06
.07
.08
.09
.10
.11
LN(MEASURED/MODEL)

Figure 4-10.

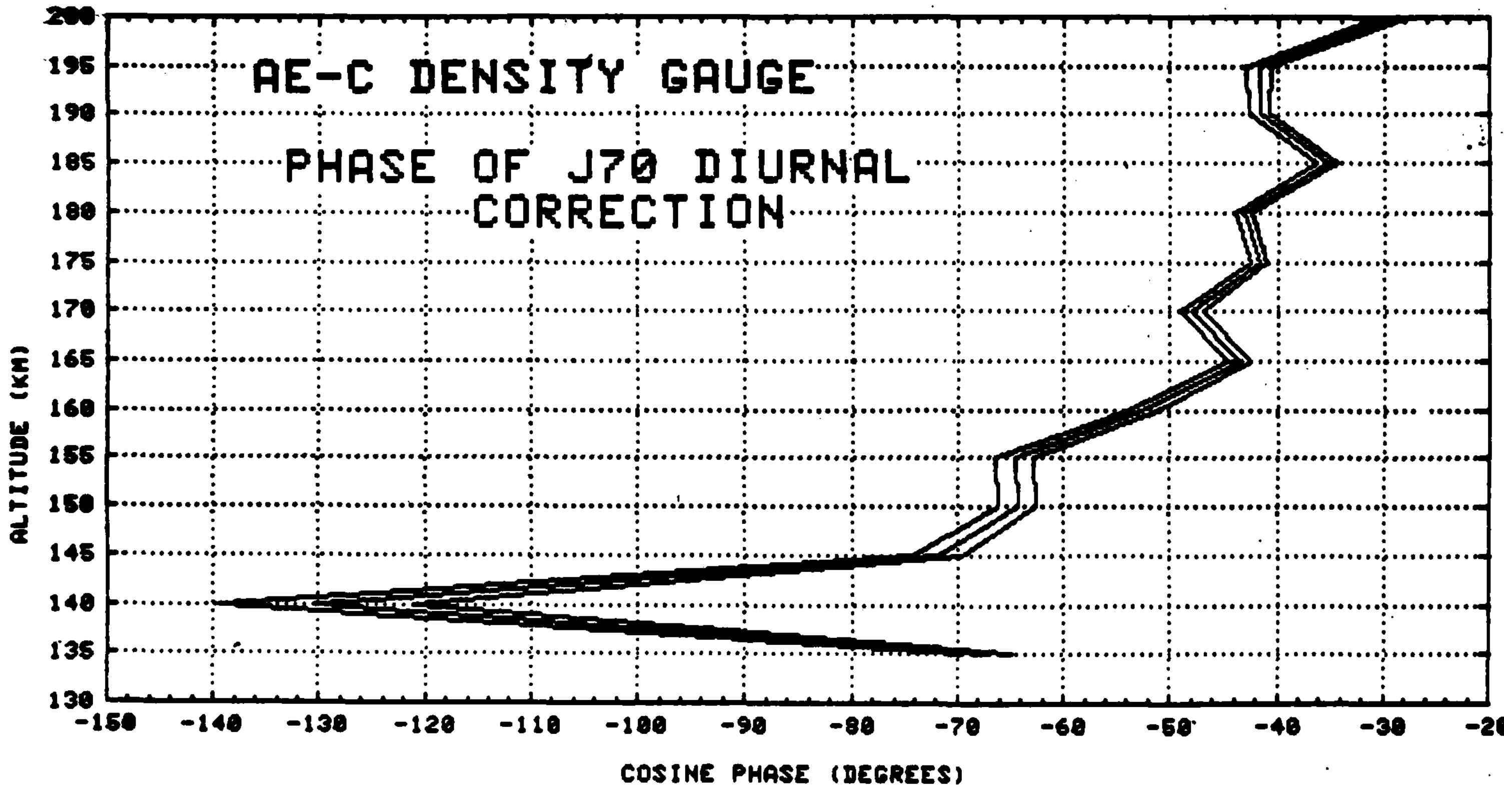

AE-C DENSITY GAUGE
PHASE OF J70 DIURNAL CORRECTION
ALTITUDE (KM)
200
195
190
185
180
175
170
165
160
155
150
145
140
135
130
-150
-140
-130
-120
-110
-100
-90
-80
-70
-60
-50
-40
-30
-20
COSINE PHASE (DEGREES)

Figure 4-11.

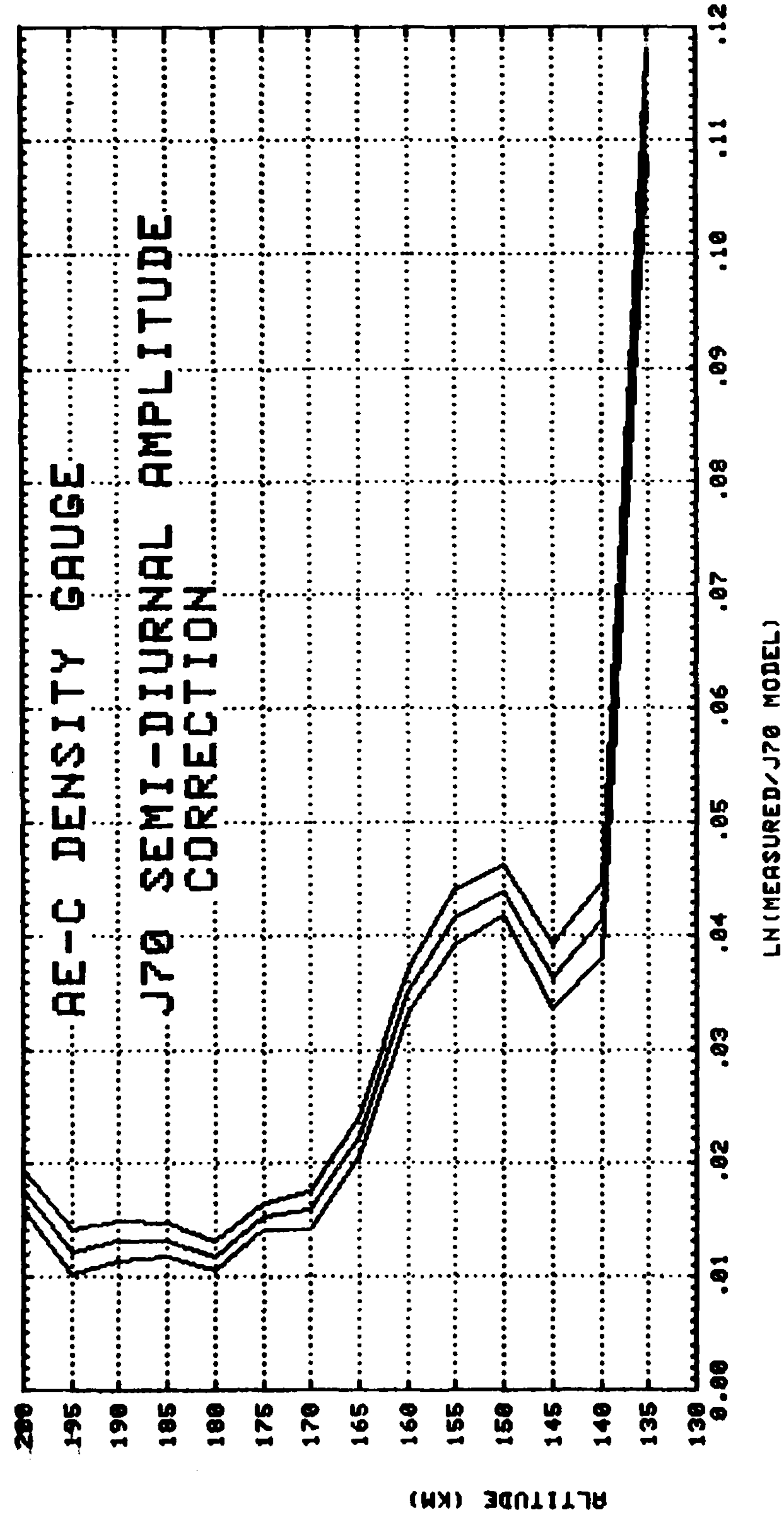
AE-C DENSITY GAUGE
J70 SEMI-DIURNAL AMPLITUDE
CORRECTION
200
195
190
185
180
175
170
165
160
155
150
145
140
135
130
ALTITUDE (KM)
0.00
.01
.02
.03
.04
.05
.06
.07
.08
.09
.10
.11
.12
LN(MEASURED/J70 MODEL)

Figure 4-12.

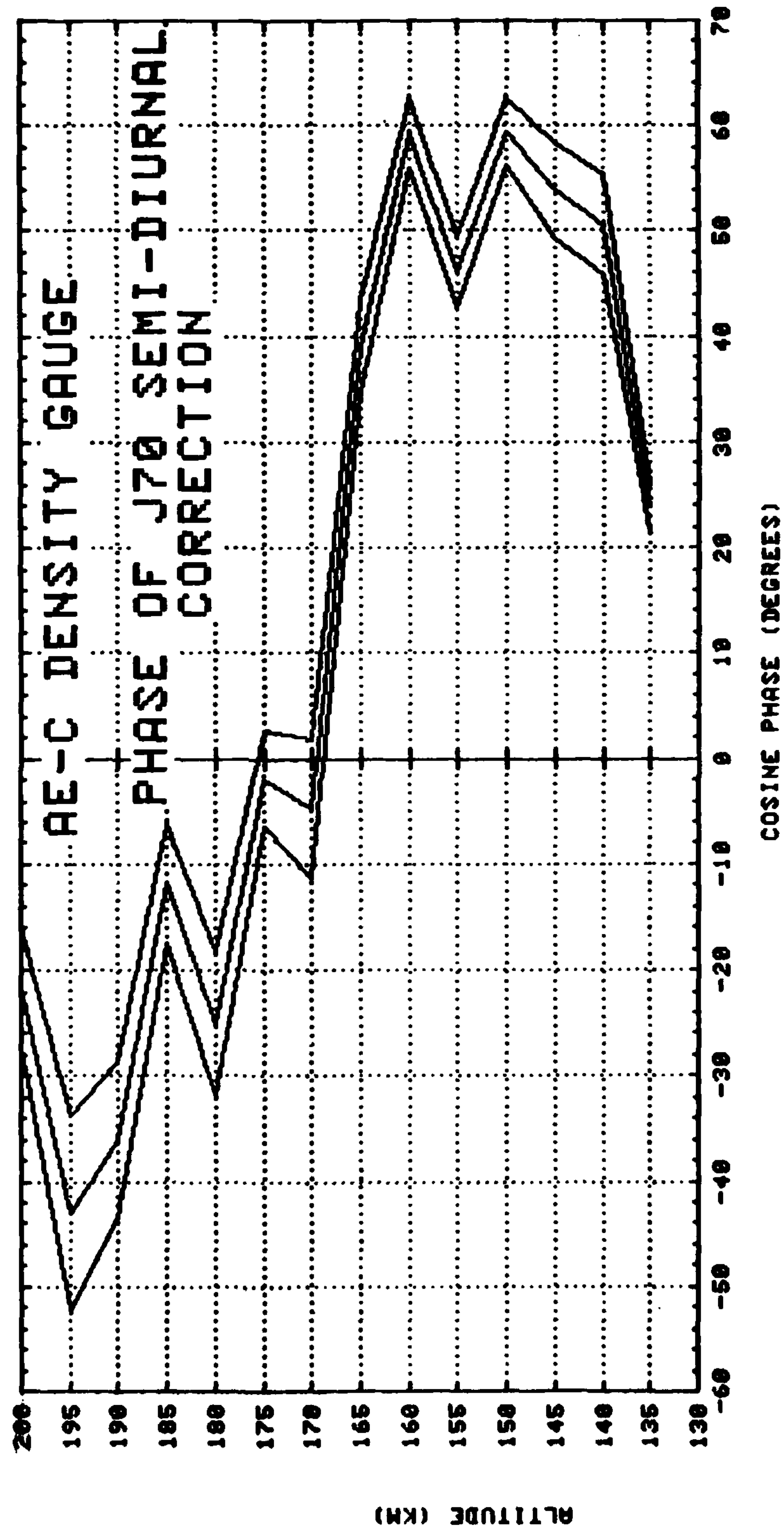
AE-C DENSITY GAUGE
PHASE OF J70 SEMI-DIURNAL
CORRECTION
COSINE PHASE (DEGREES)
ALTITUDE (KM)
-60
-50
-40
-30
-20
-10
0
10
20
30
40
50
60
70
200
195
190
185
180
175
170
165
160
155
150
145
140
135
130

Figure 4-13.

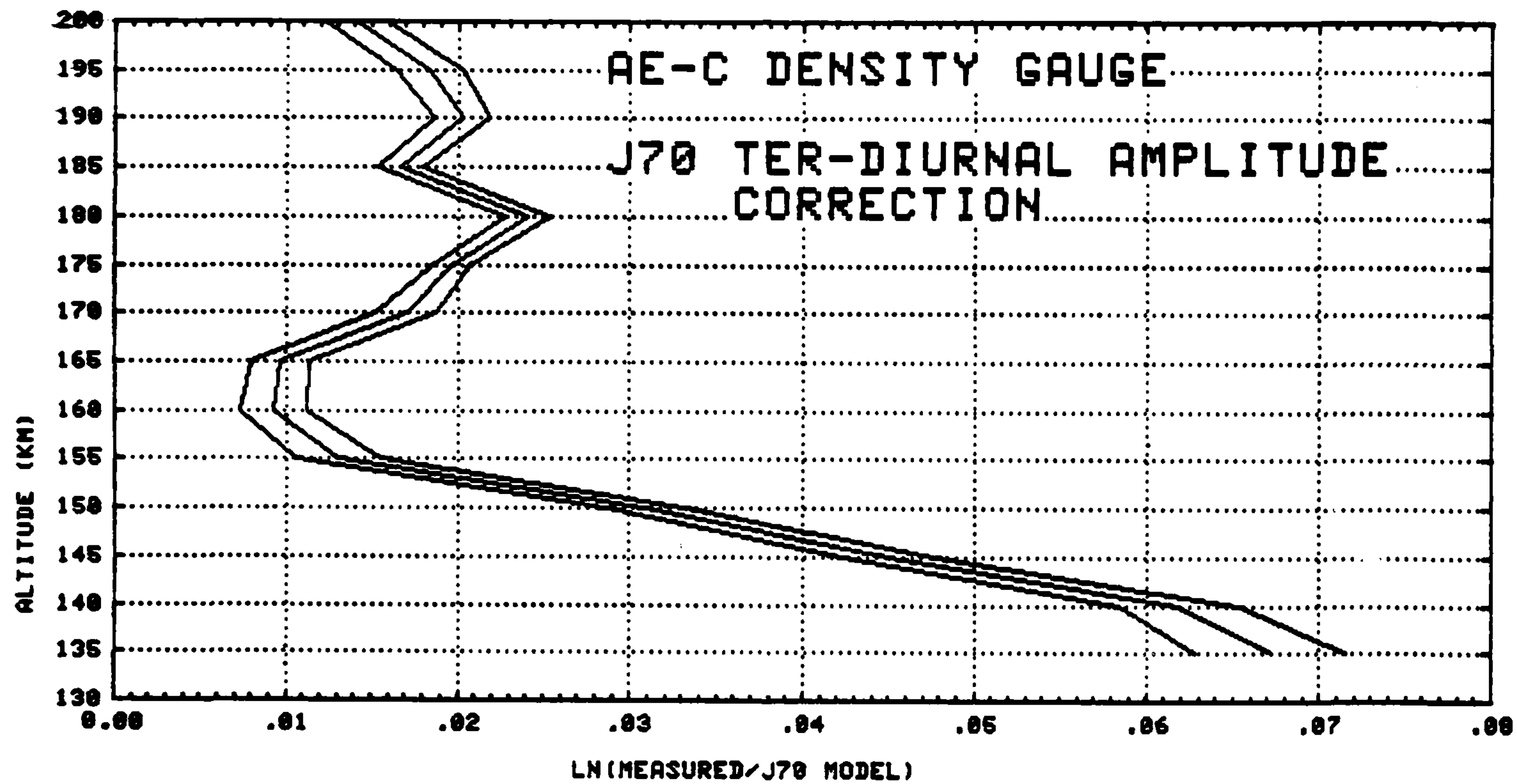
AE-C DENSITY GAUGE
J70 TER-DIURNAL AMPLITUDE CORRECTION
ALTITUDE (KM)
LN(MEASURED/J70 MODEL)
200
195
190
185
180
175
170
165
160
155
150
145
140
135
130
0.00
.01
.02
.03
.04
.05
.06
.07
.08

Figure 4-14.

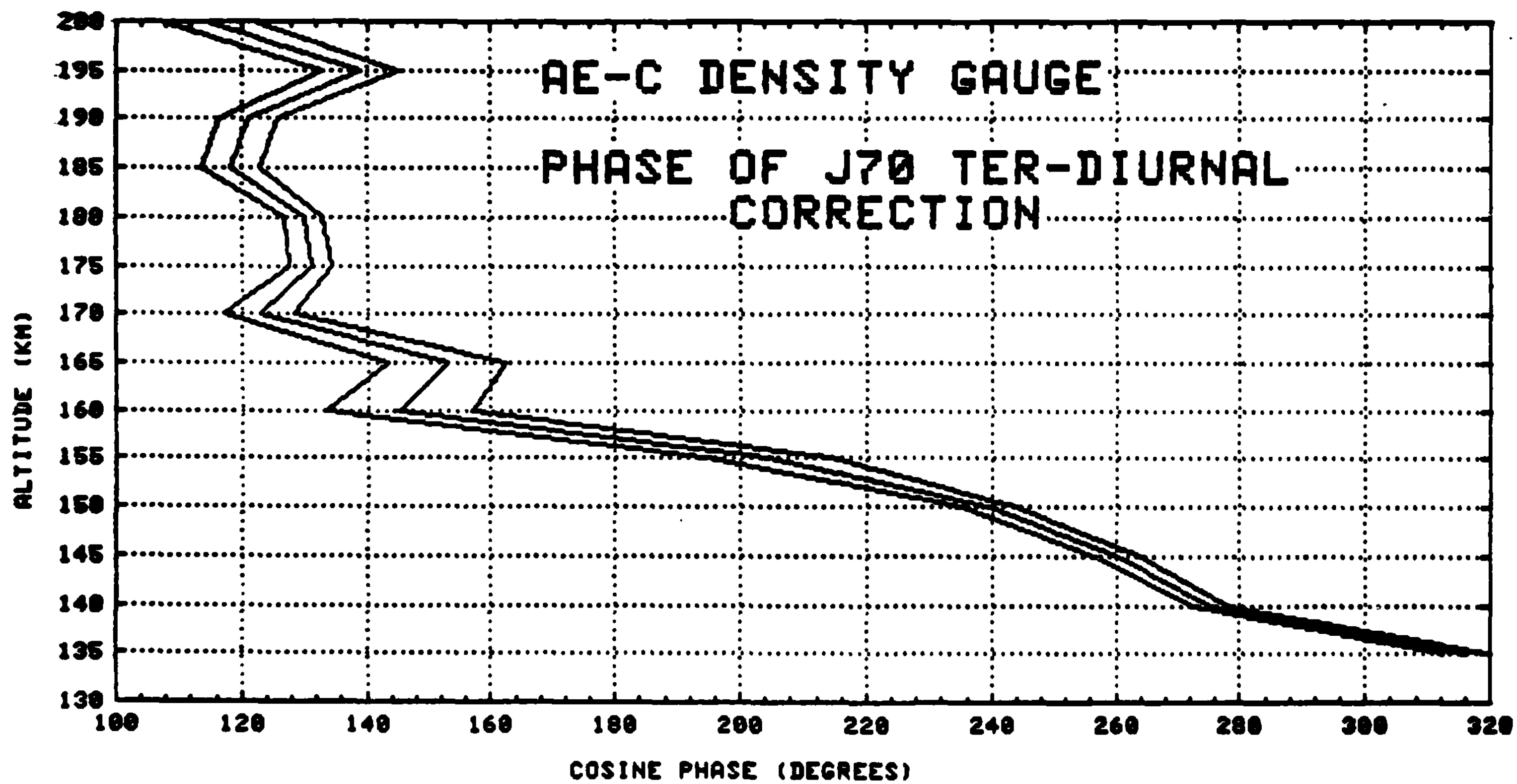
AE-C DENSITY GAUGE
PHASE OF J70 TER-DIURNAL CORRECTION
ALTITUDE (KM)
200
195
190
185
180
175
170
165
160
155
150
145
140
135
130
100
120
140
160
180
200
220
240
260
280
300
320
COSINE PHASE (DEGREES)

Figure 4-15.

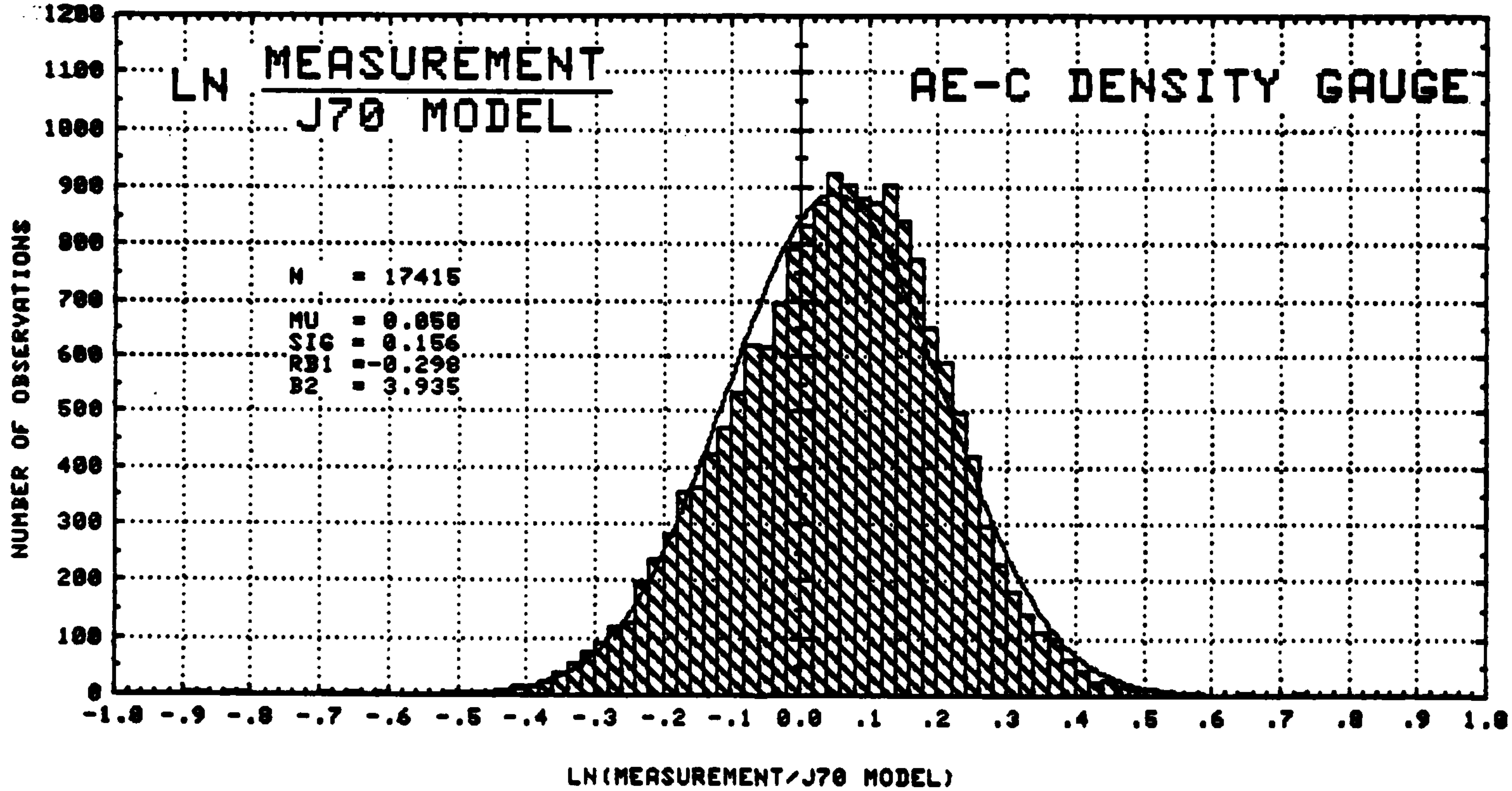

LN MEASUREMENT / J70 MODEL
AE-C DENSITY GAUGE
N = 17415
MU = 0.050
SIG = 0.156
RB1 =-0.298
B2 = 3.935
NUMBER OF OBSERVATIONS
0
100
200
300
400
500
600
700
800
900
1000
1100
1200
-1.0 -.9 -.8 -.7 -.6 -.5 -.4 -.3 -.2 -.1 0.0 .1 .2 .3 .4 .5 .6 .7 .8 .9 1.0
LN(MEASUREMENT/J70 MODEL)

Figure 4-16.

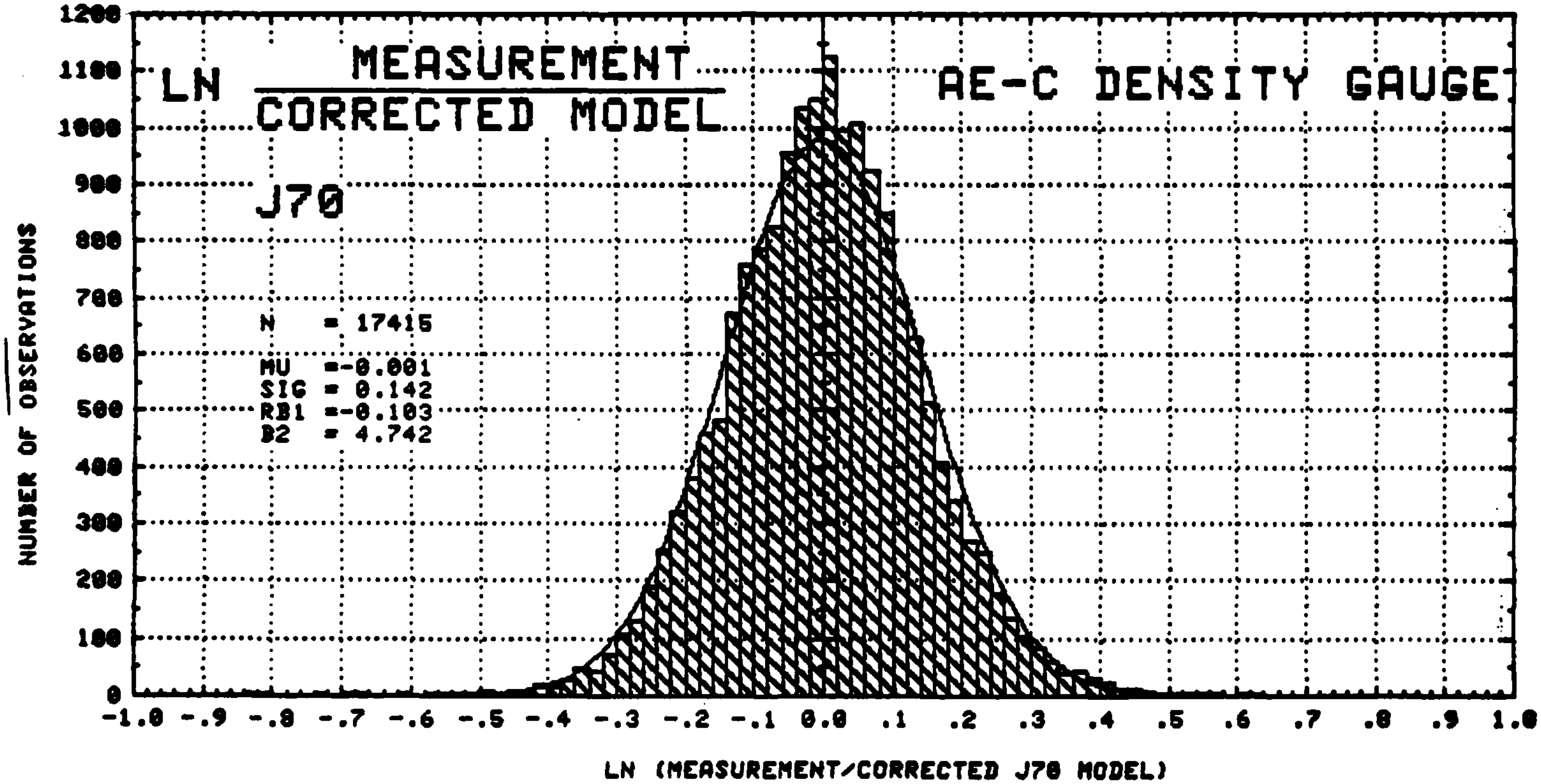
LN MEASUREMENT / CORRECTED MODEL
AE-C DENSITY GAUGE
J70
N = 17415
MU =-0.001
SIG = 0.142
RB1 =-0.103
B2 = 4.742
NUMBER OF OBSERVATIONS
0
100
200
300
400
500
600
700
800
900
1000
1100
1200
-1.0 -.9 -.8 -.7 -.6 -.5 -.4 -.3 -.2 -.1 0.0 .1 .2 .3 .4 .5 .6 .7 .8 .9 1.0
LN (MEASUREMENT/CORRECTED J70 MODEL)

Figure 4-17.

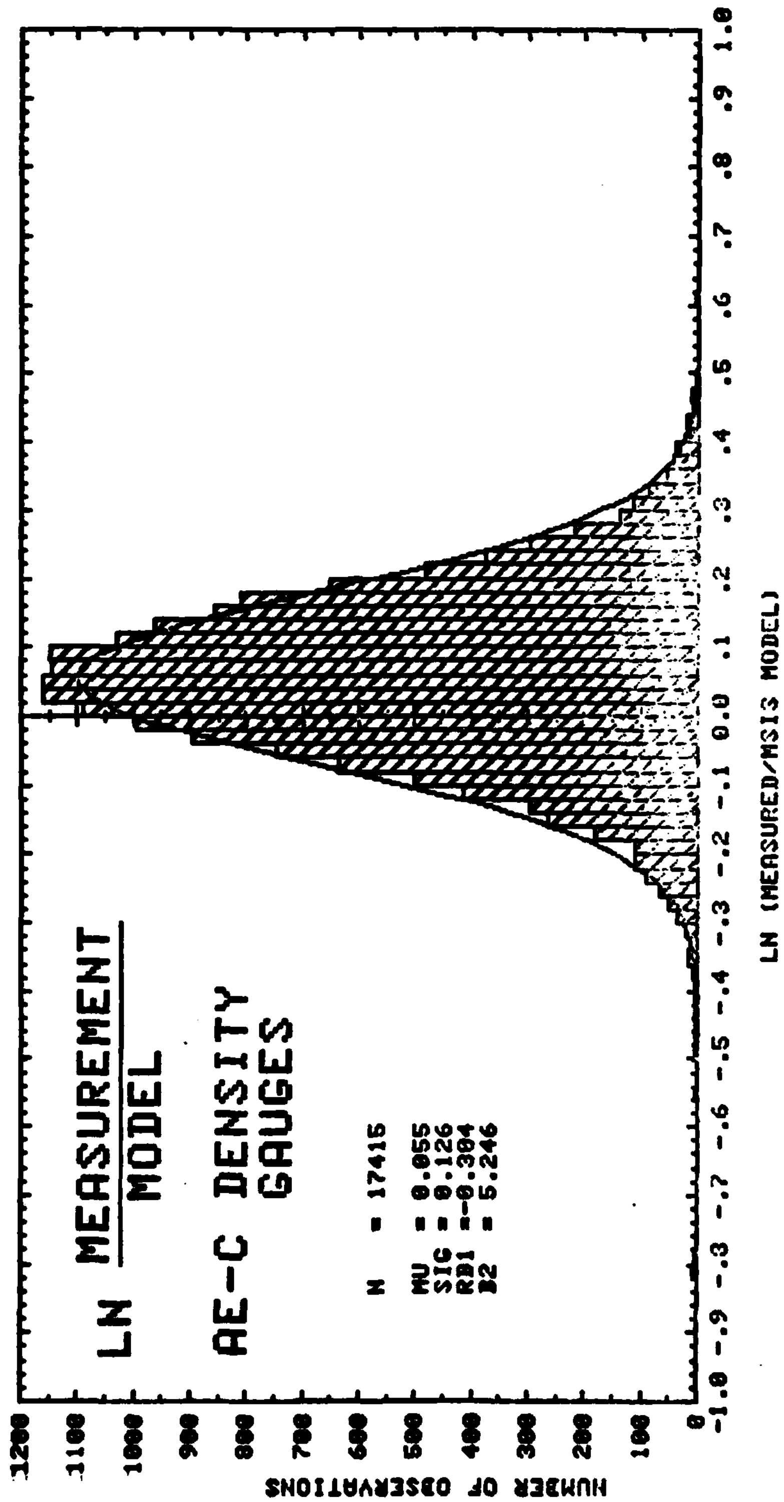

LN MEASUREMENT / MODEL
AE-C DENSITY GAUGES
N = 17415
MU = 0.055
SIG = 0.126
RB1 =-0.304
B2 = 5.246
NUMBER OF OBSERVATIONS
0 100 200 300 400 500 600 700 800 900 1000 1100 1200
-1.0 -.9 -.8 -.7 -.6 -.5 -.4 -.3 -.2 -.1 0.0 .1 .2 .3 .4 .5 .6 .7 .8 .9 1.0
LN (MEASURED/MSIS MODEL)

Figure 4-18.

LABORATORY OPERATIONS

The Laboratory Operations of The Aerospace Corporation is conducting experimental and theoretical investigations necessary for the evaluation and application of scientific advances to new military space systems. Versatility and flexibility have been developed to a high degree by the laboratory personnel in dealing with the many problems encountered in the nation's rapidly developing space systems. Expertise in the latest scientific developments is vital to the accomplishment of tasks related to these problems. The laboratories that contribute to this research are:

Aerophysics Laboratory: Launch vehicle and reentry aerodynamics and heat transfer, propulsion chemistry and fluid mechanics, structural mechanics, flight dynamics; high-temperature thermomechanics, gas kinetics and radiation; research in environmental chemistry and contamination; cw and pulsed chemical laser development including chemical kinetics, spectroscopy, optical resonators and beam pointing, atmospheric propagation, laser effects and countermeasures.

Chemistry and Physics Laboratory: Atmospheric chemical reactions, atmospheric optics, light scattering, state-specific chemical reactions and radiation transport in rocket plumes, applied laser spectroscopy, laser chemistry, battery electrochemistry, space vacuum and radiation effects on materials, lubrication and surface phenomena, thermionic emission, photosensitive materials and detectors, atomic frequency standards, and bioenvironmental research and monitoring.

Electronics Research Laboratory: Microelectronics, GaAs low-noise and power devices, semiconductor lasers, electromagnetic and optical propagation phenomena, quantum electronics, laser communications, lidar, and electro-optics; communication sciences, applied electronics, semiconductor crystal and device physics, radiometric imaging; millimeter-wave and microwave technology.

Information Sciences Research Office: Program verification, program translation, performance-sensitive system design, distributed architectures for spaceborne computers, fault-tolerant computer systems, artificial intelligence, and microelectronics applications.

Materials Sciences Laboratory: Development of new materials: metal matrix composites, polymers, and new forms of carbon; component failure analysis and reliability; fracture mechanics and stress corrosion; evaluation of materials in space environment; materials performance in space transportation systems; analysis of systems vulnerability and survivability in enemy-induced environments.

Space Sciences Laboratory: Atmospheric and ionospheric physics, radiation from the atmosphere, density and composition of the upper atmosphere, aurorae and airglow; magnetospheric physics, cosmic rays, generation and propagation of plasma waves in the magnetosphere; solar physics, infrared astronomy; the effects of nuclear explosions, magnetic storms, and solar activity on the earth's atmosphere, ionosphere, and magnetosphere; the effects of optical, electromagnetic, and particulate radiations in space on space systems.